

https://dspace.org/

Design of an intravaginal composite polymeric system for the reduction and prevention of STI and HIV transmission

Mashingaidze, Felix

2014-08-22
http://hdl.handle.net/10539/15217

Downloaded from a DSpace repository. https://dspace.org/

DESIGN OF AN INTRAVAGINAL COMPOSITE POLYMERIC SYSTEM FOR THE REDUCTION AND PREVENTION OF STI AND HIV TRANSMISSION

FELIX MASHINGAIDZE

A dissertation submitted to the Faculty of Health Sciences, University of the Witwatersrand, in fulfilment of the requirements for the degree of Master of Pharmacy



Supervisor:

Professor Viness Pillay, Department of Pharmacy and Pharmacology, University of the Witwatersrand, Johannesburg, South Africa

24 March 2014

Co-Supervisors:

1. Associate Professor Yahya Essop Choonara, Department of Pharmacy and Pharmacology, University of the Witwatersrand, Johannesburg, South Africa

2. Professor Eckhart Buchmann, Department of Obstetrics and Gynaecology, Faculty of Health Sciences, University of the Witwatersrand, Johannesburg, South Africa

3. Doctor Vinesh Maharaj, Department of Biosciences, Council for Scientific and Industrial Research, Pretoria, South Africa

4. Doctor Lisa Clare du Toit, Department of Pharmacy and Pharmacology, University of the Witwatersrand, Johannesburg, South Africa

DECLARATION

I, Felix Mashigaidze, declare that this dissertation is my own work. It is being submitted for the degree of Master of Pharmacy in the Faculty of Health Sciences at the University of the Witwatersrand, Johannesburg, South Africa. It has not been submitted before for any degree or examination at this or any other University.



Signature

This 24th day of March, 2014

RESEARCH OUTPUTS

PUBLICATIONS, CONFERENCE PROCEEDINGS AND PATENT

A. Publications

1. Qualitative and quantitative intravaginal targeting: key to anti-HIV-1 microbicide delivery from test-tube to *in vivo* success. 2012. Viness Pillay, Felix Mashingaidze, Yahya E. Choonara, Lisa C. du Toit, Eckhart Buchmann, Vinesh Maharaj, Valence M.K. Ndesendo, Pradeep Kumar. Journal of Pharmaceutical Sciences. 101, 1950-1968 (Abstract in Appendix A).

2. Exploration of the biomacromolecular interactions of an interpenetrating proteo-saccharide hydrogel network at the mucosal interface. 2013. Felix Mashingaidze, Yahya E. Choonara, Pradeep Kumar, Lisa C. du Toit, Eckhart Buchmann, Vinesh Maharaj, Valence M.K. Ndesendo, Viness Pillay. Journal of Biomedical Materials Research A, 101A, 3616-3629 (Abstract in Appendix B).

B. Conference proceedings

Podium presentation

1. Formulation, optimization and characterization of mucin-pectin-polyethylene glycol microspheres for intravaginal anti-HIV-1 drug delivery. 12 September, 2012. Felix Mashingaidze, Viness Pillay, Yahya E. Choonara, Pradeep Kumar, Lisa C. du Toit, Eckhart Buchmann, Vinesh Maharaj, Valence M.K. Ndesendo. UKPharmSci Conference. East Midlands Conference Centre, Nottingham, United Kingdom (Abstract in Appendix C).

2. Pectin-mucin interactions: implication and application in microsphere formulation for drug delivery. 24 August 2011. Felix Mashingaidze, Viness Pillay, Yahya E. Choonara, Pradeep Kumar, Lisa C. du Toit, Eckhart Buchmann, Vinesh Maharaj, Valence M.K. Ndesendo. School of Therapeutic Sciences Research Day, University of Witwatersrand, Johannesburg, South Africa (Abstract in Appendix D).

Poster presentation

1. Formulation, optimization and characterization of mucin-pectin-polyethylene glycol microspheres for intravaginal anti-HIV-1 drug delivery. 12 September, 2012. Felix Mashingaidze, Viness Pillay, Yahya E. Choonara, Pradeep Kumar, Lisa C. du Toit, Eckhart Buchmann, Vinesh Maharaj, Valence M.K. Ndesendo. UKPharmSci Conference. East Midlands Conference Centre, Nottingham, United Kingdom (Abstract in Appendix C).

C. Patents

1. Pharmaceutical dosage form. 2011. Viness Pillay, Yahya E. Choonara, Felix Mashingaidze. South Africa Patents and Trade Mark Office, Patent Journal, volume 44, number 9, provisional patent filed on 08 September 2011 (Copy in Appendix E).

RESEARCH FUNDING

1. Awarded a travel grant by the Faculty of Health Sciences Research Office, University of the Witwatersrand, to present a paper and poster at the UKPharmSci Conference that took place from the 12-14th September 2012 at the East Midlands Conference Centre, University of Nottingham, Nottingham, United Kingdom.

2. Awarded a travel grant from the Postgraduate Merit Award/Bursary Funds, Financial Aid and Scholarship Office, University of the Witwatersrand, to present a paper and poster at the UKPharmSci 2012 Conference that took place from 12-14th September at the East Midlands Conference Centre, University of Nottingham, Nottingham, United Kingdom.

3. Awarded a Faculty Research Committee Individual Research Grant from the Medical Faculty Research Endowment Fund (MFREF), Faculty of Health Sciences, University of the Witwatersrand, Johannesburg, South Africa. Grant Number: 00140184911065121105MASH012RM.

4. Funded under Professor Viness Pillay's Research Chair Grant of the South African National Research (NRF), to complete a Master of Pharmacy degree in the department of Pharmacy and Pharmacology, University of the Witwatersrand.

5. Awarded a CSIR BioSciences South Africa Research Bursary to complete a Master of Pharmacy degree in the Department of Pharmacy and Pharmacology, University of the Witwatersrand.

ACCOLADES

1. Awarded a “First Time Inventor” certificate by the Technology Transfer Office of the University of the Witwatersrand (located in Wits Enterprise) in recognition for disclosing my first Wits innovation (copy of Certificate in Appendix F).

2. A target selection team identified a publication that I co-authored for being of special interest to the drug development sector and was listed on the Global Medical discovery Series 2012. This publication is “Qualitative and quantitative intravaginal targeting: key to anti-HIV-1 microbicide delivery from test-tube to *in vivo* success. 2012. Viness Pillay, Felix Mashingaidze, Yahya E. Choonara, Lisa C. du Toit, Eckhart Buchmann, Vinesh Maharaj, Valence M.K. Ndesendo, Pradeep Kumar. Journal of Pharmaceutical Sciences. 101, 1950-1968”.

ABSTRACT

This dissertation discusses anti-HIV-1 microbicide research. In particular, it concentrates on microbicide formulation and delivery. Microbicides are anti-HIV-1 agents that when applied in the human vagina or rectum may prevent sexual HIV-1 transmission. Although most of the anti-HIV-1 agents being developed as microbicides are active *in vitro*, they have proved to be ineffective *in vivo*. A review of microbicide development over the last decade expounds the view that unsatisfactory microbicide failures may be a result of inefficient delivery systems employed. Thus, necessitating a thorough scientific qualitative and quantitative investigation of important aspects involved in HIV-1 transmission as a prerequisite for microbicide development. In this dissertation it is postulated that intravaginal targeting of HIV-1 increases the chances of microbicide success, wherein vaginal micro-environmental factors including pH would be maintained at HIV-1 prohibitive acidic levels to ward off other sexually transmitted diseases which compromise vaginal epithelial barrier properties. Furthermore, targeting early stages of the HIV-1 infection accompanied by computation and delivery of appropriate microbicide quantities could result in an effective microbicide formulation.

In an effort to address microbicide formulation challenges, an intravaginal delivery system able to deliver anti-HIV-1 agents (zidovudine and BP36) over 28 days was formulated. This delivery system is a caplet-shaped composite system comprising zidovudine (AZT) and BP36-loaded pectin-mucin-polyethylene glycol submicrospheres embedded within a poly(D,L-lactide), magnesium stearate, polyvinyl acetate/polyvinylpyrolidone (Kollidon® SR) and poly(acrylic acid) based polymeric caplet matrix. The delivery system was tested *in vitro* and *in vivo* in the pig model. X-ray imaging illustrated the delivery system swelling and its matrix contrast fading over time as vaginal fluid permeated the matrix's core. Plasma, vaginal fluid and tissue drug was detected and quantified using ultra performance liquid chromatography-tandem photodiode array detector. AZT plasma and vaginal fluid concentrations measured on days; 3, 7, 14, 21 and 28 decreased gradually with time. Vaginal tissue AZT concentrations (after 28 days) were higher than plasma AZT concentrations and were in the same range as vaginal fluid AZT concentrations. The herbal extract, BP36, was detected in plasma, vaginal fluid and tissue but was only qualitatively analysed due to its lack of standardization. Histopathological analysis of excised vaginal tissue revealed different scores of abnormalities comprising mild to moderate epithelial proliferation and exocytosis, subepithelial leukocyte influx, perivascular cell cuffing and isolated epithelial erosion, stromal fibrosis and isolated tissue necrosis.

DEDICATION

I dedicate this dissertation to my parents Michael H. and Lydia Mashingaidze for believing in me and supporting me throughout my scholarly journey. I thank them for all the sacrifices they have made for me to reach this academic level.

ACKNOWLEDGEMENTS

This dissertation is a culmination of the contribution and inspiration provided by several people, few of whom I would like to acknowledge.

I acknowledge Prof. Viness Pillay, my supervisor, for encouraging me to pursue postgraduate studies and for providing me with an opportunity to study under his expert guidance. The financial support he sourced for me enabled me to complete my studies. I also thank him for creating a conducive research environment that includes highly equipped advanced laboratories where I was able to learn about several pharmaceutical science techniques.

I thank Ass. Prof. Yahya E. Choonara, my co-supervisor, for his critical analysis and input in my research work and the support he provided, especially when colaborating with our colleagues from Council for Scientific and Industrial Research (CSIR) BioSciences, Pretoria, South Africa.

I acknowledge Dr. Lisa C. du Toit, my co-supervisor, for the advice she provided me about my research, her contribution in the optimization of my formulations and her reviews and recommendations to the publications I co-authored and other written work.

I utilized Prof. Eckhart Buchmann, my co-supervisor's expert obstetrics and gynaecology contribution in my research and his reviews of our publications were notable. For that I am grateful.

I would like to thank Dr. Vinesh Maharaj, my co-supervisor and research group leader at CSIR Biosciences and CSIR BioSciences for providing financial support for my research, tuition fees and stipend, which enabled me to complete my research work. In addition, I would like to thank him and all the team members at CSIR BioSciences that include, Dr. Collin Kenyon and Dr. Pamisha Pillay for the collaborative work they performed on BP36, a novel anti-HIV-1 plant extract and microbicide candidate.

I thank Dr. Divya Bijukumar, a postdoctoral fellow in the Department of Pharmacy and Pharmacology at the University of the Witwatersrand for meticulously reviewing this dissertation.

I would like to thank Ass. Prof. Michael P. Danckwerts, head of the Department of Pharmacy and Pharmacology, University of the Witwatersrand, for the support he provided me as the head of department.

I thank the Animal Ethics Screening Committee (AESC) and members of staff of the Central Animal Services (CAS), University of the Witwatersrand who include; Prof. Graham Alexander, Dr. Douglas M. Eide, Ass. Prof. Kennedy H. Erlwanger, Dr. Leith Meyer, Ms. Mary-Anne Costello, Ms. Amelia Rammekwa, Ms. Kershnee Chetty, Ms. Lorraine Setimo, Mr. Patrick Selahle and Mr. Nico Douths, for the animal ethics approval and the technical assistance they provided me in performing my *in vivo* studies.

Having completed his PhD on microbicide drug delivery research in the same department, Ass. Prof. Valence M.K. Ndesendo provided me with technical and scientific advice that made my research work easier. I thank him for his contribution to my work because I did not have to reinvent the wheel on some of the techniques involved as I used his work as reference.

I am privileged to have been part of the WADDP postgraduate student group and I will always cherish my interaction with my fellow students as we faced various challenges and attained several successes in our work. I thank them for all the assistance and support they provided.

Mr. Pradeep Kumar, my fellow postgraduate research student's contribution to my studies was profound. He assisted me in technical and scientific work in the laboratories as well as in the analysis and writing of scientific posters, papers and in the preparation for conferences. I thank him very much for that.

I thank the technical staff in the Department of Pharmacy and Pharmacology, University of Witwatersrand including; Mr. Sello Ramarumo, Mr. Bafana Themba, Mr. Kleinbooi Mohlabi, Ms. Busisiwe Damane for all the assistance they provided which made my work in the laboratories and office easier.

ANIMAL ETHICS DECLARATION

I, Felix Mashingaidze, hereby confirm that the study entitled "*In vivo* intravaginal delivery of a drug combination (zidovudine and BP36) in the pig model employing a composite polymeric delivery system" was approved by the Animal Ethics Committee of the University of Witwatersrand with Ethics Clearance Number 2011/44/05 (Abstract in Appendix 7).

TABLE OF CONTENTS

		Page
Declaration		iii
Research Outputs		iv
Research Funding		vi
Accolades		vii
Abstract		viii
Dedication		ix
Acknowledgements		x
Animal Ethics Declaration		xii
List of Figures		xix
List of Tables		xxvi
List of Equations		xxix

Chapter 1

Background and Motivation for the Formulation of an Intravaginal Delivery System to Prevent Transmission of STIs Particularly HIV-1

1.1.	Introduction	1
1.2.	Rational and motivation for this study	3
1.3.	An intravaginal composite polymeric system: concept and outline	6
1.4.	Aims and objectives of this study	7
1.5.	Overview of this dissertation	8

Chapter 2

A Review of the Key Aspects Essential for Anti-HIV-1 Microbicide Delivery Success

2.1.	Introduction	11
2.2.	Mechanism of HIV-1 infection: determinants and dynamics	19
2.3.	The vagina as a target site for microbicide delivery	22
2.4.	Qualitative microbicide targeting	23
2.4.1.	Direct viral and cellular targeting	24
2.4.2.	Targeting the vaginal microenvironment	26
2.4.3.	Targeting the vaginal epithelia	26

2.4.4. Vaginal subepithelia targeting 28
2.4.5. Microbicide multi-targeting 29
2.5. Quantitative microbicide targeting 31
2.6. Concluding remarks 36

Chapter 3

Characterization and Preformulation Analysis of Drug (AZT and BP36) and Polymer (pectin, mucin and poly ethylene glycol) intended for submicrosphere preparation

3.1. Introduction 37
3.2. Materials and methods 40
3.2.1. Materials 40
3.2.2. Attenuated total reflection Fourier transform infrared spectroscopic (ATR-FTIR) analysis of drugs and polymers 40
3.2.3. Morphological characterization of lyophilized samples of MUC, PEC and MUC-PEC blends 41
3.2.4. Thermal and thermodynamic analysis of AZT and BP36 powder samples, MUC, PEC_{USP} and MUC-PEC_{USP} lyophilized samples 41
3.2.5. Thermal and thermodynamic analysis of AZT and BP36 powder samples; MUC, PEC_{USP} and MUC-PEC_{USP} lyophilized samples 41
3.2.6. Ultraviolet (UV) spectrophotometry analysis of MUC, PEC and MUC-PEC combination aqueous dispersions 42
3.2.7. Rheology analysis of MUC, PEC and MUC-PEC combination aqueous dispersions 42
3.2.8. Static lattice atomistic simulations of MUC PEC interactions 44
3.3. Results and discussion 44
3.3.1. ATR-FTIR spectroscopy of AZT, B36, MUC, PEC and MUC-PEC 44
3.3.2. Morphological characterization by scanning electron microscopy of lyophilized samples of MUC, PEC_{USP} and MUC-PEC_{USP} 49
3.3.3. Thermogravimetric analysis of AZT and BP36 50
3.3.4. Thermal and thermodynamic analysis of AZT, BP36, MUC, PEC_{USP}, MUC-PEC_{USP} 52
3.3.5. Ultraviolet spectrophotometry analysis 56
3.3.6. Rheological characterization of porcine gastric mucin (MUC), pectin (PEC) and their respective combination aqueous dispersions 59

3.3.7.	Effect of plasticizer (PEG 400) and calcium ions on the viscosity and dynamic moduli of dilute MUC-PEC_{USP} aqueous dispersions	60
3.3.8.	Molecular Mechanics Assisted Model Building and Energy Refinements	64
3.3.9.	MMER analysis	65
3.3.10.	Elucidation of MUC and PEC molecular interactions and the simulation of a MUC-PEC submicrosphere	66
3.4.	Concluding remarks	71

Chapter 4

Formulation and Characterization of Drug Loaded Pectin-mucin-poly ethylene glycol Submicrospheres

4.1.	Introduction	72
4.2.	Materials and methods	73
4.2.1.	Materials	73
4.2.2.	Box-Behnken design optimization for the preparation of AZT-loaded PEC-MUC-PEG SMs	73
4.2.3.	*In vitro* preparation of AZT–loaded PEC-MUC-PEG SMs	75
4.2.4.	Determination of the stability of the optimized SM emulsion	75
4.2.5.	Characterization of the SMs	76
4.2.6.	Drug encapsulation and release from the submicrospheres	76
4.2.7.	Attenuated total reflectance Fourier transform infrared (ATR-FTIR) spectroscopy analysis	79
4.2.8.	Thermal analysis using differential scanning calorimetry (DSC)	79
4.2.9.	Thermogravimetric analysis	79
4.2.10.	X-ray diffraction (XRD) analysis	80
4.3.	Results and discussion	81
4.3.1.	Preparation and optimization of the macromolecular SMs	81
4.3.2.	Submicrosphere emulsion stability	83
4.3.3.	Morphological characterization of AZT-loaded PEC-MUC-PEG SMs	84
4.3.4.	Drug release from PEC-MUC-PEG SMs	85
4.3.5.	ATR-FTIR analysis of PEC, MUC, PEG, AZT and AZT-loaded PEC-MUC-PEG SMs	90
4.3.6.	Differential scanning calorimetry (DSC)	91

4.3.7.	Thermogravimetric analysis of AZT-loaded SMs and their native constituents	92
4.3.8	X-ray diffraction (XRD)	94
4.4.	Concluding remarks	96

Chapter 5

Fabrication, Optimization and *In vitro* Testing of a Composite Polymeric Delivery System

5.1.	Introduction	97
5.2.	Materials and methods	98
5.2.1.	Materials	98
5.2.2.	Box-Behnken design optimization of the composite polymeric drug delivery system (caplet)	99
5.2.3.	Polymeric matrix texture profiling	100
5.2.4.	Effect of the quantity of poly(acrylic acid) on the caplet matrix dimensions	101
5.2.5.	Polymeric caplet matrix friability determination	101
5.2.6.	Drug release studies of the composite polymeric delivery system	102
5.3.	Results and discussion	103
5.3.1.	Fabrication and optimization of the composite polymeric delivery system	103
5.3.2.	Effect of the quantity of poly(acrylic acid) on caplet matrix swelling	106
5.3.3.	Polymeric caplet matrix texture profile	109
5.3.4	Polymeric caplet friability	110
5.3.5	Drug release from the composite polymeric delivery system	110
5.4.	Concluding remarks	114

Chapter 6

***In Vivo* Extended Analysis of a Composite Drug Delivery System in the Pig Model**

6.1.	Introduction	115
6.2.	Materials and methods	116
6.2.1.	Materials	116
6.2.2.	Preparation of the drug-loaded composite polymeric delivery system	117
6.2.3.	Transportation and housing of the experimental animals (Large White	117

pigs)
6.2.4. *In vivo* experimental design and procedure 118
6.2.5. *In vivo* X-ray imaging of the intravaginal polymeric delivery system 121
6.2.4.2. Vaginal swab collection 122
6.2.4.3. Blood sample collection 122
6.2.4.4. Vaginal tissue sample collection 122
6.2.5. Quantitative chromatographic determination of drug (AZT and/or BP36) in plasma, vaginal fluid and vaginal tissue 123
6.2.5.1. Chromatographic detection and quantification of AZT 123
6.2.5.2. Diluent, stock and working standard preparation 124
6.2.5.3. Solid phase extraction and measurement of AZT from plasma 124
6.2.5.4. Chromatography assay validation 125
6.2.5.4.1. Selectivity 125
6.2.5.4.2. Recovery 125
6.2.5.4.3. Linearity 125
6.2.5.4.4. Limit of detection and limit of quantification 125
6.2.5.4.5. Precision and accuracy 126
6.2.5.4.6. Stability of AZT and 3TC in plasma 126
6.2.5.5. Analysis of AZT concentration in plasma, vaginal fluid and tissue samples of group B pigs 126
6.2.6. Chromatographic detection and quantification of BP36 127
6.2.7. Histopathology analysis of porcine vaginal epithelia 127
6.3. Results and discussion 128
6.3.1. Pilot study using one pig from group C 128
6.3.2. *In vivo* X-ray imaging of the intravaginal polymeric delivery system 130
6.3.3. Quantitative chromatographic determination of plasma drug released from the delivery system 132
6.3.3.1. Chromatographic conditions and separation of AZT from 3TC 132
6.3.3.2. AZT chromatographic assay validation 133
6.3.3.2.1. Selectivity 133
6.3.3.2.2. Recovery 133
6.3.3.2.3. Linearity, limit of detection and limit of quantification 134
6.3.3.2.4. Precision and accuracy 134
6.3.3.2.5. Stability of analyte and internal standard 135

6.3.3.3. Concentration of AZT in porcine plasma, vaginal fluid and vaginal tissue samples 135
6.3.3.4. Detection and quantification of BP36 in porcine plasma, vaginal fluid and vaginal tissue 137
6.3.4. Histopathology analysis of porcine vaginal epithelia 138
6.4. Concluding remarks 143

Chapter 7

Conclusions and Recommendations

7.1: Conclusions 144
7.2: Recommendations 146

References 147

Appendices 173
Appendix A: Abstract for a review paper published from this dissertation 174
Appendix B: Abstract for a research paper published from this dissertation 175
Appendix C: Abstract for the UKPharmSci 2012 conference poster and podium presentations 176
Appendix D: Abstract for The University of the Witwatersrand School of Therapeutics Sciences Research Day conference podium presentation 177
Appendix E: Patent Journal issue (September 2011) where a filed provisional patent for the work provided in this dissertation was published. (provisional patent number 72) 178
Appendix F: “First Time Inventor” certificate issued by Wits Enterprise 181
Appendix G: Animal Ethics Clearance certificate 182
Appendix H: First animal ethics “Modification and Extension of Experiments” certificate 183
Appendix I: Second animal ethics “Modification and Extension of Experiments” certificate 184

LIST OF FIGURES

		Page
Figure 1.1:	A composite polymeric delivery system inserted into the human posterior vaginal fornix	6
Figure 2.1:	Schematic of HIV-1 infection pathway and mechanism	20
Figure 2.2:	HIV-1 interactions with receptors and co-receptors on Langerhans cells (LCs) and dendritic cells (DCs)	21
Figure 2.3:	Transmission electron micrograph (TEM) of: a) HIV-1 virus captured by a dendritic cell; b) HIV-1 virus attached to a dendritic cell	21
Figure 2.4:	Epithelia monolayers showing tight junction down-regulation on exposure to different HIV-1 strains that include; a) normal unexposed epithelia, b) wildtype HIV-1 strain exposed epithelia and c) gp120-lacking mutant HIV-1 exposed epithelia	27
Figure 2.5:	Illustration of microbicide-HIV-1 virus confrontation in the vaginal cavity	28
Figure 2.6:	Post-exposure HIV-1 virus census in cervicovaginal epithelia	32
Figure 2.7:	HIV-1 neutralization schematics by microbicide formulations with different anti-HIV-1 release profiles; a) acute HIV-1 intravaginal infection: no microbicide, b) quick release microbicide formulation and c) sustained release microbicide formulation	34
Figure 3.1:	ATR-FTIR absorbance spectrum of zidovudine (AZT)	45
Figure 3.2:	ATR-FTIR absorbance spectrum of BP36	45

Figure 3.3: Split ATR-FTIR absorbance spectra of lyophilized aqueous dispersions of different types of pectin; PEC_{AS-FS}, PEC_{AS} and PEC_{USP} 47

Figure 3.4: Split ATR-FTIR absorbance spectra of lyophilized aqueous dispersions PEC_{USP}, MUC and MUC-PEC_{USP} 48

Figure 3.5: Overlay ATR-FTIR absorbance spectra of lyophilized aqueous dispersions of porcine gastric mucin (MUC) and pectin (PEC_{USP}) that compares the different MUC:PEC_{USP} ratios in MUC-PEC_{USP} lyophilized aqueous dispersions, thus depicting the type and extent of macromolecular interactions between MUC and PEC_{USP} 48

Figure 3.6: SEM images, taken at 510X magnifiifation, depicting membranous scaffolds of lyophilized MUC-PEC_{USP} combinations; (a) MUC, (b) PEC_{USP}, (c) MUC-PEC_{USP}1:1, (d) MUC-PEC_{USP}1:4 and (e) MUC-PEC_{USP}1:9. Bar =50.0μm 50

Figure 3.7: TGA (solid) and DTGA (dotted) thermogram of AZT obtained when AZT was analyzed from 50ºC to 500ºC 51

Figure 3.8: TGA (solid) and DTGA (dotted) thermogram for BP36 obtained when BP36 was analyzed from 25ºC to 500ºC 51

Figure 3.9: First run DSC thermogram of AZT measured from -10ºC to 500ºC 52

Figure 3.10: First and second run DSC thermograms of AZT measured from -10ºC to 200ºC 52

Figure 3.11: First run DSC thermogram of BP36 measured from -10ºC to 500ºC 53

Figure 3.12: First and second run DSC thermograms of BP36 measured from -10ºC to 250ºC 53

Figure 3.13: DSC thermogram of; MUC, MUC-PEC_{USP} (ratio 1:1, 1:4 and 1:9) and 54

PEC evaluated from -10°C to 250°C

Figure 3.14: Rheology profile properties of MUC, PEC_{USP} and MUC-PEC_{USP} 9:1 illustrating non-Newtonian shear thinning (pseudoplastic) flow and rheological synergism 62

Figure 3.15: Rheological pseudoplastic flow and viscosity profiles of MUC, PEC_{USP} and MUC-PEC_{USP} 9:1 illustrating the effect of addition of PEG 400 and crosslinking with calcium ions on viscosity 63

Figure 3.16: Effect on dynamic moduli of PEG 400 and crosslinking with calcium ions as measured by dynamic oscillatory rheology 64

Figure 3.17: Energy minimized molecular structures of, (a) glycosylated MUC and (b) PEC generated by HyperChem™ 8.0.8 Molecular Modeling System (Hypercube Inc., Gainesville, Florida, USA). Colour codes: C (cyan), O (red), N (blue) and H (white) 68

Figure 3.18: Visualization of geometrical preferences of; (a) MUC:PEC::1:1, (b) MUC:PEC::1:2, (c) MUC:PEC::1:3 and (d) MUC:PEC::1:4 along with H-bonds after molecular simulation in vacuum. MUC is rendered as stick model (red) with coiled (yellow) secondary structure. Colour codes: C (cyan), O (red), N (blue) and H (white) 69

Figure 3.19: Connolly molecular electrostatic potential surfaces of a simulated submicrosphere in wire mesh display mode 70

Figure 4.1 Response mesh plots correlating dependent formulation parameters/responses; PS, ZP and MDT to their independent parameters; ST, SC and D:P ratio 82

Figure 4.2: Delta transmission and delta backscattering profiles of an optimized SM emulsion obtained through continuous scans every 6 minutes for 1 hour 83

Figure 4.3:	Transmission electron micrograph of AZT-loaded MUC-PEC-PEG SMs observed at 40 000X magnification using a JEOL S100 transmission electron microscope	84
Figure 4.4:	Showing, (a) Particle size distribution with intensity and (b) zeta potential distribution profile of the optimized SMs obtained using a zetasizer	85
Figure 4.5:	SM dissolution profiles of; (a) formulations F1-F5, (b) formulations F6-F10, (c) formulations F11-F15 and (d) the optimized formulation in SVF and PBS	86
Figure 4.6:	Comparison of AZT release from; (a) PEC-MUC-PEG SMs in SVF pH 4.2 to AZT release in PBS pH 7.4, (b) crosslinked PEC SMs to release from uncrosslinked PEC SMs both in SVF, (c) PEC-MUC-PEG SMs to AZT release from PEC-MUC SMs both in SVF and (d) PEC-MUC-PEG SMs to AZT release in PEC-PEG SMs both in SVF	88
Figure 4.7:	ATR-FTIR spectra of; (a) AZT-loaded PEC-MUC-PEG SMs, (b) MUC, (c) PEC, (d) AZT and (e) PEG	91
Figure 4.8:	DSC thermograms of; (a) PEC-MUC-PEG +AZT, (b) MUC, (c) PEC and (d) AZT	92
Figure 4.9:	The TGA (solid) and DTGA (dotted) thermograms of: (a) PEC-MUC-PEG+AZT SMs; (b) (i) MUC, (ii) PEC, (iii) AZT, (iv) PEC-MUC-PEG+AZT MS and (v) PEG; (c) PEC; (d) MUC; (e) AZT and (f) PEG	94
Figure 4.10:	Three dimensional X-ray diffractograms of; (a) AZT-loaded PEC-MUC-PEG SMs (black), PEC (green), MUC (blue) and AZT (red)	95
Figure 5.1:	Digital photographs of a steel punch and die set and a polymeric caplet punched using the set	104

Figure 5.2: Response surface plots correlating responses; fractional of mass increase (FMI), matrix hardness (H) and fractional drug release (FDR) to independent parameters; masses of magnesium stearate (MS), polyvinyl acetate/polyvinylpyrolidone (KSR) and poly(D,L-lactide) (PDLL) used in fabricating the polymeric caplet 105

Figure 5.3: Depicts (a) digital photographs of polymeric caplets, from left to right; before 30 day dissolution in SVF and after dissolution for the caplets containing 1%, 2% or 3% of poly(acrylic acid) and (b) a bar graph illustrating the different percentage dimensional increases in length, width and thickness of the polymeric caplet containing 1%, 2% and 3% poly(acrylic acid) that was measured after 30 days of caplet dissolution in SVF 107

Figure 5.4: Depicts; (a) digital photograph of the caplet's cross-section (from left to right); before dissolution and after 1% poly(acrylic acid) containing caplet's dissolution in SVF and PBS then 2% and 3% poly(acrylic acid) containing caplet's dissolution in SVF respectively (b) SEM micrograph acquired at 500X magnification of the caplet's cross-section before dissolution and (c-f) SEM micrograph of the caplet cross-section after a 30 day dissolution of the caplet containing, (c) 1% poly(acrylic acid) in SVF (d) 1% poly(acrylic acid) in PBS (e) 2% poly(acrylic acid) in SVF and (f) 3% poly(acrylic acid) in SVF 108

Figure 5.5: Force versus time texture analysis profile used to determine the caplet matrix hardness (H) and percentage matrix resilience 109

Figure 5.6: Fraction of AZT released from the optimised caplet in SVF and PBS over 30 days 111

Figure 6.1: Large White female pigs housed in Central Animal Services, University of the Witwatersrand, (a) together in one pen upon delivery 118

and (b) separately in each cage during experimentation

Figure 6.2: Flow diagram depicting a step-by-step *in vivo* experimental approach 119

Figure 6.3: Pig shown, (a) under anaesthesia in the pen before being taken to the procedures room and (b) during intravaginal insertion of a delivery system that was tied right round using a silk suture material then sutured onto the vaginal mucosa 121

Figure 6.4: Large White female pig lying on the operating table in the dorsal position whilst under anaesthesia during the X-ray procedure 121

Figure 6.5: Digital images of the delivery system and X-rays images of the delivery system observed *in situ* in the vaginal cavity during the pilot study when; (a) the delivery system was inserted using a metal speculum and a radio opaque string lined sponge was used to ensure the caplet stays in place in the vaginal cavity, (b) the engraved delivery system was tied right round and attached to the mucosa in the vaginal cavity using a silk suture material and (c) the delivery system was enclosed in a silk material pouch and the pouch was attached to the mucosa in the vaginal cavity 129

Figure 6.6: X-ray images of the pig pelvic region depicting the composite polymeric delivery system: with no drug loaded observed on days 3 a.i), 7 (a.ii), 14 (a.iii), 21 (a.iv) and 28 (a.v); loaded with AZT (300mg) observed on days 3 (b.i), 7 (b.ii), 14 (b.iii), 21 (b.iv) and 28 (b.v); loaded with BP36 (600mg) observed on days 3 (c.i), 7 (c.ii), 14 (c.iii), 21 (c.iv) and 28 (c.v) and; loaded with BP36 (150mg) and AZT (150mg) observed on days 3 (d.i), 7 (d.ii), 14 (d.iii), 21 (d.iv) and 28 (d.v) 131

Figure 6.7: Chromatograms obtained for; (a) IS and AZT spiked in diluent, (b) typical blank plasma sample and (c) IS and AZT spiked in plasma sample 132

Figure 6.8:	Chromatograms of the analyte (AZT, 5µg/mL) and IS (3TC, 3µg/mL) spiked plasma samples obtained at times; (a) 0hrs, (b) 12hrs, (c) 24hrs, (d) 48hrs and (e) 72hrs revealing analyte and IS stability during the chromatographic assay	135
Figure 6.9:	Typical UPLC chromatogram obtained for plasma, vaginal fluid and tissue samples	135
Figure 6.10:	AZT concentration measured in, (a) plasma and (b) vaginal fluid samples collected on days; 3, 7, 14, 21 and 28 from group B pigs	136
Figure 6.11:	AZT concentration measured in vaginal tissue samples excised from group B pigs after the 28 day study	137
Figure 6.12:	UPLC-PDA chromatogram of BP36	138
Figure 6.13:	Digital photographs of the excised vaginal tissue; (a) soon after being excised from the pig on day 28 of the experiment with the composite delivery system still attached and (b) placed in 10% normal buffered formalin for storage before histopathology analysis	140
Figure 6.14:	Histopathology images of excised pig vaginal tissue depicting; (a) normal epithelia and lamina propria, pig C1, (b) epithelial erosion/ulceration, pig B4, (c) epithelial proliferation, pig A1, (d) epithelial exocytosis, pig A4, (e) subepithelial leukocyte influx, pig B4, (f) stromal fibrosis, pig B5, (g) perivascular cell cuffing, pig B4 and (h) tissue necrosis and polymorphonuclear exudation, pig B4	142

LIST OF TABLES

		Page
Table 2.1:	Microbicide clinical trials	13
Table 2.2:	Different microbicide formulations	17
Table 2.3:	HIV-1 invasion sites, location and the type of epithelial cells	22
Table 2.4:	HIV-1 receptor targets and their corresponding inhibitory agents	24
Table 2.5:	Microbicide combination formulations	30
Table 3.1:	Rheometer parameters	43
Table 3.2:	Midpoint melting point and heat of fusion of different MUC:PEC_{USP} weight and volume fractions	54
Table 3.3:	Thermodynamic interaction energy density (*B*) and the Flory-Huggins interaction parameter (χ_{12}) which were determined at 25°C of MUC-PEC_{USP} blends at different MUC:PEC_{USP} ratio; 1:1, 1:4 and 1:9	56
Table 3.4:	UV absorbance of dilute aqueous dispersions of MUC, PEC and MUC-PEC combinations	57
Table 3.5:	Viscosity of MUC-PEC dispersions of three different pectin types at different MUC: PEC ratios	60
Table 3.6:	Viscosity of MUC-PEC_{USP}: effect of addition of PEG 400 and crosslinking with calcium ions on aqueous dispersions of MUC-PEC_{USP} at MUC: PEC_{USP} ratio 9:1	61
Table 3.7:	Effect on dynamic moduli of PEG 400 and crosslinking with calcium ions	63
Table 3.8:	Total potential energies of pectin, mucin, pectin-mucin and the MUC PEC interation energies at MUC:PEC ratios of; 1:1, 1:2, 1:3 and 1:4	70

Table 4.1:	Independent parameters and responses from the Box-Behnken statistical design used to optimize AZT-loaded PEC-MUC-PEG SMs	74
Table 4.2:	Formulations generated using a Box-Behnken statistical design for the optimization of AZT-loaded PEC-MUC-PEG SMs	74
Table 4.3:	Simulated vaginal fluid (SVF), 1L	77
Table 4.4:	Responses obtained from *in vitro* testing of the 15 design formulation's independent parameters	82
Table 4.5:	Goodness of fit and best fit parameters obtained by fitting the SM dissolution profiles (obtained in SVF and PBS) to different kinetic models	89
Table 5.1:	Box-Behnken design independent parameter limits and response objectives	99
Table 5.2:	Box-Behnken design template of the 15 polymeric caplet formulations	100
Table 5.3:	Texture analyzer parameters used in caplet matrix texture analysis	101
Table 5.4:	Experimental responses to the 15 design formulations used in the optimization for the polymeric caplet	104
Table 5.5:	Best fit parameters and adjusted coefficients of determination obtained after fitting the optimized caplet drug release profile to different kinetic models	113
Table 6.1:	Chromatographic gradient elution conditions	123
Table 6.2:	Solvent elution efficiency of methanol, ethanol and acetonitrile as given by drug recovery after SPE	133
Table 6.3:	Mean recoveries of AZT after SPE from spiked blank plasma (n=3)	133
Table 6.4:	Calibration curve parameters obtained through linear regression on	134

three different days (n=3)

Table 6.5: Intra-day and inter-day precision and accuracy calculated as RSD and RE for three AZT concentration levels; 1, 5 and 10µg/mL (n=3) 134

Table 6.6: Histopathological observations of the vaginal sections excised from the pigs from groups; A, B, C and D 141

LIST OF EQUATIONS

Page

Equation 3.1: $\Delta A = A_{MUC\text{-}PEC} - (A_{PEC} + A_{MUC})$ 42

Where:

ΔA: UV absorbance difference

$A_{MUC\text{-}PEC}$: UV absorbance obtained for the aqueous mucin-pectin combination dispersion

A_{MUC}: UV absorbance obtained for the aqueous mucin dispersion

A_{PEC}: UV absorbance obtained for the aqueous pectin dispersion

Equation 3.2: $\Delta\eta = \eta_{MUC\text{-}PEC} - (\eta_{PEC} + \eta_{MUC})$ 43

Where:

Δη: viscosity difference between the mucin-pectin aqueous dispersion viscosity and that of the sum of the individual viscosities of mucin and pectin

$\eta_{MUC\text{-}PEC}$: mucin-pectin aqueous dispersion's viscosity

η_{PEC}: viscosity of the pectin aqueous dispersion

η_{MUC}: viscosity of the mucin aqueous dispersion

Equation 3.3: $\Delta G' = G'_{MUC\text{-}PEC} - (G'_{PEC} + G'_{MUC})$ 43

Where:

ΔG': storage moduli difference between the mucin-pectin aqueous dispersion storage modulus and that of the sum of the individual storage modulus of mucin and pectin

$G'_{MUC\text{-}PEC}$: mucin-pectin aqueous dispersion's storage modulus

G'_{PEC}: storage modulus of the pectin aqueous dispersion

G'_{MUC}: storage of the mucin aqueous dispersion

Equation 3.4: $\Delta G'' = G''_{MUC\text{-}PEC} - (G''_{PEC} + G''_{MUC})$ 43

Where:

ΔG'': loss moduli difference between the mucin-pectin aqueous dispersion loss modulus and that of the sum of the individual storage modulus of mucin and pectin

$G''_{MUC\text{-}PEC}$: mucin-pectin aqueous dispersion's loss modulus

G''_{MUC}: loss modulus of the mucin aqueous dispersion

G''_{PEC}: loss modulus of the pectin aqueous dispersion

Equation 3.5: $T_m = T_m^0 + T_m^0 (V_2/\Delta H_2) B\phi_1^2$ 55

Where:

T_m: melting temperature of the mucin-pectin blend

T_m^0: melting temperature of pure pectin

V_2: molar volume fraction of pectin

ΔH_2: change in heat of melting

B: molecular interaction energy density

ϕ_1: volume fraction of mucin

Equation 3.6: $T_m = T_m^0 + T_m^0 (V_2/\Delta H_2) B (1-\phi_2)^2$ 55

Where:

T_m: melting temperature of the mucin-pectin blend

T_m^0: melting temperature of pure pectin

V_2: molar volume fraction of pectin

ΔH_2: change in heat of melting

B: molar interaction energy density

ϕ_2:volume fraction of pectin

Equation 3.7: $B = (\chi_{12} TR)/V$ 55

Where:

B: molar interaction energy density

χ_{12}: Flory-Huggins interaction parameter

T: absolute temperature

R: molar gas constant

V: total volume

Equation 3.8: $E_{molecule/complex} = V_\Sigma + V_b + V_\Theta + V_\varphi + V_{ij} + V_{hb} + V_{el}$ 65

Where:

$E_{molecule/complex}$: total potential energy of a molecular complex

V_Σ: steric potential energy contribution of the optimized structure

V_b: potential energy contribution caused by bond stretching

V_Θ: bond angle potential energy contribution

V_φ: torsional potential energy contribution

V_{ij}: potential energy contributed by van der waals interactions as a result of non-bonded interatomic distances

V_{hb}: potential energy contributed by hydrogen bonding

V_{el}: potential energy contributed by electrostatic interactions

Equation 3.9: $\Delta E_{Total} = \Delta E_{Total\ (MUC\text{-}PEC)} - [\Delta E_{Total\ (MUC)} + \Delta E_{Total\ (PEC)}]$ 65

Where:

ΔE_{Total}: total potential energy deviation

$\Delta E_{Total\ (MUC\text{-}PEC)}$: total potential energy of the mucin-pectin complex

$\Delta E_{Total\ (MUC)}$: total potential energy deviation in mucin

$\Delta E_{Total\ (PEC)}$: total potential energy in pectin

Equation 3.10: E_{MUC}=-166.812 V_{Σ}= 5.474V_b + 70.351V_{θ} + 55.173V_{φ} - 29.066V_{ij} - 7.096V_{hb} - 261.649V_{el} 65

Where:

E_{MUC}: potential energy of mucin

V_{Σ}: steric potential energy contribution of the optimized structure

V_b: potential energy contribution caused by bond stretching

V_{Θ}: bond angle potential energy contribution

V_{φ}: torsional potential energy contribution

V_{ij}: potential energy contributed by van der waals interactions as a result of nonbonded interatomic distances

V_{hb}: potential energy contributed by hydrogen bonding

V_{el}: potential energy contributed by electrostatic interactions

Equation 3.11: E_{PEC}= 6.539 V_{Σ}= 2.316V_b + 11.957V_{θ} + 10.407V_{φ} + 13.335V_{ij} - 31.477V_{el} 66

Where:

E_{PEC}: potential energy of pectin

V_{Σ}: steric potential energy contribution of the optimized structure

V_b: potential energy contribution caused by bond stretching

V_{Θ}: bond angle potential energy contribution

V_{φ}: torsional potential energy contribution

V_{ij}: potential energy contributed by van der waals interactions as a result of nonbonded interatomic distances

V_{hb}: potential energy contributed by hydrogen bonding

V_{el}: potential energy contributed by electrostatic interactions

Equation 3.12: $E_{MUC\text{-}PEC1} = -222.143\ V_{\Sigma} = 8.556V_b + 111.66V_{\theta} + 104.151V_{\varphi} - 45.460V_{ij} - 13.159V_{hb} - 387.892V_{el}$ 66

Where:

$E_{MUC\text{-}PEC1}$: potential energy of the mucin-pectin complex were a single mucin molecule interact with a single pectin molecule

V_{Σ}: steric potential energy contribution of the optimized structure

V_b: potential energy contribution caused by bond stretching

V_{Θ}: bond angle potential energy contribution

V_{φ}: torsional potential energy contribution

V_{ij}: potential energy contributed by van der waals interactions as a result of nonbonded interatomic distances

V_{hb}: potential energy contributed by hydrogen bonding

V_{el}: potential energy contributed by electrostatic interactions

Equation 3.13: $E_{MUC\text{-}PEC2} = -299.723\ V_{\Sigma} = 10.725V_b + 132.77V_{\theta} + 137.173V_{\varphi} - 61.557V_{ij} - 20.086V_{hb} - 498.747V_{el}$ 66

Where:

$E_{MUC\text{-}PEC2}$: potential energy of the mucin-pectin complex were a single mucin molecule interact with a two pectin molecules

V_{Σ}: steric potential energy contribution of the optimized structure

V_b: potential energy contribution caused by bond stretching

V_{Θ}: bond angle potential energy contribution

V_{φ}: torsional potential energy contribution

V_{ij}: potential energy contributed by van der waals interactions as a result of nonbonded interatomic distances

V_{hb}: potential energy contributed by hydrogen bonding

V_{el}: potential energy contributed by electrostatic interactions

Equation 3.14: $E_{MUC\text{-}PEC4} = -385.041V_{\Sigma} = 20.132V_b + 170.443V_{\theta} + 231.344V_{\varphi} - 55.159V_{ij} - 25.026V_{hb} - 26.775V_{el}$ 66

Where:

$E_{MUC\text{-}PEC4}$: potential energy of the mucin-pectin complex were a single mucin molecule interact with a three pectin molecules

V_{Σ}: steric potential energy contribution of the optimized structure

V_b: potential energy contribution caused by bond stretching

V_{Θ}: bond angle potential energy contribution

V_{φ}: torsional potential energy contribution

V_{ij}: potential energy contributed by van der waals interactions as a result of nonbonded interatomic distances

V_{hb}: potential energy contributed by hydrogen bonding

V_{el}: potential energy contributed by electrostatic interactions

Equation 3.15: $E_{MUC\text{-}PEC4} = -385.041V_{\Sigma} = 20.132V_b + 170.443V_{\theta} + 231.344V_{\varphi} - 55.159V_{ij} - 25.026V_{hb} - 26.775V_{el}$ 66

Where:

$E_{MUC\text{-}PEC4}$: potential energy of the mucin-pectin complex were a single mucin molecule interact with a four pectin molecules

V_{Σ}: steric potential energy contribution of the optimized structure

V_b: potential energy contribution caused by bond stretching

V_{Θ}: bond angle potential energy contribution

V_{φ}: torsional potential energy contribution

V_{ij}: potential energy contributed by van der waals interactions as a result of nonbonded interatomic distances

V_{hb}: potential energy contributed by hydrogen bonding

V_{el}: potential energy contributed by electrostatic interactions

Equation 3.16: $\Delta E_{(x:y)} = V_{\Sigma\ MUC\text{-}PEC\ (x:y)} - (x.V_{\Sigma\ MUC} + y.V_{\Sigma\ PEC})$ 70

Where:

$\Delta E_{(x:y)}$: MUC PEC interaction energy of x molexules of MUC and y molecules of PEC

$V_{\Sigma\ MUC\text{-}PEC\ (x:y)}$: total potential energy of the MUC-PEC complex

$V_{\Sigma\ MUC}$: total potential energy of MUC

$V_{\Sigma\ PEC}$: total potential energy of PEC

Equation 4.1: $$BS = \frac{1}{\sqrt{\lambda^*}}$$ 75

Where:

BS: back scattered light

λ^*: photon transport mean free path

Equation 4.2: $$\lambda^*(d, \Phi) = \frac{2d}{[3\Phi(1-g)Q_s]}$$ 75

Where:

λ^*: photon transport mean free path

d: particle mean diameter

Φ: volume fraction of particles

g: asymmetry factor

Q_s: light scattering efficiency factor

Equation 4.3: $EE\ (\%) = Actual\ amount\ of\ AZT\ in\ SMs / theoretical\ amount\ of\ AZT \times 100$ 76

Where:

EE: encapsulation efficiency

Equation 4.4: $$MDT = \frac{\sum_{i=1}^{n} t_i M_t}{M_\infty}$$ 78

Where:

MDT: mean dissolution time

M_t: drug released in time t

M_∞: loading dose

Equation 4.5: $$DE = \frac{\int_0^t y \times dt}{y_{100} \times t} \times 100\%$$ 78

Where:

DE: dissolution efficiency

y: percentage of drug dissolved in time t

Equation 4.6: $$f_2 = 50 \log \left\{ \left[1 + {}^1/_n \sum_{t=1}^{n} W_t (R_t - T_t)^2 \right]^{-0.5} \times 100 \right\}$$ 78

Where:

f_2: similarity factor

W_t: optional weight factor

R_t: reference assay at time t

T_t: test assay at time t

n: number of sampling points

Equation 4.7: $$f_1 = \frac{\sum_{t=1}^{n} |R_t - T_t|}{\sum_{t=1}^{n} R_t} \times 100\%$$ 78

Where:

f_1: difference factor

R_t: reference assay at time t

T_t: test assay at time t

n: number of sampling points

Equation 4.8: $PS=-1719.600+163.070[ST]+1247.470[SC]+637.950[D:P]-3.900[ST]^2-158.33[SC]^2-127.530[D:P]^{2-}66.800[ST*SC]+24.600[ST*D:P]-227.200[SC*D:P]$ 81

Where:

PS: particle size

ST: ultrasonication time

SC: surfactant concentration

D:P: drug:polymer ratio

Equation 4.9: $ZP=40.125-4.925[ST]+13.250[SC]-189.100[D:P]+0.580[SC]^2-20.400[SC]^2-26.400[D:P]^2-4.160[ST*SC]+3.000[ST*D:P]+122.800[SC*D:P]$ 81

Where:

ZP: zeta potential

ST: ultrasonication time

SC: surfactant concentration

D:P: drug:polymer ratio

Equation 4.10: $MDT=-34.951+3.267[ST]+41.139[SC]-20.998[D:P]-0.093[ST]^2-11.896[SC]^2-4.624[D:P]^2-0.921[ST*SC]-0.415[ST*D:P]+10.104[SC*D:P]$ 81

Where:

MDT: mean dissolution time

ST: ultrasonication time

SC: surfactant concentration

D:P: drug:polymer ratio

Equation 5.1: $$\%\ dimensinal\ increase = \frac{D_2 - D_1}{D_1} \times 100$$ 101

Where:

D_1: length, width or thickness of caplet before dissolution in simulated vaginal fluid (SVF)

D_2: length, width or thickness of caplet after dissolution in simulated vaginal fluid (SVF) for 7 days

Equation 5.2: $$Friability\ (\%) = \frac{M_1 - M_2}{M_1} \times 100$$ 102

Where:

M_1: total mass of 10 caplets before the friability test

M_2: total mass of 10 caplets after the friability test

Equation 5.3: $$FMI=1.616-0.002[PDLL]+0.668[MS]-0.001[KSR]$$ 103

Where:

FMI: fractional caplet mass increase

PDLL: mass of poly(D,L-lactide)

MS: mass of magnesium stearate

KSR: mass of polyvinyl acetate/polyvinylpyrolidone

Equation 5.4: $$H=-14.465+0.101[PDLL]-0.706[MS]-0.109[KSR]-0.005[MS*MS]+0.001[PDLL*MS]+ 0.001[MS*KSR]$$ 103

Where:

H: caplet matrix hardness

PDLL: mass of poly(D,L-lactide)

MS: mass of magnesium stearate

KSR: mass of polyvinyl acetate/polyvinylpyrolidone

Equation 5.5: $FDR=3.964-0.008[PDLL]+0.009[MS]+0.007[KSR]$ 103

Where:

FDR: fractional drug released from caplet after 7 days of dissolusion

PDLL: mass of poly(D,L-lactide)

MS: mass of magnesium stearate

KSR: mass of polyvinyl acetate/polyvinylpyrolidone

Equation 5.6: $$Matrix\ resilience\ (\%) = \frac{\int_2^3 f(t)dt}{\int_1^2 f(t)dt} \times 100$$ 110

Where:

$\int_2^3 \mathrm{f(t)dt}$: area under the curve between anchors 3 and 2

$\int_1^2 \mathrm{f(t)dt}$: area under the curve between anchors 2 and 1

Equation 6.1: $LOD= 3.3\sigma/S$ 125

Where:

σ: standard deviation (SD) of y-intercepts obtained by performing regression analysis on the calibration curve

S: calibration curve slope

Equation 6.2: $LOQ=10\sigma/S$ 125

Where:

σ: standard deviation (SD) of y-intercepts obtained by performing regression analysis on the calibration curve

S: calibration curve slope

CHAPTER 1
BACKGROUND AND MOTIVATION FOR THE FORMULATION OF AN INTRAVAGINAL DELIVERY SYSTEM TO PREVENT TRANSMISSION OF STIs INCLUDING HIV-1

1.1. Introduction

On average 2.5 million people worldwide were infected with HIV-1 in 2011 and approximately 1.8 million of them were from Sub-Saharan Africa (WHO Data and Statistics, 2011). Existing infection prevention measures, including education and condom use, are already being utilized to curb HIV-1 transmission. Condoms are approximately 90-95% effective in preventing HIV-1 transmission but their use is mired by improper and male-controlled usage (Pinkerton and Abramson, 1997). Therefore, HIV-1 transmission is still a major challenge, especially in South Africa and Sub-Saharan Africa. A promising new preventative modality is the use of microbicides, which are chemical entities that are proposed to reduce HIV-1 transmission when applied vaginally or rectally (Coplan et al., 2004). These pharmaceutical applications can be used discretely, therefore aiding in effective prevention of HIV-1 transmission by the volition of the female partner thereby shifting the responsibility of HIV-1 transmission prevention from the dominion of men to that of women (World Health Organization, 2009; Coplan et al., 2004). The incessant spread of HIV-1, the failure of condoms to provide foolproof protection and the still-to-be discovered or invented cure and/or vaccine make microbicides the new face of hope (UNAIDS, 2010; Gabby and Gibbs, 1996; Crosby et al., 2005; Walsh et al., 1999).

Starting with the Nonoxynol-9 (N-9) surfactant followed by a plethora of other microbicides, there has been a surge in scientific research in HIV-1 prevention using microbicides, with several potent anti-HIV-1 compounds being discovered (Cutler and Justman, 2008). However, very few tangible successes have been recorded from a human effectiveness viewpoint (Cutler and Justman, 2008). There is no microbicide that is effective against HIV-1 on the market to date, yet there are numerous patents of microbicide candidates resulting in the current paradox and inspiration for partaking on this study, whereby, there are successful *in vitro* microbicide studies but disappointing *in vivo* human studies. Leading us to point at, 'ineffective delivery systems', as exemplified by the failure of Pro2000 (Endo Pharmaceuticals Solutions, Chadds Ford, PA, USA; McCormack et al., 2010), as the cause of microbicide failures. Therefore, inept systems which have been employed to deliver microbicides, may have contributed to the lack of correlation between *in vitro* and *in vivo* efficacies. Available microbicide applications are mostly gels, thus effectiveness is dependent on gel distribution and residency intravaginally.

The route of HIV-1 infection through the vaginal wall involves a substantial amount of virons penetrating the mucosal epithelia and attacking the susceptible immune cells in the subepithelia (Fox and Fidler, 2010). The infected subepithelial cells disseminate to the regional lymph nodes leading to systemic infection (Fox and Fidler, 2010). HIV-1 epithelial cell layer bypass may occur indirectly via Langerhans cell-assisted entry or directly through the disrupted vaginal epithelia layer (Wu and KewalRamani, 2006). To prevent HIV-1 infection, potent microbicides have to create a quantitative and qualitative chemical or physical barrier. This entails the microbicide being present at the site of action longer than the residence time of HIV-1. Additionally, the microbicide has to be bioavailable in the subepithelia to prevent HIV-1 dissemination to the local lymph nodes (Cutler and Justman, 2008; Mayer and Pizer, 2009).

Therefore this study aimed at designing a composite polymeric intravaginal delivery system for dual delivery of a novel microbicide agent (BP36) and an antiretroviral (ARV) zidovudine (AZT). The composite polymeric delivery system, in caplet form would be inserted into the posterior fornix of the vaginal cavity as a way of reducing interference with normal vaginal activities such as intercourse, menstruation and micturition. Its intended position in the vaginal cavity leads to gravity-assisted microbicide agent distribution. The delivery system would be a submicrosphere-embedded erodible polymeric matrix that would release active pharmaceutical ingredients (API) to be distributed throughout the vaginal cavity. Biocompatible and biodegradable polymers such as poly(D,L-lactide), polyvinyl acetate/polyvinylpyrolidone, poly(acrylic acid), pectin, porcine gastric mucin and poly ethylene glycol were the main polymers for the assemblage of the composite polymeric delivery system. Mucoadhesive properties of the delivery system were provided by the incorporation of poly(acrylic acid). The delivery system was designed to eroded and release the active pharmaceutical ingredients (BP36 and AZT) dually encapsulated in the pectin-mucin-poly ethylene glycol submicrospheres.

The submicrospheres were to be synthesized from biocompatible and biodegradable polymers such as pectin, mucin and polyethylene glycol. The interpenetration of pectin fibres and mucin (Sriamornsak and Wattanakorn, 2008) would be exploited to encapsulate the active pharmaceutical ingredients and to modulate drug release from the delivery system. Upon hydration the submicrospheres would, in a modulaterd manner, release the active pharmaceutical ingredients (APIs) into the vaginal cavity. The APIs would then be distributed throughout the vaginal cavity through gravity and inherent vaginal movements to create a chemical barrier against HIV-1 transmission. The matrix of the composite polymeric delivery system, to be formulated from poly(D,L-lactide, polyvinyl acetate/polyvinylpyrolidone, and

poly(acrlic acid) would swell upon absorption of vaginal fluid and erosion takes place creating pores through which the anti-HIV-1 agents would percolate. The erosion of the polymeric matrix was envisaged to involve the hydrolysis of poly-D.L-lactide and the solubilization of the polyvinyl pyrolidone part of polyvinyl acetate/polyvinylpyrolidone. Poly(D,L-lactide) hydrolysis in the aqueous vaginal environment would produce acids and diacids that would help to maintain the acidic vaginal pH which is hostile to pathogens (Li and McCarthy, 1999). Absence of additional fluid from the delivery system itself renders discreetness to the composite polymeric delivery system unlike gel-based formulations.

The choice of the anti-HIV-1 agents used was made to ensure greater success in preventing HIV-1 transmission. BP36, a natural product extract has been discovered to have anti-HIV-1 properties whose mode of action include HIV-1 entry inhibition whilst zidovudine (AZT) would be employed to counter the virus that would have bypassed the viral entry-inhibition stage and it would prevent viral replication. Therefore, the composite polymeric delivery system would have two different modes of action, entry inhibition and replication prevention, thus activity will be both intracellular and extracellular. The delivery of the anti-HIV-1 agent/s using a composite polymeric delivery system was further tested *in vivo* in the pig model.

1.2. Rationale and motivation for this study

The design of a microbicide delivery system should at least ensure that the microbicide:

- Acts as a foolproof chemical and or physical barrier at the vaginal mucosal layer.
- Outlasts the virus: be always present at the site of action.
- Prevents dissemination of infected cells from the sub-epithelia to the regional lymph nodes (Mayer and Pizer, 2009).

Failed microbicides such the nonoxynol-9 surfactant showed *in vitro* success of disrupting the HIV-1 membrane. However, *in vivo* studies have shown that nonoxynol-9 also disrupts the vaginal epithelial membrane integrity thus increasing HIV-1 transmission according to the COL-1492 study (Van Damme et al., 2002). Gel microbicides formulations have failed to outlast the virus. They are as good as their distribution and residence at the site of action. These gel formulations also fall short in preventing the dissemination of infected cells from the mucosa to the lymph nodes simply because they are not bioavailable in the sub-epithelium.

With enough scientific input, analysis and innovation microbicides delivery can be improved. The understanding of the human vaginal anatomy and physiology is important when designing a

microbicide delivery system. Anatomical markers that can help and have incited us to consider this study include the presence of a posterior vaginal fornix and mucus-lined mucosal membrane that can act as a port of anchor for a long-term delivery system. Thus formulating a delivery system able to prolong anti-HIV-1 agent release for at least a month to curtail drug dosing frequency challenges and ensure that the anti-HIV-1 agent/s outlasts the virus is key. Taking a cue from the successes of triple therapy in antiretroviral treatment and the use of antiretrovirals (nevirapine therapy) in the prevention of mother to child transmission, this study employs a model antiretroviral, AZT together with a novel microbicide agent, BP36, to prevent HIV-1 transmission.

According to the Council for Scientific and Industrial Research (CSIR) BioSciences (the organization that holds the patent for BP36) BP36 is a sulfated polysaccharide containing galacturonic and methyl galacturonic moieties whose anti-HIV-1 properties involve the blockage of HIV-1's attachment to the gp120 site on T-cells. BP36 was shown to have anti-HIV-1 activity with the same potency as AZT and nevirapine as demonstrated in the multinuclear-activation galactosidase indicator (MAGI) assay they conducted. BP36 is an extract from a native plant of South Africa. Hence, its success would materialize in financial benefits for the local people as they would be involved in the agricultural production and marketing of the plant.

The microbicide pipeline has several 'inadequate' microbicide delivery systems. Most of these are gels and semi-solids which are indiscreet when used (Rohan and Sassil, 2009). These unaesthetic modalities have motivated us to look at another angle, a composite polymeric intravaginal delivery system in the form of a caplet that is not a gel or semi-solid, which does not add to the fluid in the vagina but instead uses the vaginal fluid as a vehicle to distribute the anti-HIV-1 agent/s throughout the vaginal cavity.

The exact mechanism by which the HIV-1 infection occurs is complex. The vaginal mucosa is lined by stratified squamous epithelia that traditionally do not possess receptors for HIV-1 (with the exception of Langerhans cells which can be found on the epithelia and have extensions into the sub-epithelia) but the sub-epithelial tissue contains multiple targets of the HIV-1 virus (Mayer and Pizer, 2009). There are two common theories postulated of how the virus ends up in the sub-epithelium. The first is the Langerhans cell-assisted entry and the other one is that of the breach of the vaginal mucosa thus opening the floodgates for the virus to enter the sub-epithelium (Wu and KewalRamani, 2006). Epithelial breach can be caused ether by local trauma

or by inflammation as a result of sexually transmitted infections (STIs) (Mayer and Pizer, 2009). The astute strategy therefore would be to prevent HIV-1 from entering the sub-epithelia. Therefore, this study focuses on ensuring adequate amount of the anti-HIV-1 agent is available in the vaginal fluid over an extended duration. Exploring these possibilities may lead us to create new intellectual property with possible applications of the composite polymeric delivery system that include;

- The use of the delivery system to prevent transmission of HIV-1 and other STIs.
- The intravaginal delivery of other systemic drugs that are otherwise degraded by the normal gastrointestinal environment, such as insulin.
- The delivery of drugs through the vaginal mucosa to avoid the liver's first pass metabolism.
- The delivery of personal hygiene, antibacterial and antifungal agents.
- The adaptation of the delivery system for use in other sites of the body that envisage biodegradation and extended drug delivery as preferred characteristics.

The novelty of this study involves the delivery of a combination of an antiretroviral, zidovudine, and a microbicide candidate, BP36, in a single extended release formulation using an optimized blend of polymers to yield the desired drug release properties to prevent vaginal HIV-1 transmission. Potential scientific or societal benefits that motivated us to carry out this study include;

- The possibility of adding to the HIV-1 transmission prevention arsenals already available, a composite polymeric delivery system that improves patient compliance thus aiding in the reduction of the spread and prevalence of HIV/AIDS.
- The ability to shift the HIV-1 prevention dominion from the man to the woman since the delivery system may be used discreetly by women.
- The generation of scientific data to be published in high-impact peer reviewed journals and presented at various conferences for the advancement of science and medicine**.**
- The possibility of creating a home grown functional pharmaceutical application comprising BP36, the novel compound extracted from an indigenous South African plant, that may be affordable to the local population and thus have a huge positive impact on people's quality of life, especially those living in the third world countries where HIV/AIDS prevalence rate is high.

1.3. An intravaginal composite polymeric system: concept and outline

The composite polymeric delivery system was to be made up of AZT and BP36 encapsulating submicrospheres uniformly embedded within a polymer matrix which would be directly compressed into a caplet shaped dosage form as depicted in figure 1.1. The submicrospheres were to be made from pectin, porcine gastric mucin and polyethylene glycol whilst the caplet matrix would be a proportional blend of poly-D.L-lactide, polyvinyl acetate/polyvinylpyrolidone, poly(acrylic acid) and magnesium stearate. The functionality of the composite caplet matrix would involve the vaginal fluid–modulated hydrolysis of poly-D.L-lactide, penetration of vaginal fluid into the interior of the caplet matrix as it solubilises the polyvinylpyrolidone part of the polyvinyl acetate/polyvinylpyrolidone, resulting in matrix swelling. Once vaginal fluid reaches the caplet interior it would be absorbed by the submicrospheres causing the release of AZT and BP36 which will then percolate out of the caplet matrix through the pores formed by the solubilized polyvinylpyrolidone as well as through diffusion as the caplet matrix continues to swell on absorption of more vaginal fluid. The composite polymeric device would fight HIV-1 and STI transmission on two main fronts. The first front would be the HIV-1 in the vaginal fluid. This front would be countered by the anti-HIV-1 agents released into the vaginal fluid. The second front would the subepithelia and HIV-1 in this region would be countered by the anti-HIV-1 agents that would have diffused though the epithelia.

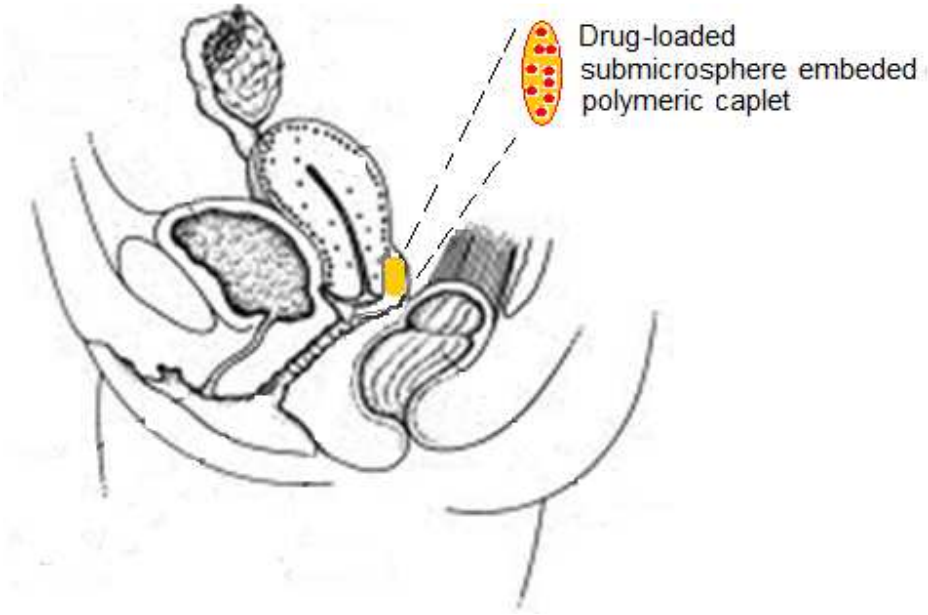


Figure 1.1: A composite polymeric delivery system inserted into the human posterior vaginal fornix

1.4. Aim and objectives of this study

The aim of this study was to formulate an intravaginal composite polymeric drug delivery system laden with submicrospheres encapsulating anti-HIV-1 agents for the purpose of reducing vaginal STI and HIV-1 transmission over and extended duration. In order to achieve this aim the following objectives had to be met;

1. Preformulation, formulation and optimization of drug encapsulating pectin-mucin-polyethylene glycol submicrospheres.
2. Elucidation of the; submicrosphere morphological characteristics, zeta potential, stability of the submicrosphere emulsion, Fourier transform infrared spectroscopy, thermal and thermogravimetric properties of the native materials and the submicrospheres.
3. Determination of drug encapsulation and drug release from the submicrospheres as well as model fitting of the submicrosphere dissolution profile.
4. Fabrication and optimization of the composite polymeric delivery system in the form of a caplet by direct compression of a material blend comprising poly(D.L-lactide) polyvinyl acetate/polyvinylpyrolidone, magnesium stearate, AZT and BP36 laden submicrospheres
5. Elucidation of the drug release kinetics of the composite polymeric delivery system *in vitro* in simulated vaginal fluid.
6. Textural profiling and determination of the friability of the composite delivery system.
7. Performance of *in vivo* animal studies in the Large White pig model to determine caplet drug release in the vaginal cavity, bioavailability of BP36 and AZT in the pig plasma and vaginal epithelial fluid and tissue.

1.5. Overview of this Dissertation

Chapter one begins with an introduction in which the epidemiological status of HIV/AIDS and the huge health burden it posses to the population especially people living in Sub-Saharan Africa is highlighted. Furthermore, ways of preventing HIV-1 transmission are discussed with their advantages and disadvantages noted. One of the disadvantages noted is that the control of HIV-1 prevention is to a greater extent controlled by the male partner. The need to find alternative ways and tools to prevent the spread of sexually transmitted infections, especially HIV-1 became the rationale and motivation of the study with endpoints that include the shifting of the dominion for preventing HIV-1 transmission from the male to the female. The conceptualization and outline of a HIV-1 prevention modality is presented in this chapter. This modality is in the form of a drug-loaded composite polymeric delivery system to be inserted into the posterior fornix of the vagina. The delivery system, which is to be inserted discreetly by the woman, would release the anti-HIV-1 active/s into the vaginal cavity over an extended duration to prevent HIV-1 transmission. Lastly the study's aims and objectives are outlined.

Chapter two is a critical review of the progress made thus far in microbicide research. It outlines the successes and failures reported, with a table containing a comprehensive summary of some of the clinical trials performed on microbicides candidates. This chapter also reviews the different factors involved in vaginal HIV-1 infection and then discusses key issues that need to be addressed during microbicide development. Among the subjects discussed are: the determinants and dynamics of HIV-1 infection; the vaginal cavity and the challenges and opportunities it presents as a site for microbicide delivery and qualitative microbicide targeting that involves, direct viral and cellular targeting, vaginal microenvironment targeting, subepithelial targeting and multitargeting. Quantitative targeting was also identified as a key element that determines the success or failure of a microbicide with two new terms coined; microbicide critical activity window (MCAW) which refers to the initial phase of HIV-1 transmission when microbicide intervention would most likely succeed and the microbicide critical concentration (MCC) which refers to the minimum amount of microbicide agent required to prevent HIV-1 transmission during the initial stages of infection.

Chapter three details the characterization and preformulation studies performed on the anti-HIV-1-agents (zidovudine and BP36) and the biocompatible and biodegradable polymers; pectin, porcine gastric mucin (mucin) and poly ethylene glycol. The aim of the preformulation studies was to infer if it was possible to harness the individually desirable characteristics of the

polymers by combining them to form submicrospheres. Therefore, the focus of the preformulation study was the formation of a macromolecular interpenetrating network of pectin, mucin and poly ethylene glycol. Techniques used to determine pectin, mucin and poly ethylene glycol interactions included; attenuated total reflection Fourier transform infrared spectroscopy (AT-FTIR), thermal and thermodynamic analysis using differential scanning calorimetry (DSC) and thermogravimetric analysis (TGA), ultraviolet spectroscopy and rheology measurements of aqueous dispersions of the polymers. Furthermore, static atomistic simulation of the pectin-mucin-poly ethylene glycol submicrospheres was performed as a precursor to the experimental formulation of the submicrospheres which was then carried out in chapter four.

Chapter four provides details on the formulation of drug loaded pectin-mucin-poly ethylene glycol submicrospheres using the emulsion crosslinking technique. A 3 factor 3 level (3^3) Box-Behnken statistical design was utilized in the optimization of the preparation of drug-loaded submicrospheres. In the Box-Behnken design; ultrasonication time, surfactant concentration and drug:polymer ratio were taken as the independent parameters whilst; particle size, zeta potential and mean dissolution time were regarded as dependent parameters or responses. Determination of the stability of the water in oil (W/O) emulsion, a crucial intermediate in the formation of submicrospheres, was performed and detailed in this chapter. In addition, the characteristics of the submicrospheres including particle size and zeta potential are presented. Submicrosphere drug encapsulation and release were measured and key parameters such as submicrosphere encapsulation efficiency and the mean dissolution time were determined. Other techniques used to confirm the composition and characteristic of the drug loaded pectin-mucin-polyethylene glycol submicrospheres include; AT-FTIR, DSC, TGA and X-ray diffraction.

Chapter five reports on the fabrication of a composite polymeric delivery system in the form of a caplet composed of drug loaded pectin-mucin-poly ethylene glycol submicrospheres embedded within a polymeric matrix blend of poly(D,L-lactide) and polyvinyl acetate/polyvinylpyrolidone. A 3^3 Box-Behnken design was employed to optimize the caplet with; mass of poly(D,L-lactide), mass of magnesium stearate and mass of polyvinyl acetate/polyvinylpyrolidone taken as independent parameters whilst the fraction of drug released in 7 days, the caplet hardness and fractional simulated vaginal fluid (SVF) intake were the dependent parameters or responses. Drug release studies performed on the caplet over 30 days are presented in this chapter. Characterization of the dissolution profiles was attained by determining specific parameters such as mean dissolution time, dissolution efficiency and fitting

the dissolution profile into different known kinetic models. Caplet characterizations provided in chapter 5 include textural profile analysis that involves the determination of caplet matrix hardness and matrix resilience using a texture analyzer. The friability of the caplet was also tested

Chapter six describes the *in vivo* studies performed which involved intravaginal application of the composite delivery system in Large White pigs with the intention of having the delivery system retained intravaginally for 30 days whilst blood samples and vaginal swabs are taken at predetermine time points. On completion of *in vivo* experimentation, the pigs were euthanized and their vaginal tissue was excised for further histopathology examination. In the chapter, detection and quantification of drug from withdrawn plasma samples, vaginal swabs and in tissue were performed using ultra performance liquid chromatography-tandem photodiode array (PDA).

Chapter seven is the conclusions and recommendations section of this dissertation. It provides the summation of various aspects discussed in the dissertation on microbicide development in general and the composite polymeric delivery system in particular. Recommendations for further research on microbicides and microbicide delivery with a focus on the observed shortcomings of the composite delivery system are provide in this chapter.

CHAPTER 2
A REVIEW OF THE KEY ASPECTS ESSENTIAL FOR ANTI-HIV-1 MICROBICIDE DELIVERY SUCCESS

2.1. Introduction

There has been an increase in interest among pharmaceutical scientists for the possible use of anti-HIV-1 agents as microbicides to prevent heterosexual vaginal HIV-1 transmission. However, clinical studies conducted have largely been disappointing. This chapter reviews the development of microbicides with an aim to expand the view that unsatisfactory microbicide failures may be a result of inefficient delivery systems employed. A thorough scientific qualitative and quantitative analysis of important aspects involved in HIV-1 transmission as a prerequisite for microbicide delivery is discussed in this chapter. Highlighting that intraluminal vaginal targeting of HIV-1 increases the chances of microbicide success, wherein the micro-environmental factors including pH is maintained at HIV-1 prohibitive acidic levels simultaneously to ward off other sexually transmitted diseases which compromise vaginal epithelial barrier properties. Furthermore, choice of receptors to target, both on HIV-1 and on target cells is vital in deterring transmission. Appropriate modeling of virus-target cell interactions as well as targeting early stages in the HIV-1 infection, accompanied by computation and delivery of appropriate microbicide quantities have the potential of delivering a women-controlled HIV-1 prevention modality.

Several novel compounds are being discovered and existing ones are being tried for the treatment of HIV/AIDS yet the eradication of the disease remains elusive, leading to a refocus towards prevention (Ndesendo et al., 2008; Hladik et al., 2010). Contemporary strategies include microbicides, vaginally or rectally applied topical chemical agents, having the ability to block HIV-1 infection (Hladik et al., 2010). Nonoxynol-9 was the first chemical entity to be extensively tried as a preventative microbicide against HIV-1. It is quite effective as a viral membrane lysis agent, however its efficacy *in vivo* as an HIV-1 prevention application was not demonstrated due to its detrimental effects on the vaginal membrane which even led to an increase in HIV-1 infection according to the COL-1492 study (Van Damme et al., 2002). Several microbicide trials have failed, restricting microbicide agents to test tube therapies (Baleta 2007; Hendrix et al., 2009). They may be highly effective *in vitro* but they are not sufficiently effective *in vivo* (Cutler and Justman, 2008). Various reasons have been postulated to explain this failure of microbicides. This chapter focuses on microbicide formulation and delivery as one of the

causes of microbicide failures and as an aspect that can be improved to enhance microbicide efficacy.

Potent anti-HIV-1 agents have been formulated into gels, creams, tablets and rings. Gels and creams are applied prior to and/or after coitus. They constitute the anti-HIV-1 agent in a gel or cream vehicle which will cover the vaginal epithelia when applied creating a chemical and physical barrier to HIV-1. The advantage of using such formulations is that the gel or cream can be tailored to enhance gel or cream adherence to the vaginal epithelia by employing mucoadhesive materials such as mucoadhesive polymers. Gels and creams may also act as lubricants needed during coitus to avoid vaginal epithelial microtrauma which compromises vaginal epithelial integrity. However gels and creams are indiscreet (i.e. messy and sticky), they are short acting thus require frequent application and their efficacy depends on the extensive and exclusive coverage of the vaginal epithelia to create a comprehensive microbicide barrier. On the other hand tablets and rings are discreet and are inserted into the vagina well before coitus. They release the potent anti-HIV-1 agent upon degradation, erosion, disintegration or diffusion of the anti-HIV-1 agent from the dosage form matrix. Their disadvantages are that they have to release the right quantity of anti-HIV-1 agent at the desired time (i.e. on exposure to HIV-1) and the anti-HIV-1 agent has to sufficiently distribute in the vaginal cavity to prevent HIV-1 transmission.

A comprehensive list of some of the microbicide trials that have been carried out thus far is illustrated in table 2.1. A closer analysis of this table reveals that most microbicide trials pass phase I tests, a few pass phase II testing and although microbicide research has recently revealed the success of a phase IIb CAPRISA 004 tenofovir gel trial (Abdool Karim et al., 2010; Mohammadi, 2010), there has not been any successful phase III trial. Therefore, there is nothing on the market in the form of a microbicide to effectively deter the HIV-1 transmission. Table 2.2 enlists microbicide agents that have been formulated into different delivery systems (i.e. gels, creams, tablets and vaginal rings) and the mechanism by which they inhibit HIV-1 transmission. These formulations include the ones that have failed at different stages of clinical trials and others still under investigation.

Table 2.1: Microbicide clinical trials

Phase I				Phase I/II	Phase II	Phase II B Phase II/IIB	Phase III Phase II/III
***IPM 010/ MTN 012** ° Male tolerance -Dapivirine gel +Ongoing[5,93,133]	***MTN 002** ° P/K and Placental transfer +Data analysis Shown to be safe for pregnant women with less transfer of drug to foetus compared to oral dosage[133]	***Invisible Condom®** ° Safety and acceptability +Result-2007: Safe, well tolerated and acceptable[6]	***HPTN 047** ° Safety and acceptability study -Pro 2000/5 gel +Result- 2006 Safe and acceptable[85]	***IPM 014A** ° Safety and acceptability -Dapivirine gel +Safe and well tolerated[93,63]	***MTN 010** ° Expanded safety -UC-781 gel +Withdrawn[133]	***VOICE (MTN 003)** ° Safety and efficacy -Tenofovir gel +Ongoing[5,64]	***IPM 009 A/B** ° Efficacy -Dapivirine ring +To be determined[93,64]
***MIV-150/Zinc Salt Gel study** +Planned[4]	***TFV 010** -Tenofovir gel +Data analysis[4]	***IPM 001** ° Safety -Dapivirine ring +Result-2009 : Safe and well tolerated[93]	***HPTN 049** ° Safety and acceptability study -6% Cellulose sulphate gel +Result-2006: Safe , well tolerated and acceptable[85]	***IPM 014B** ° Expanded safety -Dapivirine gel +Data analysis[93,64]	***MTN 001** ° Adherence and P/K -Tenofovir gel +Closed , to follow up [133,13]	***CAPRISA 004** ° Safety and efficacy -1% Tenofovir gel +Result – 2010: 39% effective[64,3]	***MDP 302** -Tenofovir gel +Planned[4]

***Vaginal Applicator Study** -Tenofovir gel [+]Planned[3]	***RMP 002/ MTN 006** ° Safety study -Tenofovir gel [+]Relatively safe [134]	***IPM 008** ° Safety -Dapivirine ring [+]Result- 2009: Safe and well tolerated[14]	***Project Gel** °Safety and acceptability in young men -Tenofovir [+]Result – Ongoing[5]	***IPM 015** ° Expanded safety -Dapivirine vaginal ring [+]Ongoing Planned[5,64]	***HPTN 059** ° Expanded safety and acceptability -1% Tenofovir gel [+]Results-2008: Safe to use daily for six months[85,133]	***MTN 003B** °Bone and mineral density study -Tenofovir Gel [+]Enrolling[5]	***FHI Cellulose Sulphate Gel** ° Safety and efficacy [+]Result- 2007: Trial stopped after CONRAD trial[56,89]
***PK/PD** ° Safety Study -UC-781 gel [+]Planned[4]	***Ethanol in emollient gel** ° Safety [+]Ongoing[6]	***IPM 012** ° P/K -Dapivirine gel [+]Results- 2010 Safe and well tolerated[93]		***NCT00136643** ° Safety and tolerability -Invisible Condom® [+]Result- 2007: Safe, well tolerated and acceptable[201]	***Praneem polyherbal vaginal tablet** ° Expanded safety [+]Result- 2008 Safe for 6 months use[6]		***CARRAGUARD Gel** ° Safety and efficacy [+]Result – 2008: Safe but no evidence of efficacy[3,4]
***Zinc Salt Gel Study** Zinc acetate gel	***AF 020** ° Safety study -Amphora™/ ACIDIFORM™	***CTV-05 LACTIN-V** ° Safety and acceptability		***IPM 003** ° Safety , tolerability and systemic	***CTV-05 LACTIN-V** ° Colonization efficiency,		***MDP 301** ° Safety and efficacy -0.5% Pro 2000/5 [+]Result – 2009

+Planned[4]	gel +Ongoing[5]	-Lactobacillus cripatus +Resullts- 2009: Safe and Acceptable[79]	absorption -Dapivirine gel +Results- Safe and well tolerated for twice daily dosage[93]	safety and acceptability -Lactobacillus cripatus +Result- 2010: High colonization efficiency, safe and accepted[80]	No evidence of efficacy[3]
***IPM 024** ° P/K -Dapivirine ring Data analysis +Result- 2010: safe and well tolerated[93]	***IPM 013** ° Safety study -Dapivirine ring +Data analysis[5,93]	***IPM 018** ° P/K feasibility -Dapivirine ring +Results-2007, Pharmacokinetic data show sufficient distribution[93]	***IPM 005B** ° Safety -Dapivirine gel +Results- 2009 Safe and well tolerated for twice daily application[93]		***NCT00000929** -Nonoxynol-9 film study ° Efficacy +Result- 1998 No evidence of efficacy[201]
***MTN 007** °Safety and acceptability -Tenofovir gel + Ongoing[4]	***Pilot Study** -UC-781 gel +Ongoing[4]	***HTPN 032** ° Male tolerance and toxicity acceptability study -BufferGel and			***COL-1492 study** ° Efficacy -Nonoxynol-9 gel +Result-2002: No evidence of efficacy. Toxicity and

	Pro 2000/5 gel +Result- Safe and tolerated[85]	increased infectivity with multiple use[204]

P/K – Pharmacokinetic

Structure:

* Study name or identifier

° Type of study

-Active pharmaceutical ingredient and/dosage form

+ Result or status

A critical review of HIV-1 infection mechanisms and pathways by analyzing the cellular components that involved; Langerhans cells, macrophages, T-cells, dendritic cells and their respective receptors and co-receptors, gp120, gp41, $CD4^+$, CXCR4, CCR5, langerin and DC-SIGN is also done in this chapter. In order to increase microbicide chances of preventing HIV-1 transmission, the choice of receptors and co-receptors to target is vital and is discussed in detail. The properties and role of the vaginal epithelia in the prevention of HIV-1 transmission, ways of enhancing those properties and how microbicides can be tailored to provide a comprehensive anti-HIV-1 barrier are also given due consideration. This chapter deliberates on the contentious issue of the appropriate microbicide quantity essential to block HIV-1 in the vaginal cavity. Due to the variability of the vaginal cavity dimensions, the concentrations of virus in semen and the frequency of coitus, different microbicide formulations have to be tailored to deliver enough anti-HIV-1 agents to deter transmission. After scientifically considering all important aspects and issues raised in this analysis and by employing techniques such as the use of combination anti-HIV-1 agents released from extended microbicide delivery systems, scientists may be able to develop an effective microbicide.

Table 2.2: Different microbicide formulations

Chemical Entity	Formulation/Delivery System	Anti-HIV-1 Activity
Carbomer® (polyacrylic acid)[207]	Gel - BufferGel™	Acidifying agent.
Carrageenan[14,159]	Gel - Carraguard®	Blocks viral infected semenal mononuclear cell migration.
Cellulose acetate phthalate (CAP)[123]	Gel	Adsorbs and inactivates virus
Cellulose sulphate[9]	Gel – Ushercell™	Viral replication inhibitor
Cetyl Betaine[54,148]	Cream - C31G , Savvy™	Broad spectrum antimicrobial
Cyanovirin-N[15,199]	Gel	Viral entry inhibitor, Blocks virus-CD4+ fusion.
Dapivirine (TMC120)[148,185]	Vaginal ring	Inhibits viral replication,

		NNRTI[148]
Monocaprin[197]	Hydrogel	Inactivates virus
Myristamine oxide[54]	Cream- C31G, Savvy™	Inactivates virus
Napthalene Sulphonate[127]	Gel – Pro 2000™	Disrupts viral cell membrane
Nonoxynol-9 (N- 9)[8]	Gel- Advantage S®	Disrupt viral cell membrane
Polystyrene sulfonate (PSS)[61,148]	Vaginal tablets Gel- (T-PSS)	Fusion inhibitor
Praneem (Azadirachta indica, Neem tree)[97,148]	Vaginal tablets	Unknown, possibly cytoadhesion inhibition
Sodium lauryl sulphate (SLS)[164]	Gel- Invisible Condom™	Fusion and entry inhibitor
SPL7013[148,96]	Gel- VivaGel ™	Fusion and entry inhibitor Uses dentrimer technology
Stapidine[142]	Gel	NRTI[88]
Tenofovir disoproxil fumarate (TDF)[148]	Gel-PMPA gel, Tenofovir™	Viral replication inhibitor NRTI[88]
Theophen-thiourea (PHI-443)[148]	Gel	Viral replication inhibitor NNRTI[148]
UC-781[148]	Gel	Viral replication inhibitor NNRTI[148]

[1] Non-nucleoside reverse transcription inhibitor

[2] Nucleoside reverse transcription inhibitor

2.2. Mechanism of HIV-1 infection: determinants and dynamics

The mode of HIV-1 transmission among humans has been under intensive investigation from the time when HIV-1 was first discovered. Technological advances in viral detection have made it easier for researchers to be able to understand the cellular and molecular mechanisms of HIV-1 transmission. Transmission can be established either by cell-free or cell-associated viruses (Hladick and Hope, 2009). Investigation has shown that in several instances HIV-1 invasion occurs when the virus penetrates the epithelia then goes into the subepithelia, passes through the lymphatic system and ultimately enters the systemic system (Haase, 2010). How it manages to penetrate the vaginal epithelia has been attributed to several pathways, simplest of which involves the free passage of the virus through breached epithelia (Morrow et al., 2007; Nazli et al., 2010). Epithelial disruption can be caused by several factors including microtrauma during sexual intercourse, use of irritating chemicals or as a result of inflammation caused by co-infection with other sexually transmitted diseases (Norvell et al., 1984; Gray and Wawer, 2007; Wilkinson, 2007; Van de Perre et al., 2008; Hayes et al., 1995; Hester and Kennedy, 2003).

Figure 2.1 is a comprehensive time-based illustration of the HIV-1 infection process. HIV-1 has been shown to transcytose the single columnar epithelia, particularly at the squamocolumnar junction where high cell turnover enhances HIV-1 penetration through epithelial transcytosis (Bomsel, 1997). Another well documented epithelial HIV-1 transmission strategy used by HIV-1 is the Langerhans-cell assisted HIV-1 transfer route (Pignet and Blauvelt, 2002; Wu, 2008). Langerhans cells (LCs) are considered to be the bastions of epithelial immunity (Pignet and Blauvelt, 2002; Wu 2008). Their immature forms abide within the subepithelia whilst having cellular projections onto the epithelial surface and into luminal compartments of the vaginal cavity. The job of LCs is to detect and interact with the invading HIV-1, after which they migrate, maturing in the process, to the T-cell rich lymph nodes where they present HIV-1, initiating an immune response. HIV-1 manipulates this process to penetrate the vaginal epithelial barrier. Immature LCs residing within the epithelial layer express $CD4^+$ receptors and CCR5 co-receptors which are essential for HIV-1 infection. The productively infected LCs migrate into the subepithelia and ultimately towards the lymph nodes where they transfer HIV-1 to T-cells (Zaitseva et al., 1997; Kawamura et al., 2003). Another chemokine co-receptor expressed by LCs is CXCR4 and is only expressed by the mature LCs (Zaitseva et al., 1997; Zhang and Moore, 1999). However, the role of CXCR4 as an HIV-1 trans-epithelial passage facilitator is limited as it has been shown that the majority of HIV-1 strains isolated from patients immediately after primary infection utilized the CCR5 co-receptor (R5 virus) as compared to the CXCR4 co-receptor (X4virus) (Zhang and Moore, 1999).

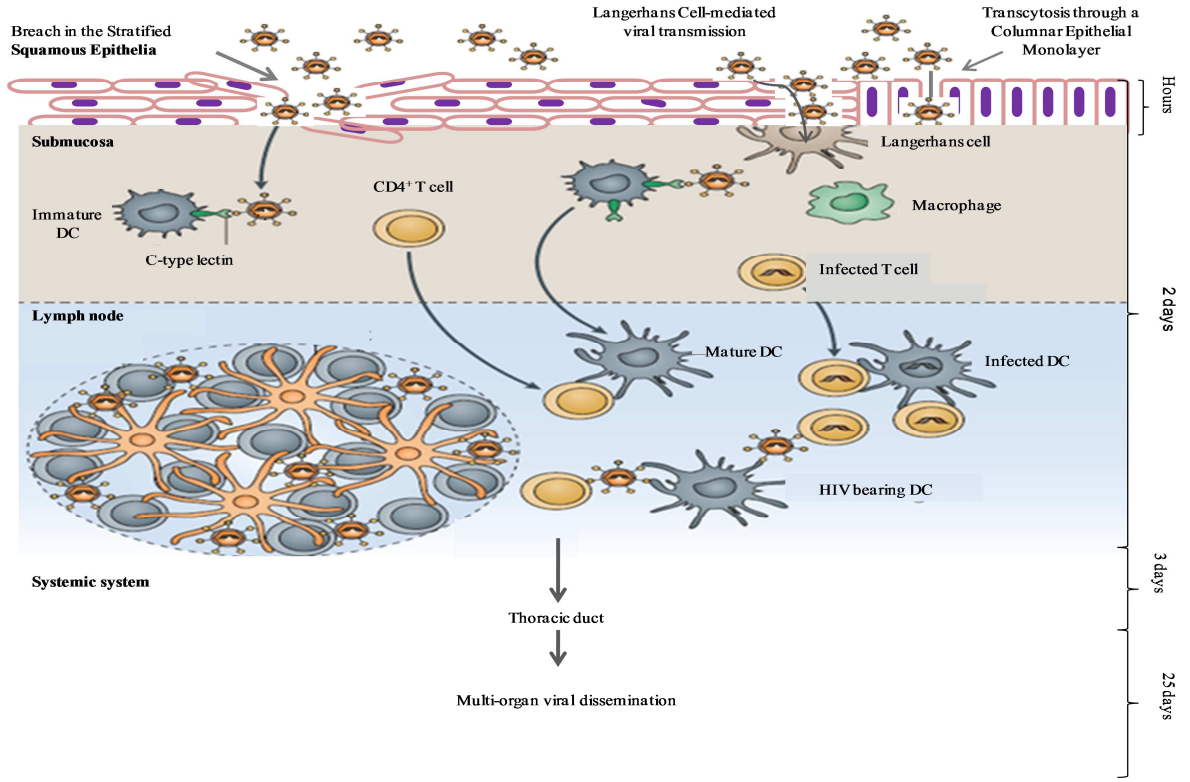


Figure 2.1: Schematic of HIV-1 infection pathway and mechanism (adapted from Wu and KewalRamani 2006).

There is a sudden increase in further HIV-1 transmission once the virus passes the vaginal epithelia and enters the subepithelia, aided by an increase in concentration of HIV-1 susceptible cells that include; T-cells, macrophages and dendritic cells (DC) (Shen et al., 2011; Wu and KewalRamani, 2006). HIV-1 either productively infects some of these cells through receptor and co-receptor interactions or it captures the virus using the dendritic cell-specific intracellular adhesion molecule (ICAM) grabbing non-integrin (DC-SIGN, CD209) whose affinity for the HIV-1 gp120 is stronger than that for CD4 (Geijtenbeek et al., 2000). Figure 2.2 illustrates the various HIV-1-receptor interactions that may occur during the infection process (De Witte et al., 2007). Monocyte derived dendritic cells (MDDC) which express DC-SIGN can bind and transfer HIV-1 without being infected in a process referred to as trans-infection, whereby HIV-1-carrying dendritic cells facilitate the infection of T-cells by concentrating the virus in an infectious synapse (Kwon et al., 2002; Donaghy et al., 2006). An augmenting process termed cis-infection occurs concurrently; this is whereby HIV-1 attached via DC-SIGN is directed onto the same DC membrane for CD4-co-receptor dependent membrane fusion (Kawamura et al., 2003).

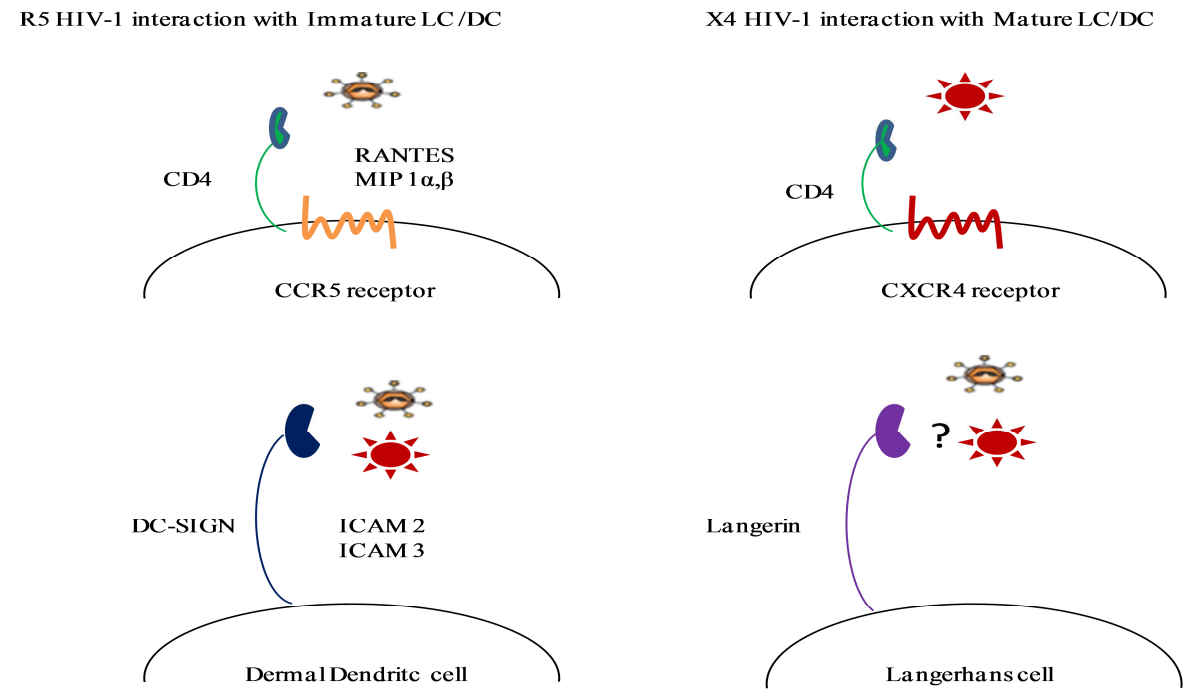


Figure 2.2: HIV-1 interactions with receptors and co-receptors on Langerhans cells (LCs) and dendritic cells (DCs) (adapted from Kawamura et al., 2005; De Witte et al., 2007).

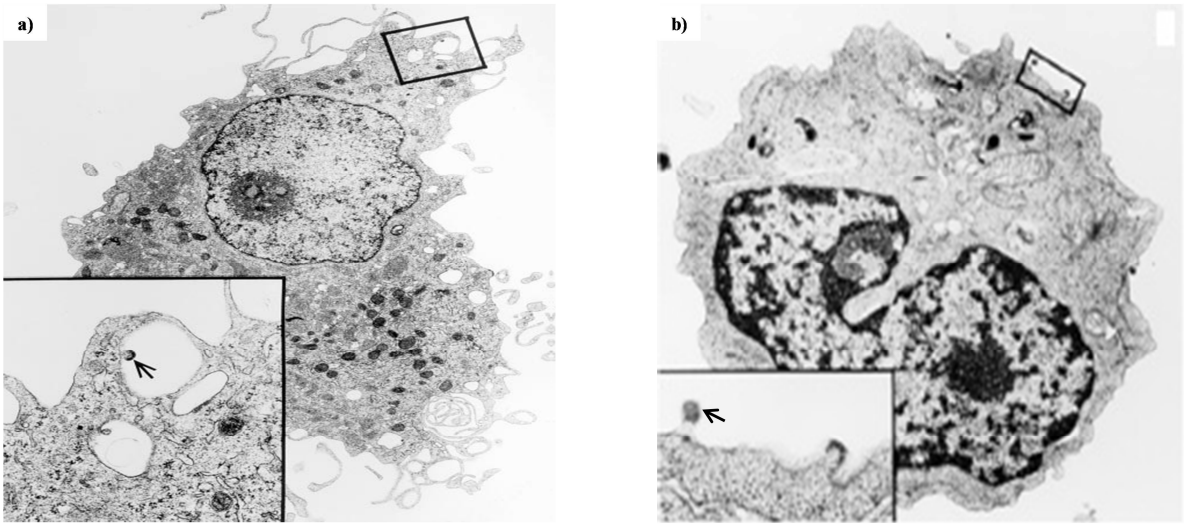


Figure 2.3: Transmission electron micrograph (TEM) of: a) HIV-1 virus captured by a dendritic cell; b) HIV-1 virus attached to a dendritic cell (adapted from Blauvelt et al., 1997).

In figure 2.3.a, C-type lectin DC-SIGN is involved in the attachment and capture of HIV-1 into a low pH non-lysosomal competency retention compartment in the DC for further trans-infection to $CD4^+$ and chemokine expressing cells (Blauvelt et al., 1997), whereas in figure 2.3.b there is direct viral and DC membrane fusion as a consequence of the attachment of the viral gp120 to the DC $CD4^+$ and the chemokine co-receptor. HIV-1 viral capture by dendritic cells is independent of DC4, CCR5 and CXCR4 whilst productive dendritic cell infection is CD4, CCR5 and CXCR4 dependent (Blauvelt et al., 1997). The complexity of the

HIV-1infection poses a huge challenge to the defence capacity of the human immune system; however it also provides numerous opportunities for external therapeutic interventions to prevent transmission. Knowing and understanding these complex HIV-1 infection pathways are a prerequisite for microbicide development since each pathway and cellular target in the infection sequence may present a possible way to prevent HIV-1 transmission.

2.3. The vagina as a target site for microbicide delivery

Research has shown that the majority of HIV-1 infections occur by passage of viral particles through the epithelia of various body organs (Pope and Haase, 2003; Epple et al., 2010). Viral particles, cell-bound or not, are carried in most body fluids and are particularly abundant in genital fluids. The type of epithelial cells lining the vaginal cavity is a major determinant in HIV-1 transmission (Epple et al., 2010). Table 2.3 shows different locations of the vaginal epithelial layer and the types of epithelial cells that constitute it (Hladick and McElrath, 2008). The vaginal cavity is partially lined by both, a columnar epithelial monolayer on the endocervix and less susceptible stratified squamous epithelia on the vagina and ectocervix (Hosein and Wilson, 2011; Celum et al., 2008).

Table 2.3: HIV-1 invasion sites, location and the type of epithelial cells located there (Hladick and McElrath, 2008).

HIV invasion site	Anatomical location	Epithelium type
Female genital tract	Vagina	Squamous Stratified Non-keratinized
	Ectocervix	Squamous Stratified Non-keratinized
	Endocervix	Columnar Monolayer

In designing microbicide delivery systems, one should always take into account the epithelial cell location and type. A good example of where the location and epithelial cell type has contributed in mitigating HIV-1 transmission is in male circumcision (Templeton, 2010; Bailey et al., 2007; Gray et al., 2007; Siegfried et al., 2005; Denniston and Hill, 2007). Circumcision in males has been found to reduce transmission by more than 50% and this can be attributed to post-circumcision reduction in the squamous epithelial layer surface area due to the removal of the foreskin, which also houses LCs that facilitate HIV-1 infection (Templeton, 2010; Bailey et al., 2007; Gray et al., 2007; Siegfried et al., 2005; Denniston and Hill, 2007). Microbicides delivery systems should maintain the epithelial barrier lining or enhance it, but not disrupt it as in the case of Nonoxynol-9 gel in the COL-1492 study (Van Damme et al., 2002).

In this dissertation, focus is on the vaginal cavity as it has been anatomically shown that chances of succeeding in deterring HIV-1 transmission occurring via the vaginal route are higher compared to other routes such as the rectal route (Hladick and McElrath, 2008). Additionally the vaginal cavity is a semi-closed pouch unlike the rectum which is an open-ended tube-like system (Stone, 2002). This makes it easier for extensive intravaginal microbicide distribution and retention to be achieved. The dimensions of the vaginal cavity vary depending on factors such as age, height and the sexual arousal state (Barnhart et al., 2006). This presents a challenge when trying to determine the sufficient microbicide formulation quantity required to prevent HIV-1 transmission. However, the use of experimentally determined average vaginal cavity dimensional values may be useful in microbicide delivery system design. Barnhart and co-workers determined the mean vaginal length from the cervix to the introitus as 62.7mm, with the vaginal width being greatest in the proximal vagina, 32.5mm, decreasing at the proximal diaphragm, 27.8, and smallest at the introitus, 26.2mm (Barnhart et al., 2006).

2.4. Qualitative microbicide targeting

The delivery of potent anti-HIV-1 agents intravaginally has to be tailored to match the pre-existing anatomical and physiological conditions. In order to effectively prevent HIV-1 transmission, certain aspects in the HIV-1 transmission pathway have to be prioritized and particular targets have to be pursued. Such targets include viral and cellular targets, vaginal epithelia, the vaginal cavity microenvironment and subepithelial microbicide bioavailability (Haase, 2010; Wu, 2008). In addition, there has to be some correlation between employing an anti-HIV-1 agent and preserving or enhancing the host defence system.

2.4.1. Direct viral and cellular targeting

Strategic targeting of HIV-1 is important to achieve an effective microbicide as HIV-1 uses a complex combination of proteins and receptors, some of which have already been mentioned earlier in this chapter. Table 2.4 gives an array of receptor targets that can be exploited by microbicide agents. The variety of HIV-1 targets is a dilemma for microbicide developers as to which anti-HIV-1 agent to use. Hu and co-workers provided some light as which receptor/s microbicide developers should prioritize (Hu et al., 2004). *Ex vivo* studies on human cervical tissue explants demonstrated that in addition to the blockage of viral gp120 cellular targets, CD4 alone or CCR5 and CXCR4 together, other non-HIV-1 receptors such as mannose-binding C-type lectin receptor (MCLR) DC-SIGN, mannose receptor (MR) and non-MCLRs should also be blocked (Hu et al., 2004; Pohlam et al., 2001; Jameson et al., 2002; Gummuluru et al., 2003; Turvile et al., 2004). Blockade of the gp120 removes downstream receptors such as the g41 from the equation and ultimately renders HIV-1 non-infectious. Additionally, Lamers and co-workers predicted the use of the R5X4 co-receptor with an accuracy of 75.5% using neural networks proving that dual tropic viruses may increase microbicide efficacy (Lamers et al., 2008).

Table 2.4: HIV-1 receptor targets and their corresponding inhibitory agents (Balzirini and Van Damme, 2007; Shattock and Solomon, 2004).

Viral envelope glycoprotein	Anti-HIV-1 microbicide agent
gp120	• mAb b12 • Carbohydrate binding agents (cyanovirin, plant lectins pradimycin A derivatives; and mAb 2G12) • CD4 IgG2 (PRO-542) • BMS-806 • CD4 mini protein
gp41	• T20 (enfuvirtide) • T-1249, • mAbs 2F5, 4E10
Viral Intracellular targets	
Viral intergrase	• Elvitegravir and MT-2048
Viral reverse transcriptase	• NNRTI : PMPA (tenofovir disoproxylfumarate) • NRTI: TMC120 (dapivirine), UC781, MIV-150 and DABO
Viral membrane	

- Nonoxynol 9
- C31G, SLS
- Cyclodextrins

Various innovative techniques for direct HIV-1 blockage have been developed to date, with the employment of nano-constructs active against the HIV-1 being the latest (du Toit, Pillay and Choonara, 2009). Nano-size gold and silver particles have been demonstrated to inhibit viral attachment to target receptors by preferentially binding to gp120 (Elechiguerra et al., 2005; Yacaman et al., 2006). Dendrimers, tri-component multi-branched three-dimensional nanostructures composed of a poly-functional core, can act as a drug carrier wherein the interior layers and the multivalent surface can be functionally modified to disrupt the normal virus-target cell interactions thus preventing viral attachment and subsequent infection (Witvrow et al., 2000). One such dendrimer, VivaGel^{TM}, has been granted "Fast Track" status by the United Stated Food and Drug Administration (FDA), as an investigational new drug (IND) against HIV-1 and other sexually transmitted diseases. Other dendrimer compounds that have shown anti-HIV-1 activity include SPL2923, SPL6195, SPL7013, SPL7304 and SPL7320 (McCarthy et al., 2005). Investigational anti-HIV-1 work has been done on the microbicide potential of carbon-60 aggregates, fullerenes, and virus targeting nano-micelles termed NanoViricides^{TM} (Marcorin et al., 2000; Schuon 2008).

Despite all these imposing anti-HIV-1 interventions, no microbicide has reached the market and this warrants a re-think on the choice of HIV-1 target receptors with an emphasis on targeting more than one receptor as discussed further in the multi-targeting section of this review. Fractionally but importantly, besides targeting the HIV-1, microbicide developers should not ignore other factors that enhance HIV-1 capabilities such as semen, since it is now known that the amyloid fibrils found in semen enhance HIV-1's ability to attach to epithelial cells and to leukocytes (Munch et al., 2007).

2.4.2. Targeting of the vaginal microenvironment

Altering some of the basic vaginal microenvironment properties, such as pH may have tremendous implications on the HIV-1 transmission sequence (Hilber et al., 2007). The approximate normal vaginal pH of 4.5 is maintained by the lactic acid produced due to anaerobic metabolism of glucose by resident lactobacilli and this acidic pH can hinder HIV-1 transmission (Lai et al., 2009). Using high resolution multiple particle tracking techniques, Lai and co-workers managed to demonstrate that at approximately pH 4.5 cervicovaginal mucus traps HIV-1-mimicking polystyrene nanoparticles causing them to diffuse 1000-fold slower than they would in water. In contrast diffusion of the HIV-1-mimicking nanoparticles in cervicovaginal mucus at pH 6-7 was found to be only 15-fold slower than in water.

On further assessment they found that in acidic pH, HIV-1 has a negative surface charge that is neutralized by lactic acid whilst at neutral pH of 6-7 this negative charge is maintained. The surface charge of the HIV-1 determines whether the virus can slip through the mucus layer, composed mostly of polyanionic mucin and water, which lines the cervicovaginal epithelia and ultimately determines infectivity (Lai et al., 2009). The success of anti-HIV-1 microbicide delivery systems thus depends upon the pharmaceutical scientist's ability to take into account the vaginal micro-environmental pH. Any measure that aims to maintain the acidic vaginal pH would be a step in the right direction, for not only will this prevent HIV-1 transmission, but it may also prevent invasion by other micro-organisms that may cause ulcers and inflammation resulting in impaired barrier properties of the vaginal epithelia. Products developed by exploiting this concept include the microbicide gels: BufferGel® and Acidiform® (Van de Wijgert, 2001; Von Mollendorf et al., 2010). Even Lime juice has been studied pre-clinically for its acidifying HIV-1 transmission prevention properties (Hemmerling et al., 2007).

2.4.3. Targeting the vaginal epithelia

The biofunctionality of the vaginal epithelia as a physical barrier that blocks invasion by pathogens from the external environment is of vital importance in the prevention of HIV-1 transmission. Maintenance and enhancement of its physical and immunological HIV-1 deterrent properties are vital in designing an effective microbicide delivery system (Kozlowski and Neutra, 2003; Bergmeier and Lehner, 2006). The integrity of the vaginal epithelia can be compromised by a plethora of varying factors such as microtrauma during coitus, sexually transmitted diseases and the mere exposure to pathogens such as HIV-1 (Templeton, 2010; Bailey et al., 2007). An investigation into microtrauma of vaginal epithelia after coitus yielded 61.1% positive colposcopy findings, thus suggesting the need for lubricants during sexual intercourse (Norvell et al., 1984). Microbicide vehicles, particularly

gels can be rheologically tailored to mitigate epithelial disruption. The gp120 envelope glycoprotein studded on the infectious HIV-1 has been reported to reduce the transepithelial resistance (TER) of genital epithelia (Nazli et al., 2010). The mechanism of this phenomenon is based on the HIV-1's ability to induce inflammatory factors in the epithelial cells leading to down-regulation of tight junction mRNA and protein levels resulting in increased epithelial permeability. Tight junction genes known to be affected include; claudin 1, 2, 3, 4, 5, ocludin and ZO-1 which were 2-17 times variably down-regulated (Nazli et al., 2010; Bai et al., 2008). Figure 2.4 illustrates the epithelial tight junction down-regulatory effects of exposing genital epithelia to a gp120-carrying HIV-1 (wildtype) strain as compared to gp120-deficient HIV-1 (mutant) strain.

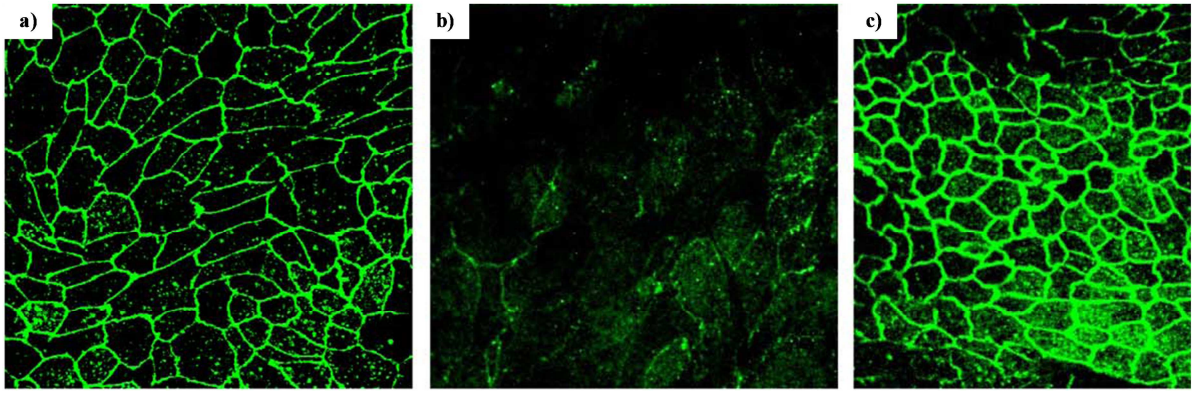


Figure 2.4: Epithelia monolayers showing tight junction down-regulation on exposure to different HIV-1 strains that include; a) normal unexposed epithelia, b) wildtype HIV-1 strain exposed epithelia and c) gp120-lacking mutant HIV-1 exposed epithelia (adapted from Nazli et al., 2010).

Nazli and co-workers standardized that in order for a microbicide to enhance its chances of effectiveness, it must neutralize HIV-1 before it reaches the epithelial layer. Vital work in this direction has been done by Geonnotti and Katz of Duke University in determining the crucial parameters in the dynamics of HIV-1 neutralization by a microbicide gel (Geonnoti and Katz, 2006). Using a Cyanovirin-N (CV-N) as a model microbicide agent, they concluded that effective pre-epithelial HIV-1 neutralization can be achieved with a postcoital vaginal epithelial gel-coating thickness of ~100μm that is extensively and exclusively distributed intravaginally. A similar principle could be a prerequisite in designing other forms of microbicide delivery systems such as vaginal tablets, rings and films where the primary goal and momentous achievement of a microbicide formulation would be to extensively and exclusively cover the vaginal epithelia and to enhance epithelia HIV-1 deterrent properties. A conventional battleground-illustration of intraluminal HIV-1 in the seminal layer drifting towards a microbicide covered vaginal epithelial mucus layer is depicted in figure 2.5.

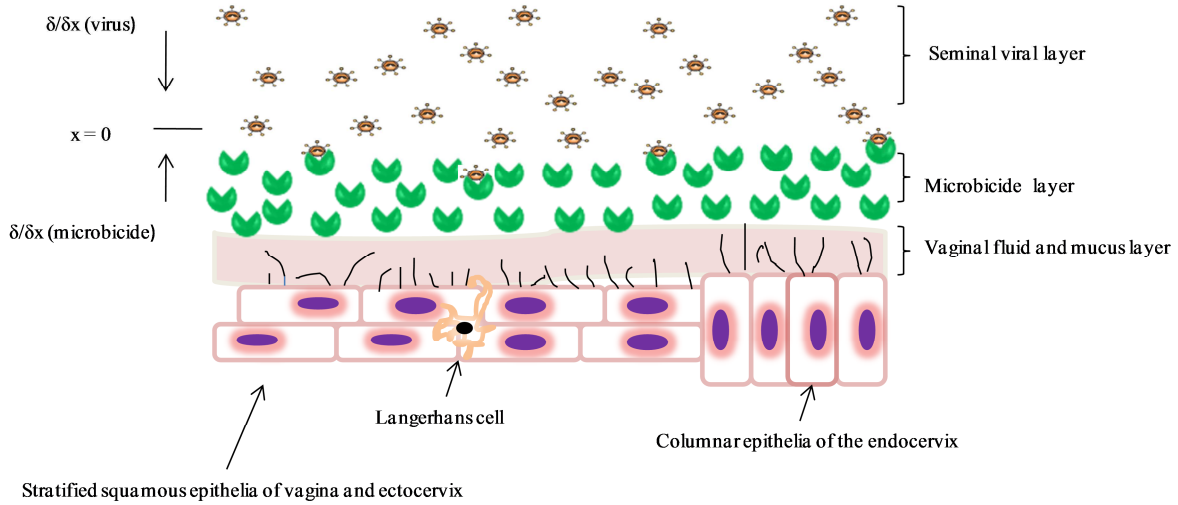


Figure 2.5: Illustration of microbicide-HIV-1 virus confrontation in the vaginal cavity (Adapted from Geonnoti and Katz, 2006).

Ways of enhancing vaginal epithelial integrity should be pursued. One such way involves the use of water soluble fibre pectin in microbicide delivery systems. Pectin has been reported to have trophic effects on the intestinal epithelia (Fukunag et al., 2003), warranting the investigation of its effects on the vaginal epithelia. Mucoadhesive delivery systems can help improve residence time of the anti-HIV-1 agent and may aid in maintaining a uniform microbicide layer covering the epithelia (Woolfson et al., 2010). Mucoadhesive delivery systems are generally composed of synthetic polymers or biological macromolecules with the ability to attach to the mucus layer lining the vagina epithelia. Polymers that have been employed in vaginal delivery systems include poly(acrylates), chitosan, cellulose derivatives, hyaluronic acid derivatives, pectin, tragacanth, starch, poly(ethylene glycol), sulfated polysaccharides, carageenan, sodium alginate and gelatine (Valenta, 2005).

2.4.4. Vaginal subepithelia targeting

Thomas and co-workers disputed the commonly held view that the majority HIV-1 particles are non-infections. They went further to demonstrate experimentally that the apparent HIV-1 non-infectivity, commonly reported maybe a result of infrequent occurrences of successful HIV-1-target cell interactions (Thomas et al., 2007; Gray et al., 2001). They highlighted the danger that comes with HIV-1 penetration into the $CD4^+$ cell-rich sub-epithelia. HIV-1 vulnerable target cells in the subepithelia including; DCs, T cells and macrophages/monocytes, that generally express CXCR4 and/or CCR5 co-receptors essential for HIV-1 infection, are concentrated in the lamina propria (Zhang et al., 1998; Zoeteweij and Blauvelt, 1998; Miller and Shattock, 2003). The increased number of $CD4^+$ and DC-SIGN expressing cells in the subepithelia enhances HIV-1 transmission (Van de Wijgert et al., 2001; Cunningham et al., 2007), making it a serious concern for microbicide

developers. It is therefore important for the microbicide agents to be able to access the subepithelia. Use of agents with high genital tissue bioavailability such as Pfizer's CCR5 blocking viral entry inhibitor, maraviroc, may be useful in this respect (Dumond et al., 2009).

Another concern that arises in the subepithelia is the ability of HIV-1 to hide in the local macrophages, away from the reach of microbicide agents. Recent discoveries reveal that macrophage-bound HIV-1 could be targeted based on the fact that the scarcity of deoxynucleoside triphosphate (dNTP) in macrophages leads HIV-1 to use abundant rebonucleoside triphosphate (rNTP) for its replication (Kennedy et al., 2010). Kennedy and co-workers discovered that by blocking HIV-1–rNTP interactions, viral replication plunged by 90% (Kennedy et al., 2010). Therefore, an agent that blocks HIV-1-rNTP interaction such as cordycepin may be used as an add-on microbicide agent to reduce post-epithelial HIV-1 transmission by minimizing intra-macrophage HIV-1 viral replication (Kennedy et al., 2010).

2.4.5. Microbicide multi-targeting

With the complex nature of HIV-1 infection and the variability of viral invasion pathways, many microbicide developers are advocating the use of agents that target either more than one receptor on HIV-1 and on the vulnerable target cells or a combination of agents in order to efficiently prevent HIV-1 transmission. Table 2.5 summarizes some of the microbicide combinations that have been developed to date. A smart choice of an anti-HIV-1 agent combination would be required to mitigate viral attachment, fusion, replication and other important steps in the infection sequence. When trying these combinations a complete pathotoxicity or safety study has to be performed to rule out any chances of epithelial barrier disruption or inflammation to avoid the danger of not only allowing free passage for the HIV-1, but inflammation-driven recruitment of target cells as well.

Table 2.5: Microbicide combination formulations (Alliance for Microbicides Development, 2007; Liu et al., 2005).

Microbicide combination	Developer/Researcher
BufferGel® + dentrimers (SPL7013 + optimized dentrimers)	ReProtect , Starpharma
CAP + UC781 or NCp7 nucleoside/zinc finger inhibitors	New York Blood Centre , NIH
CVN-12pl chimeras and combinations, HNG-105	Drexel
Dolabellane diterpene	Instituto Oswaldo Cruz (FIOCRUZ) Universidade Federal Fluminense, Fundacão Atanipho de Paiva
M167+ BMS+ other ARV	IPM
PC-710 (Carraguard + zinc) , ZCM (Carraguard + zinc + MIV-150)	Population Council
SJ3366	ImQuest
Tri-molecular microbicidal–immunising construct (MHC antigents + microbial HSP70 +CCR5 peptides)	Allomicrovac
Cellulose acetate 1,2-Benzenedicarboxylate + UC781	Liu S, Lu H, Neurath R, Jiang S (Liu et al., 2005)
mAb b12 and CV-N	Sexton A, Harman S, Shattock RJ, Ma K-C (Sexton et al., 2009)
WHI-07 and vanadocene dithiocarbamate	D'Cruz OJ, Uckun FM (D'Cruz and Uckun 2007)

2.5. Quantitative microbicide targeting

Post-exposure cervicovaginal HIV-1 population in humans is difficult to quantify due to ethical and experimental constrains. However by sequentially analyzing simian immunodeficiency virus (SIV) quantities after intravaginal inoculation in Indian rhesus macaques, researchers have been able to measure viral populations at each stage in the HIV-1 infection process (Miller et al., 1989). An important finding from these SIV studies discovered that after intravaginal inoculation of the order of 1 billion virons, only a small fraction of the inoculum was detected 2-24 hours later in the cervicovaginal tissues (Miller et al., 2005). Therefore, only a small fraction of the virons gets to cross into the subepithelia to establish the founder population (Miller et al., 2005).

This founder viral population cannot solely establish systemic infection because local viral population expansion is a prerequisite for systemic infection (Alliance for Microbicide Development, 2007; Lukashov and Goudsmit, 1997). The relatively low number of virons at this stage of infection provides a rare opportunity for microbicides to prevent systemic HIV-1 infection. Microbicides must target this stage of HIV-1 transmission since the virus will be at its quantitative weakest. Here, microbicide agents that can cross the epithelial barrier and be active in the subepithelia can play a major role. Figure 2.6 depicts the quantitative viral post-exposure profile with eclipse, exponential growth, peak viral replication and decline at different stages in the infection sequence. A microbicide delivery system should prolifically deliver the anti-HIV-1 agent within the first few days to take advantage of this quantitative-vulnerability of the virus. In figure 2.6 we have referred this opportune arbitrary time necessary to counteract the virus as the “Microbicide Critical Activity Window” (MCAW).

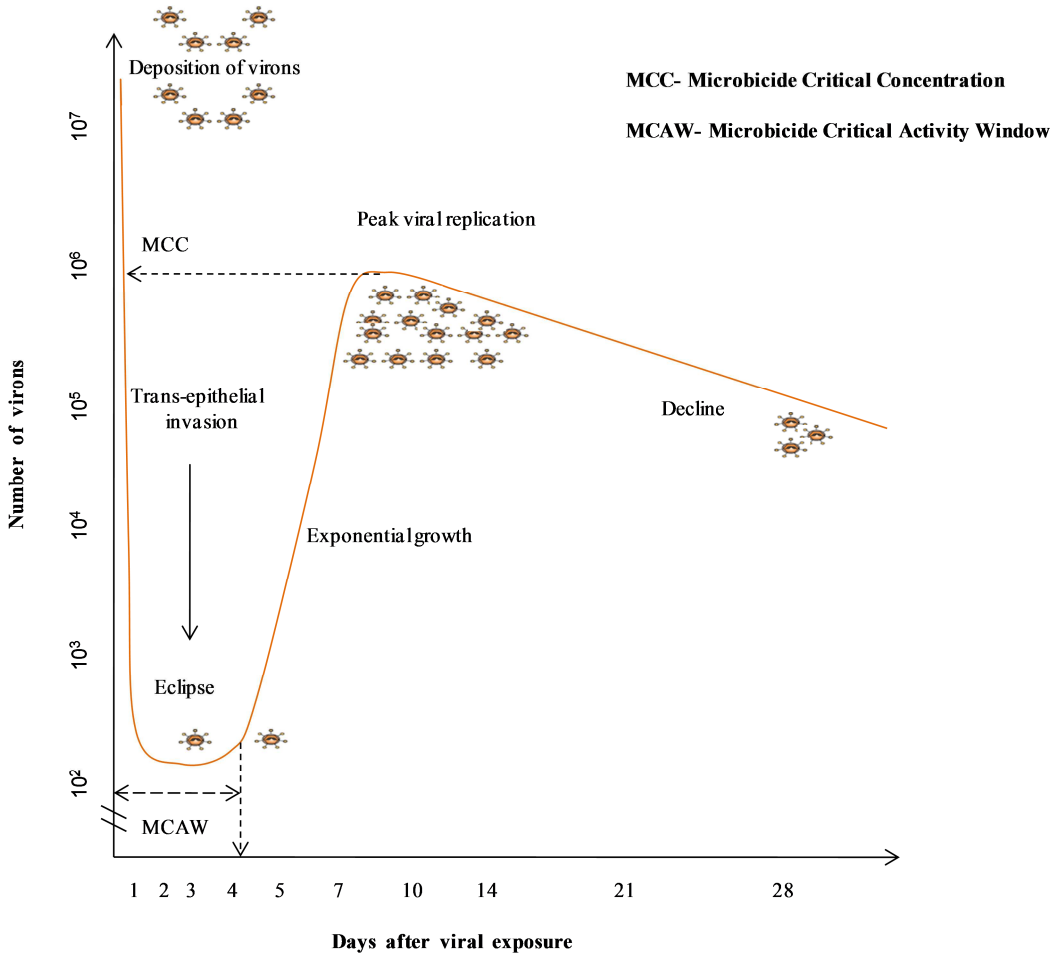


Figure 2.6: Post-exposure HIV-1 virus census in cervicovaginal epithelia (adapted from Miller et al., 2005; Haase, 2005).

After the MCAW, viral dynamics become complicated as the founder HIV-1 population attacks the 'resting' $CD4^+$ cells, $CD4^+$ T-cells, macrophages and DCs in the subepithelia followed by replication, leading to dissemination to draining lymph nodes. Lymph nodes hold high concentration of $CD4^+$ cells, hence once the virus reaches the lymph nodes, there is rampant replication and broadcasting of HIV-1 leading to an exponential growth in viral population as depicted in figure 2.6 (Haase, 2005). Viral replication reaches a peak concentration in 10-14 days then declines steadily (Miller et al., 2005). For microbicides, fortunes diminish drastically after the exponential growth stage due to increased number of virons, production of mutant viruses that may present an extraordinary challenge to anti-HIV-1 agents and the ability of the HIV-1 to hide in cells such as macrophages. However, Anti-HIV-1 agents released from microbicide delivery systems should surpass this peak viral concentration [designated as "Microbicide Critical Concentration" (MCC) in figure 2.6] to have a chance of deterring systemic viral infection (Richman et al., 2003). Microbicide success depends on a comprehensive quantitative excess of the microbicide agent/s to HIV-1 from the introitus to the cervix in the vagina (Hendrix et al., 2009; Lacey et al., 2006). The

variability in semen-borne HIV-1 quantities further adds to this quantitative complexity, as the semen viral quantity depends upon the individual's stage of HIV-1 infection and the seminal volume, which in turn depends on ones ejaculation frequency (Vernazza et al., 1997; Tachet et al., 1999).

Various microbicide delivery systems with different anti-HIV-1 agent release profiles can be formulated in the form of gels, films, rings, tablets or sponges (Pillay et al., 2012). Their common goal should be to deliver the anti-HIV-1 agent in sufficient quantity to prevent infection. The majority of delivery systems are quick release formulations applied prior to sexual intercourse for exclusive and extensive distribution within the vaginal or rectal cavity before exposure to HIV-1 during sexual intercourse. Extensive *in vitro* and *in vivo* studies need to be performed to determine the ability of the delivery system to release the anti-HIV-1 agent thus ensuring complete and sufficient vaginal distribution of the anti-HIV-1 agent. Figure 2.7.b displays a failed typical microbicide quick release profile. Such delivery systems usually fail to stay at inhibitory concentrations for a long enough time to avert transmission that may be a result of viral shedding, typical observed in acute HIV-1 infection. This limitation may be resolved by employing sustained and extended release delivery systems with a typical profile shown in figure 2.7.c. In addition to preventing infection due to viral shedding, these systems can improve compliance and ensue that an inhibitory anti-HIV-1 agent concentration is always available *in situ.* The major disadvantage of these extended microbicide delivery systems is the toxic or inflammatory effects that may occur as a result of sustained exposure to the anti-HIV-1 agent and the delivery system, making pathotoxicity studies mandatory to exclude inflammation and breach of the vaginal epithelia (Cone et al., 2006).

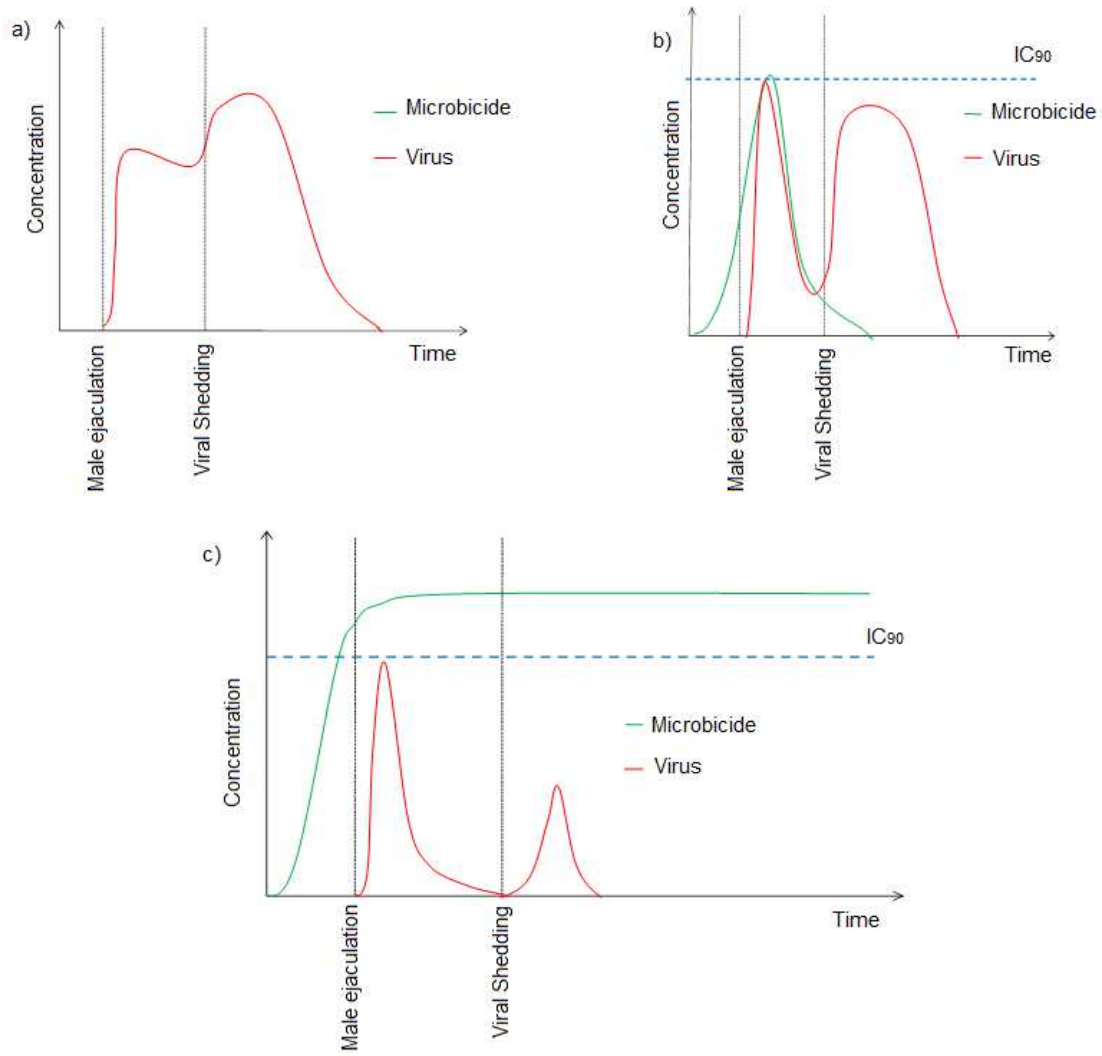


Figure 2.7: HIV-1 neutralization schematics by microbicide formulations with different anti-HIV-1 release profiles; a) acute HIV-1 intravaginal infection: no microbicide, b) quick release microbicide formulation and c) sustained release microbicide formulation (Gupta, 2008).

In designing a microbicide delivery system, a lot of other aspects should be considered such as how the anti-HIV-1 agent interacts with the virus, the means by which HIV-1 enters target cells, and the ways by which it can be neutralized (Chan and Kim, 1998). However, more knowledge is required regarding the quantitative aspects of both viral entry and neutralization. Advanced microscopy has shown that HIV-1 is surrounded by lipid coated bilayer studded with heterodimeric envelop proteins made up of three transmembrane subunits (gp41) which are capped by extensively glycosylated triple surface moieties (gp120) (Zhu et al., 2006; Zhu et al., 2003). Gp120 has been identified as an integral component in the viral entry mechanism where it binds to CD4 of the target cells causing conformational changes that allow co-receptor binding leading to a rearrangement in the transmembrane gp41 thus triggering viral-cellular fusion (Poignard et al., 2001; Chan et al., 1997).

The number of trimers needed for infection, stoichiometry of entry (Yang et al., 2005; Yang et al., 2006), as well as those of blocking the HIV-1, stoichiometry of neutralization (Magnus et al., 2009; Magnus and Regoes, 2010; Klaase, 2007; O'keefe et al., 2000), has been a subject of controversy among researches. Inspired by this, Yang and co-workers arrived at an experimental conclusion that just one trimer is capable of enabling HIV-1 entry. Whilst an incremental model elaborates that all trimers contribute equally to HIV-1 entry, the laminal model postulates that a threshold number of gp120s should be available for viral entry to occur (Yang et al., 2005; Yang et al., 2006; Magnus et al., 2009; Magnus and Regoes, 2010; Klaase, 2007; O'keefe et al., 2000). The determination of which part of the virus should the anti-HIV-1 agents target and how many of them are required is yet to be determined for an appropriate microbicide delivery system to be developed. With proper modeling and use of Yang and co-workers' stoichiometric conclusion, which provides the worst case scenario, the appropriate quantity of anti-HIV-1 agent that is to be utilized in the microbicide formulation can be determined and seriously considered when developing microbicide delivery systems.

2.6. Concluding remarks

The prevention of vaginal HIV-1 transmission requires the employment of a multiple-front strategy. Primarily, the evasive HIV-1 has to be intraluminally neutralized before it reaches the epithelial layer. Maintenance of the integrity of the epithelial layer is of paramount importance and can be achieved by deliberately avoiding agents that may instigate inflammation whilst increasing lubrication to minimize microtrauma during sexual intercourse. Anti-HIV-1 agents should not only be extremely potent but should also be in a quantitative excess in relation to HIV-1, and their distribution intraluminally has to be extensive and exhaustive. Use of agents that can penetrate the vaginal epithelia and remain active in the subepithelia to further protect HIV-1 susceptible cells may help prevent HIV-1 transmission. In addition, being able to have the anti-HIV-1 agents at the site (vaginal cavity) for a prolonged period reduces HIV-1 transmission.

An appropriate strategy would be to design a microbicide delivery system capable of: maintaining the luminal acidic micro-environment by employing acidifying biodegradable and biocompatible polymers such as poly(D,L-lactide), polylactic-co-glycolic acid, polyanhydrides including poly(sebacic) anhydride and poly(ortho-esters) as matrices for either vaginal tablets, rings, sponges or films which degrade to their respective acids and diacids in a rate controlled manner without destroying the normal vaginal flora. Polymeric macromolecules such as pectin may be used to enhance epithelial integrity. Proper scientific experimentation and mathematical modeling may result in the sustained and extended delivery of the active agents from the appropriately engineered polymers or polymer blends that may be mucoadhesive.

These innovative microbicide delivery systems have the potential to enhance patient compliance and ensure optimum anti-HIV-1 agent concentration whilst reducing side effects normally caused by frequent dosing. Use of multiple anti-HIV-1 agents with different mechanisms of action may further enhance microbicide efficacy. Engineering rheological properties of the delivery systems to achieve extensive and exhaustive target-epithelial coverage is necessary, particularly in gels. In the following chapters a composite polymeric delivery system which aims to address the concerns raised in this chapter is formulated and tested *in vitro* and *in vivo* as a potential anti-HIV-1 microbicide delivery system. In conclusion, researchers might discover countless highly potent anti-HIV-1 agents to be used as microbicides, but unless they deliver them effectively and efficiently to the appropriate site, their work will be far from translational.

CHAPTER 3

CHARACTERIZATION AND PREFOMULATION ANALYSIS OF DRUG (AZT AND BP36) AND POLYMER (PECTIN, MUCIN AND POLY ETHYLENE GLYCOL) INTENDED FOR SUBMICROSPHERE PREPARATION

3.1. Introduction

Research into microbicides that prevent HIV-1 transmission has led researchers to consider different chemical agents of varying potency and mechanisms of action against HIV-1. These anti-HIV-1 agents range from; vaginal acidifying agents (polyacrylic acid), virus inactivators (monocaprin and myristamine oxide), agents that adsorb to HIV-1 and inactivate it (cellulose acetate phthalate), broad spectrum antimicrobials such as cetyl betaine, viral cell membrane disrupting agents (nonoxynol-9 and napthalene sulphonate), viral fusion inhibitors (polysterene sulfornate, cyanovirin-N and sodium lauryl sulfornate) and HIV-1 replication inhibitors such as dapivirine, stapidine, tenofovir disproxil fumarate and theophen thiourea (Pillay et al., 2012). Research has also been carried out on plant extract agents such as praneem whose mechanism of action is not yet clearly understood.

The apex of microbicide research thus far has been the relative success of a study (phase IIb CAPRISA 004 tenofovir gel trial) performed using a 1% tenofovir gel (nucleoside reverse transcription inhibitor) which showed 39% efficacy in preventing vaginal HIV-1 transmission thus proving right the viability of the concept of using microbicides as a HIV-1 transmission prevention tool (Abdool karim et al., 2010). There is also scope in using a combination of different anti-HIV-1 agents with different mechanisms of action (Pillay et al., 2012).

The study reported in this dissertation employs a combination of two anti-HIV-1 agents, zidovudine and BP36. Zidovudine was the first antiretrovirals to be developed and used to treat HIV/AIDS. It is a nucleotide reverse transcriptase inhibitor (NRTI), which means that it prevents HIV-1 from replicating. It was chosen in this study to reduce the viral load thus reducing the risk of transmission since HIV-1 that initially infects a person has to reach a quantitative threshold for transmission to occur (Pillay et al., 2012). The second anti-HIV-1 agent is an experimental herbal extract (leaves and sterm) from a South African plant identified as BP36. BP36 has been studied and patented for its anti-HIV-1 properties by the Council for Scientific and Industrial Research (CSIR) BioSciences, South Africa.

Scientists at CSIR BioSciences, South Africa, found the composition of BP36 to be a percentage carbohydrate content of; arabinose 11.5%, rhamnose 5.5%, xylose 1.9%, mannose 4%, galactose 10.5%, glucose 26%, glucuronic acid 4.3% and galacturonic acid 36.3%. On its anti-HIV-1 properties, BP36 was reported to be active against HIV-1 subtype C pseudoviruses, with an IC_{50} of 0.1–7.9µg/mL as compared to T20:0.1 – 7.5µg/mL and tenofovir:0.2 – 1.2µg/mL (van den Berg et al., 2011). In addition BP36 was found to act within 8 hours thus proposing that its mechanism of action was probably viral fusion inhibition. Therefore, BP36 was employed together with zidovudine because its mechanism against HIV-1 is different and complimentary to that of zidovudine.

In this chapter zidovudine and BP36 are identified and characterized using attenuated Fourier transform infrared microscopy and their physical properties are elucidated through differential scanning calorimetry, and thermogravimetric analysis. This study involved dual encapsulation of zidovudine and BP36 in submicrospheres prepared from biodegradable and biocompatible macromolecules porcine gastric mucin, pectin, and polyethylene glycol, of which submicrospheres are then embedded within a polymeric caplet matrix. Therefore, this chapter also focused of elucidating the physicochemical, thermal and thermodynamic properties of porcine gastric mucin, pectin and polyethylene glycol and their interaction in aqueous media in an effort to understand and predict how they would form submicrospheres that would encapsulate zidovudine and BP36.

Mucin, a glycosylated protein that forms the major structural component of the mucus gel that covers most human body cavities (urogenital, gastrointestinal, eye, lungs and other mucosal membranes) plays a major role in various frontline interactions with different materials from the external environment (Dekker et al., 2002; Bansil and Turner, 2006). Mucus is composed of approximately 95% water, about 2% lipids (fatty acids, phospholipids and cholesterol) and electrolytes with the remaining 3% being mucin. Research has shown interest in mucin as the structural backbone of the gel-like layer that serves various functions such as; lubrication of mucosal membranes to avoid abrasions, protection of mucosal lining from self digestion as in the case of gastric mucus and it also acts as a gate keeper, keeping at bay unwanted external environmental materials and organisms such as bacteria and viruses (Patel et al., 2003; McGuckinet al., 2011).

The major functions of mucus are owed to the structure and molecular properties of mucin. Mucin is a large (0.5-20MDa) glycoprotein consisting of a protein core composed of 4-5 amino acids (proline, serine, threonine, glycine and glutamate) arranged in detached regions, namely, a bulky (60%) central repeating serine, threonine and proline (STP) region.

Interspaced within this STP region and at the terminals are N-linked oligosaccharides and von Willebrand factor (vWF)-like cysteine rich regions (Dekker et al., 2002; Bansil and Turner, 2006). The STP region is linked to oligosaccharide side-chains made up of 5-15 sugars such as N-acetylglucosamine, fucose, N-acetylneuramic acid, N-acetylgalactosamine, mannose and sulfate that account for approximately 80% by weight of mucin and are responsible for mucin's hydrophilic properties through its sialic acid content (Bansil and Turner, 2006). The cysteine rich regions form disulfide bonds responsible for mucin's dimeric structure (Dekker et al., 2002; Bransil and Turner, 2006). Therefore mucin is a complex biomaterial with peculiar structural and chemical properties to interact with a diverse range of materials of external origin. Of particular interest in this chapter was the manner in which mucin interacts with a biocompatible and biodegradable macromolecule, pectin, under different conditions and how these macromolecular interactions can be demonstrated through diverse techniques.

Pectin, a plant cell wall constituent, is a linear polysaccharide composed of (1-4)-α-D-galacturonic acid units randomly interrupted by (1,2)-linked L-rhamnoside-chains and other neutral sugars (Rolin, 1993; Sriamornasak et al., 2008). Chemical and physical properties of pectins are mostly defined by the degree of methyl esterification (DE) and the degree of amidation (DA) of its carboxylic groups. The DE is used as a pectin classification system with pectins having less than 50% DE referred to as low methoxy pectins and those with DE greater than 50% regarded as high methoxypectins (Rolin, 1993). Pectin is used as a thickener or gelling agent in the food industry (Thakur et al., 1997). In the cosmetic industry it has been employed to encapsulate fragrances in microspheres as well as being utilized in various formulations such as gels, films and as a stabilizer in emulsions, suspensions and foams (Thakur et al., 1997; Liu et al., 2005). Pectin's use extends to the pharmaceutical industry where it is used as a binding agent, gelling agent and in conventional and modified drug delivery to modulate the release of the active pharmaceutical ingredient from nanoparticles, microspheres, beads and tablets (Wong et al., 2002; Liu et al., 2005; Vaidya et al., 2009; Srivastava et al., 2010). In tissue engineering and biotechnology it finds applications as a wound dressing and cell regeneration matrix (Munarin et al., 2011). In the majority of these applications pectin interacts with the mucus layer and hence interacts with mucin.

Several techniques have been developed over the years to assess the type and extent of mucin-pectin interactions. Among them, the rheological technique has demonstrated viscosity and dynamic moduli synergism involved in mucin-pectin aqueous dispersions (Hassan and Gallo, 1990; Liu et al., 2005; Sriamornsak et al., 2008; Sriamornsak and

Wattanakorn, 2008; Thirawong et al., 2008). This technique has been widely utilized to determine and explain mucoadhesion of pectin (Sriamornsak et al., 2008; Thirawong et al., 2008). Scanning electron microscopy and atomic force microscopy have also been employed to demonstrate mucin-pectin interactions (Liu et al., 2005; Sriamornsak et al., 2008; Sriamornsak et al., 2010). This chapter further demonstrates mucin pectin interactions using full attenuated total reflection Fourier transform infrared (ATR-FTIR) spectroscopy analysis, ultraviolet (UV) spectrophotometric analysis, thermal and thermodynamic analysis as well as *in silico* static lattice atomistic simulations of mucin-pectin interactions. In addition, an investigation of the effect of calcium ions (Ca^{2+}), the mucin:pectin ratio and a plasticizer polyethylene glycol 400 (PEG 400), on the formation of a mucin-pectin interpenetrating macromolecular network was investigated.

3.2. Materials and Methods

3.2.1. Materials

Zidovudine (AZT) was purchased from GlaxoSmithKline, Middlesex, UK and BP36 was supplied by the department of BioSciences, Council for Scientific and Industrial Research, South Africa. Porcine gastric mucin type III (MUC) with 1-1.5% bound sialic acid (M_w ~22 000 000 $gmoL^{-1}$) and polyethylene glycol 400 (PEG M_w 400) were purchased from Aldrich® (Sigma–Aldrich Inc., St. Louis, USA). Three commercially available grades of citrus pectin having different degrees of esterification (DE) and different degrees of amidation (DA) were purchased from CP KelcoApS, Lille Skensved, Denmark: GENU® pectin type USP/100 (PEC_{USP})[DE 55-65%M_w~120-130 000 $gmoL^{-1}$, average density $\rho_{PEC\text{-}USP}$~0.7gmL^{-1}]; GENU® pectin type LM-101 AS (PEC_{AS}) [DE 35%, DA 15%]and GENU® pectin type LM-104 AS FS($PEC_{AS\text{-}FS}$), [DE 28%, DA 20%]. All other chemicals employed were of analytical grade and were used as purchased.

3.2.2. Attenuated total reflection Fourier transform infrared spectroscopic (ATR-FTIR) analysis of the drugs and polymers

Powder samples of zidovudine, BP36 and lyophilized samples of MUC, PEC and MUC-PEC aqueous dispersion combinations (MUC:PEC ratios: 1:0, 1:1, 1:4, 1:9 and 0:1) were analysed by ATR-FTIR. Dilute aqueous dispersions of ($1\%^{w}/_{v}$); MUC, PEC and their combinations at different MUC:PEC ratios of 1:0,1:1,1:4,1:9 and 0:1 were prepared by dispersing the macromolecules in deionized water whilst stirring at 25°C for 30 minutes. The dispersions were frozen overnight below -72°C before being lyophilized for 48 hours. Thereafter samples were analyzed using a Perkin Elmer Spectrum 2000 FTIR spectrometer that was fitted with a MIRTGS detector (PerkinElmer Spectrum 100, Llantrisant, Wales, UK), that used a diamond crystal internal reflection element containing an ATR-FTIR cell.

Samples were analyzed at a wave number range of 650-4000cm^{1} with a resolution of 4 cm^{-1} and 64 scans per spectrum at a direct contact force of 112 N. AZT, BP36 , MUC and PEC were characterised. In addition, MUC-PEC interactions were elucidated and interpreted from the various structural transformations observed on comparing the MUC-PEC ATR-FTIR spectra to that of the native MUC and PEC.

3.2.3. Morphological characterization of lyophilized samples of MUC, PEC and MUC-PEC blends

Lyophilized aqueous dispersions of (1% $^{w}/_{v}$); MUC, PEC_{USP} and MUC-PEC_{USP} combinations with weight ratios of 1:0,1:1,1:4 1:9 and 0:1 were mounted on specimen stubs and gold coated using a SPI-Module^{TM} sputter coater (SPI Supplies, STRUCTURE PROBE INC, West Chester, Pennsylvania, USA) and then observed at 510X magnification under a scanning electron microscope (SEM) (PHENOM^{TM} Desktop SEM, FEI Company, Oregon, USA) operated at 10KV in the electron imaging mode.

3.2.4. Thermogravimetric analysis of AZT and BP36

Thermal degradation analysis was performed on 10-20mg samples of AZT and BP36 samples, put in ceramic pans and under nitrogen atmosphere, using a TGA 4000 thermogravimetric analyzer (PerkinElmer Inc, Massachusetts, USA). Thermograms obtained and their first derivatives revealed the thermal degradation properties of the AZT and BP36.

3.2.5. Thermal and thermodynamic analysis of AZT and BP36 powder samples, MUC, PEC_{USP} and MUC-PEC_{USP} lyophilized samples

Dry powder samples were used to elucidate the thermal properties of AZT and BP36 through differential scanning calorimetry. MUC-PEC_{USP} aqueous dispersions were prepared by adding PEC_{USP} and MUC to deionized water then stirring them at 25°C for 30 minutes. Each aqueous dispersion had a total macromolecule concentration of 3.33%$^{w}/_{v}$ composed of different MUC:PEC_{USP} ratios of 1:0, 1:9, 1:4, 1:1 and 0:1. The dispersions were cast into films on Petri dishes and left to dry at ambient temperature for 48hours. The resultant films were pulverized and used as samples for differential scanning calorimetry (DSC) measurements (Mettler Toledo, DSC1, STARe System, Schwerzenback, Switzerland). Calibration of temperature and enthalpy on the instrument were done using indium and zinc. Heating rate was set at 10°Cmin^{-1} under a dry nitrogen atmosphere (Afrox, Germiston, Gauteng, South Africa) with a flow rate of 200mLmin^{-1} acting as the purge gas in order to reduce oxidation. Samples (10mg) were added into 40µL aluminium pans and heated from -10°C to 110°Cand kept at 110°C for 3 minutes. This was done to evaporate any moisture in the sample and to eliminate any thermal history. The samples were then quenched from

110°C to -10°C at a rate of 20°C min^{-1}. The midpoint melting point (T_m) and heat of fusion (ΔH) obtained from the melting point depression were determined according to the peaks generated on the experimental DSC curves on heating the samples from -10 to 250 °C. To determine the interaction and miscibility of MUC and PEC_{USP}, analysis of the thermal and thermodynamic properties of MUC and PEC_{USP} were elucidated according to the Nishi-Wang and Flory-Huggins theories (Harris et al., 1983; Xie et al., 2002).

3.2.6. Ultraviolet (UV) spectrophotometry analysis of MUC, PEC and MUC-PEC combination aqueous dispersions

Ultraviolet (UV) absorbance of MUC, PEC and MUC-PEC combination dispersions in deionized water were assessed by passing UV light through a standard quartz cuvette at 600nm wavelength, thereafter UV absorbance was measured using a nanophotometer (NanoPhotometer^{TM},Implen GmbH, Munchen, Germany) at ambient temperature (25°C). Dilute aqueous dispersions of MUC-PEC were prepared at a concentration of 0.2%$^{w}/_{v.}$ MUC-PEC weight ratios examined were 1:0, 1:1, 1:4, 1:9, 0:1, 4:1, and 9:1. Three different types of pectin were used to assess the effect of the DE and DA on MUC-PEC combination UV absorbance. UV absorbance was used in this study as a measure of MUC-PEC interactions by computing and comparing the UV absorbance difference (ΔA), of pristine MUC, PEC and combination MUC-PEC dispersions. Absorbance difference (ΔA) was regarded as the difference of the UV absorbance obtained for the MUC-PEC combination ($A_{MUC\text{-}PEC}$) and that of the summation of the UV absorbance obtained when individual pristine dispersions of MUC (A_{MUC}) and pectin (A_{PEC}) were measured as in equation 3.1.

$$\Delta A = A_{MUC\text{-}PEC} - (A_{PEC} + A_{MUC}) \qquad \textit{Equation 3.1}$$

3.2.7. Rheology analysis of MUC, PEC and MUC-PEC combination aqueous dispersions

Viscosity (η), storage modulus (G') and loss modulus (G'') of (3.333% $^{w}/_{v}$) of dilute aqueous dispersions of MUC, PEC and different MUC:PEC combinations were measured using a modular advanced rheometer (HAAKE MARS Modular Advanced Rheometer, Thermo electron Corporation, Karlsruhe, Germany) with a C35/1° Ti sensor. The tests were performed employing the rheometer parameters shown in table 3.1.

Table 3.1: Rheometer parameters

Parameter	Value
Cone and plate gap	0.0051mm
Driver version	0.29
Inertia	1.721 10^{-06} Kgm^2
A-factor	89051.00 Pa
M-factor	57.010 rad/s
Temperature	25°C
Damping	30.00

Viscosity was measured on a 0.5mL sample for 60s and 180s. Dynamic oscillatory rheology measurements of the storage and loss moduli of 0.5mL samples were performed over a small frequency range of 0.1-1.0Hz which fell within the shear independent plateau of the corresponding strain amplitude sweep. All samples were prepared by dispersing PEC, MUC or MUC-PEC combinations in 15mL of deionized water. The samples were allowed to stand for 5minutes prior to testing. Rheological synergy expressed by the equations below was investigated and used as a signifier of the interpenetrating macromolecular interactions between PEC and MUC (Equations 3.2-3.4).

$$\Delta\eta = \eta_{MUC\text{-}PEC} - (\eta_{PEC} + \eta_{MUC}) \qquad \textit{Equation 3.2}$$

$$\Delta G' = G'_{MUC\text{-}PEC} - (G'_{PEC} + G'_{MUC}) \qquad \textit{Equation 3.3}$$

$$\Delta G'' = G''_{MUC\text{-}PEC} - (G''_{PEC} + G''_{MUC}) \qquad \textit{Equation 3.4}$$

Where:

$\Delta\eta$ – Difference of the viscosity of MUC-PEC ($\eta_{MUC\text{-}PEC}$) and the sum of the viscosities of individual MUC (η_{MUC}) and PEC (η_{PEC}).

$\Delta G'$- Difference of the storage modulus of MUC-PEC ($G'_{MUC\text{-}PEC}$) and the sum of the storage moduli of individual MUC (G'_{MUC}) and PEC (G'_{PEC}).

$\Delta G''$- Difference of the loss modulus of MUC-PEC ($G''_{MUC\text{-}PEC}$) and the sum of the loss moduli of individual MUC (G''_{MUC}) and PEC (G''_{PEC}).

3.2.8. Static lattice atomistic simulations of MUC PEC interactions

Molecular mechanics simulations were performed using commercial software: HyperChem™ 8.0.8 Molecular Modeling System (Hypercube Inc., Gainesville, Florida, USA) and ChemBio3D Ultra 11.0 (CambridgeSoft Corporation, Cambridge, UK).The structure of pectin (PEC; 4 saccharide units) was built from standard bond lengths and angles using the sugar builder module on HyperChem™ 8.0.8 while the structure of the glycoprotein analogue (MUC) was generated using the sequence editor module. The models were energy-minimized using a progressive-convergence-strategy where initially the MM+ force field was used followed by energy-minimization using the Amber 3 (Assisted Model Building and Energy Refinements) force field. The conformer having the lowest energy was used to create the MUC-PEC complexes. A complex of one macromolecule with another was assembled by disposing the macromolecules in a parallel way, and the same procedure of energy-minimization was repeated to generate the final models: PEC, MUC, and MUC-PEC (1:1 to 1:4). Full geometry optimization was carried out in vacuum employing the Polak–Ribiere conjugate gradient algorithm until an RMS gradient of 0.001kcal/mol was reached. For molecular mechanics calculations in vacuum, the force fields were utilized with a distance-dependent dielectric constant scaled by a factor of 1. The 1-4 scale factors employed were, electrostatic=0.5 and van der Waals=0.5 (Kumar et al., 2011).

3.3. Results and Discussion

3.3.1. ATR-FTIR spectroscopy of AZT, B36, MUC, PEC and MUC-PEC

The AT-FTIR spectrum of zidovudine showed strong band from ~3200-3500cm^{-1} which was likely a result of stretching vibration of the hydroxyl (O-H) group in AZT (Figure 3.1). The weak bands observed in figure 3.1 at about 1200cm^{-1} may be a result of the stretching vibrations of the amine group of AZT (Figure 3.1). The distinctive peak at ~2100cm^{-1} was due to the stretching vibrations of the azide group (-N=C=N-) in AZT (Figure 3.1). A strong absorption peak (~1600cm^{-1}) was observed on the AZT spectrum which may have been contributed to by the strong stretching vibrations of the amide I bond (Ravi et al., 2008). The ATR-FTIR spectrum of AZT (Figure 3.1) also depicted several peaks in the finger print region (1450-650cm^{-1}) which were consistent with what has reported in literature (Ravi et al., 2008).

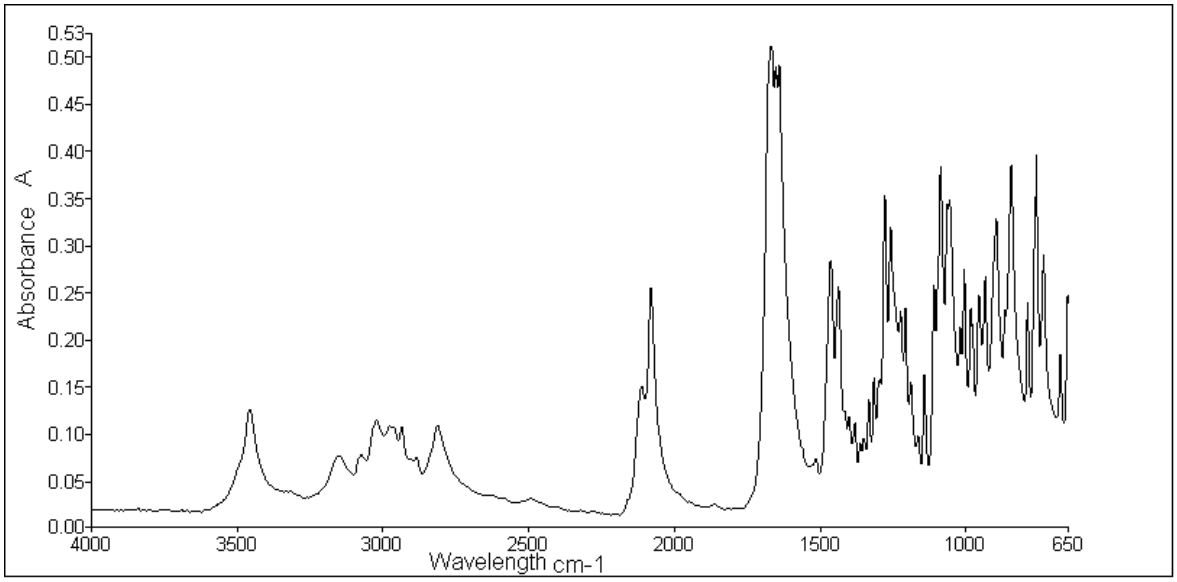


Figure 3.1: ATR-FTIR absorbance spectrum of zidovudine (AZT)

Figure 3.2 depicts the FTIR absorption spectra of BP36 which shows a broad peak from ~2800-3600cm^{-1} which was likely a result of the overlapping stretching vibration of alkane and hydroxyl groups found in BP36. A strong band at ~1700cm^{-1} may have been caused by hydrogen bonded carboxyl (C=O) groups of the BP36 (Figure 3.2). The BP36 spectrum also depicted a few peaks in the finger print region (1450-650cm^{-1}).

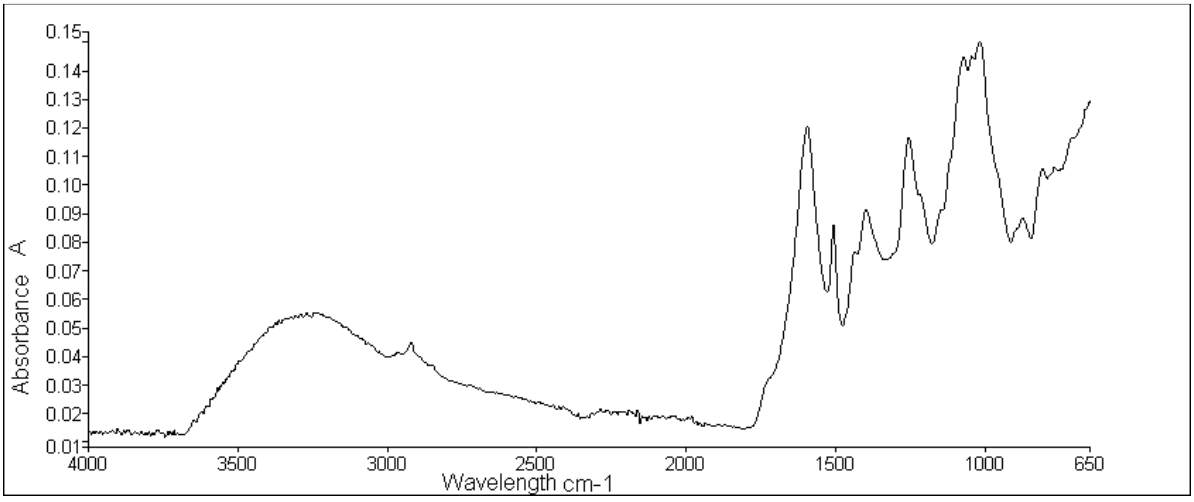


Figure 3.2: ATR-FTIR absorbance spectrum of BP36

Full ATR-FTIR split absorption spectra of the three different types of citrus pectins; PEC_{USP}, PEC_{AS} and PEC_{AS-FS}, are shown in figure 3.3 with characteristic peaks identified. The broad peaks between 3000 and 3650cm^{-1} identified in all three types of pectin were due to an overlap of strong stretching vibrations of the -O-H bond of the pectin carboxylic groups and the free -O-H bond of the hydroxyl groups found in pectin. Absorption peaks at 2933cm^{-1} for

PEC_{USP}, 2932cm^{-1} for PEC_{AS} and 2926cm^{-1}depict sp^3 stretching vibrations of the -C-H alkane groups of the different types of pectin. Absorption peaks observed at 1736cm^{-1} for PEC_{USP}, 1740cm^{-1} for PEC $_{AS}$ and PEC_{AS-FS} correspond to stretching vibrations of the -C=O ester bond.

The strength of the peaks signified the degree of esterification of the three different types of pectin. PEC_{USP} which is typically 55-65% esterified displayed the strongest peak followed by PEC_{AS}, 35% and PEC_{AS-FS}, 28%. PEC_{AS-FS} displayed strong peaks at 1672cm^{-1} and 1594cm^{-1} identifying amide I and amide II -C=O stretching vibrations respectively. Amide I and amide II peaks of PEC_{AS} observed at around 1670cm^{-1} and 1599cm^{-1} were weaker than those of PEC_{AS-FS}. This confirmed that the degree of amidation of PEC_{AS-FS} (typically 20%) was higher than that of PEC_{AS} (typically 15%). PEC_{USP} did not show any amide peaks thus confirming that it was not amidated, however a strong peak at 1607$cm^{-1}$was observed which might have been a result of -C=O stretching of the carboxylic groups. All three types of pectin displayed typical absorption bands in the carbohydrate region (1200-900cm^{-1}) (Sriamornsak et al., 2008).

Figure 3.4 compares the FTIR absorption spectra of MUC, PEC_{USP} and that of MUC-PEC_{USP}. MUC is a glycosylated protein whose characteristic absorption peaks depicted in figure 3.4 1(b) included a broad peak spanning from 3000$cm^{-1}$to 3650cm^{-1} which was likely due to an overlap of carboxylic -O-H with primary and secondary amine -N-H stretching vibrations. An absorption peak at 2919cm^{-1} was a typical -C-H stretching vibration corresponding to the alkane groups found in glycosylated mucin. Other typical MUC peaks occurred at 1638cm^{-1} due to -C=O amide I strong stretching vibration and at 1544cm^{-1} resulting from -C=O amide II stretching vibration. The gylcosylation of MUC was revealed by the typical peaks observed in the carbohydrate region of 1200cm^{-1} to 900 $cm^{-1.}$

The absorption spectra of MUC-PEC_{USP} showed peaks attributed to by both PEC_{USP} and MUC, with a very broad peak extending from 3000cm^{-1} to above 3650cm^{-1} as a result of -O-H stretching of the carboxylic groups in PEC_{USP} and the carboxylic groups in MUC overlapping the -N-H stretching bond of the primary amine. The band with its peak at 3363cm^{-1} appeared much broader than the respective peaks of PEC_{USP} and MUC which signified the occurrence of PEC_{USP} and MUC macromolecular interactions through hydrogen bonding. MUC-PEC_{USP} absorption peaks at 2932cm^{-1} belonged to -C-H alkane stretching vibrations of both PEC_{USP} and MUC. The peak at 1737cm^{-1} showed that the ester bond in the PEC_{USP} remained intact when PEC_{USP} and MUC interacted. Disappearance of the peaks at 1638cm^{-1} and 1544cm^{-1} from MUC when combined with PEC_{USP} may have been a result of

macromolecular interactions or due to masking by PEC_{USP}. MUC-PEC_{USP} spectrum showed a broad peak at 1614cm^{-1} which was likely a result of the -C=O bond stretching vibrations of carboxylic groups of PEC_{USP} and this may be attributed to hydrogen bonding involved in the IMN.

A clear view of the relative spectra peak changes is depicted in figure 3.5, which is an overlay ATR-FTIR absorption spectra displays of MUC-PEC_{USP} at different MUC:PEC_{USP} ratios of 1:1, 1:4 and 1:9. As the MUC-PEC_{USP} ratio changes from 1:1 through 1:4 to 1:9, the peaks from 3000cm^{-1} to 3650cm^{-1} (due to -O-H,-N-H stretching) and the ester -C=O bond around 1736cm^{-1} become broadened and intensified as a result of extensive intermolecular hydrogen bonding. The peaks between 1600cm^{-1} and 1630cm^{-1} shifted to the right and decreased in intensity for a PEC-PEC_{USP} ratio of 1:1 through 1:4 to 1:9 as a result of PEC_{USP} and MUC molecular interactions. The shoulder to the right of these peaks increasingly disappeared as the ratio of MUC:PEC_{USP} changed from 1:1 through 1:4 to 1:9. MUC, being a larger glycoprotein molecule as compared to PEC_{USP}, had much more groups that could participate in hydrogen bonding. These included amine, amide groups of the protein backbone, the extensive hydroxyl and carboxylic groups of the carbohydrate side chains. Consequently, there was an increase in MUC-PEC_{USP} macromolecular interactions with changing MUC:PEC_{USP} ratio from 1:1, 1:4 to 1:9.

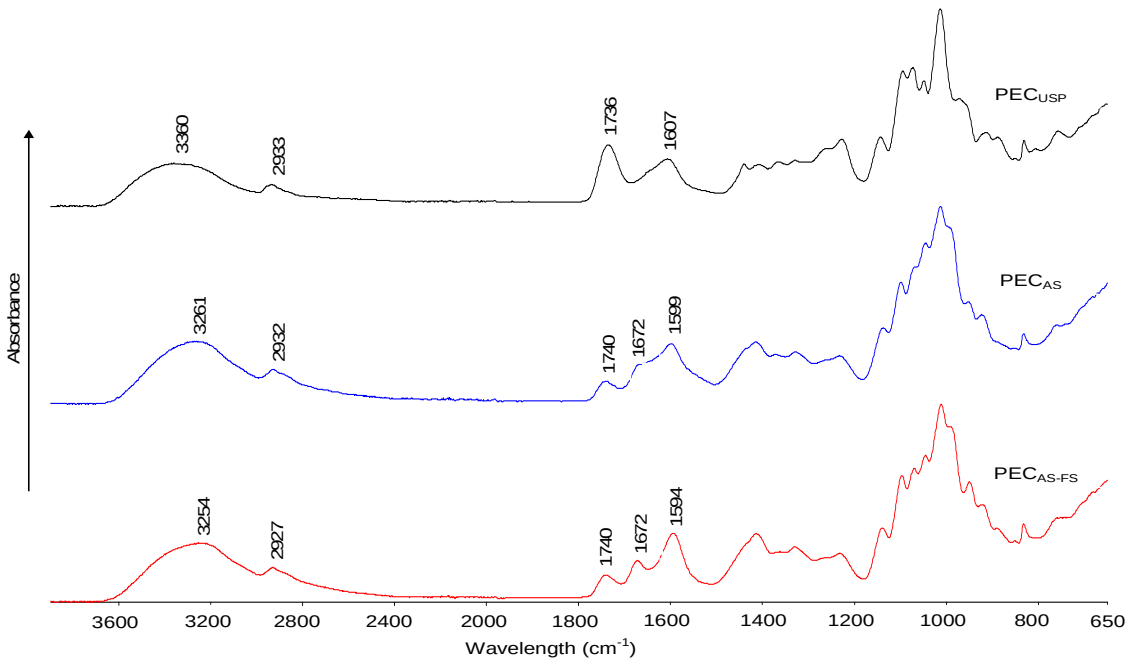


Figure 3.3: Split ATR-FTIR absorbance spectra of lyophilized aqueous dispersions of different types of pectin; PEC_{AS-FS}, PEC_{AS} and PEC_{USP}

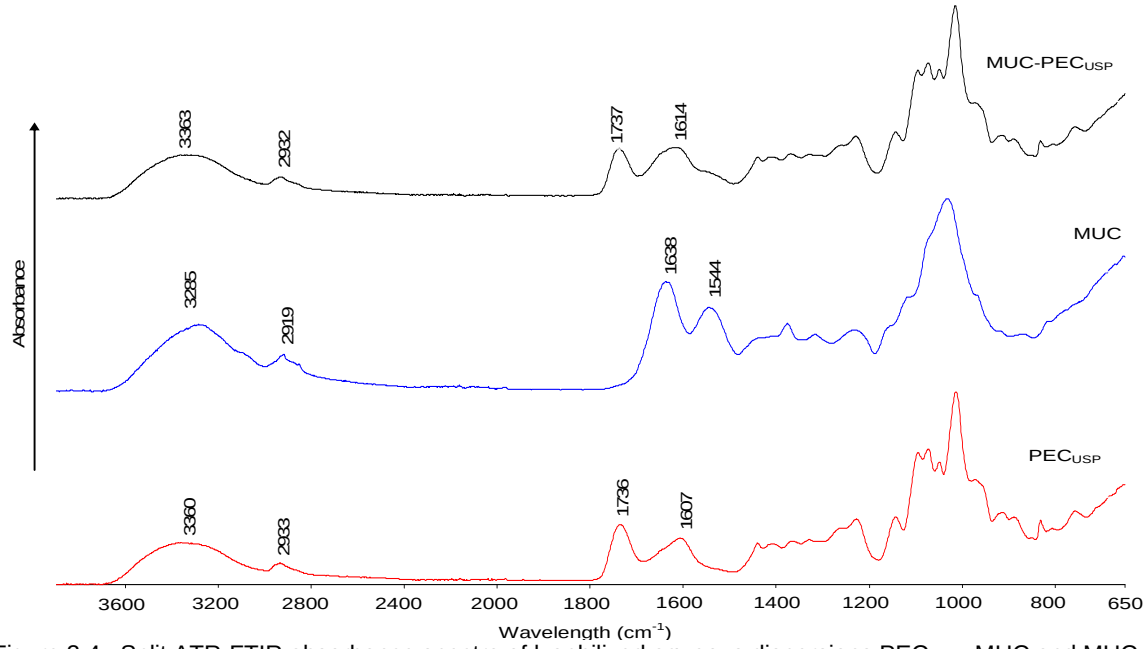


Figure 3.4: Split ATR-FTIR absorbance spectra of lyophilized aqueous dispersions PEC_{USP}, MUC and MUC-PEC_{USP}

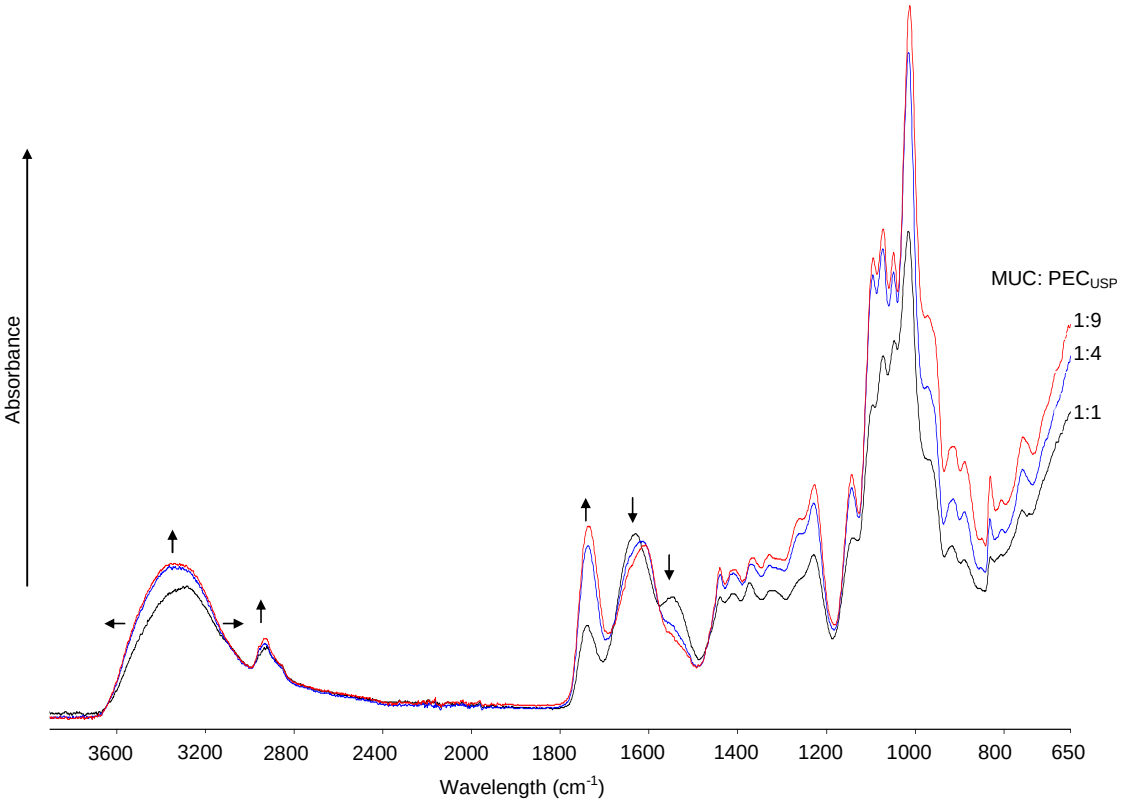


Figure 3.5: Overlay ATR-FTIR absorbance spectra of lyophilized aqueous dispersions of porcine gastric mucin (MUC) and pectin (PEC_{USP}) that compares the different MUC:PEC_{USP} ratios in MUC-PEC_{USP} lyophilized aqueous dispersions, thus depicting the type and extent of macromolecular interactions between MUC and PEC_{USP}.

3.3.2. Morphological characterization by scanning electron microscopy of lyophilized samples of MUC, PEC_{USP} and MUC-PEC_{USP}

Electron micrographs of MUC and PEC_{USP} and their various combinations at different ratios revealed the surface morphology and relative structural integrity of lyophilized scaffolds as depicted in figure 3.6. Figure 3.6(a) depicts a MUC scaffold showing a thin multidirectional membranous scaffold with less defined edges and a thin outlook with pores and micropores characterizing its membranous surface. MUC, with its bottle-brush structure composed of a protein core and random carbohydrate side chains, would most likely result in uneven surfaced, porous membranes with multidirectional edges as depicted in figure 3.6(a) (Patel et al., 2003, Bansil and Turner 2006). In contrast, the PEC_{USP} scaffold depicted in figure 3.6(b) was composed of a thicker, unidirectional rigid-looking scaffold with well defined edges and a smoother surface as compared to that of MUC.

PEC_{USP} has a linear structure with relatively well defined (1-4)-α-D-galacturonic acid repeat units which could explain its smooth unidirectional rigid structure shown in figure 3.6(b) (Rolin 1993). The MUC-PEC_{USP} combination scaffolds exhibited intermediary characteristics owing to contributions from both MUC and PEC_{USP}. The MUC-PEC_{USP} 1:1 scaffold depicted in figure 3.6(c) displayed more MUC characteristic thinness, was multidirectional and even appeared filamentous at the edges. The rigidity and smoothness of the scaffold membranes increased with changing MUC:PEC_{USP} ratio from 1:1 through 1:4 to 1:9 as they assumed a more unidirectional and thicker PEC_{USP} morphology. The morphological presentations exhibited in figure 3.6 were possibly a result of the molecular structures of MUC and PEC_{USP}.

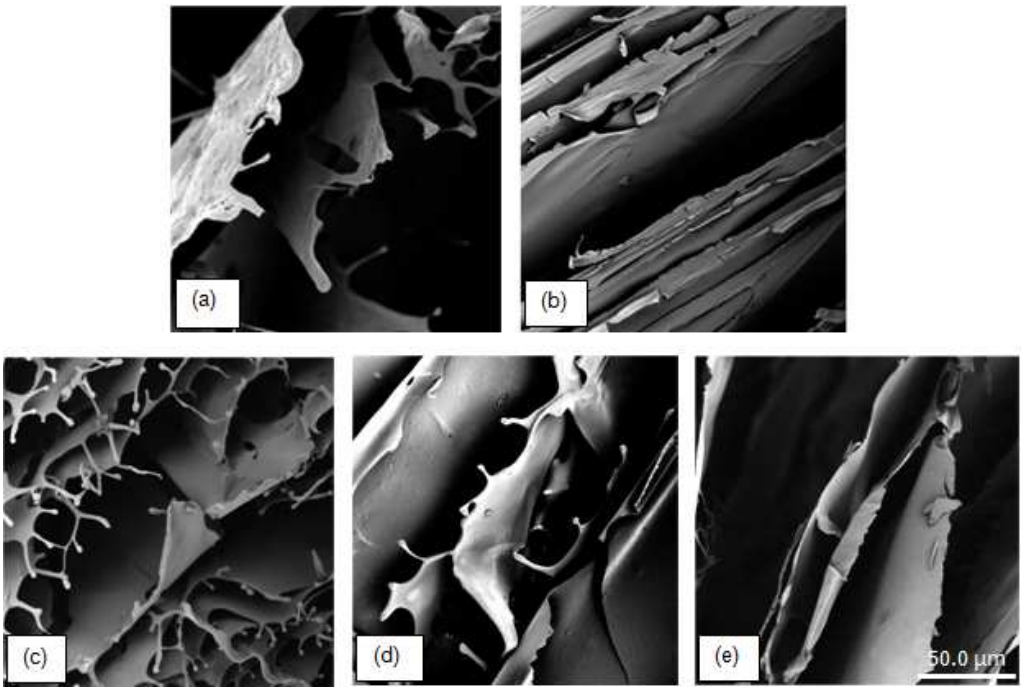


Figure 3.6: SEM images, taken at 510X magnifiifation, depicting membranous scaffolds of lyophilized MUC-PEC_{USP} combinations; (a) MUC, (b) PEC_{USP}, (c) MUC-PEC_{USP}1:1, (d) MUC-PEC_{USP}1:4 and (e) MUC-PEC_{USP}1:9. Bar =50.0µm

3.3.2. Thermogravimetric analysis of AZT and BP36

Thermogravimetric analysis of AZT yielded the thermogram depicted in figure 3.7 (solid line) and its first derivative (derivative thermogravimetric analysis, DTGA (dotted line). The first derivative reveals that AZT thermally degraded in two major steps depicted by the DTGA peaks at 244.10°C (first step) and 310.70°C (second step). Degradation of AZT started at the extrapolated onset of 230.14°C, then the second degradation step began before the first degradation step ended. The extrapolated end of the degradation of AZT was at 331.48°C and the total AZT weight loss on heating from 50-500°C was about 78%.

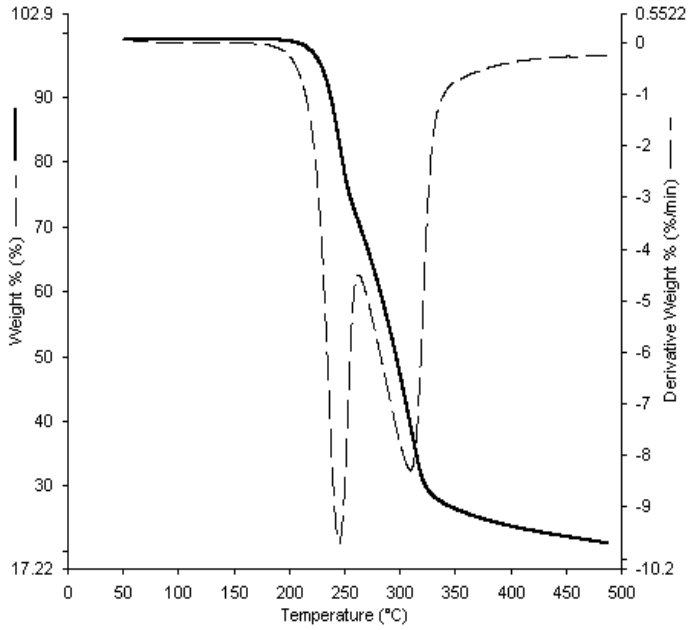


Figure 3.7: TGA (solid) and DTGA (dotted) thermogram of AZT obtained when AZT was analyzed from 50ºC to 500ºC

The TGA thermogram of BP36 [Weight (%) against Temperature (°C), 25-500°C, figure 3.8] depicts the first derivative with peak at 68.52°C that corresponds to the first thermal event and a peak at 304.02°C that corresponds to the second thermal event. The first thermal event calculations gave an extrapolated onset at 50.54°C, an inflection point at 65.70°C, an end at 98.63°C and a BP36 degradation weight loss of 10.119% measured from 25-150°C. This weight loss was most probably due to evaporation of the moisture from BP36. The second thermal event calculations showed an extrapolated onset at 251.34°C, an inflection point at 306.04°C, an end at 351.15 and a BP36 degradation weight loss of 33.393%. BP36 ash value was calculated to be 40.340%.

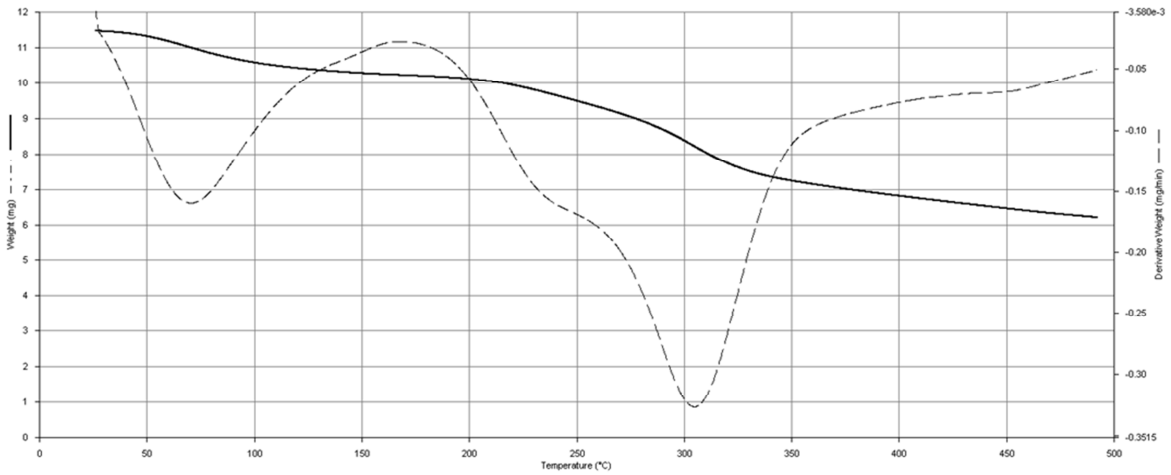


Figure 3.8: TGA (solid) and DTGA (dotted) thermogram for BP36 obtained when BP36 was analyzed from 25ºC to 500ºC

3.3.4. Thermal and thermodynamic analysis of AZT, BP36, MUC, PEC_{USP}, MUC-PEC_{USP}

DSC thermogram of AZT run from -10ºC to 500ºC revealed an onset melting point (endothermic peak) of 115ºC and a double crystallization point (exothermic peak) at 230ºC and 240ºC before degrading (Figure 3.9).

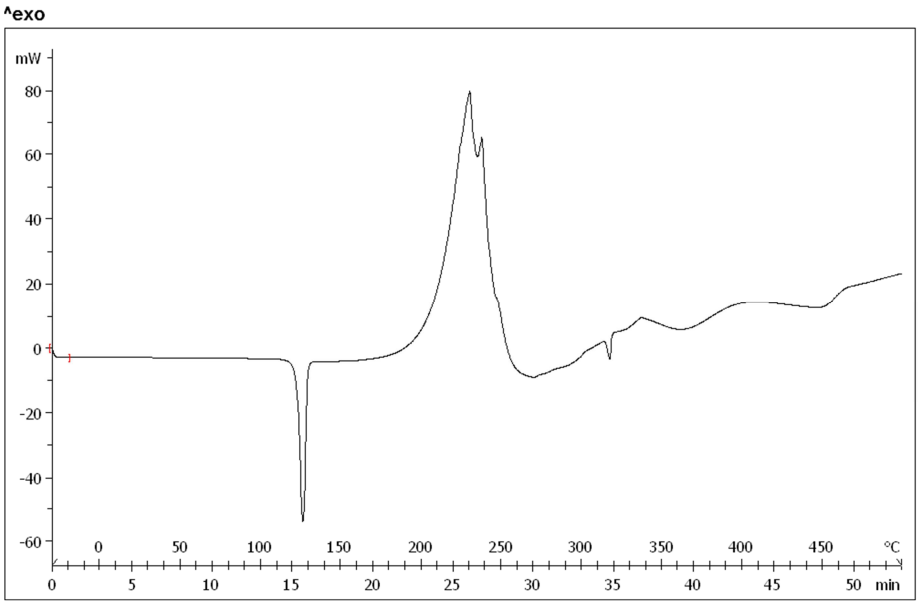


Figure 3.9: First run DSC thermogram of AZT measured from -10ºC to 500ºC

Running DSC for AZT from -10ºC to 200ºC, quenching the sample and then running it again from -10ºC to 200ºC revealed an onset zidovudine onset grass transition (T_g) of 35ºC as depicted in the 2nd run AZT thermogram in figure 3.10.

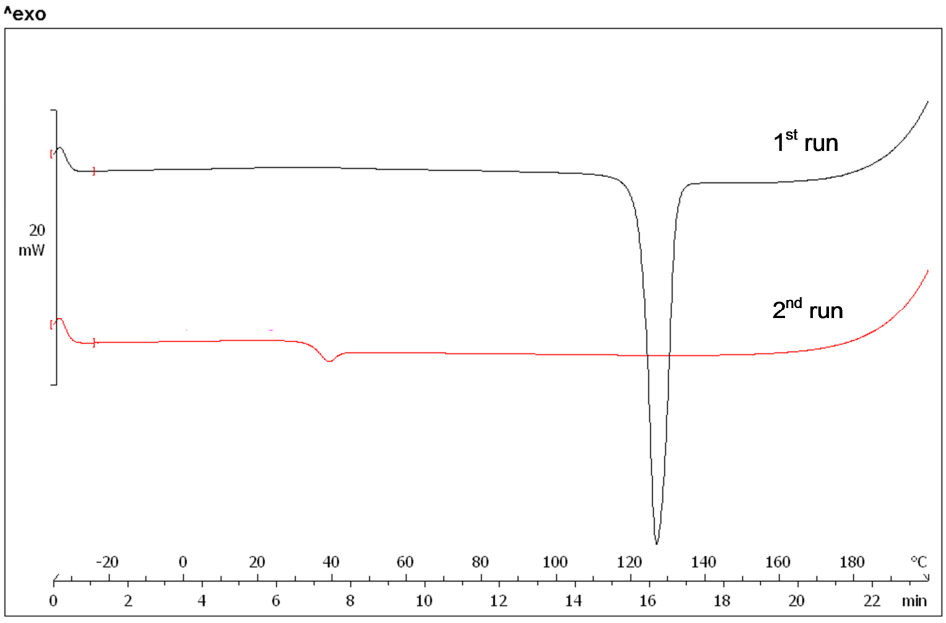


Figure 3.10: First and second run DSC thermograms of AZT measured from -10ºC to 200ºC

The BP36 DSC thermogram showed a midpoint melting point of ~105ºC which was a broad endothermic peak consistent with carbohydrate macromolecules (Figure 3.11). The thermogram showed an exothermic peak at about 390ºC that was not very sharp before degradation (Figure 3.11). This exothermic peak could be ascribed to crystallization of BP36. BP36 also showed a grass transition at ~80ºC as depicted by the 2nd run DSC thermogram of BP36 in figure 3.12.

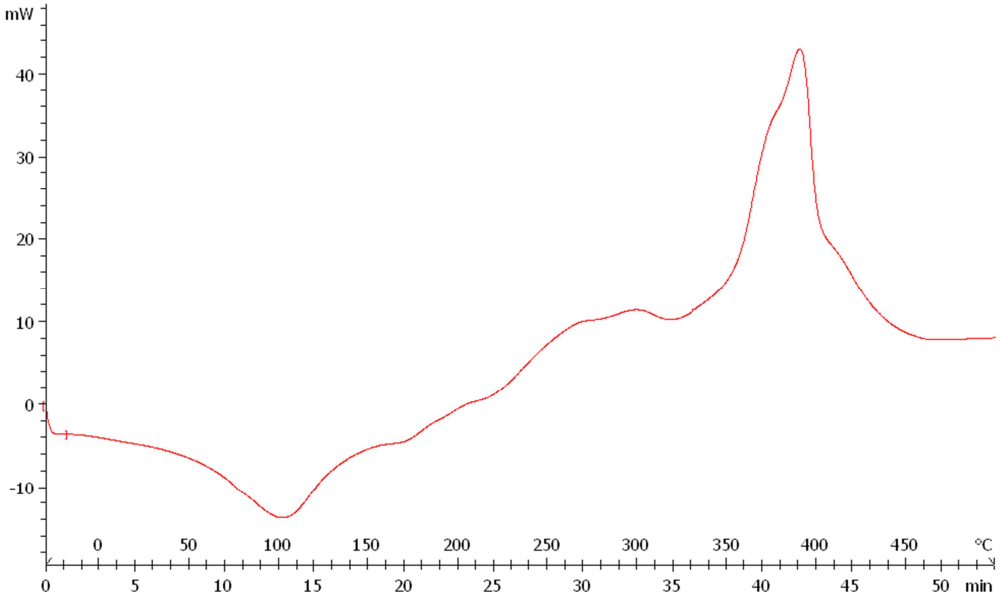


Figure 3.11: First run DSC thermogram of BP36 measured from -10ºC to 500ºC

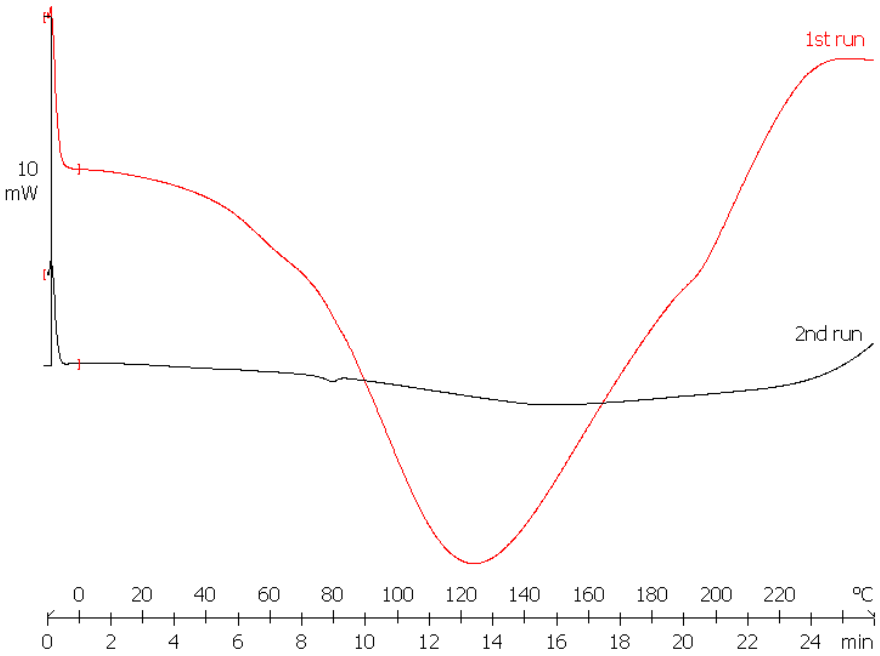


Figure 3.12: First and second run DSC thermograms of BP36 measured from -10ºC to 250ºC

Typical broad endothermic peaks were observed for MUC at 111.100°C and PEC_{USP} at 105.280°C (Sharma and Ahuja 2011). MUC-PEC_{USP} blends conformed to the same outline with melting point peaks becoming broader and shifting towards the left as the MUC:PEC_{USP} ratio changed from 1:9 through 1:4 to 1:1. The melting temperature (T_m) and the heat of fusion (ΔH_m) of the MUC-PEC_{USP} blend increased with the content of PEC_{USP} as depicted in Figure 3.13 and table 3.2.

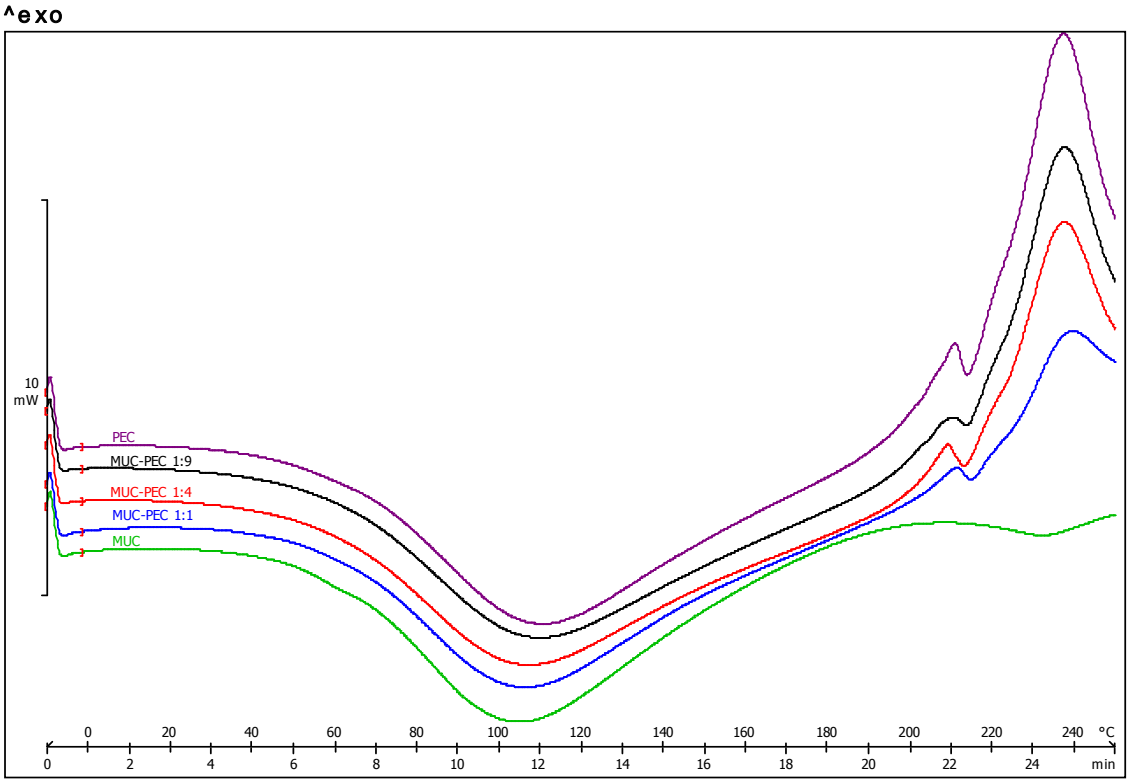


Figure 3.13: DSC thermogram of; MUC, MUC-PEC_{USP} (ratio 1:1, 1:4 and 1:9) and PEC evaluated from -10°C to 250°C.

Table 3.2: Midpoint melting point and heat of fusion of different MUC:PEC_{USP} weight and volume fractions.

MUC:PEC_{USP} weight ratio	1:0	1:1	1:4	1:9	0:1
Φ_1	1.000	0.318	0.104	0.050	0.000
ϕ_2	0.000	0.682	0.896	0.950	1.000
Peak T_m/ °C	105.280	106.630	107.280	109.770	111.100
ΔH_m/Jg^{-1}	207.580	206.500	212.190	222.810	250.290

To determine the miscibility and interaction of MUC and PEC_{USP} by differential scanning calorimetry (DSC) using the melting point depression, the Flory-Huggins lattice theory and Nishi-Wang theory of thermodynamics were employed (Harris et al., 1983; Xie et al., 2002).

Equation 3.5 and 3.6 related to the thermodynamic relationship of the melting point depression of MUC, PEC_{USP} and MUC-PEC_{USP} according to the Nishi-Wang theory. Equation 3.7 gives *B*, the MUC-PEC_{USP} interaction energy density.

$$T_m = T_m^0 + T_m^0 (V_2/\Delta H_2) B\phi_1^2 \qquad \textit{Equation 3.5}$$

$$T_m = T_m^0 + T_m^0 (V_2/\Delta H_2) B (1-\phi_2)^2 \qquad \textit{Equation 3.6}$$

$$B = (\chi_{12} TR)/V \qquad \textit{Equation 3.7}$$

Where, T_m and T_m^0 are the melting temperatures of PEC_{USP} in the blend and pure PEC_{USP} respectively. V_1 and V_2 are the corresponding molar volumes of MUC and PEC_{USP} whilst ϕ_1 and ϕ_2 are volume fractions of MUC and PEC_{USP} respectively, where $\phi_1+\phi_2=1$. *R* is the molar gas constant, *T* is the absolute temperature and χ_{12} is the Flory-Huggins interaction parameter computed at 25°C. ϕ_1 and ϕ_2 were computed from the mass of MUC and PEC_{USP} used to prepare the blends and their respective densities (ρ_{MUC})~1.500gmL^{-1} and ($\rho_{PEC\text{-}USP}$)~0.7gmL^{-1} (Nordman et al., 1997). V_1 and V_2 were calculated from the average molecular weights and the densities of MUC ($M_{w\text{-}MUC}$~22 000 000 gmoL^{-1}) and PEC_{USP} ($M_{w\text{-}PEC\text{-}USP}$~125 000 000 gmoL^{-1}). Table 3.3 displays calculated values of the MUC-PEC_{USP} interaction energy density (*B*) and the Flory-Huggins interaction parameter, χ_{12}, of the three different ratios of MUC-$PEC_{USP.}$ The χ_{12} values for the MUC:PEC_{USP} ratios examined were all negative which indicated that aqueous dispersions of MUC and PEC_{USP} were miscible as a result of possible macromolecular interactions such as hydrogen bonding of hydroxyl and carboxyl groups in both macromolecules and the amine and amide groups of the MUC. The more negative the χ_{12} value was, the stronger the interactions between MUC and PEC_{USP}.

The data in table 3.2 showed that macromolecular interactions between MUC and PEC_{USP} strengthened with decreasing MUC:PEC_{USP} ratio (from 1:1 through 1:4 to 1:9) and this may be explained by the fact that the MUC is a larger macromolecule as compared to PEC_{USP} hence one MUC macromolecule could accommodate and interact with more than one PEC_{USP} macromolecule. MUC, with its bottle brush structure had carbohydrate side-chains whose hydroxyl and carboxyl groups were available to interact via hydrogen bonding with those of PEC_{USP} (Patel et al., 2003; Bansil and Turner, 2006). The trend in the χ_{12} value from MUC:PEC_{USP} 1:1 through 1:4 to 1:9 revealed that although the macromolecular interactions became strengthened gradually, MUC it appears would reach a point of saturation with the number of PEC_{USP} macromolecules that it would able to interact with. Determination of the

optimum MUC:PEC_{USP} ratio was not the subject of this study however this trend revealed and may have resulted from the increased steric hindrance and depletion of interaction functional groups as consequence of the increase in the number of PEC_{USP} molecules.

Table 3.3: Thermodynamic interaction energy density (*B*) and the Flory-Huggins interaction parameter (χ_{12}) which were determined at 25°C of MUC-PEC_{USP} blends at different MUC:PEC_{USP} ratio; 1:1, 1:4 and 1:9.

MUC:PEC_{USP}	*B*/Jcm^{-3}	χ_{12}
1:1	- 4.607x10^{-4}	- 2.726
1:4	- 34.225x10^{-4}	-20.250
1:9	- 49.790x10^{-4}	-29.459

3.3.5. Ultraviolet spectrophotometry analysis

Both MUC and PEC could be dispersed in deionized water; however the ease and extent at which they dispersed or solubilised varied depending on their molecular structures, the type of functional groups they possessed and how these functional groups interacted with water molecules. The ultraviolet spectroscopic experiment measured the amount of UV light absorbed by the dispersed MUC and PEC macromolecules. The more the macromolecule was solubilized the less the UV light it absorbed. MUC was shown to be less soluble in deionized water than PEC_{USP} as presented in table 3.3. MUC:PEC_{USP} (1:0) absorbed more UV light than MUC-PEC_{USP} (0:1) and as the weight fraction of MUC in the aqueous dispersions was increased there was an increase in UV absorbance.

MUC as a glycoprotein has hydroxyl and carboxylic groups on the branched carbohydrate side chains as well as amine and amide groups in its protein core (Dekker et al., 2002; Bransil and Turner, 2006). These groups were involved in hydrogen bonding with water molecules leading to solubilization. However, MUC's protein core which was mostly hydrophobic prevented complete solubilization and led to conformational changes in MUC with folds being formed to protect its hydrophobic regions. This resulted in the formation of a MUC random coil that had greater absorbance of UV when dispersed in deionized water than PEC_{USP}, which has hydroxyl and carboxylic groups that interact with water molecules to form hydrogen bonds that aid in solubilization. This phenomenon is comparable to a micelle system that appears clear visually as a result of the hydrophobic core being encapsulated in the hydrophilic outer layer. Conversely, the PEC_{USP} macromolecules are much smaller, are linear and have no major hydrophobic moiety which made them more approachable by water molecules as compared to MUC macromolecules. This is reflected in table 3.4 by the lower

UV absorbance value of the aqueous dispersion of pristine PEC_{USP} (MUC-PEC_{USP}::0:1) as compared to that of pristine MUC (MUC:PEC_{USP}1:0).

Table 3.4: UV absorbance of dilute aqueous dispersions of MUC, PEC and MUC-PEC combinations

MUC:PECratio	PEC	MUC	MUC-PEC	Δ*A*
	A_{PEC}	A_{MUC}	$A_{MUC-PEC}$	
MUC:PEC_{USP}1:0	0.084±0.008	0.000±0.000	0.084±0.004	0.000±0.000
MUC:PEC_{USP} 1:9	0.070±0.001	0.064±0.001	0.168±0.010	0.034±0.008
MUC:PEC_{USP} 1:4	0.067±0.008	0.074±0.009	0.303±0.003	0.162±0.009
MUC:PEC_{USP}1:1	0.037±0.009	0.348±0.009	0.511±0.002	0.126±0.009
MUC:PEC_{USP}4:1	0.009±0.002	0.547±0.007	0.631±0.009	0.075±0.006
MUC:PEC_{USP}9:1	0.002±0.000	0.569±0.004	0.579±0.002	0.008±0.001
MUC:PEC_{USP}0:1	0.000±0.000	0.630±0.000	0.630±0.006	0.000±0.000
MUC:PEC_{AS}1:4	0.028±0.006	0.074±0.009	0.121±0.001	0.019±0.006
MUC:PEC_{AS-FS} 1:4	0.036±0.005	0.074±0.009	0.120±0.004	0.010±0.004

Data expressed as mean values (± SD); n = 3.

$A_{MUC-PEC}$ – UV absorbance of MUC-PEC aqueous dispersions

A_{PEC} – UV absorbance of aqueous PEC

A_{MUC} – UV absorbance of aqueous MUC

UV absorbance was measured at 600nm where neither MUC nor PEC has their λ max

Dispersing MUC and PEC together in deionized water may lead to intermolecular and intramolecular hydrogen and electrostatic interactions between the two macromolecules that may alter solubilization of the macromolecules and hence UV absorbance. In this study, the absorbance difference (Δ*A*) was used as a parameter to signify the presence and extent of molecular interactions between MUC and PEC. Δ*A* was computed as the difference in the UV absorbance of the MUC-PEC dispersion and the summation of the UV absorbance of individual dispersions of MUC and PEC as in Equation 3.1. A positive value for Δ*A* signified UV absorbance synergy. The extra UV absorbance may be attributed to the intermolecular interactions between MUC and PEC (Cai and Arntfield, 1997). It can be asserted that MUC and PEC would have formed hydrogen bonds, interpenetrated and electrostatically interacted with each other, in addition to interacting with the surrounding water molecules, leading to a decrease in solubility and thus an increase in UV absorbance.

Table 3.4 shows that Δ*A* values for all MUC-PEC combinations were positive. This signified the occurrence of intermolecular interactions between MUC and PEC that are stronger than

either macromolecule's interactions with water molecules. These intermolecular interactions included hydrogen bonding, chain interpenetration and electrostatic interactions as explained further in the molecular mechanics section. Δ*A* changed with the change in MUC:PEC_{USP} ratio. According to results shown in table 3.4, Δ*A* generally increased with the change in MUC:PEC_{USP} ratio from 1:0 through 1:4 and 1:9 to 0:1. However, MUC:PEC_{USP} 1:4 showed the greatest absorbance as compared to ratios 1:0, 1:1, 1:9 and 0:1. In general, more than one PEC_{USP} molecule may interact with one MUC molecule given MUC's multiblock copolymer structure, size and potential functional groups capable of intermolecular interactions. Although this study's aim was not to find out the optimum number of PEC_{USP} molecules that could potentially interact with MUC in aqueous media, the results revealed that there may be a certain ratio that would result in optimum MUC-PEC_{USP} interactions to give a stable polyelectrolyte. In this experiment the MUC:PEC_{USP} ratio 4:1 resulted in the greatest intermolecular interactions.

A Δ*A* comparison was made of three different types of pectin; PEC_{USP}, PEC_{AS} and $PEC_{AS\text{-}FS}$ which had different degrees of esterification (DE) and degrees of amidation (DA) at a MUC:PEC ratio of 4:1. It was found that *ΔA* increased with an increase in the degree of esterification in the order $PEC_{AS\text{-}FS}$ (DE 28%)<PEC_{AS}(DE 35%)<PEC_{USP} (DE 65%). Δ*A* increased with a decrease in the degree of amidation in the order $PEC_{AS\text{-}FS}$ (DA 20%)<PEC_{AS} (DA 15%)<PEC_{USP} (DE 0%). The higher PEC was esterified, the more it interacted with MUC and this may have been a result of the predominance of macromolecular chain interpenetration between MUC and PEC when PEC had more ester side groups leading to the formation of an IMN. The corresponding ester side-groups are aliphatic groups which are hydrophobic and thus can interact with the hydrophobic part of MUC to form more stable MUC-PEC interpenetrating networks. This decreased the aqueous solubility of the macromolecules and increased the UV absorbance of their aqueous dispersions. Amidation added to the hydrophilicity of PEC thus increased its hydrophilic interaction with water molecules and PEC, resulting in increased solubility and decreased UV absorbance as observed in the $PEC_{AS\text{-}FS}$ (DA 20%)<PEC_{AS}(DA 15%)<PEC_{USP} (DE 0%) trend.

3.3.6. Rheological characterization of porcine gastric mucin (MUC), pectin (PEC) and their respective combination aqueous dispersions

The viscosity of the aqueous PEC dispersion was found to be greater than that of MUC for all the three different types of PEC studied (Table 3.5). The viscosity of MUC-PEC_{USP} increased as the ratio of MUC-PEC_{USP} changed from 1:1 through 1:4 to 1:9 signifying the major role played by PEC_{USP} in the overall viscosity of the MUC-PEC_{USP} combination. In addition, the viscosities of the three different types of pectin were in the order of MUC-PEC_{USP}>MUC-PEC_{AS-FS}>MUC-PEC_{AS} which meant that highly esterified pectin PEC_{USP} (DE 65%) underwent stronger molecular interactions with MUC. This corroborated well with the previously reported work by Thirawong and co-workers, where they observed that the more pectin became esterified the higher its molecular weight became and this in-turn increased its interactions with MUC. PEC_{AS} (DE 35%) and PEC_{AS-FS} (DE 28%) are both low methoxy pectin types therefore their molecular weights are much smaller than that of the higher methoxy pectin type PEC_{USP}, thus translating to lower molecular interactions with MUC as compared to PEC_{USP} (Thirawong et.al., 2008). One would expect MUC-PEC_{AS} to have shown a greater viscosity than MUC-PEC_{AS-FS} because of its higher DE, however the opposite was observed in this study.

The greater viscosity of MUC-PEC_{AS-FS} as compared to MUC-PEC_{AS} may be explained by the higher degree of amidation of MUC-PEC_{AS-FS} (DA 20%) as compared to MUC-PEC_{AS} (DA 15%). The amide groups in the low methoxy pectin types might have taken part in hydrogen bonding with the hydroxyl, carboxyl, amine and amide groups present in MUC, therefore the greater the DA, the more the pectin interacted with the MUC which translated into a higher viscosity for MUC-PEC_{AS-FS} as compared to MUC-PEC_{AS-FS}. The viscosity difference ($\Delta\eta$), which was regarded as the difference between the viscosity of the MUC-PEC dispersion and the sum of the individual viscosities of MUC and PEC dispersions, was greater than zero for all MUC-PEC ratios studied and for all the three different pectin types used (Sriamornsak and Wattanakorn, 2008; Thirawong et al., 2008). This signified that there was viscosity enhancement and thus rheological synergy when MUC and PEC were co-dispersed in deionized water. The enhancement in viscosity could be regarded as a result of the macromolecular interactions between MUC and PEC to produce a stronger gel (Hassan and Gallo, 1990; Rossi et al., 1995; Thirawong et al., 2008).

Table 3.5: Viscosity of MUC-PEC dispersions of three different pectin types at different MUC: PEC ratios

MUC:PEC ratio	PEC	MUC	MUC-PEC	$\Delta\eta$
	Viscosity	Viscosity	Viscosity	
	η_{PEC}	η_{MUC}	$\eta_{MUC\text{-}PEC}$	
MUC:PEC_{USP}1:9	151.738±0.144	1.687±0.042	179.625±0.274	22.200
MUC:PEC_{USP}1:4	101.733±0.899	2.635±0.056	141.671±0.761	37.306
MUC:PEC_{USP}1:1	29.586±0.056	8.008±0.055	93.188±0.144	55.406
MUC:PEC_{AS}1:4	51.690±0.076	2.635±0.056	83.290±0.537	28.965
MUC:$PEC_{AS\text{-}FS}$1:4	46.640±0.066	2.635±0.056	96.941±0.217	47.135

3.3.7. Effect of plasticizer (PEG 400) and calcium ions on the viscosity and dynamic moduli of dilute MUC-PEC_{USP} aqueous dispersions

Rheology data obtained from performing viscosity and dynamic oscillatory rheology tests on MUC-PEC_{USP} aqueous dispersions showed that the viscosity, the storage, and the loss moduli of MUC-PEC_{USP}; decreased on addition of PEG 400 ($1\%^{v}/_{v}$), increased on crosslinking with calcium ions and further increased on addition of both PEG 400 and subsequent crosslinking with calcium ions. Table 3.6 reveals that the values of the viscosity difference ($\Delta\eta$) were positive when; PEG 400 was employed, after crosslinking with Ca^{2+} and when PEG 400 was added with subsequent crosslinking with Ca^{2+}. This demonstrated the occurrence of rheological enhancement when MUC and PEC_{USP} were co-dispersed as compared to the individual rheology characteristics.

Table 3.6 and figure 3.15 revealed that (η) and ($\Delta\eta$) of PEG-MUC-PEC_{USP} were less than that of MUC-PEC_{USP}. PEG 400 being a non-ionic polymer did not interact electrostatically with neither MUC nor PEC_{USP}, instead it may have adsorbed onto the surfaces of MUC and PEC_{USP} reducing their charge distribution and intensity which might have lowered the rheology parameters such as viscosity. The PEG 400 effect on MUC-PEC_{USP} dispersions was not shown to cause the "depletion effect" commonly reported and employed in biochemistry to precipitate and extract proteins (Wang and Annunziata, 2007). This is when PEG 400 was expected to attract water molecules away from MUC-PEC_{USP} thereby increasing MUC PEC macromolecular interactions which would have been observed as an increase in viscosity and dynamic moduli. Another possible explanation is that PEG 400 might have drawn water molecules away from MUC-PEC_{USP} which in turn reduced the mobility of MUC and PEC_{USP} macromolecular chains leading to a decrease in macromolecular interpenetration.

In addition, the two macromolecules were dispersed in aqueous media at neutral pH resulting in them carrying similar charges. Therefore, by depleting the surrounding water macromolecules the macromolecules would be brought closer together and this may have caused some electrostatic repulsion since at neutral pH both MUC and PEC_{USP} may have ionized carboxyl groups causing electrostatic repulsion of the two macromolecules, manifesting in a decrease in macromolecular interactions and hence lowering of viscosity and the dynamic moduli. PEG 400 may lie in between the MUC and PEC_{USP} chains and this might have sterically hindered macromolecule's mobility which resulted in decreased macromolecular interactions.

Table 3.6: Viscosity of MUC-PEC_{USP}: effect of addition of PEG 400 and crosslinking with calcium ions on aqueous dispersions of MUC-PEC_{USP} at MUC: PEC_{USP} ratio 9:1.

MUC:PEC ratio	MUC	PEC	MUC-PEC	$\Delta\eta$
	η_{MUC}	η_{PEC}	$\eta_{MUC\text{-}PEC}$	
MUC	2.138 ± 0.084	n/a	2.138 ± 0.084	
PEC_{USP}	n/a	168.662 ± 1.402	168.662 ± 1.402	
MUC-PEC_{USP}			196.440 ±1.688	25.640
PEG-MUC-PEC_{USP}			189.559 ± 1.378	18.759
cl-MUC-PEC_{USP}			211.798 ± 0.854	40.998
cl-PEG-MUC-PEC_{USP}			225.912 ± 1.331	55.112

Crosslinking MUC-PEC_{USP} in the neutral aqueous media using Ca^{2+} caused an increase in (η) and ($\Delta\eta$). Divalent cations like Ca^{2+} have been reported to interact with mucin via electrostatic interactions, particularly in neutral and basic media when the sialic acid groups found in mucin are ionized. This would cause the MUC to attain an aggregated structure (Espinosa et al., 2002). PEC_{USP} has ionized carboxyl groups at neutral pH capable of partaking in electrostatic interactions with Ca^{2+} resulting in an egg-box conformational structure (Braccini and Péres, 2001). Thus calcium ions at neutral pH cause electrostatic homo-crosslinking of MUC and PEC_{USP} leading to an increased MUC-PEC_{USP} gel strength and enhanced rheology parameters such as viscosity and the dynamic moduli as shown in figures 3.15 and 3.16 as well as in tables 3.5 and 3.6. The homo-crosslinking of MUC and PEC upon addition of Ca^{2+} created an IMN whereby the classic egg-box pectin network was intricately entangled with the MUC aggregated network, creating a thermodynamically stable macromolecular network that yielded synergistic characteristics exemplified by the

enhancement of the viscosity in table 3.5 and figure 3.15, as well as the synergistic increase in dynamic moduli as shown in table 3.7 and figure 3.16.

The addition of PEG 400 and then crosslinking with calcium ions caused a marked increase in viscosity and dynamic moduli and this might have been due to PEG adsorbing on MUC and PEC_{USP} surfaces causing the macromolecules to be more flexible for interpenetration as well as depleting the surrounding water molecules. In the presence of Ca^{2+} there was enhanced electrostatic interactions that caused the rheological synergy observed. Incorporation of PEG 400 and the subsequent addition of Ca^{2+} created a IMN that corresponded to a pseudo interpenetrating network (PDIPN) whereby PEG 400 remained linear whilst MUC and PEC were electrostatically crosslinked around it resulting in an entanglement with further enhancement in rheology characteristics than those of the Ca^{2+} crosslinked MUC-PEC IMN without PEG 400 as illustrated in table 3.7 and figure 3.16. The MUC-PEC interactions, as measured by rheological synergy were previously studied, therefore this study confirms and expands on their work (Hassan and Gallo, 1990; Mortazavi, 2003; Liu et al., 2005; Thirawong et al., 2008; Sriamornsak and Wattanakorn, 2008)

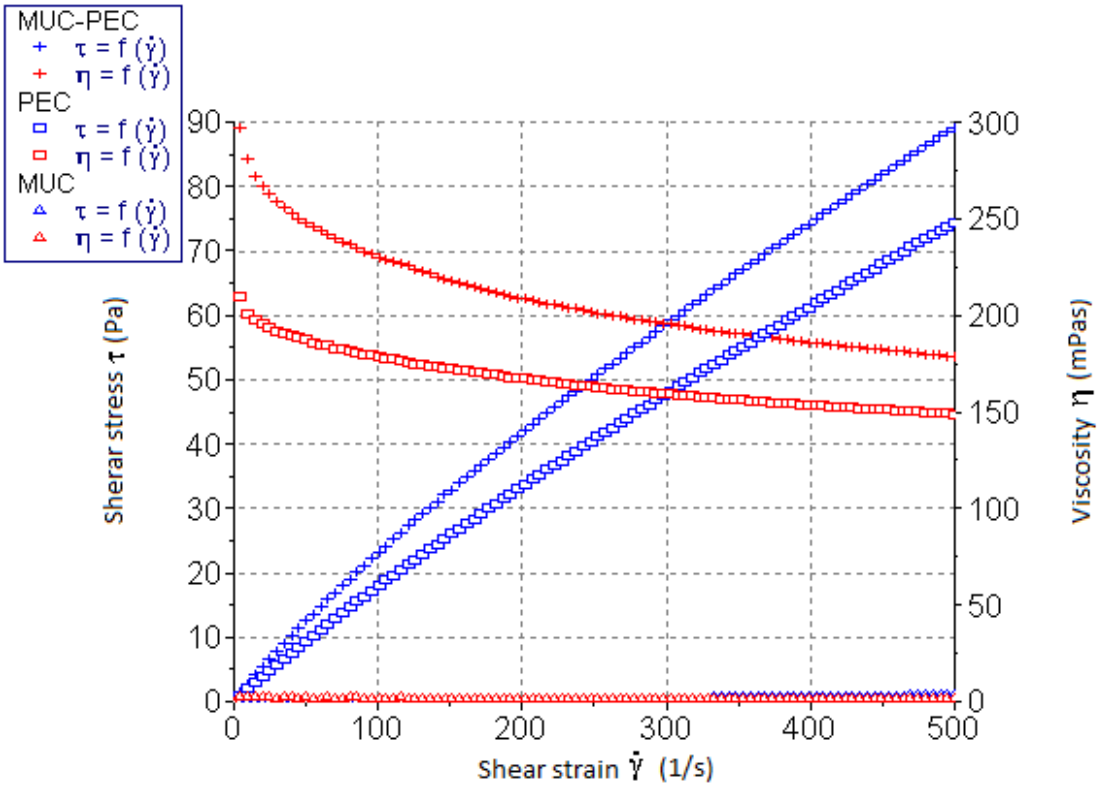


Figure 3.14: Rheology profile properties of MUC, PEC_{USP} and MUC-PEC_{USP} 9:1 illustrating non-Newtonian shear thinning (pseudoplastic) flow and rheological synergism.

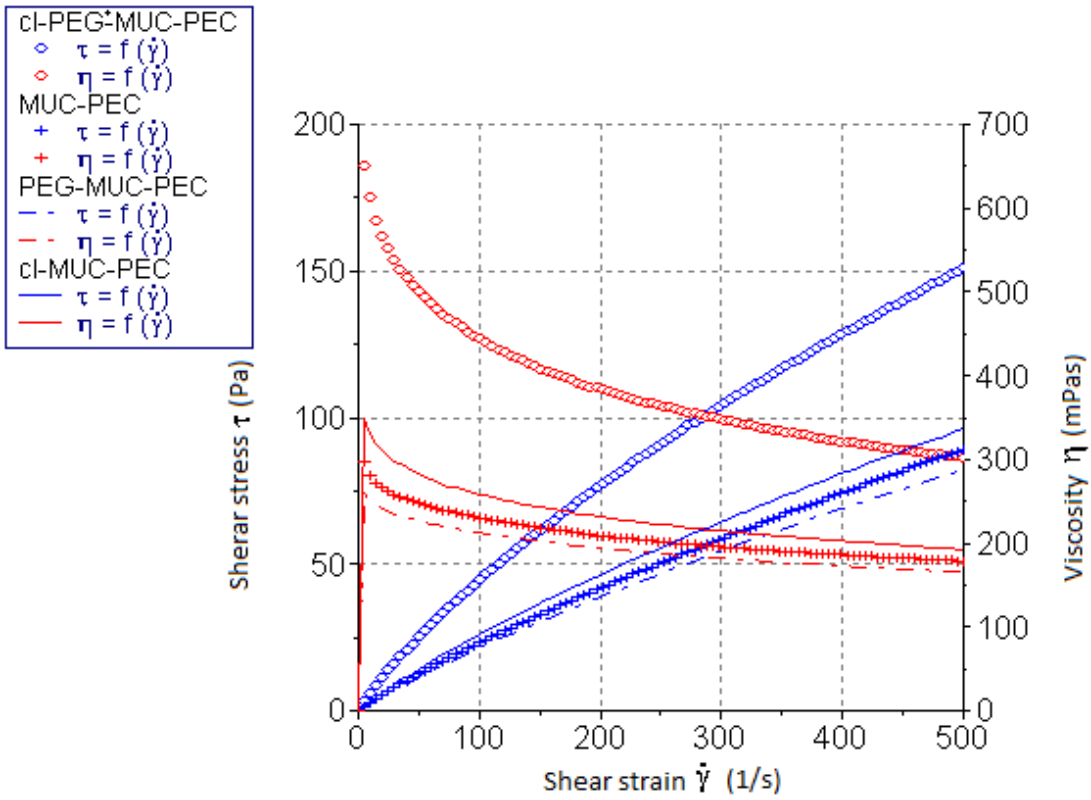


Figure 3.15: Rheological pseudoplastic flow and viscosity profiles of MUC, PEC_{USP} and MUC-PEC_{USP} 9:1 illustrating the effect of addition of PEG 400 and crosslinking with calcium ions on viscosity.

Table 3.7: Effect on dynamic moduli of PEG 400 and crosslinking with calcium ions

Dispersed components	Dynamic moduli	
	Storage modulus (*G*')	Loss modulus (*G*'')
MUC	0.002± 0.000	0.031± 0.003
PEC_{USP}	0.034 ± 0.002	0.515 ± 0.016
MUC-PEC_{USP}	0.035 ± 0.001	0.593 ± 0.027
PEG-MUC-PEC_{USP}	0.036 ± 0.005	0.584 ± 0.033
cl-MUC-PEC_{USP}	0.050 ± 0.004	0.654 ± 0.064
cl-PEG-MUC-PEC_{USP}	0.149 ± 0.011	0.808 ± 0.073

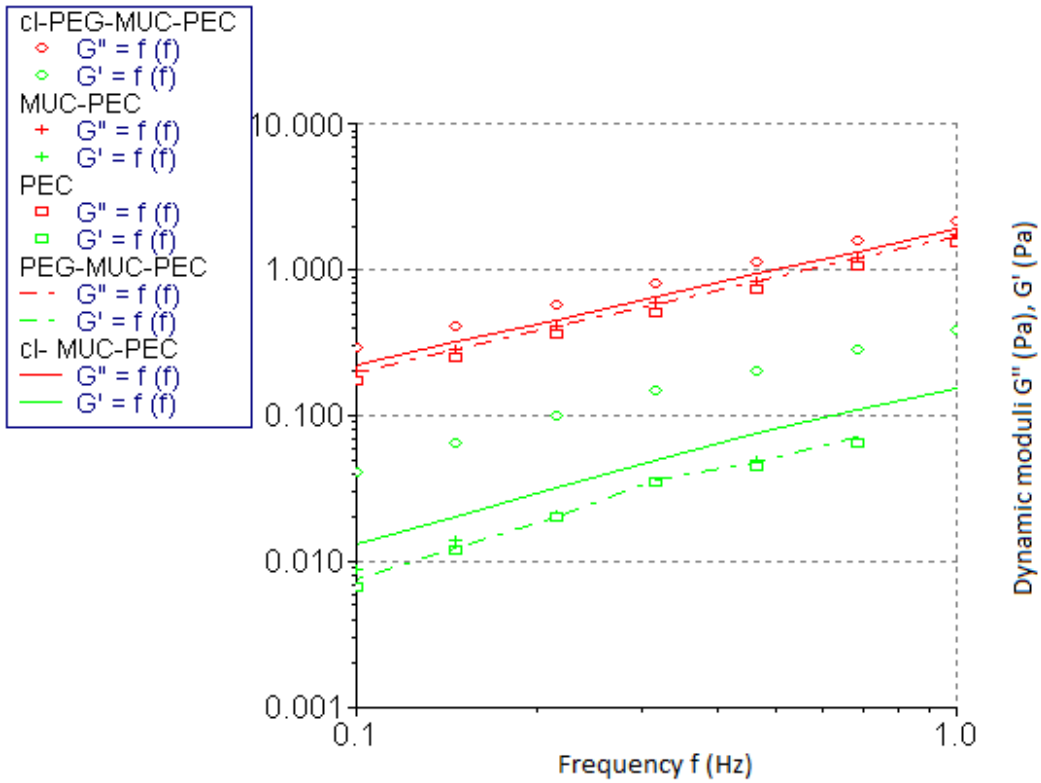


Figure 3.16: Effect on dynamic moduli of PEG 400 and crosslinking with calcium ions as measured by dynamic oscillatory rheology

3.3.8. Molecular mechanics assisted model building and energy refinements

A molecular mechanics conformational searching procedure was employed to acquire the data employed in the statistical mechanics analysis, and to obtain differential binding energies of a Polak–Ribiere algorithm, as well as to potentially permit application to macromolecular composite assemblies. MM+ is a HyperChem modification and extension of Norman Allinger's Molecular Mechanics program MM2 (Warhurst et al., 2003), whereas AMBER is a package of computer programs for applying molecular mechanics, normal mode analysis, molecular dynamics and free energy calculations to simulate the structural and energetic properties of molecules (Pearlman et al., 1995)

3.3.9. MMER analysis

Molecular mechanics energy relationship (MMER), a method for analytico-mathematical representation of potential energy surfaces, was used to provide information about the contributions of valence terms, non-covalent coulombic terms, and non-covalent van der Waals interactions for polysaccharide/mucopolysaccharides interactions. The MMER model for potential energy factor in various molecular complexes can be written as:

$$E_{molecule/complex} = V_{\Sigma} + V_b + V_{\Theta} + V_{\varphi} + V_{ij} + V_{hb} + V_{el} \qquad \textit{Equation 3.8}$$

where, V_{Σ} is related to total steric energy for an optimized structure, V_b corresponds to bond stretching contributions (reference values were assigned to all of a structure's bond lengths), V_{Θ} denotes bond angle contributions (reference values were assigned to all of a structure's bond angles), V_{φ} represents torsional contribution arising from deviations from optimum dihedral angles, V_{ij} incorporates van der Waals interactions due to non-bonded interatomic distances, V_{hb} symbolizes hydrogen-bond energy function and V_{el} stands for electrostatic energy.

In addition, the total potential energy deviation, ΔE_{Total}, was calculated as the difference between the total potential energy of the complex system and the sum of the potential energies of isolated individual molecules, as follows:

$$\Delta E_{Total} = \Delta E_{Total\ (MUC\text{-}PEC)} - [\Delta E_{Total\ (MUC)} + \Delta E_{Total\ (PEC)} \qquad \textit{Equation 3.9}$$

The molecular stability can then be estimated by comparing the total potential energies of the isolated and complexed systems. If the total potential energy of a complex system is smaller than the sum of the potential energies of isolated individual molecules in the same conformation, the complexed form is more stable and its formation is favoured (Yu et al., 2008). In the present SLAS study, different concentrations of pectin in forms of increasing number of molecules were disposed in close vicinity of the glycoprotein to represent MUC:PEC ratios of 1:1 (MUC-PEC1), 1:2 (MUC-PEC2), 1:3 (MUC-PEC3), and 1:4 (MUC-PEC4) (Figure 3.17 and 3.18). The global energy relationships for the various complexes derived after assisted model building and energy refinements were as follows:

$$E_{MUC} = -166.812\ V_{\Sigma} = 5.474V_b + 70.351V_{\theta} + 55.173V_{\varphi} - 29.066V_{ij} - 7.096V_{hb} - 261.649V_{el}$$

Equation 3.10

$$E_{PEC} = 6.539\ V_{\Sigma} = 2.316V_b + 11.957V_{\theta} + 10.407V_{\varphi} + 13.335V_{ij} - 31.477V_{el} \qquad \textit{Equation 3.11}$$

$E_{MUC\text{-}PEC1}$= -222.143 V_{Σ}=8.556V_b + 111.66V_{θ} + 104.151V_{φ} – 45.460V_{ij} – 13.159V_{hb}-387.892V_{el}

[ΔE= -61.87kcal/mol] *Equation 3.12*

$E_{MUC\text{-}PEC2}$= -299.723 V_{Σ}= 10.725V_b + 132.77V_{θ} + 137.173V_{φ} – 61.557V_{ij} – 20.086V_{hb} – 498.747V_{el}

[ΔE= -139.45kcal/mol]… *Equation 3.13*

$E_{MUC\text{-}PEC3}$= -347.445 V_{Σ}= 14.440V_b + 151.128V_{θ} + 193.723V_{φ} – 54.800V_{ij} – 24.668V_{hb} - 27.268V_{el}

[ΔE= -187.172kcal/mol] *Equation 3.14*

$E_{MUC\text{-}PEC4}$= -385.041V_{Σ}= 20.132V_b + 170.443V_{θ} + 231.344V_{φ} – 55.159V_{ij} – 25.026V_{hb} - 26.775V_{el} [ΔE= -224.768kcal/mol] *Equation 3.15*

3.3.10. Elucidation of MUC and PEC molecular interactions and the simulation of a MUC-PEC submicrosphere

For the elucidation of the mechanism inherent to the MUC-PEC complex formation, invariant factors common to mathematical description of binding energy and substituent characteristics have been ignored. The monomer length for pectin was determined on the basis of equivalent grid surface area covered by the macromolecule so that the inherent stereo-electronic factors at the interaction site can be perfectly optimized at different concentrations. The set of low-energy conformers that were in equilibrium with each other was identified and portrayed as the lowest energy conformational model. Molecular modelling studies may account for specific interactions between macromolecular segments and provide an estimate whether the two macromolecules will form a stable combination (favourable interaction) by fulfilling the necessary condition of having a negative free energy of mixing (Tiller and Gorella, 1994).

As evident from equations 3.10-3.12, a potential and steric energy stabilization of -61.87kcal/mol was accompanied with the formation of MUC-PEC1. This confirmed the favourable formation and stability of the macromolecular complex in dried state. The energy computations involved significant contributions from the bonding interactions (towards destabilization) as well as non-bonding interactions (towards stabilization). While the bonding, angle and torsional contributions destabilized the complex by inflicting strains in the

polymeric architecture, hydrogen bonding, van der Waals forces and electrostatic energy tended to balance the strain resulting in a geometrically stabilized conformation.

The formation of MUC-PEC2, MUC-PEC3, and MUC-PEC4 displayed a further energy minimization with an increase in the number of pectin molecules interacting with mucin. An interesting trend was observed here. According to equations 3.10-3.15, bond stretching and bond angle contributions displayed an upward but small increment. However, the torsional energy played a significant role in destabilizing the macromolecular complex with large increase in inherent steric energy. Similarly, for non-bonding interactions, hydrogen bonding and van der Waals forces displayed downward small increments with the electrostatic interaction playing the major stabilizing role. The above findings can be summarized as follows:

1. The energy destabilization seemed inherent from rotation of saccharide and amino acid residues creating strain due to steric interactions and this strain was further aggravated by the inclusion of bond length and angle adjustment with respect to the degrees of freedom of the system.
2. The changes in macromolecular strain above may have led to the formation of H-bonds between pectin molecules and mucin, as displayed in figure 3.19. In addition, the steric interactions might have caused pendent functional groups of pectin (-OH and –COOH) and mucin (-OH, -COOH, and $–NH_2$) to overcome torsional barriers thus presenting a larger accessible potential energy surface.
3. The above two steps may have led to the formation of an interconnected macromolecular network structure that provided the necessary physicomechanical properties to the mucin-pectin complex (Kumar et al., 2011).
4. A close look at the equations 3.12-3.15 revealed a decrease in the difference in energy values between each subsequent addition of a pectin macromolecule. This implies that the addition of pectin may have reached a maximum after which further addition might not have made any significant contribution. This was corroborated by the experimental findings where mucin:pectin::1:9 proved to be the ratio that portrayed the maximum mucin-pectin interaction.

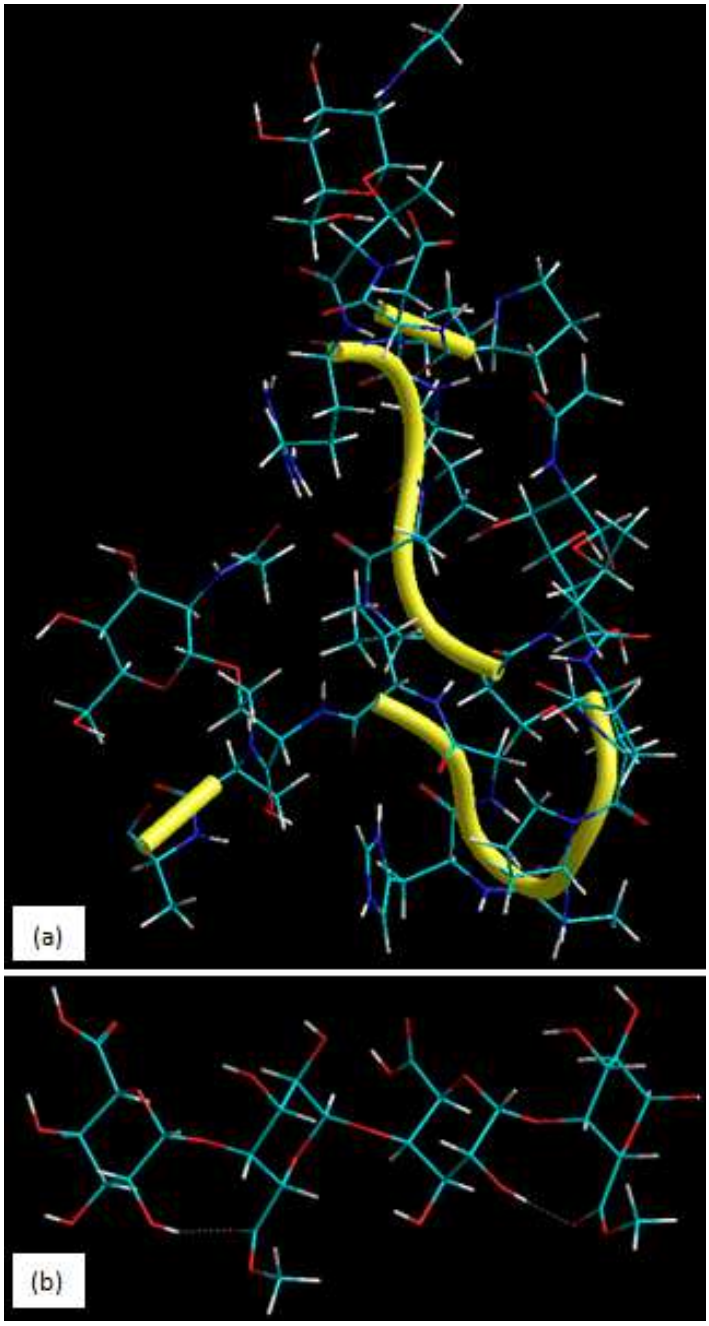


Figure 3.17: Energy minimized molecular structures of, (a) glycosylated MUC and (b) PEC generated by HyperChem^{TM} 8.0.8 Molecular Modeling System (Hypercube Inc., Gainesville, Florida, USA). Colour codes: C (cyan), O (red), N (blue) and H (white).

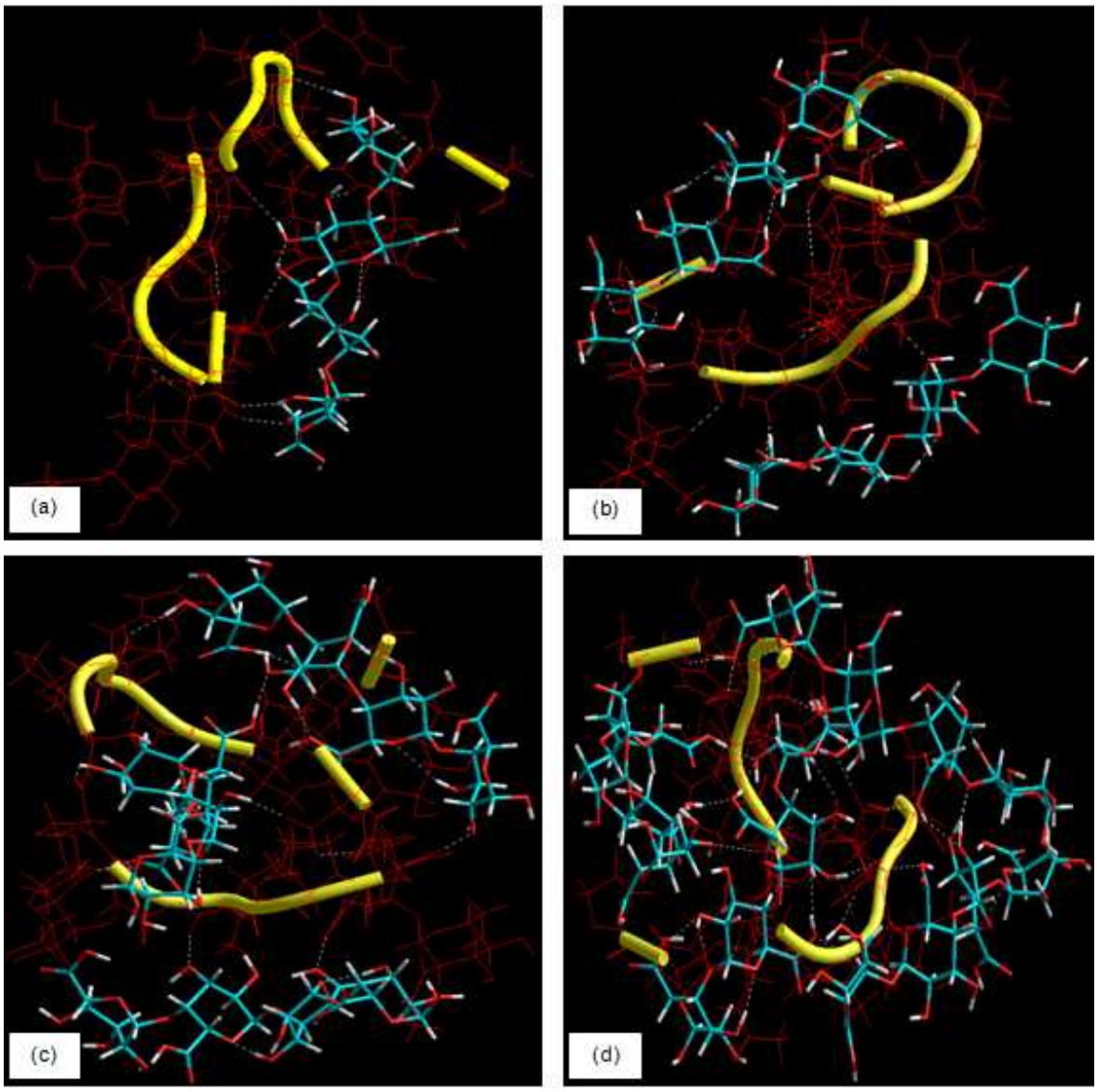


Figure 3.18: Visualization of geometrical preferences of; (a) MUC:PEC::1:1, (b) MUC:PEC::1:2, (c) MUC:PEC::1:3 and (d) MUC:PEC::1:4 along with H-bonds after molecular simulation in vacuum. MUC is rendered as stick model (red) with coiled (yellow) secondary structure. Colour codes: C (cyan), O (red), N (blue) and H (white).

The MUC PEC interaction energy was computed according to equation 3.16 and the MUC PEC interaction energy values for MUC:PEC ratios; 1:1, 1:2, 1:3 and 1:4 are provided in table 3.8. The interaction energy increased when the number of pectin molecules interating with one mucin molecule increased with the energy when the MUC:PEC ratio was 1:4 being the higest (Table 3.8). A further increase in the pectin molecules involved would probably increase the interaction energy between MUC and PEC. Connolly molecular electrostatic potential surfaces added to the simulated MUC PEC molecular interactions of the MUC:PEC ratio 1:4 (Figure 3.18d) revealed in wire mesh display mode a simulated microsphere (Figure

3.19). This in silico simulated microsphere is evidence that it is possible to form microspheres or submicrospheres using the macromolecules mucin and pectin.

$$\Delta E_{(x:y)} = V_{\Sigma\ MUC\text{-}PEC\ (x:y)} - (x.V_{\Sigma\ MUC} + y.V_{\Sigma\ PEC}) \qquad \textit{Equation 3.16}$$

Where; $\Delta E_{(x:y)}$ is the MUC PEC interaction energy of x molexules of MUC and y molecules of PEC, $V_{\Sigma\ MUC\text{-}PEC\ (x:y)}$ is the total potential energy of the MUC-PEC complex, $V_{\Sigma\ MUC}$ is the total potential energy of MUC and $V_{\Sigma\ PEC}$ is the total potential energy of PEC.

Table 3.8: Total potential energies of MUC, PEC, MUC-PEC and the MUC PEC interation energies at MUC:PEC ratios of; 1:1, 1:2, 1:3 and 1:4

MUC:PEC ratio	1:1	1:2	1:3	1:4
Total potential Energy of MUC, $V_{\Sigma\ mucin}$ (kcal/moL)	-1.668			
Total potential energy of PEC, $V_{\Sigma\ pectin}$ (kcal/moL)	6.540			
Total potential energy of MUC-PEC, $V_{\Sigma\ pectin\text{-}mucin\ (x:y)}$ (kcal/moL)	-222.143	-299.723	-247.446	-385.042
Total MUC PEC interaction energy, ΔE (kcal/moL)	-61.871	-139.451	-187.173	-224.679

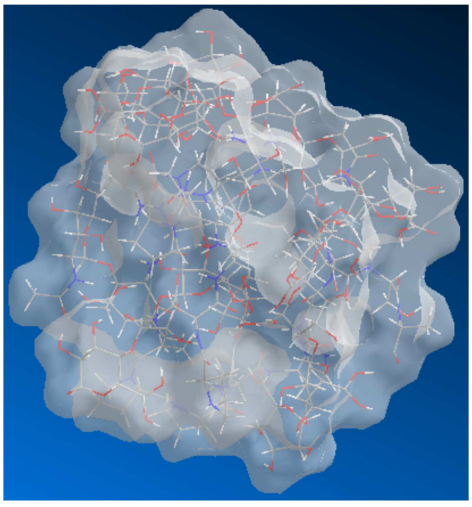


Figure 3.19: Connolly molecular electrostatic potential surfaces of a simulated submicrosphere in wire mesh display mode

In chapter 4 zidovudine loaded mucin-pectin-polyethylene glycol submicrospheres were formulated guided by the preformulation information devived from this chapter.

3.4. Concluding remarks

AT-FTIR spectroscopy, thermal and thermogravimetric characterisation of AZT and BP 36 were performed. All the techniques employed in this study demonstrated mucin-pectin interactions when the two macromolecules were co-dispersed in aqueous media. The interactions occurred in the form of hydrogen bonding, chain interpenetration, electrostatic interactions and also due to van de Waal's forces. The extent and strength of the interactions were shown to increase with the degree of esterification as well as when crosslinked with Ca^{2+} as a result of the formation of a MUC-PEC intermacromolecular network. The macromolecular interactions also decreased with an increase in the degree of amidation and upon addition of a plasticizer, PEG 400. Mucin-pectin interactions increased significantly on addition of PEG 400 and subsequently crosslinking using Ca^{2+} as a result of the formation of a MUC-PEC-PEG IMN that corresponds to a PDIPN. The ratio of mucin to pectin played a major role in their macromolecular interactions, with more and stronger macromolecular interactions observed on increasing the number of PEC macromolecules as compared to those of MUC in the aqueous dispersions. This was attributed to the relatively larger size of the MUC macromolecule compared to that of PEC, whereby the multi-oligosaccharide branches of mucin provided multiple hydroxyl and carboxyl functional groups to interact with pectin.

In addition, the formation of a MUC-PEC IMN and a MUC-PEC-PEG IMN on crosslinking with Ca^{2+} resulted in synergistic enhancement of the physicomechanical properties such as demonstrated in the rheological analysis in this chapter. These enhanced properties of the MUC-PEC IMN that results when both MUC and PEC are employed as biomaterials may be beneficially utilized in various pharmaceutical applications such as enhancing gel strength, increasing encapsulation efficiency of drugs and modulating drug release from different formulations including microspheres, nanoparticles, tablets, wafers and gels. However, MUC-PEC macromolecular interactions may also result in problems such as decreased permeability of drug and molecules through mucosal membranes where pectin and mucin would have formed an IMN barrier. A MUC-PEC microsphere was successfully simulated at a MUC:PEC ratio of 1:4. This chapter formed the basis for the *in vitro* experimentation performed in chapter 4, for the preparation of drug-loaded pectin-mucin-polyethylene glycol submicrospheres.

CHAPTER 4

FORMULATION AND CHARACTERIZATION OF DRUG LOADED PECTIN-MUCIN-POLY ETHYLENE GLYCOL SUBMICROSPHERES

4.1. Introduction

Focus on preventing vaginal HIV-1 transmission has led to the development of several different microbicides with a keen interest taken in using antiretroviral drugs as microbicides as given by their success in treating HIV/AIDS (Klaase et al., 2008). Although microbicides hold much promise and their concept is sound, clinical trials conducted up-to-date have failed to demonstrate efficacy (Hendrix et al., 2009). Several questions have been raised and some answers postulated to try and explain why anti-HIV-1 agents, effective *in vitro*, have mostly failed at different clinical stages. One common possible explanation given is that microbicide formulations did not take into consideration and did not address some fundamental anatomical, physiochemical and physiological principles involved in vaginal HIV-1 transmission. Such factors include; the presence of the anti-HIV-1 agent in appropriate quantities in the vaginal cavity where it has to be distributed extensively and exhaustively on the vaginal epithelia and having the microbicide stay at the site for a longer duration than HIV-1 (Hendrix et al., 2009).

Various formulations have been prepared to try and mitigate these concerns, among them; gels, creams, films, tablets and rings (Hendrix et al., 2009). This chapter focuses on the formulation of drug-loaded macromolecular submicrospheres (SMs) which are to be embedded within a polymeric drug delivery system in the form of a caplet as a potential microbicide drug delivery system. The submicrospheres were formulated from biocompatible materials; pectin, porcine gastric mucin and polyethylene glycol. These polymers formed the framework structure of the submicrospheres, enabling the encapsulation and controlled release of the anti-HIV-1 agent (zidovudine, one of the model antiretroviral agents used in this study). The submicrospheres were envisaged to be pH responsive and to have the ability to extend drug release by approximately 24 hours. In addition, the submicrospheres would also serve as reservoir units for the anti-HIV-1 agent, thus ensuring that there would be enough of the anti-HIV-1 agent available for the entire duration of use of the microbicide formulation.

4.2. Materials and Methods

4.2.1. Materials

Commercial grade pectin (PEC), GENU® pectin type USP/100 [Degree of esterification (DE) 55-65%] was purchased from CP Kelco ApS, Lille Skensved, Denmark. Porcine gastric mucin type III (MUC) with 1-1.5% bound sialic acid and polyethylene glycol of M_w 400 (PEG) were purchased from Aldrich® (Sigma–Aldrich Inc., St. Louis, USA). The model anti-HIV-1 active pharmaceutical ingredient (API), zidovudine (AZT), was purchased from GlaxoSmithKline, Middlesex, UK. Other materials and excipients including; calcium chloride and cyclohexane were of analytical grade and were utilized as purchased. Simulated vaginal fluid (SVF, pH 4.5) was prepared from analytical grade reagents in accordance to Owen and Katz's formulation (Owen and Katz, 1999).

4.2.2. Box-Behnken design optimization for the preparation of AZT-loaded PEC-MUC-PEG SMs

A three-factor, three-level (3^3) Box-Behnken statistical design on MINITAB® (V14, State College, Pennsylvania, USA) was employed to optimize the preparation of AZT-loaded MUC-PEC-PEG SMs (Karnachi and Khan, 1996; Box and Behnken, 1960). Upper and lower levels of three independent parameters that included; ultrasonication time (ST), surfactant concentration (SC) and drug:polymer (D:P) ratio were chosen due to their high significance in the fabrication of the SMs. The dependent parameters or responses that comprised; particle size (PS), zeta potential (ZP) and mean dissolution time (MDT) were sought, as presented in table 4.1. Fifteen formulations were generated from the Box-Behnken design (Table 4.2). These formulations were prepared and experimentally tested and the results obtained were fed into the MINITAB® design software which were then computed the optimized formulation's independent parameter and expected response values.

Table 4.1: Independent parameters and responses from the Box-Behnken statistical design used to optimize AZT-loaded PEC-MUC-PEG SMs

Independent parameter	Levels	
	Lower	Upper
ultrasonication time (min)	5	10
surfactant concentration %($^{v}/_{v}$)	1.5	2
drug:polymer ratio	0.5	1
Response	Objective	
particle size (nm)	minimize	
zeta potential (mV)	minimize	
mean dissolution time (hours)	maximize	

Table 4.2: Formulations generated using a Box-Behnken statistical design for the optimization of AZT-loaded PEC-MUC-PEG SMs

Formulation number	Ultrasonication time (min)	Surfactant concentration % ($^{v}/_{v}$)	Drug:polymer ratio
1	10	1.75	0.5
2	10	1.5	0.75
3	5	1.5	0.75
4	10	2	0.75
5	5	2	0.75
6	7.5	2	1
7	5	1.75	1
8	7.5	1.75	0.75
9	7.5	1.75	0.75
10	10	1.75	1
11	7.5	1.5	0.5
12	5	1.75	0.5
13	7.5	1.5	1
14	7.5	2	0.5
15	7.5	1.75	0.75

4.2.3. *In vitro* preparation of AZT-loaded PEC-MUC-PEG SMs.

AZT-loaded PEC-MUC-PEG SMs where prepared using a crosslinking-emulsion technique. PEC, MUC, PEG and AZT(300mg) were subsequently dispersed and dissolved in MilliQ water obtained from a MilliQ® gradient water purification system (Millipore SAS, Molsheim, France) whilst stirring for 15min to form an aqueous phase which was then crosslinked by drop-wise addition of a calcium chloride solution. The PEC:MUC ratio used was 9:1, PEG was 0.1mLs and drug (AZT):polymer (MUC, PEC and PEG) ratios used were in accordance with the Box-Behnken-design. A water-in-oil (W/O) emulsion was prepared by ultrasonication using a high intensity ultrasonic processor (Sonics Vibracell VCX 130, Sonics Materials INC, Newtown, CT, USA) with the crosslinked PEC-MUC-PEG-AZT dispersion acting as the aqueous phase and cyclohexane as the oil phase. The W:O ratio was 1:4 and span 85 was added as the surfactant in accordance with the Box-Behnken design. The emulsion was centrifuged at 4000rpm for 1min. Thereafter, excess cyclohexane was decanted. The remaining concentrated SM emulsion was frozen at -80°C for 12hrs before being lyophilized for 48hrs.

4.2.4. Determination of the stability of the optimized SM emulsion

The dispersion state of the W/O emulsion obtained in the formulation of SMs was measured using a Turbiscan Lab® (Turbiscan Lab™, Formulaction SA, L'Union, France) which assessed the degree of reversible colloidal phenomena such as creaming and sedimentation as well as irreversible phenomena such as coalescence and flocculation (Celia et al., 2009). The Turbiscan Lab® Expert software was used to analyze transmitted (T) and backscattered (BS) light according to equation 4.1 and in reference to the Mie theory represented by equation 4.2.

$$BS = \frac{1}{\sqrt{\lambda^*}} \qquad Equation\ 4.1$$

$$\lambda^*(d, \Phi) = \frac{2d}{[3\Phi(1-g)Q_s]} \qquad Equation\ 4.2$$

Where λ^* is the photon transport mean free path, Φ is the volume fraction of the particles, d is the particle mean diameter and g (asymmetry factor) and Q_s (light scattering efficiency factor) are optical parameters given by the Mie theory. A disposable flat bottomed cylindrical glass cell was carefully filled to approximately 42mm height with the optimized SM emulsion (20mLs) then placed into the Turbiscan® Lab instrument for synchronous dual measurement of light that transmitted through and light that was back-scattered at a 45º angle in reference to the incident light. Pulsed near infrared light (λ 880nm) was emitted from the source and

optical detectors (photodiodes) received the transmitted and the backscattered light. Measurements were performed at 25ºC and the Turbiscan® Lab was configured to perform continuous scans, performing a scan every 6 minutes, over a 55mm cell length from bottom to top for an hour. Variation in particle volume fraction (Φ) on particle migration (sedimentation of creaming) and the mean particle diameter (*d*) due to coalescence resulted in variation in the quantity of transmitted and backscattered light. The measured amount of transmitted and backscattered light was then interpreted and used to describe the dispersion state (stability) of the emulsion (Mengual et al., 1999; Lemarchand et al., 2003; Celia et al., 2009).

4.2.5. Characterization of the SMs

The shape and surface morphology of the SMs were determined using a transmission electron microscope (TEM) (JEOL S100 Transmission Electron Microscope, Tokyo, Japan) set at 40 000X magnification. The particle size of the SMs was determined by measuring particle diameter through a process of dynamic light scattering using a Zetasizer (Zetasizer Nano ZS, Malvern Instruments Ltd, Worcestershire, United Kingdom). Particle surface charge was evaluated by measuring the zeta potential of the SMs using the zetasizer (Garcia et al., 2011). SM powder (5mg) samples were each dispersed in 30mLs of MilliQ water and passed through 0.22µm Minisart® non-pyrogenic single use filters (Sartorius Stedim Biotech, Goettingen, Germany) into quartz cuvettes and specialized zeta potential containers respectively which were then inserted into the zetasizer to determine SM particle size and zeta potential (Garcia et al., 2011).

4.2.6. Drug encapsulation and release from SMs

The percentage encapsulation efficiency (EE) of the optimized SMs was determined according to equation 4.3 (Garcia et al., 2011).

$$EE\ (\%) = Actual\ amount\ of\ AZT\ in\ SMs / theoretical\ amount\ of\ AZT \times 100 \qquad Equation\ 4.3$$

Where the actual amount of AZT in SMs was measured on a 100mg SM sample. SMs (100mg) were added to 100mL of MilliQ water, ultrasonicated for 10 minutes, vortexed for 5 minutes and then allowed to release the remaining AZT form the SMs over 48 hours whilst in an orbital shaker bath that rotated at 20rpm and was set at 37ºC. The amount of AZT that was encapsulated in the SMs was then computed form the UV absorbance values measured using a nanophotometer (NanoPhotometer™, Implen GmbH, Munchen, Germany) at ambient temperature (25°C) and at a UV absorbance lambda max of 267nm. Determination of EE was performed in triplicate. The theoretical amount of AZT was taken as the

proportional amount of AZT in 100mg of SMs in reference to the loading dose. AZT release from PEC-MUC-PEG SMs was performed using the dialysis membrane technique over 24 hours in a 100mL container filled with SVF (Gupta et al., 2011; Woolfson et al., 2010; Shaikh et al., 2009). The dissolution media (simulated vaginal fluid, SVF), was prepared according to Owen and Katz's as presented in table 4.3 (Owen and Katz, 1999).

Table 4.3: Simulated vaginal fluid (SVF), 1L (Owen and Katz 1999)

SVF component	Quantity (g)
Sodium chloride (NaCl)	3.510
Potassium hydroxide (KOH)	1.400
Calcium hydroxide $Ca(OH)_2$	0.222
Bovine serum albumin (BSA)	0.018
Lactic acid	2.000
Acetic acid	1.000
Glycerol	0.160
Urea	0.400
Glucose	5.000

Drug release was also performed in phosphate buffered saline (PBS pH 7.4) which acted as simulated semen (Gupta et al., 2011; Woolfson et al., 2010; Owen and Katz, 2005). The AZT-loaded SMs and 2mLs of SVF or PBS (similar medium as the bulk 100mL dissolution medium) were added into a dialysis tubing which had a molecular weight cut-off of 12kDa obtained from Sigma [(Sigma–Aldrich Inc., St. Louis, USA); Gupta et al., 2011; Shaikh et al., 2009]. The tubing was securely tied at both ends and then suspended in a dissolution media filled container (100mL) that was placed in an orbital shaker incubator (Orbital Shaker Incubator, LM-530D, Yihder Technology CO., LTD, Jhonghe City, Taipei County, Taiwan, Republic of China) which was set at 37°C and rotated at 20rpm (Woolfson et al., 2010). Dissolution media aliquots (200µL) were withdrawn at predetermined time intervals and ultraviolet (UV) quantification of the amount of drug released was performed using the nanophotometer. Dissolution tests were performed in triplicate.

Dissolution profiles were generated from the amounts of AZT released over 24 hours and these profiles were used to characterize *in vitro* AZT release kinetics from the SMs. The ability of the macromolecular SMs to modulate AZT release was evaluated by determining the mean dissolution time (MDT) according to equation 4.4 and the dissolution efficiency (DE) which is the area under the dissolution curve up to a certain time, t, expressed as a

percentage of the rectangular area described by 100% dissolution in the same time, was computed according to equation 4.5 (Khan, 1975; Costa and Lobo, 2001; Garcia et al., 2011).

$$MDT = \frac{\sum_{i=1}^{n} t_i \, M_t}{M_\infty} \qquad Equation\ 4.4$$

Where M_t is the fractional dose released in time $t_i = (t_i + t_{i-1})/2$ and M_∞ corresponds to the loading dose

$$DE = \frac{\int_0^t y \times dt}{y_{100} \times t} \times 100\% \qquad Equation\ 4.5$$

Where y is the percentage of drug dissolved at time t. The pH responsiveness of the SMs was tested by comparing the dissolution efficiencies, MDTs and computing the similarity factor (f_2) and the difference factor (f_1) of the dissolution profiles obtained in SVF and PBS according to equations 4.6 and 4.7 (Moore and Flanner, 1996; O'Hara et al., 1998; Costa et al., 2001; Zhang et al., 2010).

$$f_2 = 50 \log\left\{\left[1 + {}^{1}/_{n} \sum_{t=1}^{n} W_t (R_t - T_t)^2\right]^{-0.5} \times 100\right\} \qquad Equation\ 4.6$$

$$f_1 = \frac{\sum_{t=1}^{n} |R_t - T_t|}{\sum_{t=1}^{n} R_t} \times 100\% \qquad Equation\ 4.7$$

Where n is the number of sampling points, W_t is an optional weight factor, R_t is the reference assay at time t and T_t is the test assay at time t. The dissolution profile of the PEC-MUC-PEG SMs in SVF and PBS was fitted into 14 different kinetic models and the best fit parameter, the adjusted coefficient of determination ($R^2_{adjusted}$), regarded as the goodness of fit parameter, was obtained. $R^2_{adjusted}$ was viewed as a measure of how close the dissolution profile of the SMs followed the chosen kinetic model, with values of $R^2_{adjusted}$ that increasingly approached 1 showing the closest model fit as opposed to values smaller than 1 (Zhang et al., 2010).

4.2.7. Attenuated total reflectance Fourier transform infrared (ATR-FTIR) spectroscopy analysis

ATR-FTIR spectra of native PEC, MUC, PEG, AZT and the AZT-loaded PEC-MUC-PEG SMs were obtained using a Perkin Elmer Spectrum 2000 FTIR spectrometer fitted with a MIRTGS detector (PerkinElmer Spectrum 100, Llantrisant, Wales, UK). Dry powder samples directly analyzed over a wave number range of 650-4000cm^{-1} with a resolution of 4 cm^{-1} and 10 scans per spectrum were performed at a direct contact force of 120N on a universal diamond ATR top-plate. Distinct absorption peaks were used to verify the constitution of the SMs by comparing them to the peaks on the native MUC, PEC, PEG and AZT.

4.2.8. Thermal analysis using differential scanning calorimetry (DSC)

The thermal properties of PEC, MUC, AZT and the AZT-loaded SMs were analyzed by DSC. The analysis was conducted on a differential scanning calorimeter (Mettler Toledo, DSC1, STARe System, Schwerzenback, Switzerland) which was dually calibrated for temperature and enthalpy using indium and zinc. All experiments were performed at a heating rate of 10°C min^{-1} under a dry nitrogen atmosphere (Afrox, Germiston, Gauteng, South Africa) which flowed at a rate of 200mLmin^{-1} acting as the purge gas in order to reduce sample oxidation. Samples were placed in 40µL aluminium pans and heated from -10°C to 110°C and kept at 110°C for 3 minutes. This was done to evaporate any moisture in the sample and to eliminate any thermal history. The samples were then quenched from 110°C to -10°C at a rate of 20°C min^{-1}. The midpoint melting point (T_m) and heat of fusion (ΔH) which were used for characterization were obtained from the melting point depression of the peaks generated on the experimental DSC curves on heating the samples from -10 to 300°C.

4.2.9. Thermogravimetric analysis (TGA)

Thermal degradation analysis was performed on 10-20mg samples of PEC, MUC, AZT AZT-loaded PEC-MUC-PEG SMs which were contained in ceramic pans under nitrogen atmosphere using a TGA 4000 thermogravimetric analyzer (PerkinElmer Inc, Massachusetts, USA). The experiments were run at 10°Cmin^{-1} from 50-500°C. Thermograms obtained and their first derivatives revealed the thermal degradation properties of the samples.

4.2.10. X-ray diffraction (XRD) analysis

The crystalline and amorphous nature of the AZT-loaded SMs and their individual compositional components was investigated using a Rigaku MiniFlex600 Benchtop X-ray Diffractometer (Rigaku Corporation, Tokyo, Japan) fitted with; a 600W (40Kv-15mA) X-ray generator, a counter monochromator to cut X-rays other than Cu Kα X-rays and a high intensity D/tex ultra high speed 1D detector. Experimental temperature was maintained at 19ºC. The diffractometer was operated using the Rigaku MiniFlex Guidance software, version 1.2.0.0 and data was analyzed using the Rigaku PDXL Basis software able to perform integrated intensity calculations. Measurement parameters included a divergence slit (DS) of 1.25º, scattering slit (SS) of 1.25º, a 0.3mm receiving slit (RS) and a goniometer radius of 150mm. Each powder sample of PEC, MUC, AZT and AZT-loaded PEC-MUC-PEG SMs was pressed flat onto a square grooved glass slide sample holder. Measurements were performed by scanning each sample at 0.01-100º/min over a diffraction angle range of 3º-60º 2θ. The XRD diffractograms generated were used to evaluate the crystallinity of the respective samples (Santos et al., 2003; Mishra et al., 2008; Kumar et al., 2011; Raviolo and Briñón, 2011).

4.3. Results and Discussion

4.3.1. Preparation and optimization of the macromolecular SMs

All 15 formulations from the design template produced SMs of varying particle size, zeta potential that had different MDTs (Table 4.4). The obtained results were inputted into the MINITAB® software to yield four possible optimized formulations and the most appropriate optimized formulation had a composite desirability (D) of 0.865, PS desirability (d_{PS}) of 1.000, ZP desirability (d_{ZP}) of 0.825 and MDT desirability (d_{MDT}) of 0.785. Independent and dependent parameters that had a desirability of 1,000 were regarded as the most optimum and those that had a desirability of 0.000 as the least optimum parameters. The optimal formulation had independent parameters; ST of 6.28 minutes, SC of 1.64 (% $^{v}/_{v}$) and a D:P ratio of 1:1 which gave predicted SM responses of; PS 215.19 nm, ZP -39.13mV and a MDT of 5.52 hours. Linear regression of independent parameters and responses using MINITAB® generated relationships described by the polynomial equations 4.8, 4.9 and 4.10 (Karnachi and Khan, 1996). Where the coefficient of determination of PS (R^2_{PS}) was 51.4%, ZP (R^2_{ZP}) was 90.1% and that of MDT (R^2_{MDT}) was 85.6% (Karnachi and Khan, 1996).

$$PS=-1719.600+163.070[ST]+1247.470[SC]+637.950[D:P]-3.900[ST]^2-158.33[SC]^2-127.530[D:P]^2-66.800[ST*SC]+24.600[ST*D:P]-227.200[SC*D:P] \quad \text{Equation 4.8}$$

$$ZP=40.125-4.925[ST]+13.250[SC]-189.100[D:P]+0.580[SC]^2-20.400[SC]^2-26.400[D:P]^2-4.160[ST*SC]+3.000[ST*D:P]+122.800[SC*D:P] \quad \text{Equation 4.9}$$

$$MDT=-34.951+3.267[ST]+41.139[SC]-20.998[D:P]-0.093[ST]^2-11.896[SC]^2-4.624[D:P]^2-0.921[ST*SC]-0.415[ST*D:P]+10.104[SC*D:P] \quad \text{Equation 4.10}$$

The correlation of the independent parameters; ST, SC and D:P ratio to the responses; PS, ZP and MDT was further illustrated as response mesh plots presented in figure 4.1 (Karnachi and Khan, 1996).

Table 4.4: Responses obtained from *in vitro* testing of the 15 design formulation's independent parameters

Formulation number	Particle size (nm)	Zeta potential (mV)	MDT (hours)
1	186.1±4.267	-42.7±2.350	4.852
2	311.0±13.360	-35.4±0.503	4.825
3	143.6±21.110	-33.7±1.460	3.572
4	229.1±52.030	-40.2±1.400	3.845
5	228.7±12.510	-28.1±0.894	4.895
6	220.0±4.768	-29.7±0.144	5.612
7	223.2±12.390	-30.5±0.193	6.300
8	262.9±3.964	-33.1±0.535	5.339
9	203.1±2.989	-41.6±0.671	5.952
10	231.3±4.634	-32.4±0.618	5.209
11	220.6±6.202	-34.2±0.948	5.958
12	239.5±9.255	-33.3±0.415	4.906
13	228.1±5.899	-47.4±0.536	4.349
14	269.3±13.450	-47.2±0.860	4.695
15	321.1±17.370	-35.4±0.501	5.533

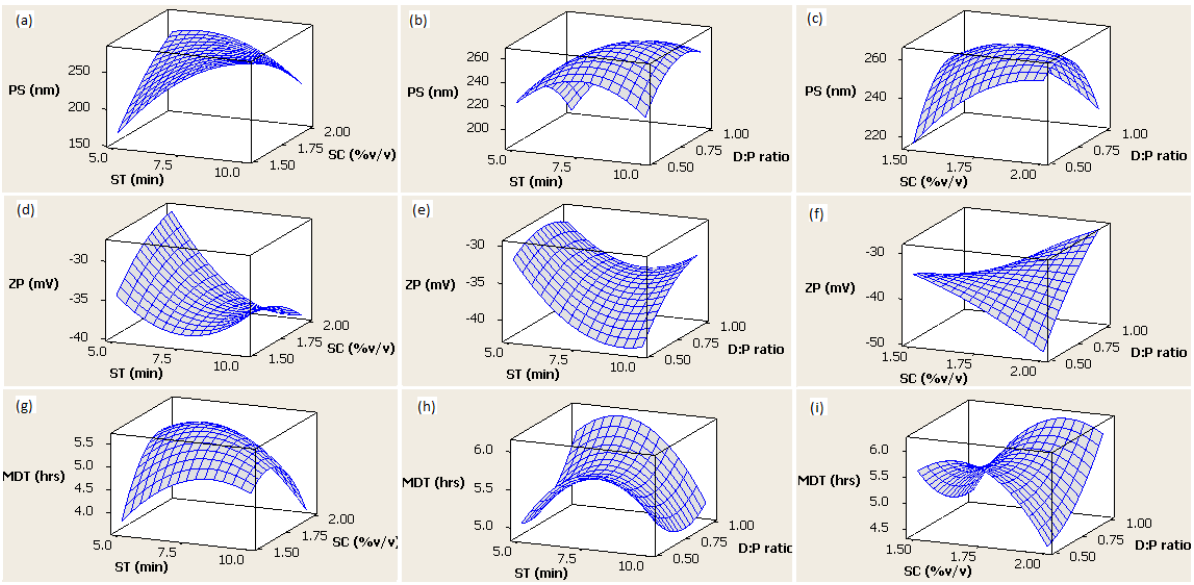


Figure 4.1: Response mesh plots correlating dependent formulation parameters/responses; PS, ZP and MDT to their independent parameters; ST, SC and D:P ratio

4.3.2. Submicrosphere emulsion stability

The delta transmission and delta back scattering profiles of the optimised SM emulsion depicted in figure 4.2 show that the SM emulsion was generally stable with some local destabilization (sedimentation) as observed by the gradual decrease in the delta backscattering (DeltaBS) signal at the top end of the glass cell. The middle and the bottom of the profile was relatively unchanged which meant that the emulsion was stable over the hour long test duration and no global destabilization (coalescence) and no creaming occurred to the SM emulsion during the total experimentation duration.



Figure 4.2: Delta transmission and delta backscattering profiles of an optimized SM emulsion obtained through continuous scans every 6 minutes for 1 hour

During the SM preparation the emulsion was centrifuged within an hour followed by freezing at -80 degrees for 24 hours then lyophilized for 48 hours, therefore a small degree of sedimentation observed does not significantly affect the AZT-loaded PEC-MUC-PEG SM formulation.

4.3.3. Morphological characterization of AZT-loaded PEC-MUC-PEG SMs

Well defined spherical SMs were observed under TEM (Figure 4.3). The mean particle size of the SMs prepared from the 15 design formulations ranged from 143.6±21.110nm, F3, to 321.1±17.370nm, F15, (Table 4.4). The optimized formulation had a mean particle size of 270.6±5.53nm and a stable polydispersity index (PDI) of 0.303±0.028 as depicted in figure 4.4a which also shows zeta potential for the 15 design formulations that ranged from -28.1±0.894mV to -47.4±0.536mV (Table 4.4). The optimized formulation had a zeta potential of -34.4±0.539mV signifying that the SMs were not agglomerated (Figure 4.4b).

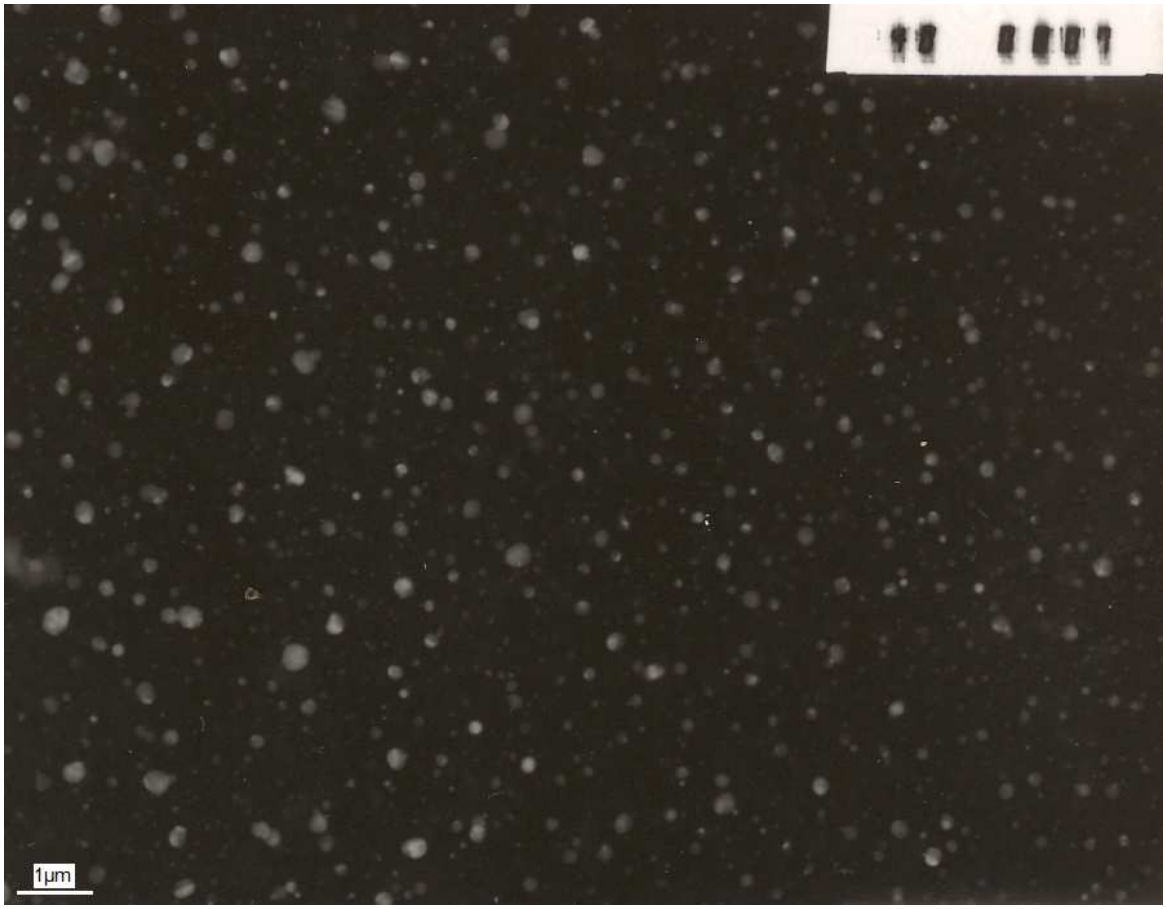


Figure 4.3: Transmission electron micrograph of AZT-loaded MUC-PEC-PEG SMs observed at 40 000X magnification using a JEOL S100 transmission electron microscope

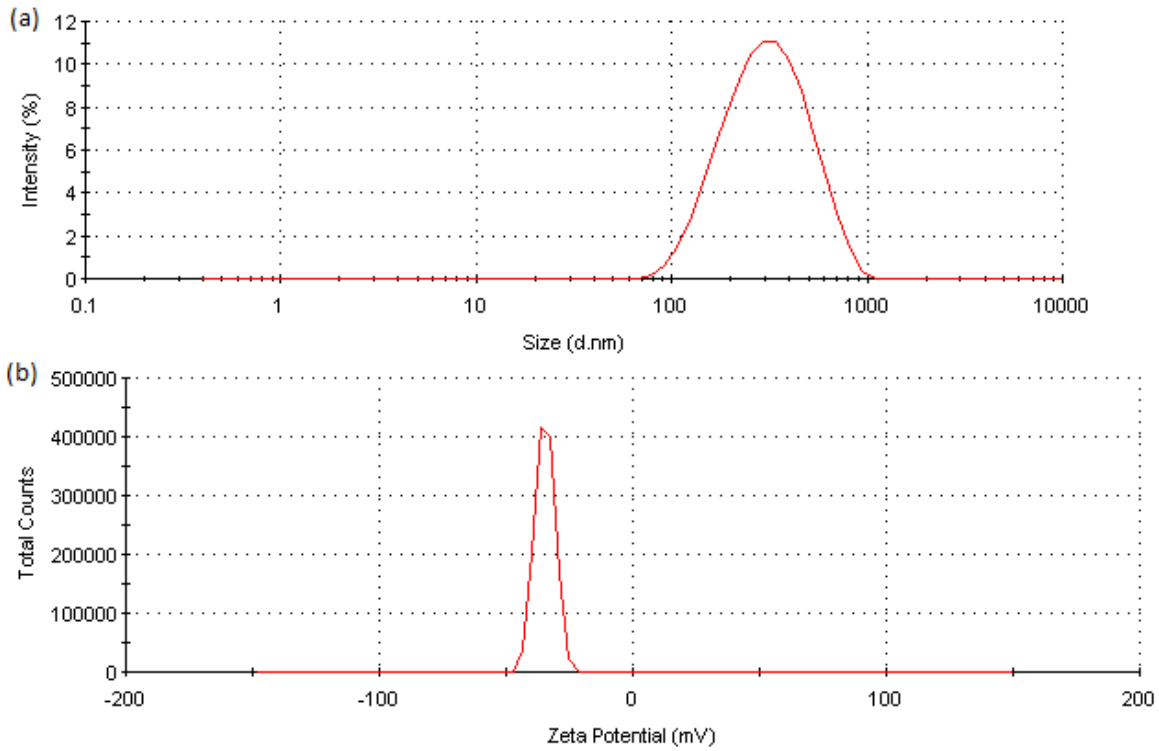


Figure 4.4: Showing, (a) particle size distribution with intensity and (b) zeta potential distribution profile of the optimized SMs obtained using a zetasizer

4.3.4. Drug release from PEC-MUC-PEG SMs

The release of AZT from SMs in SVF occurred mostly within 24 hours for the 15 Box-Behnken design formulations as depicted in the dissolution profiles in figures 4.5a-c. All 15 formulations had similar drug release profiles (Figures 4.5a-c). The ability of the macromolecular SMs to retain drug and prolong drug release was evaluated by the MDT. MDT varied from 3.573 hours for formulation F3 to 6.300 hours for formulation F7 (Table 4.4) and was a resultant of the contribution of the independent parameters as observed in figures 4.1g, 4.1h and 4.1i. For example, the dissolution profiles observed in figure 4.4a for formulations F3 and F4 showed that the drug was relased faster from the submicrospheres and this was corroborated by the computed low MDT values (Table 4.4). Independent parameters for F3 (Table 4.2) were; minimum ST (5min), medium SC (1.75%) and medium D:P ratio (0.75) which resulted in the formation of the smallest submicrospheres (PS=1.436±21.110nm). The low MDT of F3 submicrospheres was likely because the small submicrospheres provided a large dissolution surface area. Conversly relatively larger F7 submicrospheres had the highest MDT and were a product of; minimum ST (5min), medium SC (1.75%) amd maximum D:P ratio (1) as presented in table 4.2. In this case a higher D:P ratio probably contributed more to the high MDT as the submicrospheres could better retard the dissolution of the encapsulated AZT. The optimized formulation had a MDT of 5.974 hours. Comparative drug release of the optimized formulation in PBS pH 7.4 yielded a MDT

of 5.389 hours (Figure 4.5d). Drug release from the optimized SMs within 24 hours in SVF pH 4.5 was approximately 91% as compared to approximately 94% in PBS (Figure 4.5d). The dissolution characteristics of drug from the submicrospheres was therefore a summation of the contribution of all the 3 independent variables; ST, SC and D:P ratio.

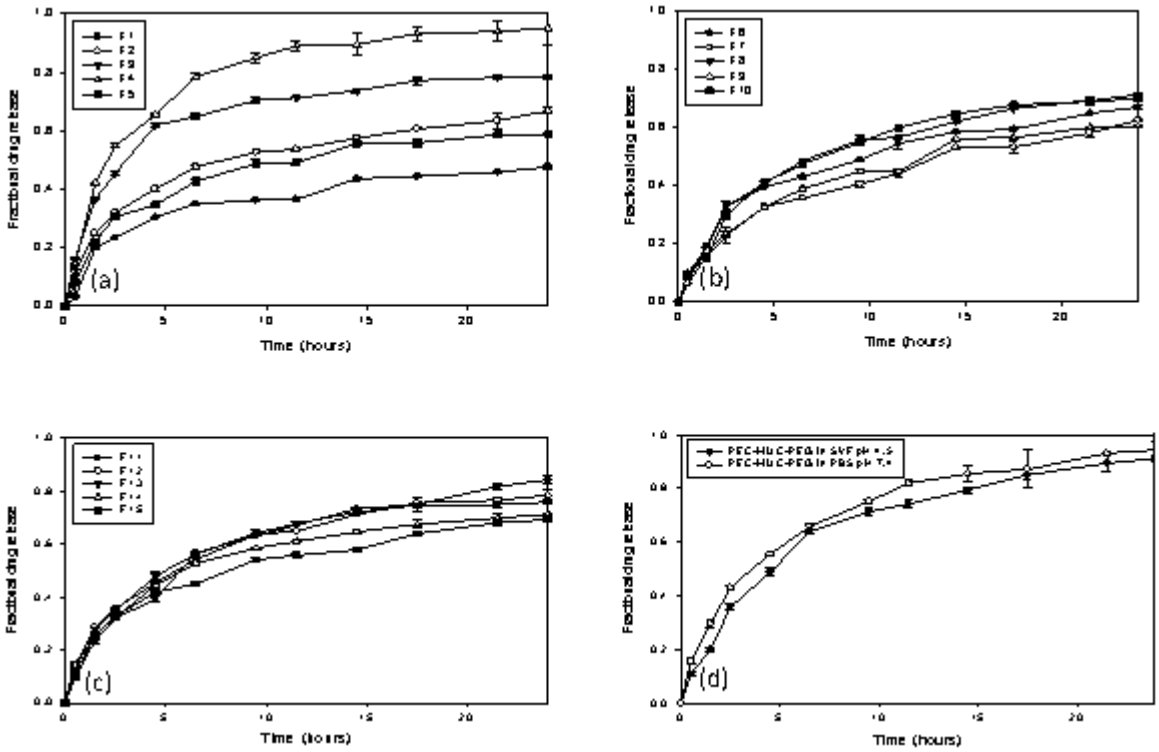


Figure 4.5: SM dissolution profiles of; (a) formulations F1-F5, (b) formulations F6-F10, (c) formulations F11-F15 and (d) the optimized formulation in SVF and PBS

An increase in pH from acidic (pH 4.5 SVF) to alkaline (pH 7.4 PBS) might have caused a destabilization in the architecture of the SMs leading to increased leakage of the encapsulated drug as shown by the increase in the fractional release in PBS as compared to that observed in SVF (Figures 4.5d and 4.6a). Additionally, the mean dissolution time for the drug released from the SMs was shorter in PBS as compared to SVF. This variation in drug release in dissolution media of a different pH may be explained by the presents of carboxyl groups in pectin and mucin which are neutral in an acidic environment (SVF pH4.5) and which are then ionized in an alkaline environment (PBS pH 7.4) which would lead to repulsion of the negatively charged moieties thus causing the architectural destabilization of the SMs thereby leading to increased drug release and a decreased mean dissolution time. However, the effect appeared not too pronounced possibly because pectin and mucin were interpenetrated and crosslinked. This was also confirmed by the similarity of the SM dissolution profiles obtained in SVF and in PBS as specified by the closeness of their dissolution efficiencies (DE =69.097% in SVF and DE=73.568% in PBS) and according to

the computed similarity and difference factors (f_2 =63.132 and f_1=8.099) (Moore and Flanner, 1996; O'Hara et al., 1998; Costa et al., 2001; Zhang et al., 2010).

From the dissolution profiles in figure 4.6b, it was noted that ionic crosslinking PEC with Ca^{2+} reduced the amount of drug released in 24 hours and this may be a result of the formation of an egg-box network structure when the Ca^{2+} electrostatically interacted with the carboxylic moieties of the macromolecular PEC (Yu et al., 2009). This egg-box structure condenses the PEC chains encapsulating AZT leading to reduced dissolution. PEG caused a slight increase in the amount of drug released and this may have occurred because PEG draws water molecules towards the SMs by forming hydrogen bonds with the surrounding water molecules of the dissolution media (SVF or PBS). There was no major difference in the dissolution profile observed for PEC-MUC-PEG submicrospheres and that for PEC-MUC or PEC-PEG submicrospheres (Figures 4.6c and 4.6d) suggesting that PEC was the main constituent that contributed to the dissolution of the submicrospheres.

Modeling of AZT-loaded SM dissolution in SVF and PBS showed that AZT release kinetics fitted with most kinetic models tested as given by the values of the adjusted coefficient of determination ($R^2_{adjusted}$) with the exception of zero order kinetic model as shown in table 4.5. The highest goodness of fit parameter ($R^2_{adjusted}$) was attained using the Logistic and Makoid-Banakar models for the dissolution profiles obtained in SVF and PBS respectively. The closeness of the best fit parameters and $R^2_{adjusted}$ underline the similarity in the SMs dissolution kinetics and profiles when dissolution was performed in SVF (pH 4.5) as compared to dissolution in PBS (pH 7.4).

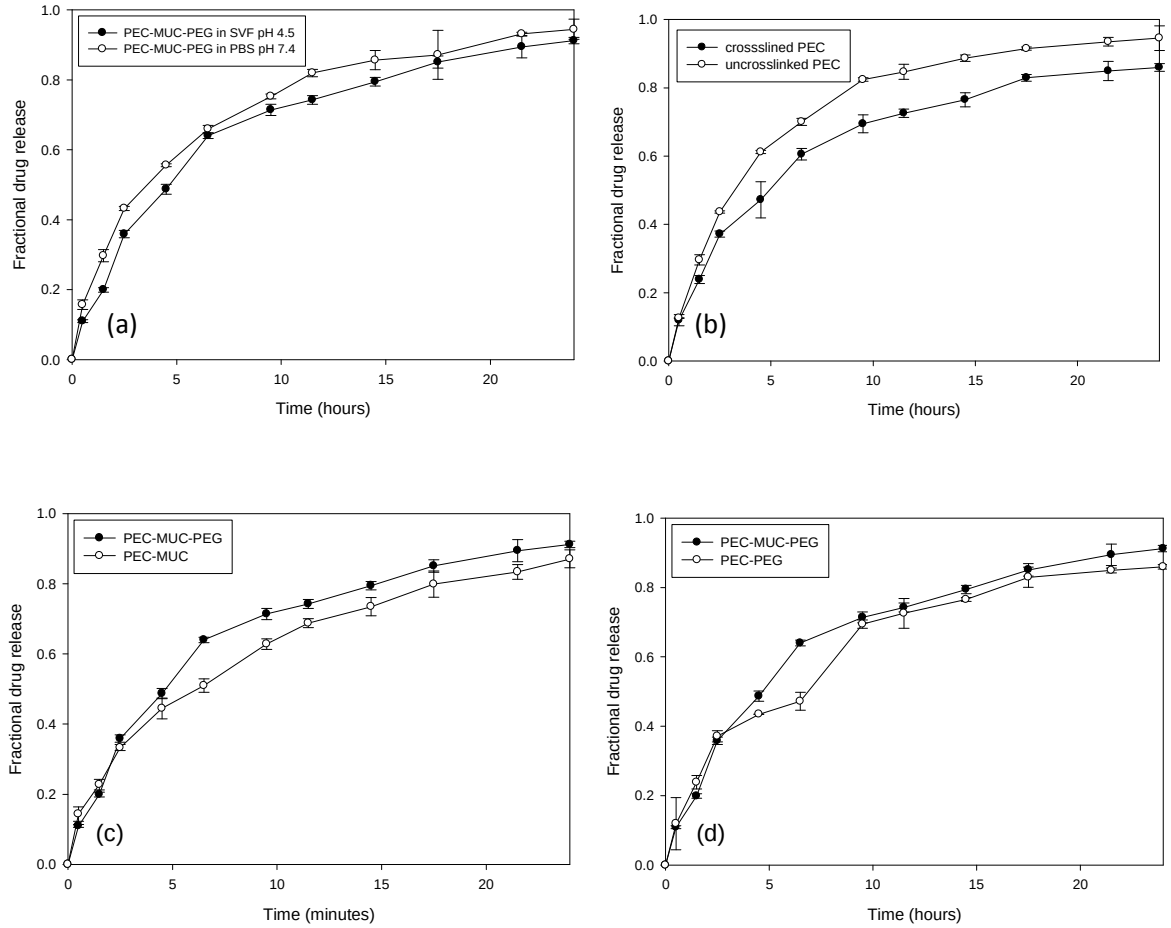


Figure 4.6: Comparison of AZT release from; (a) PEC-MUC-PEG SMs in SVF pH 4.2 to AZT release in PBS pH 7.4, (b) crosslinked PEC SMs to release from uncrosslinked PEC SMs both in SVF, (c) PEC-MUC-PEG SMs to AZT release from PEC-MUC SMs both in SVF and (d) PEC-MUC-PEG SMs to AZT release in PEC-PEG SMs both in SVF.

Table 4.5: Goodness of fit and best fit parameters obtained by fitting the SM dissolution profiles (obtained in SVF and PBS) to different kinetic models

Dissolution model	Best-fit parameter						Goodness of fit parameter $R^2_{adjusted}$	
	Parameter 1		Parameter 2		Parameter 3		pH 4.5	pH 7.4
	pH 4.5	pH 7.4	pH 4.5	pH 7.4	pH 4.5	pH 7.4		
Zero order	k_0=4.922	k_0=5.172					0.5871	0.4341
First order	k_1 =0.136	k_1=0.170					0.9768	0.9675
Higuchi	kH=20.733	kH=21.984					0.9607	0.9384
Korsmeyer-Peppas	kKP=25.198	kKP=30.806	n=0.426	n=0.372			0.9692	0.9769
Hixson-Crowell	kHC=0.037	kHC=0.046					0.9378	0.9238
Hopfenberg	kHB=0.000	kHB=0.000	n=1791.481	n=7236.567			0.9744	0.9642
Baker-Lonsdale	kBL=0.013	kBL=0.016					0.9808	0.9933
Makoid-Banakar	kMB=19.709	kMB=26.024	n=0.691	n=0.573	k=0.028	k=0.023	0.9933	0.9973
Peppas-Sahlin	k_1=20.905	k_1=27.709	k_2=-1.216	k_2=-2.058	m=0.683	m=0.597	0.9926	0.9971
Quadratic	k_1=-0.003	k_1=-0.003	k_2=0.102	k_2=0.112			0.9382	0.8882
Weibull	α=4.455	α=3.552	β=0.761	β=0.725	Ti=0.110	Ti=0.000	0.9944	0.9983
Logistic	α=-1.717	α=-1.298	β=2.751	β=2.584			0.9941	0.9918
Gompertz	α=2.290	α=1.632	β=2.2029	β=1.877			0.9817	0.9750
Probit	α=-1.027	α=-0.2772	β=1.651	β=1.546			0.9935	0.9928

k_0, k_1, kH, kKP, n, kKP, kHC, kHB, kBL, k, k_2, α and β are best fit parameters of the respective dissolution models

4.3.5. ATR-FTIR analysis of PEC, MUC, PEG, AZT and AZT-loaded PEC-MUC-PEG SMs

FTIR spectrum of AZT-loaded PEC-MUC-PEG SMs (Figure 4.7a) revealed a broad absorption peak extending from approximately 3000 to 3600cm^{-1} which may have been a result of the overlapping stretching vibrations of hydroxyl (–OH) groups found in MUC, PEC, AZT and PEG and the carboxyl (–COOH) groups of PEC and MUC (Kumar et al., 2010). The broadening of this peak as compared to the ones in PEC (Figure 4.7c), MUC (Figure 4.7b), PEG (Figure 4.7e) and AZT (Figure 4.7d) was probably due to the participation of the –OH and COOH groups in H-bonding. The SM absorption peaks observed at 2933cm-1 and 2854cm^{-1} may be attributed to strong stretching vibrations of the alkane groups; –CH_3, -CH_2, and –CH that are found in PEC (peak 2935cm^{-1}), MUC (peak 2917cm^{-1}), PEG (peak 2867cm^{-1}) and AZT (peak 2814cm^{-1}).

AZT encapsulation in PEC-MUC-PEG SM was confirmed by the presence of the absorption peak at 2105cm^{-1} which may be attributed to the stretching vibrations of the azide (-N_3) group of AZT (Figure 4.7a). The reduction in intensity of this peak as compared to the one observed on the AZT ATR-FTIR spectrum (Figure 4.7d) may be a result of the shielding of AZT as it was encapsulated within the PEC-MUC-PEG SMs and possibly due to the participation of the –N_3 group in hydrogen bonding with -OH and –COOH groups found in PEC, MUC and PEG. The peak that was observed at 1742cm^{-1} on the AZT-loaded PEC-MUC-PEC SM ATR-FTIR spectra (Figure 4.7a) may have resulted from the contribution made by strong stretching vibrations of the ester bond found in PEC which was approximately 55-65% esterified (GENU® pectin USP/100, CP Kelco ApS, Lille Skensved, Denmark). A strong amide I (-C=O) peak (1682cm^{-1}) was observed on the SM spectrum which may have been dually contributed to by the strong stretching vibrations of the amide I bond in MUC (peak 1636cm^{-1}) and AZT, peak 1641cm^{-1} and 1670cm^{-1} (Patel et al., 2003, Tam et al., 2005). The ATR-FTIR spectra of SMs, PEC, MUC, PEG and AZT depicted several peaks in the finger print region (1450-650cm) which were consistent with what is reported in literature and expected for the AZT-loaded SMs (Mishra et al., 2008; Patel et al., 2003; Ravi et al., 2008).

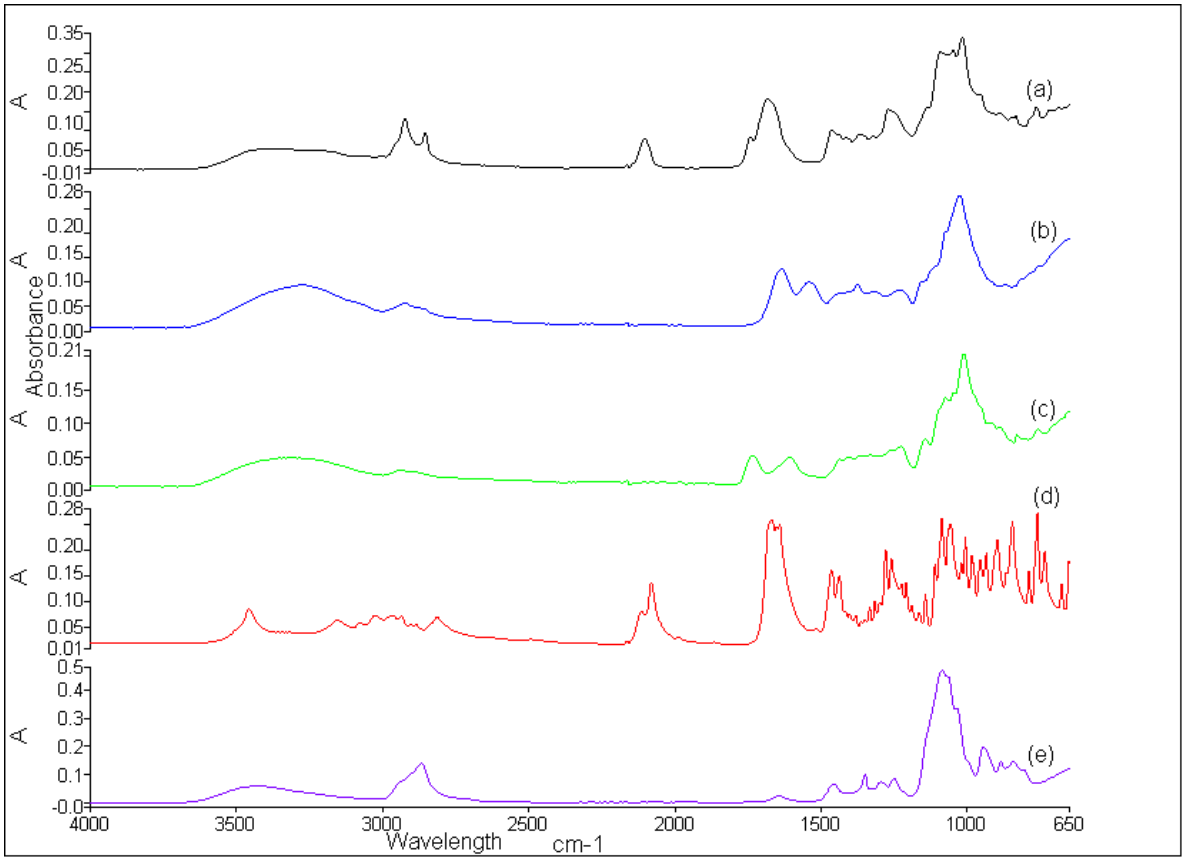


Figure 4.7: *ATR-FTIR spectra of; (a) AZT-loaded PEC-MUC-PEG SMs, (b) MUC, (c) PEC, (d) AZT and (e) PEG*

4.3.6. Differential scanning calorimetry (DSC)

DSC thermograms of AZT-loaded PEC-MUC-PEG SMs, MUC, PEC and AZT are depicted in figure 4.8. AZT-loaded PEC-MUC-PEG SMs had a broad endothermic peak with melting point peak maxima at 113.67°C and a measured heat of fusion of 9.75Jg^{-1} as well as an exothermic crystallization peak at 230.81°C (Figure 4.8a). SM components; MUC had an melting point represented by an endothermic peak maxima at 101.36°C (Figure 4.8b), PEC had a melting endothermic peak at 120.73°C as well as an exothermic crystallization peak at 236.17°C (Figure 4.8c) and the model drug, AZT, had an onset melting point at 122.88°C and an exothermic crystallization peak at 240.34°C (Figure 4.8d) that were consistent with results reported in literature (Araújo et al., 2003). The thermal DSC thermogram of AZT-loaded PEC-MUC-PEG SMs confirmed the SM composition and was a result of the thermal contribution of PEC, MUC, PEG and AZT.

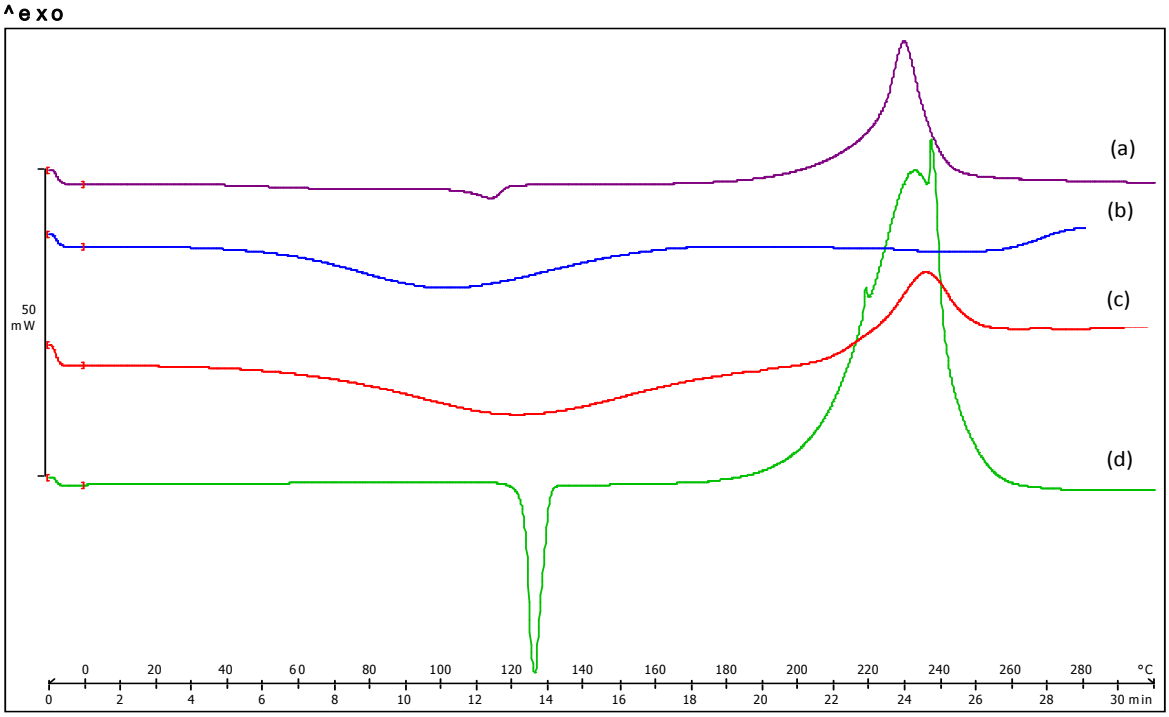


Figure 4.8: DSC thermograms of; (a) PEC-MUC-PEG +AZT, (b) MUC, (c) PEC and (d) AZT

4.3.7. Thermogravimetric analysis of AZT loaded SMs and their native constituents

The thermal degradation of AZT-loaded PEC-MUC-PEG SMs as measured by TGA produced the thermogram depicted in figure 4.9a (solid). The SM TGA thermogram depicts a one-step degradation with weight loss of approximately 84% on heating from 50-500°C. However, its first derivative TGA (DTGA, dotted) revealed that the SMs degraded in three major steps as revealed by DTGA peaks at 239.60°C, 287.90°C and 409.77°C that correspond to the points of inflection on the SM TGA thermogram. It is vital to compare the SM TGA thermogram with that of all the components from which the SMs were formulated i.e. PEC, MUC, PEG and AZT as presented in figure 4.9b. Figure 4.9c shows the TGA (solid) and DTGA (dotted) thermograms of PEC. Thermal degradation of PEC was shown to take place in two steps; the first was a minor step that took place from 50-150°C resulting in 7.919% weight loss and a point of inflection at 95.03°C which may have been a result of dehydration. The second and major PEC degradation step had an extrapolated onset and end at 233.54°C and 276.92°C respectively with its point of maximum degradation represented by the DTGA (peak 246.01°C). This second degradation step resulted in a weight loss of approximately 59% and was most likely due to the depolymerization of PEC carbohydrate chains (Kumar et al., 2010). PEC weight loss of approximately 66.98% occurred from 50-500°C. The first DTGA peaks of the SMs, 239.60°C (Figure 4.9a) and PEC, 246.01°C (Figure 4.9c) are observed to be close; therefore, PEC degradation might have contributed to the initial degradation of the SMs (Figure 4.9a).

Thermal degradation of MUC was also observed to occur in two steps, with the first minor step occurring from 50-150°C which resulted in a corresponding DTGA peak at 90.63°C that resulted in weight loss of approximately 9.14% (Figure 4.9d). This step was likely a result of the evaporation of bound water molecules from the MUC macromolecules. This first step was then followed by a major degradation step which had an extrapolated onset and end at 264.58°C and 330.64°C respectively with its point of inflection corresponding to the DTGA peak at 286.50°C. This major degradation step was possibly a result of the depolymerization of oligosaccharide side-chains in MUC. Overall, there was a total weight loss of 66.17% on heating MUC from 50-500°C. Due to the closeness of the DTGA peaks of the corresponding second degradation steps of MUC, peak at 286.50°C (Figure 4.9d) and SMs, peak at 287.90°C (Figure 4.9a), MUC was likely a contributor to the second degradation step of the AZT-loaded PEC-MUC-PEG SMs (Figure 4.9a).

The model drug, AZT, thermally degraded in two major steps depicted by the DTGA peaks at 244.10°C (first step) and 310.70°C (second step) which might have contributed to the first and second SM degradation steps (Figures 4.9a and 4.9e). Degradation of AZT started at the extrapolated onset of 230.14°C then the second degradation step began before the first degradation step ended. The extrapolated end of the degradation of AZT was at 331.48°C and the total AZT weight loss on heating from 50-500°C was 77.935%. The third degradation step of the SMs, DTGA peak 409.77°C (Figure 4.9a) was likely due to the degradation of PEG which degraded almost completely (99.084%) in one major step with an extrapolated onset and end of 338.89°C and 393.97°C respectively (Figure 4.9f). The point of maximum degradation of PEG corresponds to the DTGA peak at 395.15°C (Figure 4.9f).

All the three degradation steps of the SMs were shifted to the right as compared to the corresponding degradation steps of the respective components of the SMs (PEC, MUC, AZT and PEG) signifying SM thermal stability. The SM thermal stability might have been brought about by the macromolecular ionic crosslinking using Ca^{2+} done during the formulation of the SMs as well as the intermolecular interactions possibly due to hydrogen bonding of the carboxyl, hydroxyl, amide, amine and azide groups of the SM components.

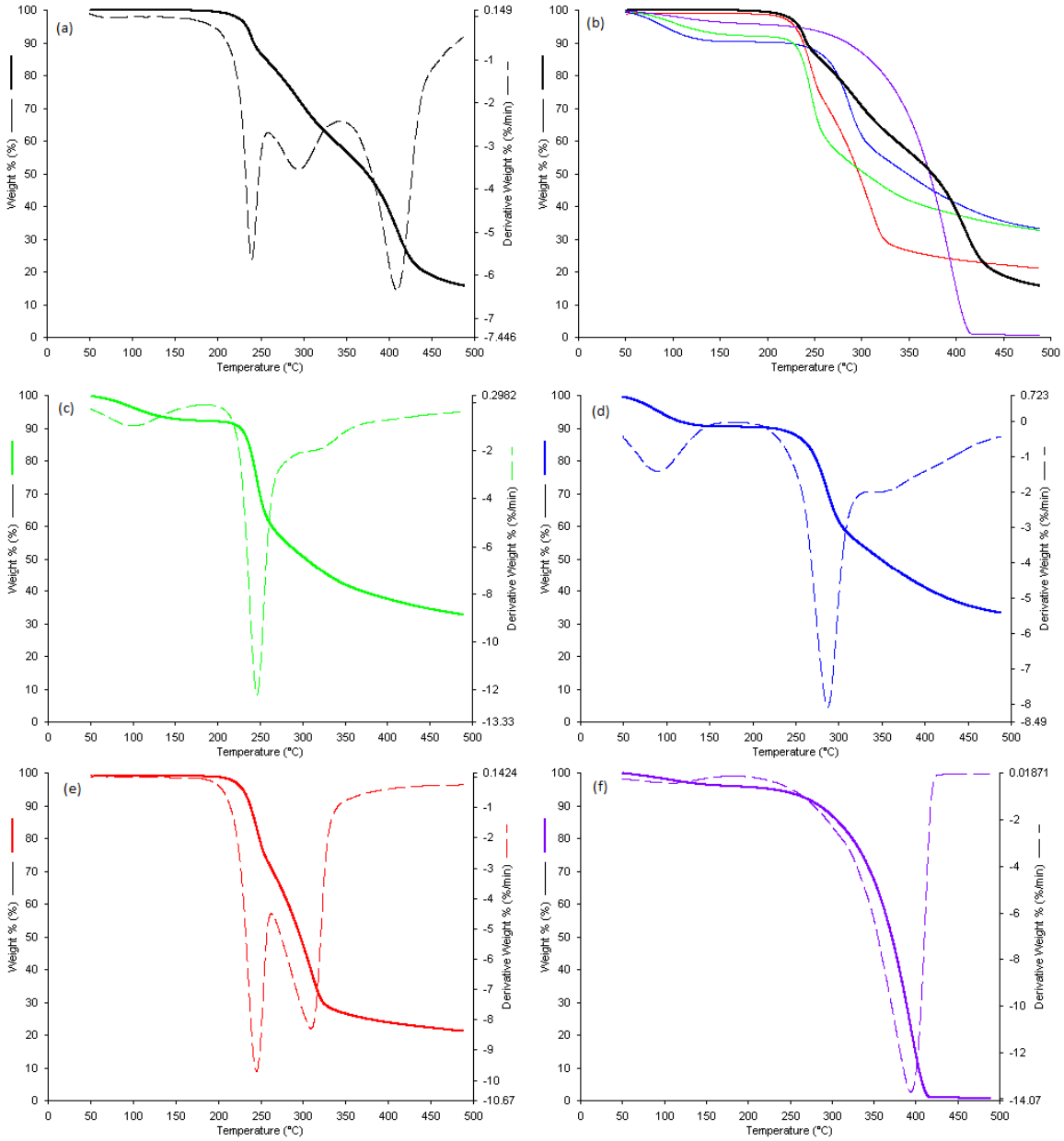


Figure 4.9: The TGA (solid) and DTGA (dotted) thermograms of: (a) PEC-MUC-PEG+AZT SMs; (b) (i) MUC, (ii) PEC, (iii) AZT, (iv) PEC-MUC-PEG+AZT MS and (v) PEG; (c) PEC; (d) MUC; (e) AZT and (f) PEG

4.3.8. X-ray diffraction (XRD)

Figure 4.10 depicts the XRD diffractograms of; AZT-loaded PEC-MUC-PEG SMs , PEC, MUC and that of AZT. The diffractogram of AZT-loaded PEC-MUC-PEG SMs shows several sharp peaks that include major peaks at 2θ equal to; 8.725º, 14.535º, 15.374º, 15.726º, 16.987º, 21.265º, 22.093º, 24.064º, 26.825º, 27.677º, 29.181º and 29.181º which signify the crystalline nature of the AZT-loaded PEC-MUC-PEG SMs (Figure 4.10a). The diffractogram of PEC depicts a broad peak at 2θ equal to 21.274º indicating the amorphous nature of PEC (Figure 4.10c) and the difractogram of MUC depicts a broad peak at 2θ equal to 21.525º illustrating also the amorphous nature of MUC (Figure 4.10b). AZT was shown to be

crystalline due to several sharp peaks that include major peaks at 2θ equal to 9.000º, 14.891, 15.725º, 16.040º, 17.304º, 21.41º, 21.640º, 24.513º, 27.140º, 28.050º and 29.500º observed on its diffractogram shown in Figure 4.10d which are similar to the ones previously reported by Raviolo and Briñón (Raviolo and Briñón, 2011). The observed patten in the diffractograms in Figure 4.10 shows that the crystallinity of AZT-loaded PEC-MUC-PEG SMs was a result of the contribution by the highly crystalline AZT. The peaks observed in the diffractogram of AZ-loaded PEC-MUC-PEG SMs were sharp as those observed for AZT but were shifted slightly to the left by less than 1º and peak intensities were lower that those of observed for AZT which was probably because of the formation of a less crystaline complex when AZT was ecapsulated in the amorphous MUC and PEC based SMs (Banthia et al., 2008; Mishra et al., 2008; Santos et al., 2003; Shaikh et al., 2009).

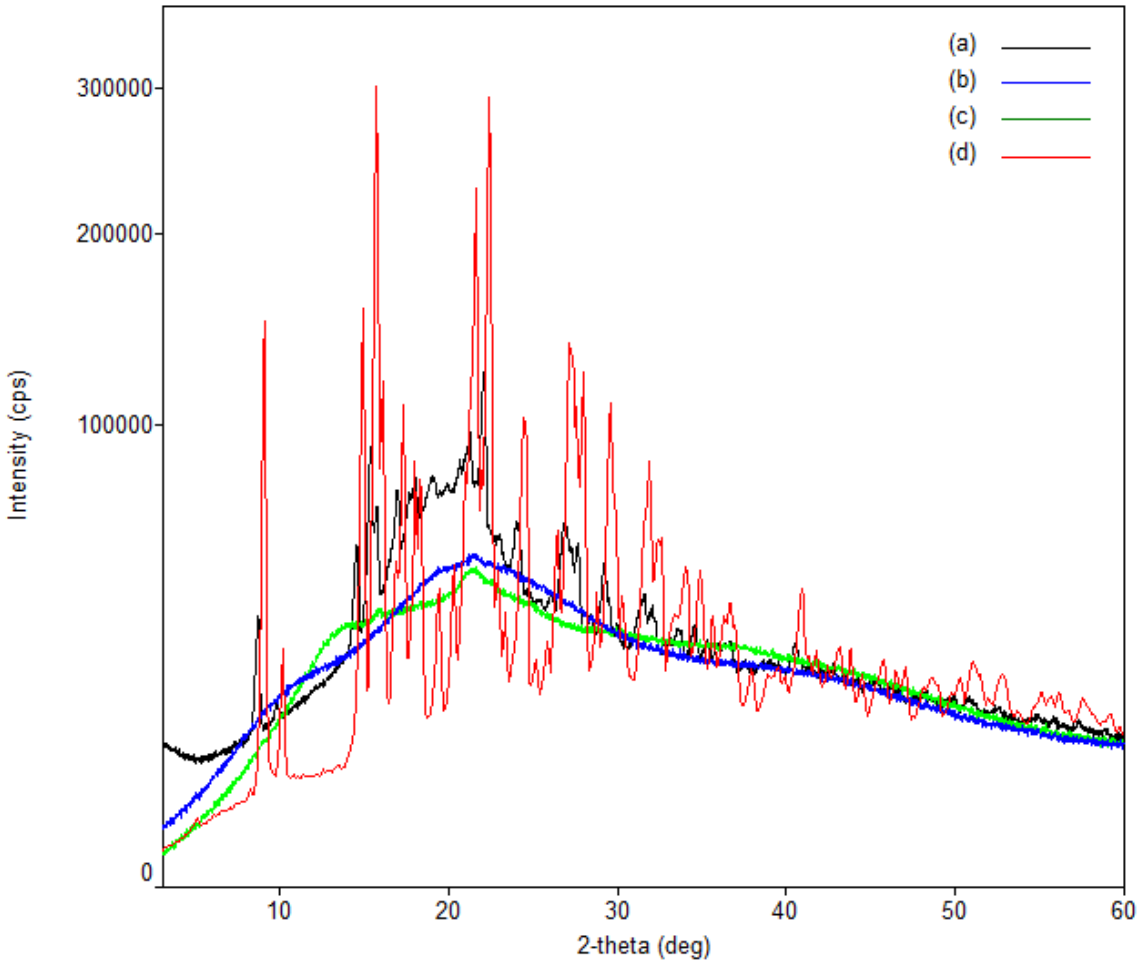


Figure 4.10: Three dimensional X-ray diffractograms of; (a) AZT-loaded PEC-MUC-PEG SMs (black), PEC (green), MUC (blue) and AZT (red)

4.4. Concluding remarks

AZT-loaded MUC-PEC-PEG submicrospheres were successfully designed and optimized using the Box-Behnken design. The optimised submicrospheres prepared by a crosslinking-emulsion technique were spherical and not agglomerated. Drug release studies performed over 24 hours showed that approximately 91% and 94% of AZT was released in SVF and PBS (which acted as simulated semen) respectively. There was no major difference between the submicrosphere AZT dissolution profile in SVF and the one in PBS. Drug release kinetics of the submicrospheres were found to fit most models tested with the highest goodness of fit parameter ($R^2_{adjusted}$) being observed with the Logistic and Makoid-Banakar models for the dissolution profiles obtained in SVF and PBS respectively.

In conclusion, submicrospheres which act as a reservoir for an anti-HIV-1 agent and capable of delivering it over a 24 hour duration were successfully formulated from biocompatible materials and tested *in vitro*. These AZT-loaded submicrospheres embedded in a polymeric matrix, as in chapter 5, and used *in vivo* in the human vaginal cavity, would likely ensure that there is enough of the anti-HIV-1 agent present in the vaginal cavity to counter HIV-1 in the seminal fluids interposed into the vaginal cavity during coitus, with no frequent dosing required prior to or after each coital act. Further studies including *in vivo* animal studies and toxicity studies necessary would be presented in chapter 6 to test the performance of these submicrospheres embedded within a composite polymeric delivery system and used *in vivo* in the pig model.

CHAPTER 5
FABRICATION, OPTIMIZATION AND *IN VITRO* TESTING OF A COMPOSITE POLYMERIC DELIVERY SYSTEM

5.1. Introduction

Heterosexual HIV-1 transmission from males to females occurs mostly via the vaginal route where free and/or cell bound HIV-1 from the seminal fluid transcytose the vaginal epithelia to enter the subepithelium where they target $CD4^+$ cells such dendritic cells, macrophages and T cells (Haase, 2010). Scientists and researchers have recognized that the human vaginal cavity is an important port of entry of HIV-1 thus contemporary thought and experimentation has been directed at trying to prevent HIV-1 infection by targeting the vaginal cavity as a site for anti-HIV-1 agent delivery with the hope that by intervening at this early stage of infection there would be greater chances of success in preventing HIV-1 transmission.

Motivation for targeting vaginal HIV-1 transmission has been heightened by the success in the development and usage of a physical polymeric barrier/sheath commonly known as a condom, which is worn during coitus to prevent the mixing of male and female genital fluids thus preventing HIV-1 infection. Though largely effective in preventing HIV-1 transmission, the condom has been hampered by inappropriate (leading to breakage), infrequent usage and to some extent it has suffered problems of cultural and religious unacceptability. As an alternative to the condom, microbicides have failed to demonstrate efficacy *in vivo* yet they are potent *in vitro* (Hendrix et al., 2009). Possible reasons for current microbicide formulations failure may lie in their inability to; maintain or augment the vaginal mucosal barrier properties, sustain the HIV-1 prohibitive acidic pH (~4.5) of the vaginal cavity, deliver appropriate quantities of the anti-HIV-1 agent/s in the vaginal cavity where it has to be distributed extensively and exhaustively on the vaginal mucosa, ensure presence of the anti-HIV-1 agent/s in the subepithelia to counteract HIV-1 that would have transcytosed the vaginal epithelia and deliver and ensure bioavailability of the anti-HIV-1 agent over longer duration to outlast HIV-1 in the vaginal cavity (Hendrix et al., 2009).

Formulations prepared thus far that include gels, creams, films, tablets and rings have tried to mitigate these microbicide formulation shortcomings but have often fallen short (Hendrix et al., 2009). Gels, creams and films were found to be indiscrete, sticky and short acting thus require frequent application before and after every coital act whilst tablets and rings are discrete and may be formulated to deliver the anti-HIV-1 agent over an extended duration (Klaase et al., 2008).

This chapter discusses the formulation of a composite polymeric drug delivery system in the form of a caplet embedded with drug-loaded submicrospheres. The delivery system was tested *in vitro* as a potential microbicide drug delivery system. The submicrospheres were formulated from biocompatible materials; pectin, porcine gastric mucin and polyethylene glycol which formed the framework structure of the submicrospheres enabling the encapsulation and controlled release of zidovudine and BP36, the model antiretroviral agents used in the study. The polymeric matrix part of the delivery system was mostly formed from poly(D,L-lactide), a hydrophobic, biocompatible and biodegradable polymer. Poly(D,L-lactide) was chosen to ensure extended drug release from the caplet in line with the principle of having the microbicide outlasting HIV-1. The choice of poly(D,L-lactide) helps maintain the HIV-1 prohibitive acidic environment since it hydrolyses to form lactic acid which is in itself the acidifying agent normally produced by the anaerobic breakdown of glucose in the human vagina. The polymeric caplet is intended to be inserted into the posterior human vaginal fornix where it would be resident for an extended duration of time whilst releasing the anti-HIV-1 agent (Ndesendo et al., 2010). Only zidovudine and not BP36 was used in the formulation and testing of the composite delivery system in this chapter since BP36 is a herbal extract of low purity which was difficult to standardize and utilize in the experiments performed.

5.2. Materials and Methods

5.2.1. Materials

Polyvinyl acetate/polyvinylpyrolidone [Kollidon® SR (KSR)] and phosphate buffered saline (PBS, pH 7.4) were purchased from Aldrich® (Sigma–Aldrich Inc., St. Louis, USA). Poly(D,L-lactide) was purchased from Boehringer Ingelheim, Ingelheim, Germany. Poly(acrylic acid) (Carbopol 794P NF) was purchased from Noveon Inc, Cleveland, OH, USA. The optimised zidovudine-loaded pectin-mucin-polyethylene glycol submicrospheres were prepared as provided in chapter 4. Other materials and excipients including magnesium stearate (MS) were of analytical grade and were utilized as purchased. Simulated vaginal fluid (SVF, pH 4.5) was prepared from analytical grade reagents in accordance to Owen and Katz's formulation (Owen and Katz, 1999).

5.2.2. Box-Behnken design optimization of the composite polymeric drug delivery system (caplet)

A three-factor, three-level (3^3) Box-Behnken statistical design was employed to optimize the fabrication of the composite polymeric caplet. The upper and lower levels of three independent parameters; mass of PDLL, mass of MS and the mass of KSR are shown in table 5.1 (Karnachi and Khan, 1996; Box and Behnken, 1960). The responses; fractional mass increase (FMI) after 7 days of caplet dissolution in SVF, caplet matrix hardness (H) and fractional drug released (FDR) after 7 days of caplet dissolution in SVF were sought (Table 5.1). The 15 formulations generated by the Box-Behnken design (Table 5.2) were experimentally tested and the results obtained were fed into the MINITAB® software which then computed the optimized formulation's independent parameters and expected responses.

Table 5.1: Box-Behnken design independent parameter limits and response objectives

Variable	Limits (mg)	
	Lower	Upper
mass of poly(D,L-lactide)	1102.5	937.5
mass of magnesium stearate	7.5	22.5
mass of polyvinyl acetate/polyvinylpyrolidone	75	
Response	*Objective*	
fractional drug release after $t_{7\ days}$	minimize	
hardness (N)	maximize	
fractional mass increase after t_{7days}	minimize	

Table 5.2: Box-Behnken design template of the 15 polymeric caplet formulations

Formulation	Mass of PDLL	Mass of MS	Mass of KSR
F1	1102.5	15	225
F2	1102.5	7.5	150
F3	1020	22.5	225
F4	937.5	15	225
F5	1020	7.5	225
F6	1102.5	22.5	75
F7	1020	22.5	75
F8	937.5	22.5	150
F9	1020	705	225
F10	937.5	7.5	150
F11	1020	15	150
F12	1102.5	15	75
F13	1020	15	150
F14	937.5	15.0	75
F15	1020	7.5	75

5.2.3. Polymeric caplet matrix texture profiling

Caplet matrix hardness was tested using a calibrated texture analyzer (Texture Analyzer TA.*TX plus,* Stable Microsystems, Surrey, UK) fitted with a 5kg load cell and set according to the parameters shown in table 5.3. The peak compression force was measured in triplicate on three different locations along the caplet length using a 2mm flat cylindrical probe and the mean peak compression force value was computed and regarded as a measure of the matrix hardness of the caplet. Measurements were performed on all the caplets fabricated according to the 15 Box-Behnken design template formulations (Table 5.2) and on the optimized caplet. In addition, the percentage caplet matrix resilience was also determined (Pillay and Danckwerts, 2002).

Table 5.3: Texture analyzer parameters used in caplet matrix texture analysis

Parameter	Value
test mode	compression
pre-test speed	1.00mm/sec
test speed	2.00mm/sec
post- test speed	10.00 mm/sec
target mode	force
force	4N
trigger type	auto force
trigger force	0.05N

5.2.4. Effect of the quantity of poly(acrylic acid) on the caplet matrix dimensions

The effect of the amount (percentage of the total caplet mass) of poly(acylic acid) on the dimensional increase of the polymeric caplet after exposure to SVF for a month were measured at 1%, 2% and 3% poly(acrylic acid) content in the caplet. Caplets were immersed for 30 days in 100mL SVF filled containers which were then put in an orbital shaker incubator (Orbital Shaker Incubator, LM-530D, YIHDER TECHNOLOGY CO., LTD, Jhonghe City, Taipei County, Taiwan, Republic of China) which was kept at 37°C and rotated at 20rpm. The dimensional increase of the caplet was then computed according to equation 5.1.

$$\%\ dimensional\ increase = \frac{D_2 - D_1}{D_1} \times 100 \qquad Equation\ 5.1$$

Where D_1 is the length, width or thickness of the caplets before being immersed in SVF for 30 days and D_2 is the length, width or thickness of the caplet after it was immersed in SVF for 30 days

5.2.5. Polymeric caplet friability determination

The uniformly blended powder of the optimized formulation composed of poly(acrylic acid) (1%), PDLL (62.50%), MS (0.5%), KSR (5%) and AZT-loaded PEC-MUC-PEG SMs (20%) was used to directly compress 10 caplets at a compression force of 2.5 tonnes using a hydraulic Carver Press (Carver Inc, Wabash, IN, USA). The mass of each caplet was above 650mg and the mean caplet mass was 1266.61±9.50mg. Caplet friability was determined according to a USP 23 method using an Erweka friability apparatus made of a transparent smooth-surfaced polymer drum that had an internal diameter of 285mm and a depth of 39mm attached to a horizontal axis. The 10 caplets were dusted then placed in the drum

through the removable side of the apparatus. The drum was rotated 100 times at a constant rate of 25rpm and the caplets were tumbled at each turn of the drum by a curved projection from the middle of the drum to the outer wall. Caplets were then removed from the drum, dusted and reweighed. The caplet friability was then calculated according to equation 5.2.

$$Friability\ (\%) = \frac{M_1 - M_2}{M_1} \times 100 \qquad Equation\ 5.2$$

Where M_1 is the total mass of the 10 caplets before the experiment and M_2 is the total mass of the 10 caplets after the experiment

5.2.6. Drug release studies of the composite polymeric drug delivery system

Drug release studies were performed for the AZT containing composite polymeric caplet. The caplet was placed in a container filled with 100mL of SVF (pH 4.5) dissolution media (Gupta et al., 2011; Woolfson et al., 2010; Owen and Katz, 1999). The container was then placed in an orbital shaker incubator (Orbital Shaker Incubator, LM-530D, YIHDER TECHNOLOGY CO., LTD, Jhonghe City, Taipei County, Taiwan, Republic of China) which was kept at 37°C and rotated at 20rpm. An aliquot (200µL) was withdrawn at predetermined time intervals and an equal volume of fresh SVF was replaced after each withdrawal. The fraction of drug released from the caplet was then computed from the UV absorbance values measured on 4µL of the withdrawn samples at 25°C using a nanophotometer which was set to detect UV absorbance at λ_{max} of 267nm. Drug release studies were performed in triplicate.

Drug release studies were also performed in phosphate buffered saline (PBS pH 7.4) which acted as a simulant for semen (Owen and Katz, 2005). The MDT computed from the drug release data revealed the extent to which AZT release from the composite polymeric caplet could be sustained. A comparison was made of dissolution of AZT in SVF and in PBS by noting their calculated dissolution efficiencies (DE) according to equation 4.5 and through the determination of the similarity factor (f_2) and the difference factor (f_1) according to equations 4.6 and 4.7 (Moore and Flanner, 1996; O'Hara et al., 1998; Costa et al., 2001; Zhang et al., 2010). The coefficient of determination ($R^2_{adjusted}$) obtained from fitting the dissolution profile of the caplet into 14 different kinetic models gave an indication as to which model drug release from the caplet followed (Zhang et al., 2010).

5.3. Results and Discussion

5.3.1. Fabrication and optimization of the composite polymeric delivery system

The polymeric caplets fabricated by direct compression (using a custom made punch and die set depicted in figure 5.1) according to the 15 Box-Behnken design formulations had variable masses and dimensions depending on the amount of material that was used to fabricate them. The optimized formulation caplet had an approximate length of 25mm, width of 10mm and thickness of 6mm. Experimental procedure yielded varying results of, FMI, H and FDR (Table 5.4). These results were then inputted into the MINITAB® software to yield an optimized formulation with a composite desirability (D) of 0.997, fractional mass increase desirability (d_{FMI}) of 1.000, hardness desirability (d_H) of 1.000 and fractional drug release desirability (d_{FDR}) of 0.991.The optimum independent parameters were computed to be; PDLL mass of 937.50mg, MS mass of 7.5mg and KSR mass of 75mg. These independent parameters yielded computed responses; FMI of 0.279, H of 21.849 FDR of 0.401. The relationships between the independent parameters and responses assessed by linear regression using MINITAB® were described by the polynomial equations; 5.3, 5.4 and 5.5 (Karnachi and Khan, 1996). Where the coefficient of determination of FMI (R^2_{FMI}) was 87.30%, H (R^2_H) was 61.70% and that of FDR (R^2_{FDR}) was 77.90% (Karnachi and Khan 1996).

FMI=1.616-0.002[PDLL]+0.668[MS]-0.001[KSR] *Equation 5.3*

*H=-14.465+0.101[PDLL]-0.706[MS]-0.109[KSR]-0.005[MS*MS]+0.001[PDLL*MS]+ 0.001[MS*KSR]* *Equation 5.4*

FDR=3.964-0.008[PDLL]+0.009[MS]+0.007[KSR] *Equation 5.5*

The correlation of the responses, FMI, H and FDR to the independent parameters, PDLL, MS and KSR was also illustrated as response surface plots (Figure 5.2).



Figure 5.1: Digital photographs of the steel punch and die set and a polymeric caplet punched using the set.

Table 5.4: Experimental responses to the 15 design formulations used in the optimization for the polymeric caplet

Formulation	Fractional mass increase after 7days in SMV[a]	Hardness (N)	Fractional drug release in SVF after 7 days
F1	0.320	20.152	0.227
F2	0.314	18.438	0.245
F3	0.678	21.634	0.346
F4	0.502	18.400	0.376
F5	0.474	19.849	0.369
F6	0.358	19.634	0.332
F7	0.394	19.997	0.274
F8	0.635	20.977	0.419
F9	0.314	18.636	0.264
F10	0.404	21.473	0.320
F11	0.386	21.384	0.288
F12	0.330	20.158	0.330
F13	0.366	21.286	0.261
F14	0.507	21.031	0.328
F15	0.284	20.164	0.243

a - simulated vaginal fluid

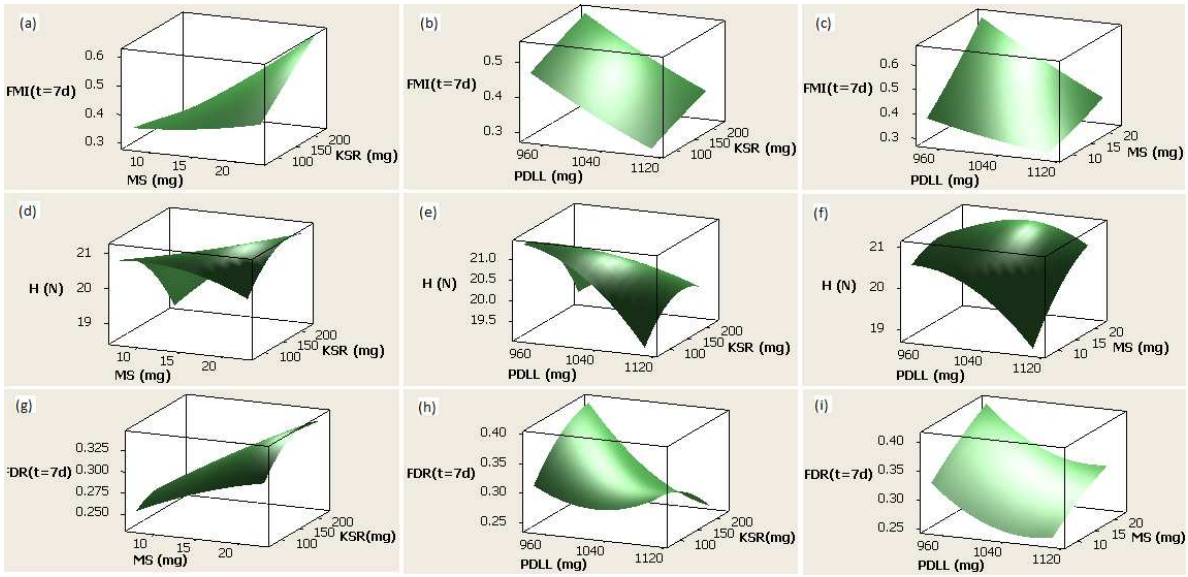


Figure 5.2: Response surface plots correlating responses; fractional of mass increase (FMI), matrix hardness (H) and fractional drug release (FDR) to independent parameters; masses of magnesium stearate (MS), polyvinyl acetate/polyvinylpyrolidone (KSR) and poly(D,L-lactide) (PDLL) used in fabricating the polymeric caplet.

5.3.2. Effect of the quantity of poly(acrylic acid) on caplet matrix swelling

The amount of poly(acrylic acid) in the caplet determined the degree of SVF or PBS uptake and hence the caplets' percentage dimensional increase (swelling; increase in length, width and thickness). Figure 5.3a depicts digital photographs of the polymeric caplets containing; 1%, 2% and 3% poly(acrylic acid) before and after being immersed in SVF for a month. The percentage dimensional increase in length, width and thickness of the caplet are illustrated by the bar graph in figure 5.3b. An increase in the content of poly(acrylic acid) meant an increase in the hydroxyl and carboxyl groups in the caplet which would lead to more SVF or PBS being drawn into the caplet through the possible formation of hydrogen bonds between the hydroxyl and carboxyl groups of poly(acrylic acid) and the water molecules in SVF or PBS resulting in caplet matrix swelling. The alkaline PBS (pH 7.4) caused the ionization and repulsion of carboxyl groups resulting in more swelling than in the acidic SVF (pH 4.5) where the carboxyl groups remained neutral as depicted in figures 5.4 and 5.5. The same phenomena are expected *in vivo* where normal vaginal fluid is acidic and seminal fluid is alkaline (Owen and Katz, 1999; Owen and Katz, 2005). In addition, increase in poly(acrylic acid) concentration would therefore affect the drug release rate (Khan and Zhu, 1998).

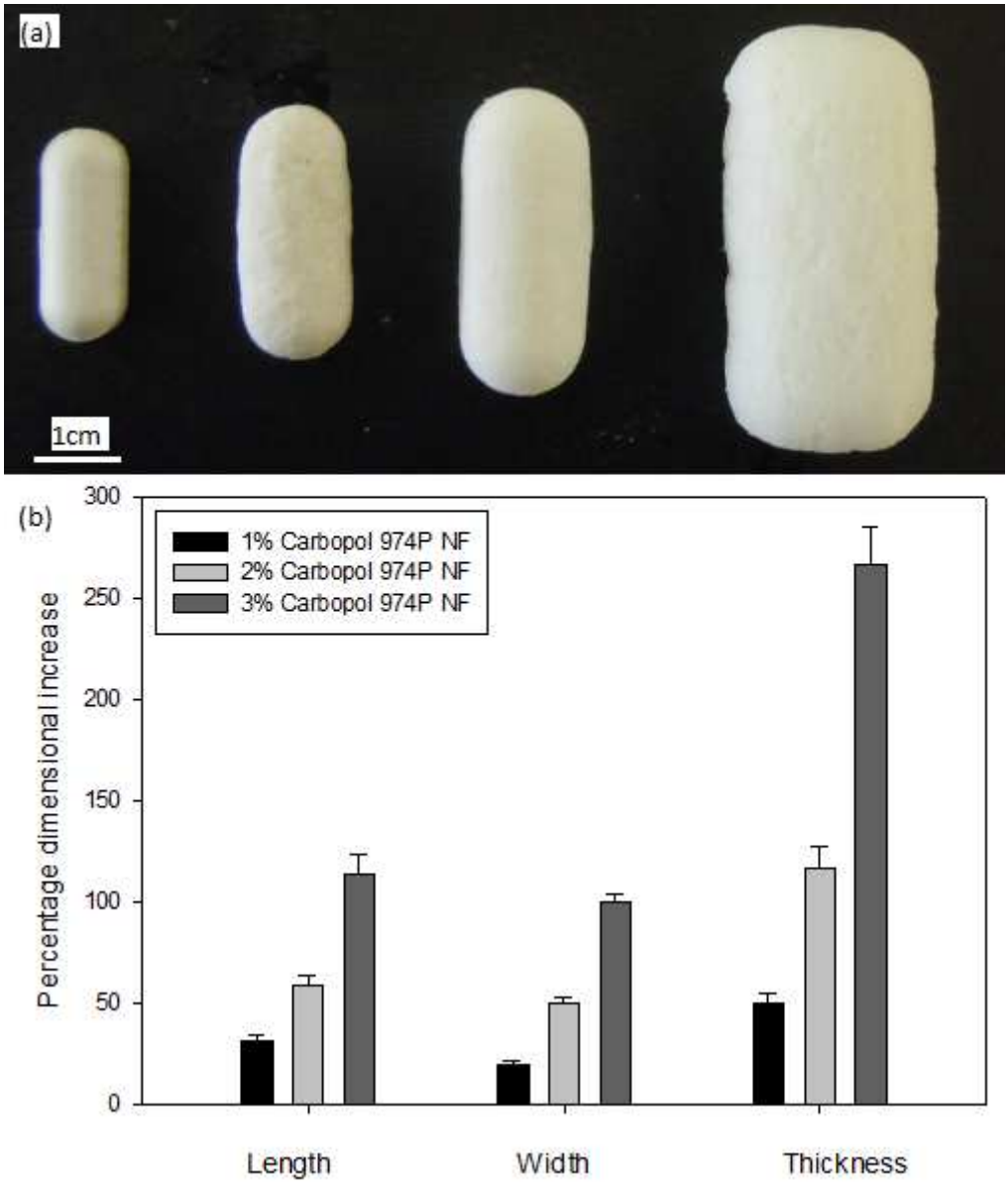


Figure 5.3: Depicts (a) digital photographs of polymeric caplets, from left to right; before the 30 day dissolution in SVF and after dissolution for the caplets containing 1%, 2% or 3% of poly(acrylic acid) and (b) a bar graph illustrating the different percentage dimensional increases in length, width and thickness of the polymeric caplet containing 1%, 2% and 3% poly(acrylic acid) that was measured after 30 days of caplet dissolution in SVF.

Figure 5.4 shows a digital photograph and SEM micrographs of the cross-sectional area of the caplet before and after dissolution in SVF or PBS for 30 days. Figure 5.4a clearly illustrates the positive effect of poly(acrylic acid) on the swelling of the polymeric caplet, with the caplets containing more poly(acrylic acid) (2% and 3%) having larger cross-sectional areas. SEM micrographs (Figure 5.4c-e) reveal that there were pores formed within the caplet in addition to the swelling of the caplet. The pores observed might have been due to the bulk erosion of the caplet matrix that possibly involved the hydrolytic degradation of

poly(D.L-lactide) and the solubilization and leaching out of the polyvinylpyrolidine part of polyvinyl acetate/polyvinylpyrolidone, KSR (Li and McCarthy 1999, Siepmann et al., 2010).

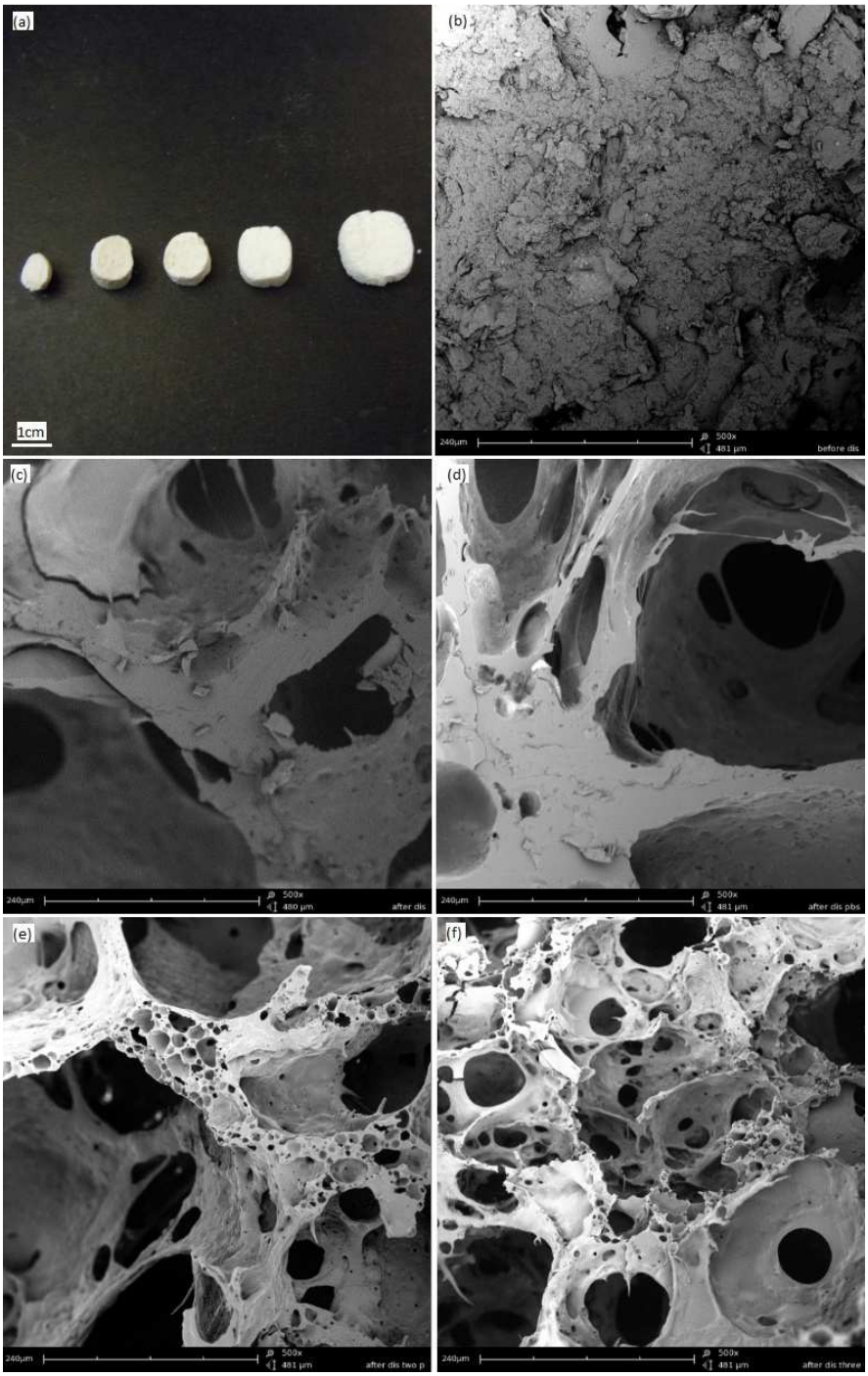


Figure 5.4: Depicts; (a) digital photograph of the caplet's cross-section (from left to right); before dissolution and after 1% poly(acrylic acid) containing caplet's dissolution in SVF and PBS then 2% and 3% poly(acrylic acid) containing caplet's dissolution in SVF respectively (b) SEM micrograph acquired at 500X magnification of the caplet's cross-section before dissolution and (c-f) SEM micrograph of the caplet cross-section after a 30 day dissolution of the caplet containing, (c) 1% poly(acrylic acid) in SVF (d) 1% poly(acrylic acid) in PBS (e) 2% poly(acrylic acid) in SVF and (f) 3% poly(acrylic acid) in SVF.

5.3.3. Polymeric caplet matrix texture profile

Caplet matrix hardness (H) values for the 15 design formulations were measured and are presented in table 5.4. Caplet hardness varied from 18.400N in Formulation F11 to 21.634N in Formulation F15 (Table 5.4). The optimized formulation had a Box-Behnken computed caplet matrix hardness of 21.849N whilst the experimentally measured hardness was 22.061±0.261N (Figure 5.5). From the response surface plots in figure 5.2d, e and f as well as the hardness response values of the 15 design formulations in table 5.4, it was observed that hardness decreased with increasing percentage content of PDLL and generally increased with increase in the percentage content of the plastically deforming KSR (El-Bragory et al., 2010). The percentage composition of MS in the caplet had an ambiguous effect on caplet hardness as previously reported by Matsuda and co-workers (Matsuda et al, 1976). Both, relatively low and high amounts of MS resulted in decreased caplet hardness (Figure 5.2d).

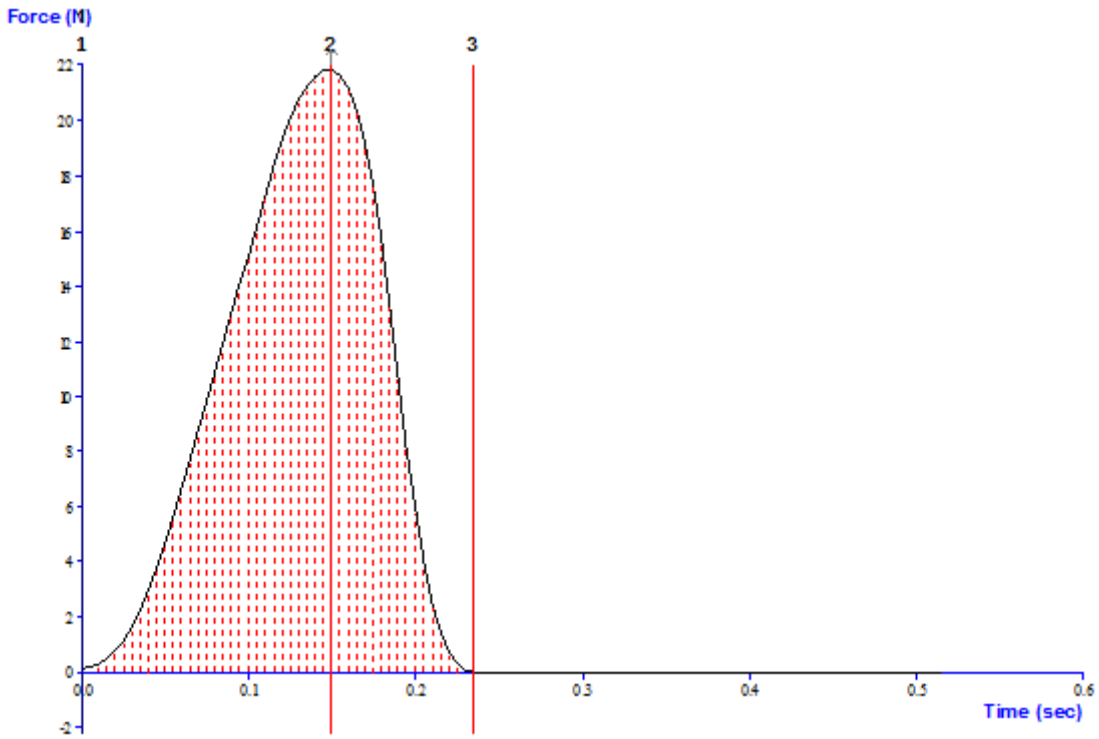


Figure 5.5: Force versus time texture analysis profile used to determine the caplet matrix hardness (H) and percentage matrix resilience

In addition, the percentage matrix resilience of the caplet was computed from the force versus time curve according to equation 5.6 (Pillay and Danckwerts, 2002).

$$Matrix\ resilience\ (\%) = \frac{\int_2^3 f(t)dt}{\int_1^2 f(t)dt} \times 100 \qquad Equation\ 5.6$$

Where $\int_2^3 f(t)dt$ is the area under the curve between the anchors 3 and 2 and $\int_1^2 f(t)dt$ is the area under the curve between the anchors 2 and 1. The anchors are depicted as red vertical lines in Figure 5.5. The mean percentage polymeric caplet matrix resilience was 62.444±0.583%.

5.3.4. Polymeric caplet friability

All 10 caplets employed were neither cracked nor broken after the friability test. Their total mass before and after the experiment was 12662.9mg and 12656.0mg respectively. Their friability was computed to be 0.054%, which is less than 1%.

5.3.5. Drug release from the composite polymeric delivery system

The fraction of AZT released from the polymeric caplet was measured over 7 days for the 15 design formulations and results obtained are presented in table 5.4. The fraction of drug released varied from 0.227 in formulation F1 to 0.419 in formulation F8 (Table 5.4). The optimized formulation had a computed fraction of drug released within 7 days of 0.401. The fraction of drug released from the optimised formulation was then experimentally tested in both SVF and PBS (acted as a semen simulant) over 30 days to obtain the drug release profiles depicted in figure 5.6. The fraction of drug released after 30 days in SVF (pH 4.5) was 0.743±0.010 and that released in PBS (pH 7.4) was 0.806±0.210. There was a MDT decrease when dissolution was performed in PBS (MDT=7.675 days) as compared to in SVF (MDT=10.556 days) as well as a marginal increase in the fraction of drug released in PBS (pH 7.4) to that released in SVF (pH 4.5). This may be attributed to the 1% poly(acrylic acid) composition of the polymeric caplet. Poly(acrylic acid) is pH responsive due to the several carboxylic groups it possesses which are ionized in basic media (PBS pH 7.4) and unionized in acidic media (SVF pH 4.5). Therefore, these ionized carboxylic groups, in basic media (pH 7.4), might have repelled each other and polarized as well as attracted dissolution media's water molecules resulting in an increase in dissolution media uptake thus leading to caplet matrix swelling as depicted in figure 5.3. This matrix destabilization and increase in basic dissolution media uptake by the caplet then resulted in an increase in drug release and a decrease in MDT (Khan and Zhu, 1998).

The effect of the dissolution media pH in conjunction with the 1% poly(acrylic acid) on the caplet dissolution kinetics is illustrated in figure 5.6 and confirmed by the similarity factor (f_2=44,821) and the difference factor (f_1=28.738) whose computed values show that the dissolution profile obtained in SVF was different from that obtained in PBS. Since f_2 values from 50-100 relate to the sameness of dissolution profiles and f_1 values from 0-15 means there is little difference in the dissolution profiles. Values of f_2 (44.821) and f_1 (28.738) were not within these ranges which means that the dissolution profiles were different (O'Hara et al., 1998, Costa et al., 2001). The increase in DE when dissolution was performed in PBS (DE=59.598%) as compared to dissolution in SVF where DE was 48.125% also confirmed the pH responsiveness of caplet dissolution (Moore and Flanner, 1996; O'Hara et al., 1998; Costa et al., 2001; Zhang et al., 2010).

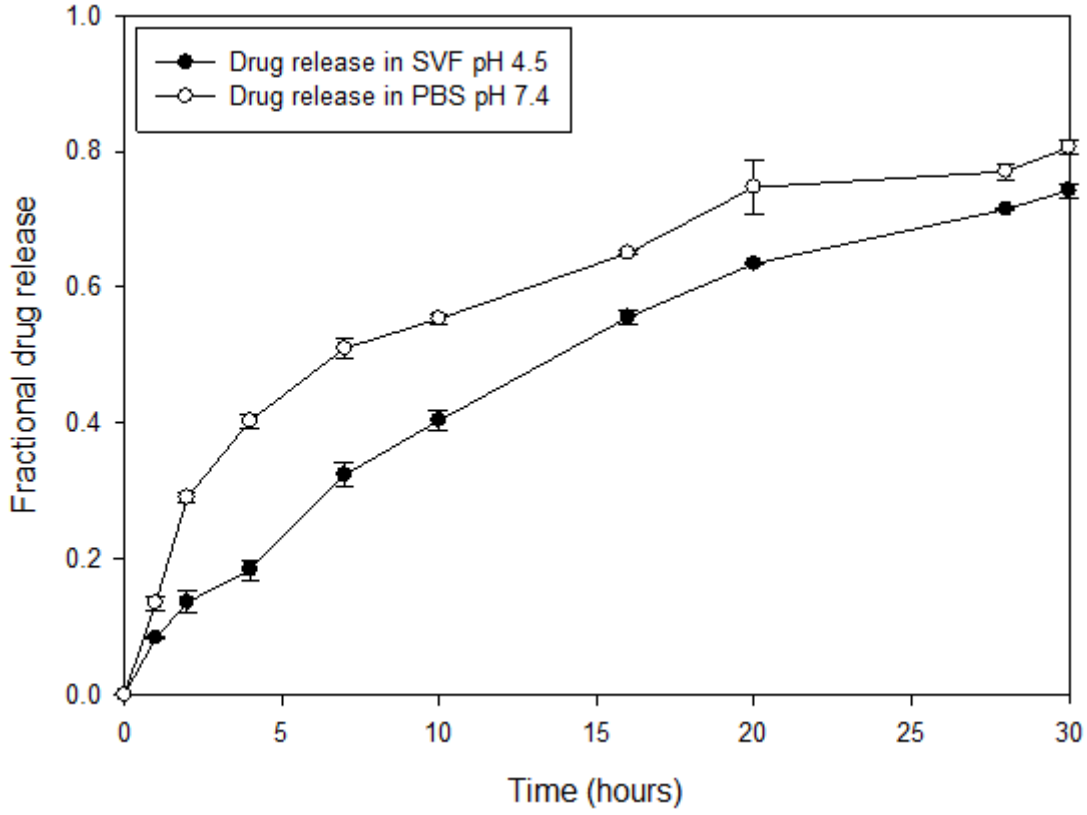


Figure 5.6: Fraction of AZT released from the optimised caplet in SVF and PBS over 30 days

The drug release mechanism, in both SVF and PBS, from the composite polymeric caplet was shown to follow most kinetic models it was fitted into as given by the adjusted coefficient of determination, $R^2_{adjusted}$, which was high, ranging from 0.8848 for the zero order kinetic model to 0.9973 for the Makoid-Banakar model in SVF and from 0.5021 for zero order kinetic model to 0.9947 in PBS Weibull model (Table 5.5). AZT release mechanism from the caplet was a sum of the release mechanism from the macromolecular SMs and that from the

main polymeric matrix. Drug release from the matrix was extended due to the hydrophobic PDLL whose hydrolytic degradation is known to be slow (Li and McCarthy, 1999). The dissolution media was drawn into the interior of the caplet by the hydrogen bond forming poly(acrylic acid) and the hydrophilic polyvinylpyrolidine part of KSR. Polyvinylpyrolidine was then dissolved and leached out of the caplet matrix together with the drug released from the SMs leaving pores as depicted in figure 5.4 (Siepmann et al., 2010). The pores formed enabled more dissolution media to enter the caplet matrix leading to more percolation based AZT release (Siepmann et al., 2010). Drug release from the caplet matrix was therefore swelling and diffusion dependent.

Table 5.5: Best fit parameters and adjusted coefficients of determination obtained after fitting the optimized caplet drug release profile to different kinetic models (Costa and Lobo, 2001; Zhang et al., 2010; Dash et al., 2010).

Dissolution model	Best-fit parameter						Goodness of fit parameter (R^2 adjusted)	
	Parameter 1		Parameter 2		Parameter 3		pH 4.5	pH 7.4
	pH 4.5	pH 7.4	pH 4.5	pH 7.4	pH 4.5	pH 7.4		
Zero order	k_0=2.839	k_0=3.287					0.8848	0.5021
First order	k_1 0.050	k_1=0.078					0.9903	0.8829
Higuchi	kH=13.294	kH=16.000					0.9772	0.9515
Korsmeyer-Peppas	kKP=9.659	kKP=22.126	n=0.609	n=0.388			0.9908	0.9786
Hixson-Crowell	kHC=0.14	kHC=0.020					0.9725	0.8030
Hopfenberg	kHB=0.000	kHB=0.00	n=3016.319	n=5886.059			0.9891	0.8683
Baker-Lonsdale	kBL=0.004	kBL=0.007					0.9516	0.9865
Makoid-Banakar	kMB=6.985	kMB=18.728	n=0.842	n=0.545	k=0.017	k=0.014	0.9973	0.9885
Peppas-Sahlin	k_1=-24.048	k_1=19.701	k_2=30.807	k_2=-1.203	m=0.205	m=0.576	0.9932	0.9889
Quadratic	k_1=-0.001	k_1=-0.002	k_2=0.049	k_2=0.072			0.9928	0.8821
Weibull	α=888.973	α=3.619	β=0.566	β=0.513	Ti=0.545	Ti=0.686	0.9917	0.9947
Logistic	α=-0.2973	α=-0.1644	β=2.674	β=1.988			0.9938	0.9920
Gompertz	α=4.457	α=2.032	β=1.715	β=1.375			0.9741	0.9884
Probit	α=-1.783	α=-1.005	β=1.609	β=1.218			0.9904	0.9929

k_0, k_1, kH, kKP, n, kKP, kHC, kHB, kBL, k, k_2, α and β are best fit parameters of the respective dissolution models

5.4. Concluding remarks

A composite polymeric delivery system in the form of a hard, resilient and non-friable caplet embedded with AZT-loaded MUC-PEC-PEG submicrospheres was successfully formulated, optimised using a 3^3 Box-Behnken design and fabricated by direct compression. The drug release mechanism from the caplet was likely due to a combination of matrix swelling and diffusion. Matrix swelling was proportional to the amount of poly(acrylic acid) in the caplet and pores were formed in the matrix as a result of the solubilisation of the polyvinylpyrolidine part of polyvinyl acetate/polyvinylpyrolidone (KSR). The dissolution media percolated into the matrix through the formed pores and AZT then diffused out. Fractional drug release over 30 days was 0.743±0.010 in SVF and 0.806±0.210 in SVF. Dissolution of AZT from the caplet matrix was observed to be affected by the pH of the dissolution medium. This was confirmed by the reduction in the mean dissolution time, the increase in dissolution efficiency and computed values of the similarity factor (f_2<50) and difference factor (f_1>15) for the dissolution profiles obtained in SVF and PBS. Dissolution kinetics of AZT release from the composite polymeric caplet fitted best with the Makoid-Banakar model when SVF was used as the dissolution medium and with the Weibull model when PBS was used as the dissolution media.

In conclusion a caplet delivery system which was able to act as a reservoir for an anti-HIV-1 agent and capable of delivering such an agent over an extended duration of a month was successfully formulated from biocompatible materials and tested *in vitro*. This delivery system, used discretely *in vivo*, would likely ensure that there is enough of the anti-HIV-1 agent present in the vaginal cavity to counter HIV-1 in the seminal fluids interposed into the vaginal cavity during coitus, with no frequent dosing required prior to or after each coital act. In addition, this delivery system provides for increased anti-HIV-1 agent release when the pH of the vaginal cavity is increased as a result of the presence of the normally alkaline seminal fluid. Further tests including performance of the composite delivery system *in vivo* in the pig model and pathotoxicity studies necessary to judge the efficacy and safety of the delivery system were performed and the results presented in chapter 6.

CHAPTER 6

IN VIVO ANALYSIS OF AN EXTENDED COMPOSITE DRUG DELIVERY SYSTEM IN THE PIG MODEL

6.1. Introduction

The development of topically applied chemical agents that may effectively prevent vaginal HIV-1 transmission (microbicides) has been a major challenge for pharmaceutical scientists (Hendrix et al., 2009; Adams and Kashuba, 2012; Pillay et al., 2012). The difficulties have included; microbicide acceptance as an alternative HIV-1 prevention modality, pharmacokinetic inadequacy whereby the microbicide has to be distributed throughout the vaginal mucosa in sufficient quantities to prevent HIV-1 transmission and mucosal toxicity which diminishes the vaginal mucosa's barrier properties resulting in easy HIV-1 mucosal transcytosis and transmission (Adams and Kashuba, 2012; Pillay et al., 2012). Despite having vast potential as a preventative tool against vaginal HIV-1 transmission, research conducted thus far has failed to provide an effective anti-HIV-1 microbicide product to the market.

Motivation for further research is still present in that, HIV/AIDS is still a pandemic, new infections are still occurring each day and the use of microbicides may be advantageous in that they may be used discreetly by the female partner thus shifting the control of HIV-1 prevention from the male to the female (Shattock and Solomon, 2004). Microbicides provide a frontline defense approach where HIV-1 is targeted at the vagina mucosal surface when it is still vulnerable since the quantity of viruses that initially transcytoses the vaginal mucosa (founder population) has been shown to be inadequate to sustain transmission until viral replication occurs (Haase, 2010; Shattock and Solomon, 2004; Stone, 2002; Haase, 2005; Pillay et al., 2012). Therefore, microbicides may act at this juncture to contain HIV-1 replication hence prevent transmission. Acting at the mucosal surface where fewer $CD4^+$ cells are present as compared to the submucosa, microbicides have the capacity to cub HIV-1 transmission (Haase, 2005).

The feasibility of the development and use of microbicides to prevent vaginal HIV-1 trasmission has continuously been hightened by the; discovery of several highly potent anti-HIV-1 agents, microbicide success stories exemplified by the 39% success rate of the 1% tenofovir gel observed in the CAPRISA study and the increase in scientific knowledge accumulated thus far including the postulated reasons for the failure of some microbicides, for example, vaginal mucosal integrity disruption by microbicides that inturn causes

increased HIV-1 transmission (Abdool Karim et al., 2010; Pillay et al., 2012). Microbicide research is now focused intensely on microbicide developmental aspects such as bioavailability enhancement (targeted and extended release formulations) and Toxicological exclusion (Klaase et al., 2008; Pillay et al., 2012; Hendrix et al., 2009).

Future microbicides would therefore be formulated to ensure that enough of the potent anti-HIV-1 agent is available at the vaginal mucosal interface and distributed throughout the entire target site for an extended duration of time to outlast HIV-1 (Pillay et al., 2012). Strict toxicology and tolerance protocols using appropriate animal models would have to be followed to exclude irritancy and disruption of the vaginal mucosa barrier properties caused by the use of microbicides (D'cruz et al., 2005; D'cruz and Uckun, 2008; D'cruz et al., 2003; Cone et al., 2006). Microbicide formulations have to satisfy these pharmacokinetic, and pathotoxicity preconditions to achieve *in vivo* microbicide success (das Neves and Bahai, 2006; Adams and Kashuba, 2012; Pillay et al., 2012). This chapter discusses a study in which a composite polymeric drug delivery system intended for intravaginally microbicide delivery was tested *in vivo* over 28 days in the pig model. Large White female pigs were chosen as test animals because of their costs, availability and the physiological and anatomical resemblance they have with humans. Zidovudine and BP36 which were used as model microbicide drugs/agents were encapsulated in pectin-mucin-polyethylene glycol submicrospheres which were then embedded within a polymeric caplet shaped matrix which was thereafter inserted into the vaginal cavity of Large White female pigs. *In vivo* performance of the delivery system was observed by taking X-ray images and drug concentration in vaginal fluid, vaginal tissue and plasma was measured at predetermined time points. In addition, histopathological analysis was performed on the pig vaginal tissue excised from the euthanized pigs after 28 experimental days. This study aimed at testing an alternative microbicide delivery system *in vivo*, with the possibility of providing extended microbicide delivery and to determine the level of vaginal epithelia pathotoxicity that such a delivery system might produce.

6.2. Materials and Methods

6.2.1. Materials

Poly(D,L-lactide), polyvinyl acetate/polyvinylpyrolidone [Kollidon® SR (KSR)], magnesium stearate, porcine gastric mucin, polyethylene glycol 400, barium sulphate, acetonitrile and formic acid were purchased from Aldrich® (Sigma–Aldrich Inc., St. Louis, USA). Poly(acrylic acid) was purchased from Noveon Inc, Cleveland, OH, USA. Pectin, GENU® pectin type USP/100 [Degree of esterification (DE) 55-65%] was purchased from CP Kelco ApS, Lille Skensved, Denmark. Active pharmaceutical ingredients (APIs); 1-[(2*R*,4*S*,5*S*)-4-azido-5-

(hydroxymethyl)oxolan-2-yl]-5-methylpyrimidine-2,4-dione commonly known as zidovudine (AZT) and 2',3'-dideoxy-3'-thiacytidine, commonly known as lamivudine (3TC) were purchased from GlaxoSmithKline, Middlesex, UK. BP36 was obtained from the Council for Scientific and Industrial Research (CSIR), South Africa. UPLC grade water was purified using a Milli-Q® gradient water purification system (Millipore SAS, Molsheim, France). Other materials and excipients employed were of analytical grade and were utilized as purchased.

6.2.2. Preparation of the drug-loaded composite polymeric delivery system

A composite polymeric delivery system composed of drug-loaded submicrospheres embedded within a caplet-shaped polymeric matrix was prepared by first preparing the drug loaded microspheres separately (chapter 5) then blended them with other caplet constituent materials to prepare the caplet as shown in chapter 5 (Sriamornsak et al., 2010; Brannon-Peppas, 1992). The drug encapsulated submicrospheres were formulated through a crosslinking-emulsion technique where a Ca^{2+} crosslinked dispersion of pectin, porcine gastric mucin, polyethylene glycol 400, BP36 and AZT acted as the aqueous phase whilst cyclohexane was the oil phase. The optimized independent parameters of ultrasonication time 6.28min, drug:polymer ratio 1:1 and surfactant (span 85) concentration 1.64 ($\%^{v}/_{v}$) were utilised in the formulation of the submicrospheres. The caplet shaped polymeric matrix was directly compressed from uniformly blended poly(D,L-lactide) (937.50mg), polyvinyl acetate/polyvinylpyrolidone (75.00mg), magnesium stearate (7.50mg) poly(acrylic acid) (1% $^{w}/_{w}$) and the drug-loaded submicrospheres (20% $^{w}/_{w}$).

6.2.3. Transportation and housing of the experimental animals (Large White pigs)

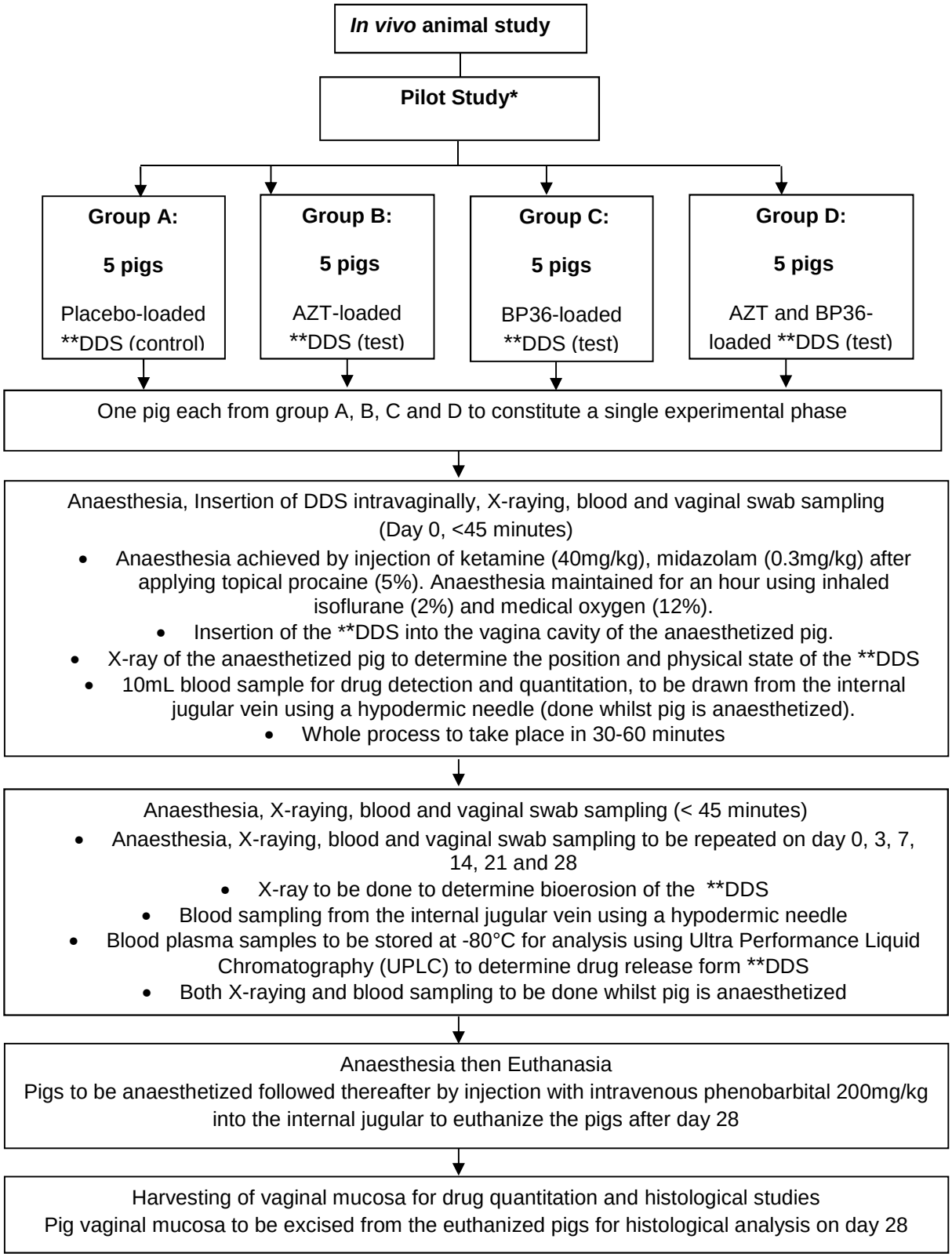
The pigs were purchased and transported from certified suppliers according to the South Africa Laws. Appropriate pre-transportion handling, loading, journeying and unloading at the Central Animal services (CAS), University of the Witwatersrand, were performed according to CAS standard operating procedures (SOPs). On arrival at CAS the pigs were assessed for any signs of disease, injury or distress and then socialized accordingly before the experimental procedures were conducted (Grandin, 1997; McEwen, 2002; Grandin, 2007; Nanni Costa, 2009). The pigs were housed at the CAS under the care of the researcher with the assistance of suitably qualified and trained CAS staff. Initially the delivered pigs were housed together in a single pen (Figure 6.1a). Thereafter, each pig was housed separately in a pen once the experimental procedures began as portrayed in figure 6.1b (i.e. after intravaginal insertion of the composite polymeric delivery system). Separation of each pig during experimentation was done for easy identification and monitoring. There was enough clean, adequately drained space for all pigs to stand on or lie down (Broom et al., 1995).



Figure 6.1: Large White female pigs housed in the Central Animal Services, University of the Witwatersrand (a) together in one pen upon delivery and (b) separately in each pen during experimentation.

6.2.4. In vivo experimental design and procedure

In vivo experimentation involved intravaginal insertion of a composite polymeric drug delivery system in 20 Large White female pigs weighing approximately 45kg. For statistical significance 20 Large White female pigs were chosen and divided into 4 groups of 5 pigs each. A statistical significant level of (p=0.05) was applied (Dell et al., 2002; Festing, 1994). This study was approved by the Animal Ethics Screening Committee (AESC) of the University of the Witwatersrand, Johannesburg, South Africa (AESC clearance No. 2011/44/05). The 20 pigs were divided into 4 groups of 5 pigs each, with group A having the delivery system with no drug (control) inserted in the vaginal cavity; group B, AZT-loaded delivery system inserted in the vaginal cavity; group C, BP36-loaded delivery system inserted intravaginally and finally group D which had a combination of AZT and BP36 loaded in the composite delivery system and inserted into the pigs' vaginal cavity as depicted in the flow diagram (figure 6.2).



* Main study to commence when the pilot study has proven that the BP36 is safe in the pig model.

** DDS- drug delivery system

Figure 6.2: Flow diagram depicting a step-by-step *in vivo* experimental approach

All groups including the pilot study underwent the same experimental procedures. Blood sampling from the internal jugular vein and X-raying was performed on day: 0, 3, 7, 14, 21 and 28 whilst the pig is anaesthetized. Study was staggered with only one pig from each group undergoing experimentation at a particular stage.

A pilot study was performed to test the experimental procedure and to determine the safety of BP36 (a novel anti-HIV-1 herbal extract) in one pig from group C. The pig was anaesthetised by an intramuscular injection of ketamine (11mg/kg) and midazolam (0.3mg/kg) on the thigh muscle (Figure 6.3a). The pig was then laid in the ventral position on an operating table where it was maintained under general anaesthesia using inhalation 2% isoflurane and 12% medical oxygen (Kaiser et al., 2006; Ndesendo et al., 2010). The BP36-loaded drug delivery system was inserted 13cm deep in the vaginal cavity using a metal speculum. The drug delivery system was expelled within 2 hours. Therefore, a different technique was used whereby the delivery system was tied right round using a silk suture material over an engraved shallow groove and then sutured to the vaginal mucosa (Figure 6.3b). In this case the delivery system was retained for three days but the suture material cut through the delivery system leading to the loss of the delivery system. This technique was also abandoned.

Finally, the BP36-loaded composite polymeric delivery system was enclosed in a silk material pouch that was then secured in the vaginal cavity by suturing the silk pouch onto the vaginal mucosa at a position distal to the urethra and proximal to the cervix and this technique proved to be the best method to ensure that the delivery system stayed in the vaginal cavity for 28 days. Therefore, all the proceeding experimentation was performed according to this successful technique achieved during the pilot study. Throughout experimentation the pig's cardiac activity (electrocardiogram), pulse, blood pressure and temperature were monitored (Kaiser et al., 2005). In addition, the pig's weight was measured and recorded every week.

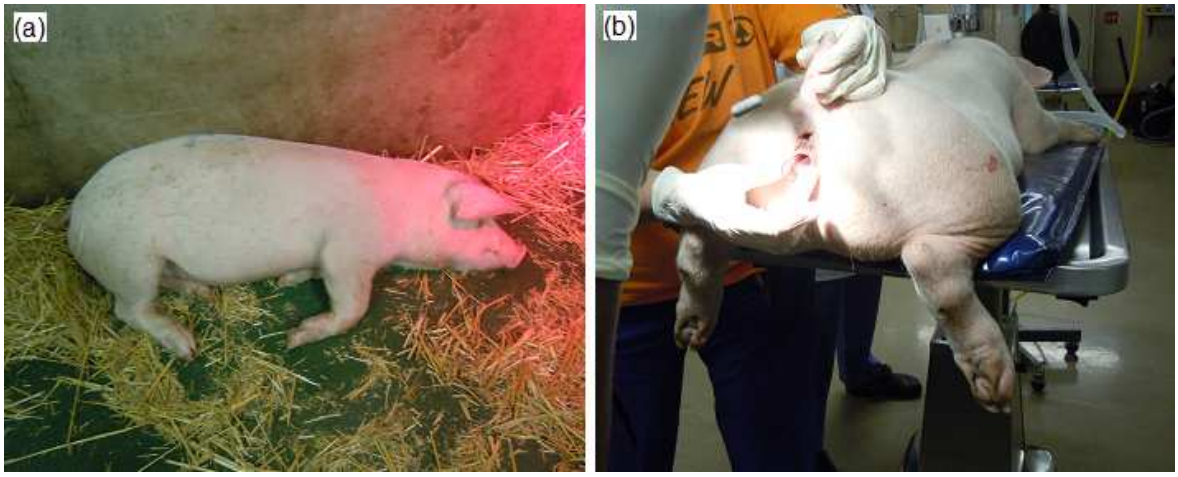


Figure 6.3: Pig shown, (a) under anaesthesia in the pen before being taken to the procedures room and (b) during intravaginal insertion of a delivery system that was tied right round using a silk suture material then sutured onto the vaginal mucosa.

6.2.4.1. *In vivo* X-ray imaging of the intravaginal polymeric delivery system

The composite polymeric delivery system contained barium sulphate (10% $^{w}/_{w}$), the radio opaque material which enabled X-ray detection of the delivery system *in situ*. The pig was laid on an operating table in the dorsal position whilst under anaesthesia and an X-ray of its pelvic region was taken using a Shimadzu MobileArt Evolution X-ray system (model MUX 200, Shimadzu Corporation, Kyoto, Japan) as depicted in figure 6.4. X-ray images of the delivery system were taken on days; 3, 7, 14, 21 and 28 after the delivery system was inserted in the vaginal cavity in order to detect its presence and location intravaginally, as well as to observe any dimensional changes that may occur to the delivery system *in situ* (Ndesendo et al., 2010).



Figure 6.4: Large White female pig lying on the operating table in the dorsal position whilst under anaesthesia during the X-ray procedure.

6.2.4.2. Vaginal swab collection

Vaginal swabs were performed to collect vaginal fluids whilst the pig was under anaesthesia before the insertion of the delivery system and on days; 0, 3, 7, 14, 21 and 28 after the delivery system was insertion. The procedure to collect the vaginal fluids involved the insertion of a cotton bud into the vaginal cavity about 4cm deep and allowing it to absorb vaginal fluids for approximately 1min (Clark and Friend, 2012). On removal of the cotton bud, a swab of the vaginal mucosa was performed with care taken not to contact the delivery system. The cotton buds were placed in 2mL Eppendorf tubes and then stored at -80ºC until analysis.

6.2.4.3. Blood sample collection

Blood samples (10mL) were withdrawn directly from the internal jugular vein whist the anaesthetized pig lay in the dorsal position starting on the day of delivery system insertion (day 0, before delivery system insertion) followed by blood sampling on days; 3, 7, 14, 21 and 28 after the delivery system was inserted in the vaginal cavity (Clark and Friend, 2012; Ndesendo et al., 2010). Withdrawn blood samples were immediately placed in heparinised tubes which were centrifuged at 1200rpm and the supernatant was stored in 2mL Eppendorf tubes at -80ºC for further analysis.

6.2.4.4. Vaginal tissue sample collection

On day 28, after X-ray taking, vaginal swab collection and blood sampling, the pigs were euthanized by means of an intravenous injection of Phenobarbital (200mg/kg) to one of the ear veins to enable vaginal tissue collection. The vaginal tract was excised from the pelvic canal after midline dissection through the symphysis pubis. Thereafter the vaginal tract was dissected to expose the vaginal mucosa. Two tissue samples were collected from each pig, one for quantitative bioanalysis to determine drug tissue concentration and the other for histopathology analysis. Tissue samples for quantitative tissue drug determination were placed in cryotubes and stored at -80ºC until analysis whist the tissues for histopathology assessment were fixed in 10% neutral-buffered formalin and stored at 4ºC until analysis (D'cruz et al., 2005, Cone et al., 2006).

6.2.5. Quantitative chromatographic determination of drug (AZT and/or BP36) in plasma, vaginal fluid and vaginal tissue

Detection and quantification of AZT and BP36 in porcine plasma samples was performed on a Waters Acuity™ ultra performance liquid chromatographic (UPLC) system (Waters Corporation, Milford, Massachusetts, USA) consisting of a binary solvent manager, a sample manager and fitted with a photodiode array detector (PDA) synchronously controlled using the Waters Empower 2 software which collected and processed the chromatography data (Iriarte et al., 2009). An Acuity UPLC® HSS T3 1.8µm; 2.1x150mm analytical column (Waters Corporation, Dublin, Ireland), fitted subsequent to a VanGuard™ Pre-column 3/Pk 2.1x5mm column (Waters Corporation, Dublin, Ireland), was used to detect and separate AZT and BP36.

6.2.5.1. Chromatographic detection and quantification of AZT

AZT was detected and separated from the internal standard (IS), 3TC using the gradient method as presented in table 6.1. The eluent was composed of varying proportions of 0.2% formic acid in water (A) and acetonitrile (B).

Table 6.1: Chromatographic gradient elution conditions

Time (min)	Flow rate (mL/min)	% A	% B
0	0.5	90	10
1.0	0.5	70	30
1.5	0.5	90	10

Chromatographic separation was performed at 40ºC column and sample temperature. UV detection was carried out at 267nm, the AZT λ_{max}. Samples were filtered through 0.2µm membrane filters (GHP Acrodisc® 13mm Syringe Filters, Pall Corporation, New York, USA) and placed into 1.5mL Waters glass vials kept at room temperature in the sample compartment. Sample volume used during analysis was 2µL and total analysis runtime was 3 minutes.

6.2.5.2. Diluent, stock and working standard solutions preparation

Acetonitrile:water (50:50 v/v) was prepared and used as the diluent. AZT stock solution (100µg/mL) was prepared by dissolving 10mg of AZT into 100mL of the diluent in a volumetric flask and the working standard solutions were prepared by serial dilutions of the stock solution to obtain solutions of concentrations 10-100µg/mL (n=10).

6.2.5.3. Solid phase extraction and measurement of AZT from plasma

Plasma samples (500µL) placed in 2mL Eppendorf tubes were pre-treated to remove proteins by the addition of 1mL acetonitrile (Polson et al., 2003). The mixture was vortexed for 2 minutes then centrifuged for a further 2 minutes at 1200rpm [Table Top High Speed Centrifuge (TG16-WS), Hunan Xiangyi Laboratory Instrument Development Co., Ltd, Hunan, China]. The supernatant was transferred to new 2mL Eppendorf tubes and zinc sulphate (500µL, 0.1%$^{w}/_{v}$) was added, vortexed and centrifuged again and the supernatant was transferred to new 2 mL Eppendorf tubes. Thereafter, the organic phase was evaporated at 30ºC under a nitrogen stream to obtain samples to be used in the solid phase extraction (SPE) procedure (Samanidou et al., 2009).

SPE was performed under vacuum using Waters Oasis® HLB 3cc (60mg) extraction cartridges mounted on a 20 hole Waters glass block vacuum manifold processing station (Waters Corporation, Milford, Massachusetts, USA). The Oasis® HLB cartridges were preconditioned by first passing through methanol (2mL) followed by Milli-Q water (2mL) at 5psi then the pre-treated plasma samples were passed through the column with minimum suction to allow maximum drug adsorption onto the Oasis® HLB cartridge. Finally the drug was eluted using different solvents. The solvent with the highest elution efficiency (high drug recovery) among methanol, ethanol and acetonitrile was the elution solvent of choice and used throughout the study. The eluates were dried at 30ºC under a nitrogen stream and the residue was reconstituted with the diluent (1mL), filtered through 0.2µm membrane filters (GHP Acrodisc® 13mm Syringe Filters, Pall Corporation, New York, USA) and placed into the 1.5mL Waters glass vials for UPLC-PDA analysis.

6.2.5.4. Chromatography assay validation

6.2.5.4.1. Selectivity

The selectivity of the chromatographic assay was assessed by comparing the chromatograms obtained using the diluent and blank plasma from five different Large White pigs to those obtained from the diluent and porcine plasma spiked with AZT (final concentration, 3µg/mL) and IS (final concentration, 3µg/mL) in an effort to identify and rule out interfering peaks.

6.2.5.4.2. Recovery

Drug recovery was measured by comparing the analyte/IS peak area ratios obtained after the blank plasma that was pooled from 5 different pigs was spiked with three different concentrations of the analyte (final concentrations; 1, 5 and 10µg/mL) and the IS (final concentration, 3µg/mL) before and after the SPE procedure (Iriarte et al., 2009; Samanidou et al., 2009). The recovery tests were performed in triplicate.

6.2.5.4.3. Linearity

Plasma calibration standard solutions were prepared by spiking blank plasma with the working standard solution to obtain AZT concentrations of 1-10µg/mL, n=10 and IS (3µg/mL) prior to solid phase extraction (Samanidou et al., 2009; Iriarte et al., 2009). A calibration curve of analyte/IS peak area ratios against analyte concentration was plotted to validate the linearity of the chromatographic assay. Measurement of the analyte/IS area ratio was performed in triplicate and the computed mean was used to construct the calibration curves on three different days.

6.2.5.4.4. Limit of detection and limit of quantification

The limit of detection (LOD) and Limit of quantification (LOQ) were computed according to the equations 6.1 and 6.2:

$$LOD = 3.3\sigma/S \qquad \textit{Equation 6.1}$$

$$LOQ = 10\sigma/S \qquad \textit{Equation 6.2}$$

Where σ is the standard deviation (SD) of y-intercepts obtained by performing regression analysis on the calibration curve and *S* is the calibration curve slope (Samanidou et al., 2009).

6.2.5.4.5. Precision and accuracy

The precision/repeatability of the chromatography assay was calculated in terms of the percentage relative standard deviation (RSD) examined at three different analyte concentrations levels of; low (1µg/mL), medium (5µg/mL) and high (10µg/mL) (Samanidou et al., 2009, Iriarte et al., 2009, Mason 2007). Accuracy, expressed as the relative error (RE), was taken as a measure of the deviation of the mean from the true value (Iriarte et al., 2009). The three different analyte concentrations were analysed in three replicates on three different days in order to determine intra- and inter-day accuracy and precision (Samanidou et al., 2009; Iriarte et al., 2009; Mason, 2007).

6.2.5.4.6. Stability of AZT and 3TC in plasma

Quality control samples (n=3) comprising blank porcine plasma spiked with AZT (final concentration, 5µg/mL) working solution and IS (final concentration, 3µg/mL) were injected into the UPLC to determine the stability of AZT and the internal standard. Samples were exposed to light and kept at ambient temperature (25ºC) and tested at time points; 0, 12, 24, 48 and 72 hours (Iriarte et al., 2009; Gonzalez et al., 2009).

6.2.5.5. Analysis of AZT concentration in plasma, vaginal fluid and tissue samples of group B pigs

Frozen plasma samples obtained on days; 0, 3, 7, 14, 21 and 28 were allowed to thaw over 24hrs and then subjected to the SPE phase as described section 2.4.3. Thereafter, UPLC-PDA AZT detection and quantification was performed. After defrosting vaginal swab samples (cotton buds) for 24hrs, 1mL of diluent (acetonitrile:water 50:50) was added to the Eppendorf tubes containing the vaginal swab samples to extract AZT. The samples were vortexed for 5min then centrifuged at 1200rpm and the supernatant was subjected to SPE as described in section 2.4.3 before AZT detection and quantification was performed using the UPLC-PDA. To measure the amount of free AZT in the excised vaginal tissue for each pig in group B, frozen samples (1g, n=3) were separately ground in a coffee grinder into a fine tissue sample, placed in 2mL Eppendorf tubes then the diluent (1mL, acetonitrile:water 50:50) was added as the AZT extraction solvent (Clark and Friend, 2012). The samples were vortexed for 10min, centrifuged at 1200rmp and the collected supernatant was subjected to SPE as in section 2.4.3 before AZT detection and quantification by UPLC-PDA.

6.2.6. Chromatographic detection and quantification of BP36

Due to the low level of purity of BP36 and the consistency (standardization) within the herbal extract, it was difficult to accurately quantify it. However, qualitative analysis that involved UPLC detection of BP36 in vaginal fluid, swarbs and plasma using a PDA detector was performed using an isocratic method on a UPLC® HSS T3 1.8µm; 2.1 x 150mm column at a column temperature of 40°C and eluents, A_1 80% acetonitrile and B_1 20% 0.2% Formic acid water (MilliQ). The runtime was 6min and sample volume that was used was 3µL.

6.2.7. Histopathology analysis of porcine vaginal epithelia

Histopathology tests were performed to determine the level of abnormality (such as inflammation and toxicity) that may have been caused by the presence of the composite polymeric delivery system in the vaginal cavity over 28 days (Ndesendo et al., 2011; D'cruz et al., 2003; Clark and Friend, 2012). Excised pig vaginal tissue was fixed in 10% normal buffered formalin (Cone et al., 2006; D'cruz et al., 2005; D'cruz and Uckun, 2008; Clark and Friend, 2012). Cut vaginal tissue sections were put in and automated tissue processor and then stained with haematoxylin and eosin (H/E) for microscopy analysis (Cone et al., 2006; D'cruz et al., 2005; D'cruz and Uckun, 2008; Clark and Friend, 2012).

The type of vaginal epithelia, thickness of the epithelial cell layer, degree of inflammation, ulceration, fibrosis and mononuclear inflammatory infiltration as well as tissue necrosis, fibrosis and the integrity of the lamina propria and the submucosa were examined. Different areas (8-10 fields) of the vaginal mucosa were examined, compared with the normal vaginal mucosa and then scored for histopathological changes such as epithelial ulceration, epithelial proliferation and epithelial exocytosis (inflammatory cell influx into the epithelium), subepithelial leukocytic influx, stromal fibrosis, perivascular cell cuffing and tissue necrosis. The histopathology scores included: 0, no abnormality; 1, minimum abnormality; 2, mild abnormality; 3, moderate abnormality and 4, severe abnormality (D'cruz and Uckun, 2008).

6.3. Results and Discussion

6.3.1. Pilot study using one pig from group C

The pilot study performed for 7 days using one pig from group C to determine the safety of BP36 and to test the experimental procedure before the main study commenced enabled us to decide the right procedure which kept the delivery system in the vaginal cavity for a longer duration of at least 28 days. The caplet that was inserted into the pig vaginal cavity by means of a metal speculum followed by a sponge lined with radio opaque string was expelled from the pig vaginal cavity within 3 days (Figures 6.5ai and 6.5aii). Figure 6.5bi and 6.5bii show the delivery system tested in the pilot study that was tied to a silk suture material before being attached to the vaginal mucosa in the pig's vaginal cavity. This deliver system lasted for about 5 days before breaking into two parts along the groove where the suture material was tied (Figure 6.5bii).

The technique that managed to keep the delivery system for much longer (in most cases for 28 days) was the one represented by figures 6.5.ci and 6.5cii where the caplet was enclosed in a silk pouch which was then attached to the vaginal wall in the vaginal cavity using silk suture material. This technique was then used for all pigs in the *in vivo* study. Ideally one would like to just insert the delivery system in the vagina and it stays in there for the desired duration without having to perform a surgical procedure to secure the delivery system. The need for attaching the caplet was a result of the caplet being expelled by the pig. Although a mucoadhesive material, poly(acrylic acid), formed part of constituents of the delivery system its mucoadhesive properties were diminished because the pig vaginal environment is always moist leading to poly(acrylic acid) over hydrating and loosing its mucoadhesiveness.

Another reason why the pig managed to expel the delivery system easily is that there is no anatomical place in the pig vaginal cavity where the delivery system may be secured unlike in humans where there is the vaginal fornices (especially the posterior vaginal fornix) where the delivery system may be secured and this results in its retention for a longer duration in the study. The pig cervix is continuous with the vaginal canal hence the delivery system can only be place in the canal where it can be easily pushed out through peristaltic-like vaginal wall movements.

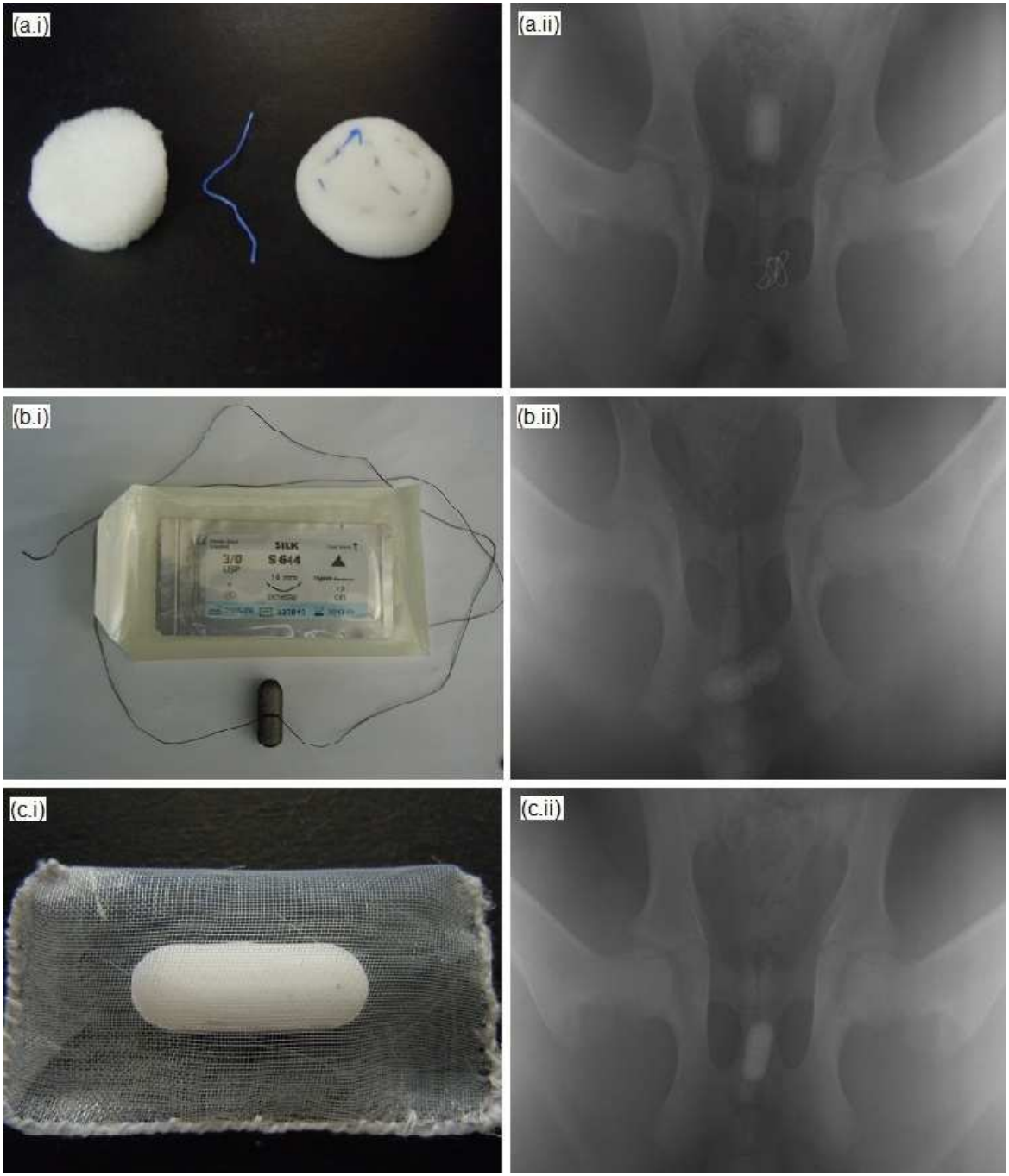


Figure 6.5: Digital images of the delivery system and X-rays images of the delivery system observed *in situ* in the vaginal cavity during the pilot study when; (a) the delivery system was inserted using a metal speculum and a radio opaque string lined sponge was used to ensure the caplet stays in place in the vaginal cavity, (b) the engraved delivery system was tied right round and attached to the mucosa in the vaginal cavity using a silk suture material and (c) the delivery system was enclosed in a silk material pouch and the pouch was attached to the mucosa in the vaginal cavity.

6.3.2. In vivo X-ray imaging of the intravaginal polymeric delivery system

The composite polymeric delivery system was observed *in situ* in the vaginal cavity by X-ray of the pelvic region of the Large White pigs as depicted in figure 6.6. Figures 6.6a.i-v (delivery system with no drug) show that the polymeric delivery system increasingly swells with the increase in its residence time in the vaginal cavity. The swelling was likely caused by the absorption of vaginal fluids by the poly(acrylic acid) and polyvinyl acetate/polyvinylpyrolidone (KSR) which constitute the polymeric delivery system. Figures 6.6b.i-v depicts the AZT loaded composite polymeric delivery system on days; 3, 7, 14, 21 and 28 after it was inserted in the vaginal cavity. The delivery system in group B pigs was observed to increasingly fade in contrast, from the outside inwards, with time which may have been due to drug and polymer solubilization and possibly the formation of pores within the polymeric delivery system as a result of the solubilization of the polyvinyl pyrolidone part of polyvinyl acetate/polyvinylpyrolidone (KSR) as vaginal fluids penetrated the interior of the delivery system. The drug-loaded delivery system was observed to swell more than the delivery system with no drug. This was likely a result of the drug, zidovudine, which is partially hydrophilic, which dissolved as vaginal fluid permeated into the polymeric delivery system matrix and percolation out (Figure 6.6). X-ray images of the delivery system in pigs from group C and D (Figure 6.6c.i-v and 6.6d.1-v) show that the swelling was more pronounced and this was most likely caused by the absorption and solubilisation of BP36 which is more hydrophilic than AZT. Some of the caplets were pushed out before 28 days (Figure 6.6c.iii-v and 6.6d.v).

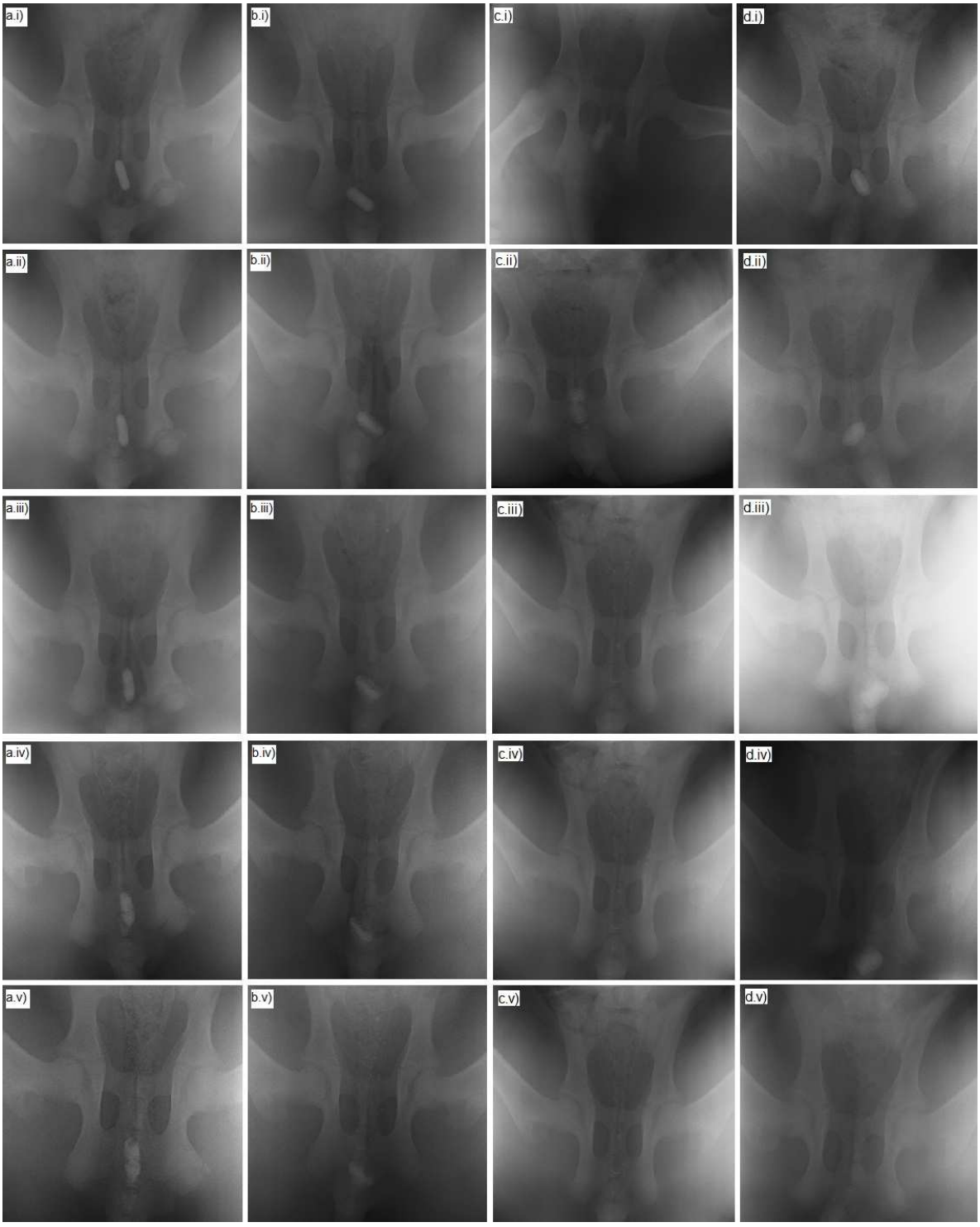


Figure 6.6: X-ray images of the pig pelvic region depicting the composite polymeric delivery system: with no drug loaded observed on days 3 a.i), 7 (a.ii), 14 (a.iii), 21 (a.iv) and 28 (a.v); loaded with AZT (300mg) observed on days 3 (b.i), 7 (b.ii), 14 (b.iii), 21 (b.iv) and 28 (b.v); loaded with BP36 (600mg) observed on days 3 (c.i), 7 (c.ii), 14 (c.iii), 21 (c.iv) and 28 (c.v) and; loaded with BP36 (150mg) and AZT (150mg) observed on days 3 (d.i), 7 (d.ii), 14 (d.iii), 21 (d.iv) and 28 (d.v).

6.3.3. Quantitative chromatographic determination of plasma drug released from the delivery system

6.3.3.1. Chromatographic conditions and separation of AZT from 3TC

High resolution chromatographic peaks of the internal standard (lamivudine) and the analyte (AZT) were obtained by UPLC-PDA (Figure 6.7a). The IS and analyte spiked in diluent were both eluted within two minutes and effectively separated by approximately one minute with an observed IS retention time (R_t) of 0.894min and that of the analyte being 1.854min (Figure 6.7a). Figure 6.7b shows the chromatogram of blank plasma depicting several peaks. There was no change in IS or analyte peak shape when they were spiked in blank plasma. In addition, there was a minor shift in the IS and analyte R_t when both were spiked with the IS R_t shifting to 0.893min whist analyte's R_t became 1.852min (Figure 6.7c).

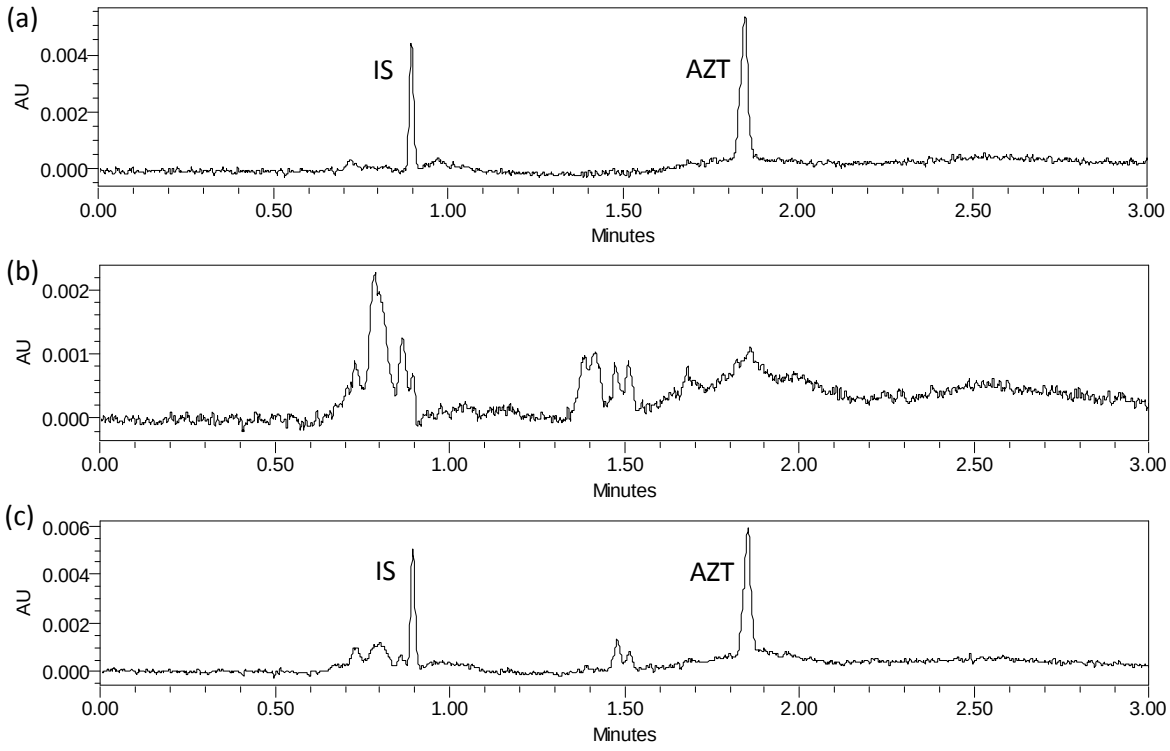


Figure 6.7: Chromatograms obtained for; (a) IS and AZT spiked in diluent, (b) typical blank plasma sample and (c) IS and AZT spiked in plasma sample

6.3.3.2. AZT Chromatographic assay validation

6.3.3.2.1. Selectivity

Chromatograms of five plasma samples obtained from five different Large White pigs showed peaks at R_t= 0.786, 1.418, 1.550, 1.679, 1.859 minutes as exemplified by figure 6.7b. Although plasma chromatogram peaks at R_t= 0.786min and 1.859min are closer to the peaks due to the IS (R_t= 0.893min) and the analyte (R_t= 1.852min), due to their relative intensity they did not interfere with the IS and analyte peaks as depicted in figure 6.7c, indicating satisfactory selectivity.

Acetonitrile was shown to be more efficient than methanol and ethanol at eluting the analyte, with an analyte recovery of 87.1705% (Table 6.2). Therefore, all other chromatographic assays were performed using acetonitrile as the eluent.

Table 6.2: Solvent elution efficiency of methanol, ethanol and acetonitrile as given by drug recovery after SPE

	Elution solvent		
	Methanol	Acetonitrile	Ethanol
AUC (AZT/IS) before SPE	1.5608	1.5608	1.5608
AUC (AZT/IS) after SPE	0.7297	1.1743	0.9371
Recovery (%)	46.7497	87.1705	60.0059

6.3.3.2.2. Recovery

Mean recoveries (n=3) calculated for analytes of concentrations; 1, 5 and 10µg/mL are presented in table 3 (approximately 78-94%). Analyte recovery increased as the concentration of the spiked analyte was increased (Table 6.3).

Table 6.3: Mean recoveries of AZT after SPE from spiked blank plasma (n=3)

	AZT concentration (µg/mL)		
	1	5	10
Recovery (%)	78.2750	94.1276	94.493
RSD (%)	4.4037	12.1093	9.4753

6.3.3.2.3. Linearity, limit of detection and limit of quantification

Calibration curves plotted, using SigmaPlot 12.0 (Systat Software Inc, San Jose, California, USA), of area under the curve of analyte/IS area ratio against the analyte concentration over a standard analyte concentration range of 1-10µg/mL (n=10) were analysed by linear regression to produce slopes, intercept and correlation coefficients given in table 6.4. The computed limit of detection (LOD) and limit of quantification (LOQ) were 1.1045µg/mL and 3.3470µg/mL respectively.

Table 6.4: Calibration curve parameters obtained through linear regression on three different days (n=3)

Curve (day)	Slope (estimate ± SD)	Intercept (estimate ± SD)	Correlation coefficient (R^2)	Linear range (µg/mL)
Curve (day 1)	0.6694±0.0348	0.2873±0.2160	0.9707	1-10
Curve (day 2)	0.5778±0.0411	0.2188±0.2550	0.9611	1-10
Curve (day 3)	0.6077±0.0328	0.2294±0.2034	0.9773	1-10

6.3.3.2.4. Precision and accuracy

Chromatographic assay precision and accuracy were determined by analyzing three different analyte concentrations (1, 5 and 10µg/mL). Precision was given by the RSD values and the accuracy by the RE values (Table 6.5). Intra-day and inter-day precision (RSD) ranged from 1.2461% to 4.8946% and 0.4653% to 2.84975% respectively whilst Intra-day and inter-day accuracy (RE) ranged from 1.8174% to 18.7545% and 3.4762% to 14.8580% respectively (Table 6.5). Both precision and accuracy were acceptable since they were less than 20% (Iriarte et al., 2009).

Table 6.5: Intra-day and inter-day precision and accuracy calculated as RSD and RE for three AZT concentration levels; 1, 5 and 10µg/mL (n=3)

	Concentration level					
	Low (1µg/mL)		Medium (5µg/mL)		High (10/mL)	
	intra-day	inter-day	intra-day	inter-day	intra-day	inter-day
RSD (%)	4.8946	0.4653	1.8688	1.1044	1.2461	2.8497
RE (%)	18.7545	14.8580	1.8174	4.9049	2.1037	3.4762

6.3.3.2.5. Stability of analyte and internal standard

Chromatographic conditions employed [column and sample temperature of 40ºC, light exposure, diluent of acetonitrile:water (50:50) and eluent, 0.2% formic acid water and acetonitrile] to detect and quantify AZT did not affect the stability of the analyte and the internal standard as their peak shapes remained similar and their retention times did not significantly shift when tested after 0, 12, 24, 48 and 72 hours (Figure 6.8).

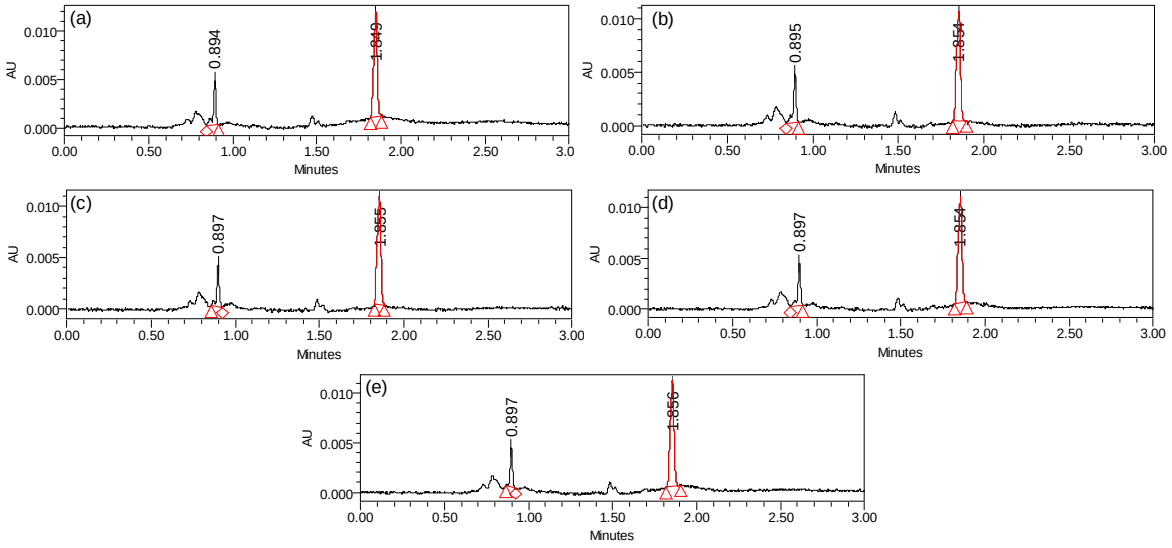


Figure 6.8: Chromatograms of the analyte (AZT, 5µg/mL) and IS (3TC, 3µg/mL) spiked plasma samples obtained at times; (a) 0hrs, (b) 12hrs, (c) 24hrs, (d) 48hrs and (e) 72hrs revealing analyte and IS stability during the chromatographic assay.

6.3.3.3. Concentration of AZT in porcine plasma, vaginal fluid and vaginal tissue samples

Figure 6.9 depicts a typical chromatogram obtained for plasma, vaginal fluid and tissue samples showing suitable IS and analyte separation with the IS peak observed at R_t≈0.95min, AZT peak R_t≈1.85min. Other peaks that may be attributed to plasma, vaginal fluid and tissue constituents were also observed at R_t≈ 0.8min and R_t≈1.5min.

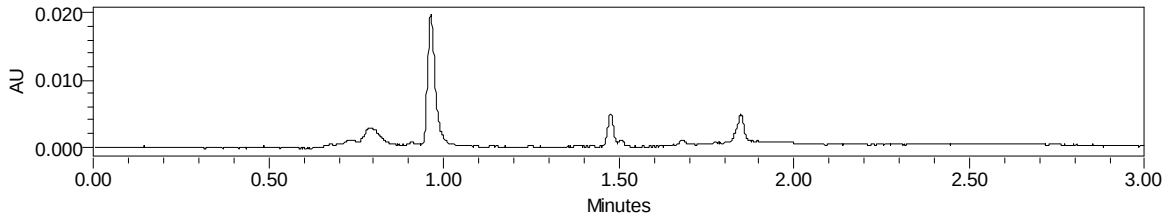


Figure 6.9: Typical UPLC chromatogram obtained for plasma, vaginal fluid and tissue samples

AZT concentration in plasma and vaginal fluids computed from the area under the curve of analyte/IS ($AUC_{analyte/IS}$) with reference to the calibration curve ($AUC_{analyte/IS}$=0.6077t+ 0.9773)

for days 3, 7, 14, 21 and 28 were plotted against time and presented in figure 6.10. Generally, both plasma and vaginal fluid AZT concentrations were observed to decrease with time (Figure 6.10) with low AZT plasma concentrations ranging from 1.1838±0.0124µg/mL to 1.1304±0.0153µg/mL. The highest plasma concentration (C_{max}) was obtained on day 7 (Figure 6.10a). AZT concentrations in vaginal fluid (range: 4.9966±0.9839µg/mL to 2.8679±0.8123µg/mL) were higher than those in plasma (Figure 6.10) which may be explained in that, AZT needed to permeate through the vaginal mucosa for it to get to the blood (plasma), therefore the majority of the drug was entrapped within the vaginal tissue.

The decreasing trend observed in vaginal fluid AZT concentrations may have been due to the fact that vaginal fluid has to penetrate the polymeric matrix of the delivery system, dissolve AZT out of the submicrospheres and percolate out of the caplet matrix for it to be measured in the vaginal fluid. Therefore, with the time, vaginal fluid will have to permeate through a longer distance into the matrix interior and percolate out with increasing resistance from the hydrophobic part of the polymeric matrix [poly(D,L-lactide) and the polyvinyl acetate part of the polyvinyl acetate/polyvinylpyrolidone (KSR)]. Vaginal tissue AZT concentrations (range: 4.2176±0.3396µg/mL to 2.9604±0.1901µg/mL) taken after 28 days were higher than plasma AZT concentrations and were in the same range as vaginal fluid (Figure 6.11).

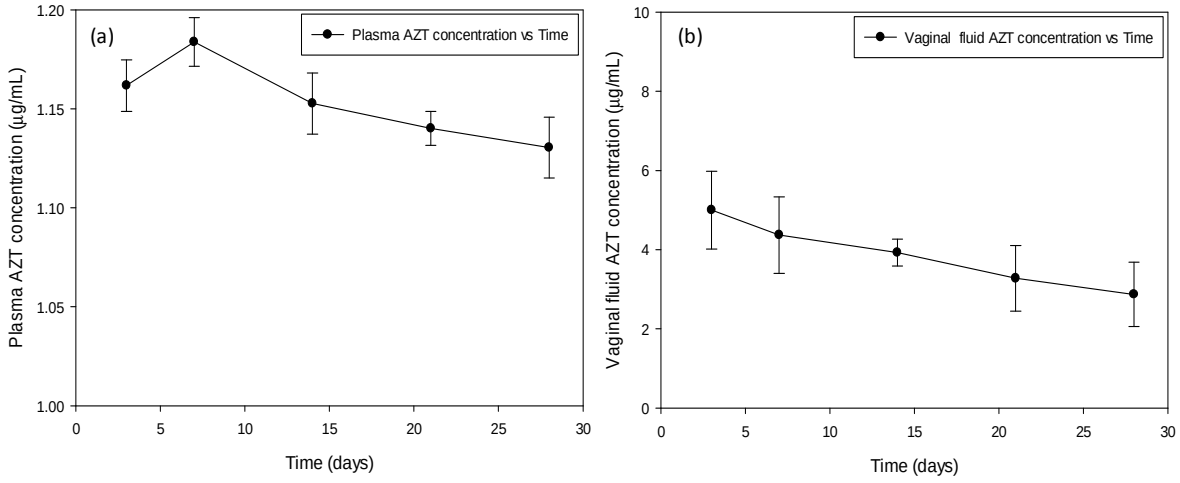


Figure 6.10: AZT concentration measured in, (a) plasma and (b) vaginal fluid samples collected on days; 3, 7, 14, 21 and 28 from group B pigs.

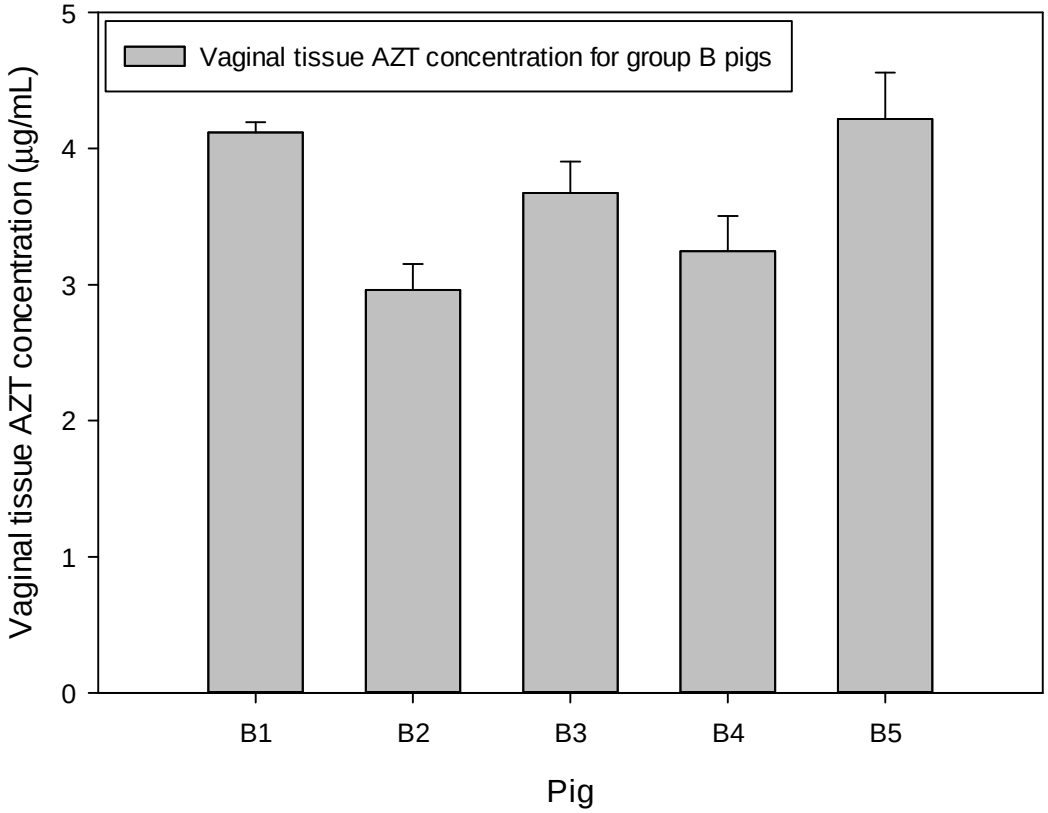


Figure 6.11: AZT concentration measured in vaginal tissue samples excised from group B pigs after the 28 day study

6.3.3.4. Detection and quantification of BP36 in porcine plasma, vaginal fluid and vaginal tissue

Figure 6.12 depicts a chromatogram of BP36 showing several peaks at different retention times. The presence of several peaks indicates the low level of purity of BP36. BP36 is a herbal extract that is still undergoing standardization and its chromatogram presented in figure 6.12 suggests that BP36 may be composed of several different molecules which may include impurities (possibly 8 molecules). BP36 was detected in the pig vaginal fluid (vaginal swab) and vaginal tissue but not in the pig plasma. Therefore, BP36 concentration in samples from pigs in group C and D were qualitatively analysed.

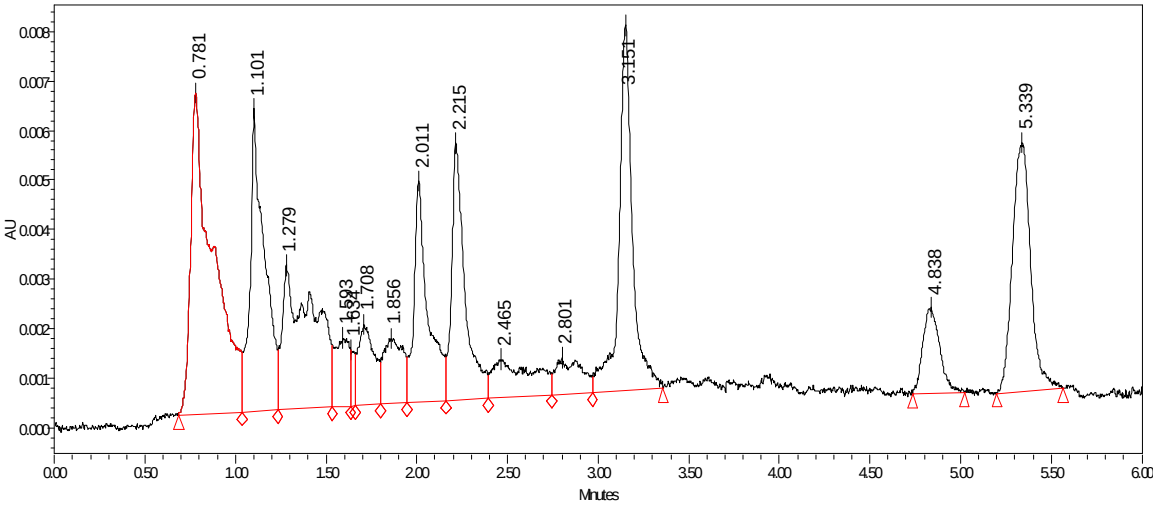


Figure 6.12: UPLC-PDA chromatogram of BP36

6.3.4. Histopathology analysis of porcine vaginal epithelia

Histological analysis of cut and formalin fixed sections (Figure 6.13) of the excised porcine vaginal mucosa after extended vaginal delivery of AZT and BP36 by means of a composite polymeric intravaginal drug delivery system resulted in the scored abnormality observations that include; epithelial erosion/ulceration, epithelial proliferation, epithelial exocytosis, subepithelial leukocyte influx, stromal fibrosis, perivascular cell cuffing and tissue necrosis as shown in table 6.6 and figure 6.14. Vaginal epithelia and lamina propria that were normal or had minimum abnormality were mostly observed in pigs from group C (Table 6.6, Figure 6.14a). On microscopy examination, superficial loss of epithelial cells (epithelial erosion) was observed in 3 pigs from group A, 2 pigs from group B, 2 pigs form group C and none from group D (Table 6.6, Figure 6.14b). Most of the erosion was minimal to moderate except in pigs A4 and C3 were there was enhanced loss of the epithelium (Table 6.6, Figure 6.14b). The observed erosion of the porcine vaginal epithelia might have been caused by irritation, inflammatory process, leukocyte influx and exocytosis into the epithelia as a result of the presence of the drug delivery system. The epithelial erosion observed in pigs in group A may have been slightly enhanced as compared to that of pigs in other groups because the delivery system in group A pigs was not drug loaded hence did not swell as much and did not allow vaginal fluid to infiltrate its interior as it did in the delivery system in other groups, which had a hydrophilic drug encapsulated within. This resulted in the delivery systems in group A pigs remaining more solid and rigid as compared to the ones in other groups as depicted in figure 6.6, which might have led to the slight increase in the delivery system's abrasiveness hence increased group A pig epithelial erosion. Epithelial erosion is bad because it diminishes the barrier properties of the vaginal epithelia and may lead to an increase in HIV-1 transcytosis and transmission.

Epithelial proliferation (due to epithelial hyperplasia) normally associated with low-grade subacute to chronic irritation was found to be mild to moderate in all group pigs (Table 6.6, Figure 6.14c). An increased level of influx (epithelial exocytosis) may be a result of inflammation as was observed in the vaginal mucosa of most pigs (Table 6.6, Figure 6.14d). In the lamina propria directly underneath the vaginal epithelium, inflammatory infiltrates (subepithelial leukocyte influx), mainly neutrophils, some eosinophils and macrophages were detected in almost all vaginal mucosa examined with scoring varying from minimum to severe abnormality signifying minimum to severe inflammation (Table 6.6, Figure 6.14e). There was more severe inflammation in group A pig vaginal epithelia as compared to other group epithelia (Table 6.6). Inflammation of the vaginal mucosa weakens the epithelial barrier properties leading to possible HIV-1 transmission.

Stromal fibrosis, observed as fibroplasia in the deeper layers of the lamina propria underneath the vaginal epithelium, was scored minimum to mild in the epithelial sections examined (Table 6.6, Figure 6.14f). Perivascular cell cuffing identified as lymphocytic infiltrates and small nodules of lymphocytic perivascular inflammation was detected and scored as minimum to moderate in the epithelial sections examined except for one (B5) which was scored as severe (Table 6.6, Figure 6.14g). Only in one vaginal epithelial section examined (B4) where a focal area of muscle and tissue necrosis where glaucomatous inflammation was observed (Table 6.6, Figure 6.14h). Within the area of tissue necrosis, numerous mononuclear cells as well as polymorphonuclear exudation were found and macrophages as well as few multinucleated giant cells could be identified. There seemed to be an infectious granuloma in the wall of the porcine vagina in pig B4. Pig B4's tissue necrosis might have been an isolated case.

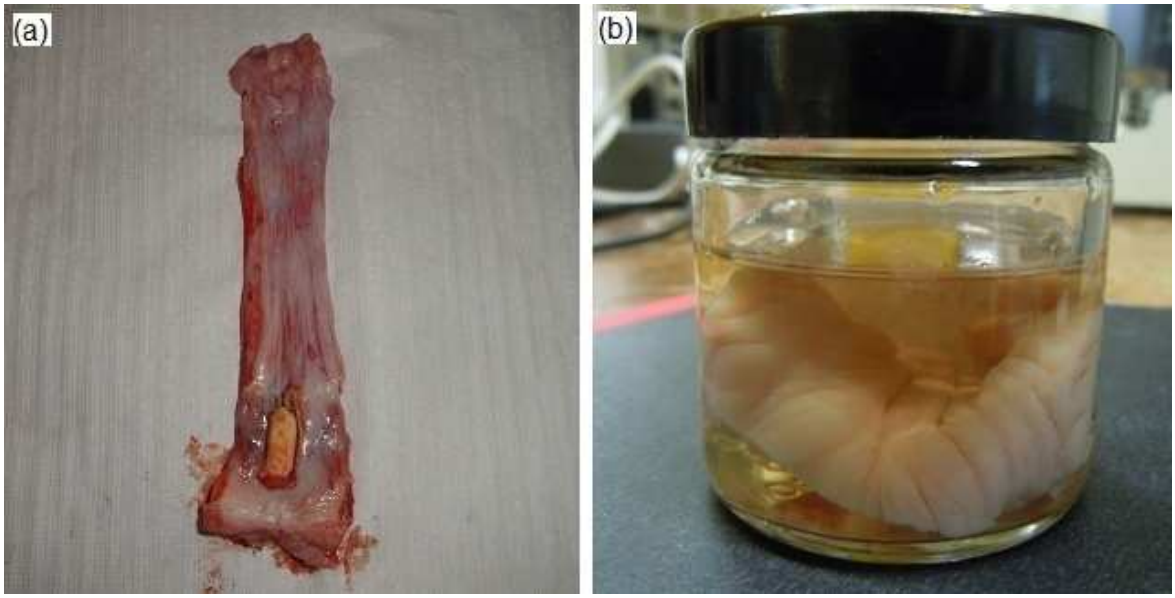


Figure 6.13: Digital photographs of the excised vaginal tissue; (a) soon after being excised from the pig on day 28 of the experiment with the composite delivery system still attached and (b) placed in 10% normal buffered formalin for storage before histopathology analysis

Table 6.6: Histopathological observations of the vaginal sections excised from the pigs from groups; A, B, C and D

Group	A					B					C					D				
Pig identity	A1	A2	A3	A4	A5	B1	B2	B3	B4	B5	C1	C2	C3	C4	C5	D1	D2	D3	D4	D5
Epithelial erosion/ulceration	-	1+	3+	4+	-	-	-	-	1+	2+	-	-	+4	-	+1	-	-	-	-	-
Epithelial proliferation	2+	1+	-	-	-	-	-	1+	2+	2+	-	-	-	-	+2	+2	+2	-	-	-
Epithelial exocytosis	3+	4+	4+	4+	1+	3+	3+	1+	3+	4+	+1	+1	+3	+1	+4	+3	+3	+2	+3	+2
Subepithelial leukocyte influx	3+	4+	4+	4+	1+	2+	2+	1+	3+	4+	-	-	+3	+1	+3	+3	+2	+1	+3	+2
Stromal fibrosis	-	-	1+	1+	-	-	-	-	2+	2+	-	+1	+3	-	+1	+2	+2	+1	+3	+2
Perivascular cell cuffing	1+	2+	3+	3+	1+	1+	1+	-	3+	4+	-	+1	+3	-	+1	+2	+2	+1	+3	+2
Tissue necrosis	-	-	-	-	-	-	-	-	3+	-	-	-	-	-	-	-	-	-	-	-

- no abnormality

1+ minimal abnormality

2+ mild abnormality

3+ moderate abnormality

4+ severe abnormality

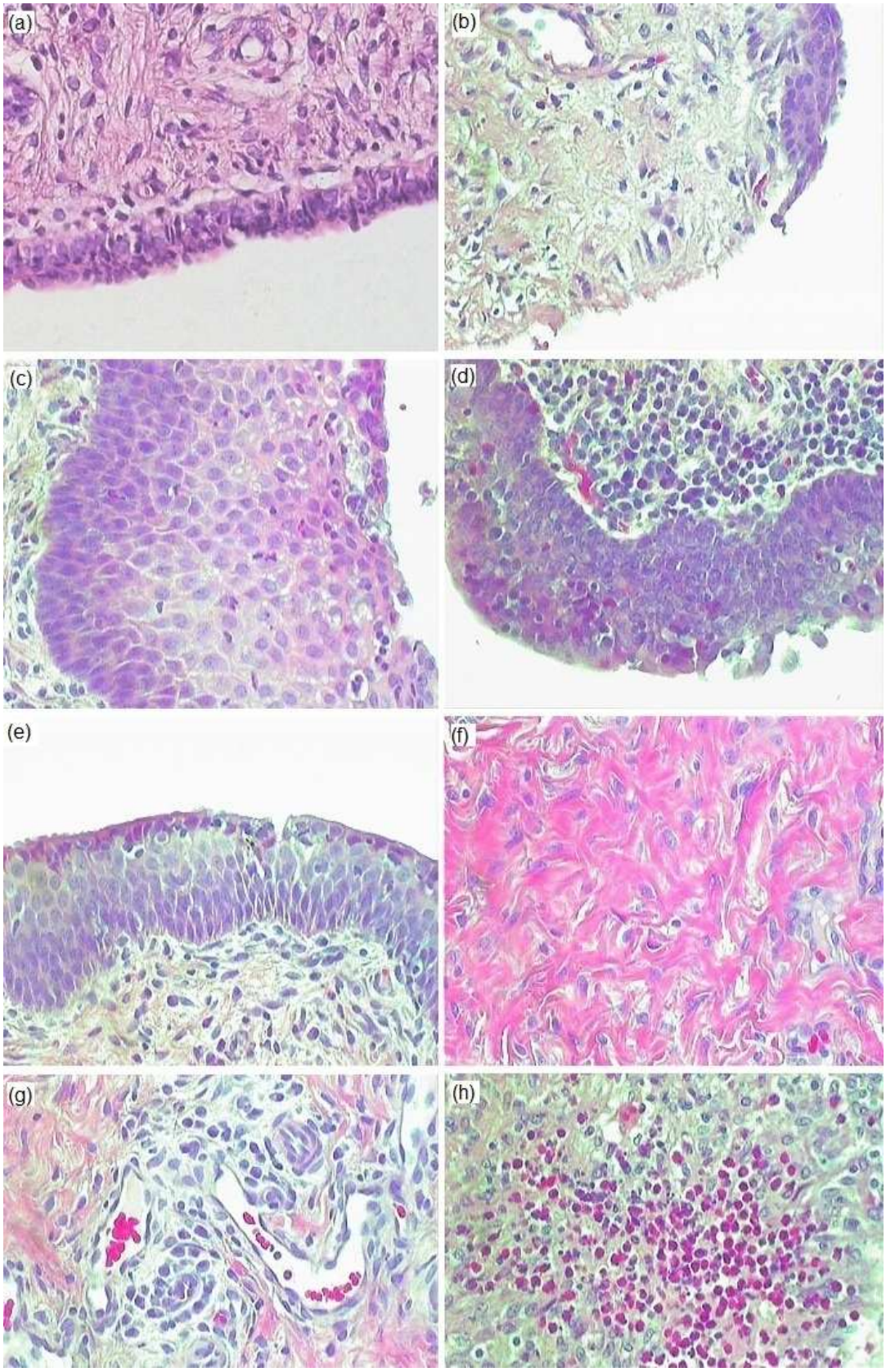


Figure 6.14: Histopathology images of excised pig vaginal tissue depicting; (a) normal epithelia and lamina propria, pig C1, (b) epithelial erosion/ulceration, pig B4, (c) epithelial proliferation, pig A1, (d) epithelial exocytosis, pig A4, (e) subepithelial leukocyte influx, pig B4, (f) stromal fibrosis, pig B5, (g) perivascular cell cuffing, pig B4 and (h) tissue necrosis and polymorphonuclear exudation, pig B4.

6. 4. Concluding remarks

The *in vivo* study reported in this chapter successfully tested an intravaginal composite polymeric delivery system in the pig as a model for extended microbicide delivery intended to prevent heterosexual vaginal HIV-1 transmission. The delivery system was observed *in situ* over 28 days and X-ray images showed that the drug loaded delivery system swelled and faded gradually with time once vaginal fluid permeated into its matrix core. An ultra performance liquid chromatography-photodiode array assay was developed and optimised for selectivity, recovery, linearity, precision, accuracy and analyte stability then used to determine AZT concentrations in plasma, vaginal fluid samples obtained at predetermined time points over 28 days and in vaginal tissue samples excised on day 28 after experimentation. Retention times shown as distinguishable peaks at approximately 0.9min for the internal standard at 1.9min for the analyte were observed.

The assay was relatively precise (RSD<5%) and accurate (RE<20%). Vaginal fluid and plasma AZT concentrations were shown to decrease gradually over the 28 days and the plasma AZT concentrations were lower than those of the vaginal fluid. AZT concentration in excised vaginal tissue samples were relatively constant and were in the same range as those of the vaginal fluid. BP36 was also detected using UPLC-PDA but could not be quantified due to low purity and inconsistence in the BP36 herbal extract. It was difficult to pinpoint which peak belonged to the active anti-HIV-1 agent in BP36 thus there is need to standardize the BP36 extract. Drug kinetics (AZT) in this study was positive since much of the drug was detected in the vaginal fluid and vaginal tissue samples which normally receive the first exposure to HIV-1 during heterosexual intercourse and little drug was detected in the plasma suggesting less systemic drug side effects would be caused by the drug. However, this study does not address the issue of how much drug should be in the vaginal fluid, vaginal tissue and plasma for successful HIV-1 prevention. Further research is necessary in this regard.

Histopathological analysis exposed different scores of abnormalities on the excised vaginal tissue. Although the majority of abnormalities were minimum to moderate including; epithelial proliferation and exocytosis, subepithelial leukocyte influx and perivascular cell cuffing, there were isolated cases of epithelial erosion, stromal fibrosis and tissue necrosis which raise concern regarding the breakdown of the barrier properties of the vaginal mucosa which may lead to HIV-1 transmission. More research is necessary to improve microbicide pharmacokinetics and reduce pathotoxicity if we are to use microbicides as an alternative female-controlled pharmaceutical tool to reduce HIV-1 transmission.

CHAPTER 7
CONCLUSIONS AND RECOMMENDATIONS

7.1. Conclusions

HIV/AIDS is a debilitating disease that diminishes ones immune system, exposing the body to other opportunistic infections such as tuberculosis. HIV/AIDS also impacts negatively on a person's social and economic activity. Although antiretrovirals are being used to manage people living with HIV/AIDS with relative success, prevention of HIV-1 transmission in the first place would reduce the disease burden and all the social and economic downturns that are brought about by HIV/AIDS. The use of microbicides as a prevention modality for male to female HIV-1 transmission is advantageous in that it has the ability to shift the control of HIV-1 prevention from the male to female. In essence use of microbicides empowers women in the fight against HIV-1 transmission.

This dissertation details the successful design and formulation of a composite polymeric microbicide delivery system to be inserted in the posterior fornix of the human vagina as an alternative to the gel, cream, tablet, sponges and ring delivery systems developed thus far. This delivery system is a caplet-shaped composite system comprising zidovudine (AZT) and BP36-loaded pectin-mucin-polyethylene glycol submicrospheres embedded within a poly(D.L-lactide), magnesium stearate, polyvinyl acetate/polyvinylpyrolidone (KSR) and poly(acrylic acid) based polymeric caplet matrix. The delivery system was able to deliver anti-HIV-1 agents (zidovudine and BP36) over 28 days in both *in vitro* experiments and *in vivo* in the pig model. X-ray illustrated the delivery system swelling and its matrix contrast fading over time as vaginal fluid permeated the matrix's core. Plasma, vaginal fluid and tissue drug was detected and quantified using ultra performance liquid chromatography-tandem photodiode array detector. AZT plasma and vaginal fluid concentrations measured on days; 3, 7, 14, 21 and 28 decreased gradually with time. Vaginal tissue AZT concentrations (after 28 days) were higher than plasma AZT concentrations and in the same range as vaginal fluid AZT concentrations. BP36 was also detected in plasma, vaginal fluid and tissue and qualitatively analysed.

This study saves as a significant contribution towards addressing the questions surrounding microbicide research whereby potent anti-HIV-1 agents are successfully tested *in vitro* but fail to pass all clinical trials. The aim and objectives of the study were mostly achieved since the formulated and optimised microbicide delivery system was able to deliver a combination of anti-HIV-1 agents over 28 days which means that there would be less dosing and more

patient compliance, the anti-HIV-1 agents would be bioavailable in the vaginal cavity long enough to outlast HIV-1 and the delivery system may be used discretely by women. In addition there is scope for the delivery system to be adopted to delivery other therapeutic agents such as antibacterials, antifungals and insulin. The benefits of a cheap, safe, easy to use and effective microbicide formulation are far reaching in the fight against HIV/AIDS and this work is a contribution to the extensive microbicide research taking place worldwide.

7.2. Recommendations

Given the failure of microbicides to pass all clinical trials, pharmaceutical scientists and developers have come to the conclusion that it is just not enough for microbicides agents to be potent against HIV-1. There are other variables at play such as the maintenance and enhancement of the vaginal barrier properties against HIV-1, the need to use different approaches that include employing two or more anti-HIV-1 agents that have different mechanisms of action and the determination and use of the appropriate quantities of the anti-HIV-1 agents. As research on microbicide agents is ongoing, there is need to focus more on these and many other variables as opposed to just looking at how potent an anti-HIV-1 agent may be. Much of the work performed in this study in designing and formulating a composite delivery system was largely successful. However, there is need for further work on some aspects that include; partaking on further tests such as immunohistopathology to determine the safety of the delivery system and determining the quantity of the microbicide that has to be delivered for sufficient anti-HIV-1 prevention.

Although this study involved the delivery of two anti-HIV-1 agents with different mechanisms of action, one of the agents (BP36) is a raw herbal extract that is still undergoing standardization. As much as BP36 showed potency against HIV-1 *in vitro*, drug delivery is a more precise science and there is need to further isolate and purify the anti-HIV-1 active pharmaceutical ingredient. This should generally be standard for any herbal based microbicide candidate to ensure easy formulation, delivery, detection and quantification.

Another issue that arose in the *in vivo* studies using the pig as a model which particularly affected the caplet delivery system was that although the human and the pig reproductive systems are similar, there are some differences that include the absence of vaginal fornices in the pig where the cervix is continuous with the vagina as opposed to in human females where the cervix protrudes into the vaginal cavity to form the anterior and posterior fornices where the caplet could be inserted securely for extended residence and microbicide delivery. This difference resulted in the pigs pushing out the caplet once inserted in the vaginal cavity. In this regard, use of other animal models, such as primates, that have vaginal fornices similar to humans would be advantageous. With continuous research and review of the pitfalls of microbicides, a female controlled HIV-1 transmission prevention modality with huge health and economic benefits may be developed.

REFERENCES

1. Abdool Karim, Q., Abdool Karim, S.S., Frohlich, J.A., Grobler, A.C., Baxter, C., Mansoor, L.E., Kharsany, A.B., Sibeko, S., Mlisana, K.P., Omar, Z., Gengiah, T.N., Maarschalk, S., Arulappan, N., Mlotshwa, M., Morris, L., Taylor, D. & CAPRISA 004 Trial Group., 2010, 'Effectiveness and safety of tenofovir gel, an antiretroviral microbicide, for the prevention of HIV infection in women, *Science* 329(5996), 1168-1174.

2. Adams, J.L. & Kashuba, D.M., 2012, 'Formulation, pharmacokinetics and pharmacodynamics of topical microbicides', *Best Practice & Research Clinical Obstetrics & Gynaecology* 26(4), 451-462.

3. AIDS Vaccine Advocacy Coalition, *Microbicide trial results*, viewed 14 July 2011, from http://www.avac.org/ht/d/sp/i/3513/pid/3513.

4. AIDS Vaccine Advocacy Coalition, *Ongoing and planned clinical trials of topical microbicide candidates Sep 2010*, viewed 14 July 2011, from http://www.avac.org/ht/a/GetDocumentAction/i/5849.

5. AIDS Vaccine Advocacy Coalition, *Ongoing clinical trials of topical microbicide candidates 2011*, viewed 25 July 2011, from http://www.avac.org/ht/a/GetDocumentAction/i/3109.

6. Alliance for Microbicide Development, *Pipeline Update of Microbicides and PrEP Candidates 2009*, viewed 14 February 2011, from http://www.microbicide.org/uploads/3/1/2/1/3121935/microbicide_pipeline_update_1_oct_2009.pdf.

7. Alliance for Microbicides Development, *Microbicide candidates in pre-clinical development as of Feb 2007*, viewed 25 July 2011, from http://www.microbicide.org/uploads/3/1/2/1/3121935/mapping_the_microbicide_effort.pdf.

8. Amaral, E., Perdigao, A. & Souza, M.H., Mauck, C., Waller, D., Zaneveld, L. & Faúndes A., 2004, 'Postcoital testing after use of acid buffering gel (ACIDIFORM) and

a 2% nonoxynol-9 product', *Contraception* 70(6), 492-497.

9. Anderson, R.A., Feathergill, K.A., Diao, X.H., Cooper, M.D., Kirkpatrick, R., Herold, B.C., Doncel, G.F., Chany, C.J., Waller, D.P., Rencher, W.F. & Zaneveld, L.J., 2002, 'Preclinical evaluation of sodium cellulose sulfate (Ushercell) as a contraceptive antimicrobial agent', *Journal of Andrology* 23(3), 426-438.

10. Araújo, A.A.S., Storpirtis, S., Mercuri, L.P., Carvalho, F.M.S., dos Santos Filho, M. & Matos, J.R., 2003, 'Thermal analysis of the antiretroviral zidovudine and evaluation of the compatibility with excipients used in solid dosage forms', *International Journal of Pharmaceutics* 260(2), 303-314.

11. Bai, L., Zhang, Z., Zang, H., Li X, Yu Q, Lin H & Yang W., 2008, 'HIV-1 Tat protein alter the tight junction integrity and function of pigment epithelium: an *in vitro* study', *BMC Infectious Diseases* 8, 6 June, 1471-2334.

12. Bailey, R.C., Moses, S., Parker, C.B., Agot, K., Maclean, I., Krieger, J.N., Williams, C.F., Campbell, R.T. & Ndinya-Achola, J.O., 2007, 'Male circumcision for HIV prevention in young men in Kisumu, Kenya: a randomised controlled trial', *Lancet* 369(9562), 643–56.

13. Baleta, A., 2007, 'A second chance for microbicides', *Lancet* 370(9581), 17-18.

14. Balzarini, J. & Van Damme, L., 2007, 'Microbicide drug candidates to prevent HIV infection' *Lancet* 369(9563), 787-789.

15. Balzarini, J., 2005, 'Targeting the glycans of gp120: a novel approach aimed at the achilles heel of HIV', *Lancet Infectious Diseases* 5(11), 726–731.

16. Bansil, R. & Turner, B.S., 2006, 'Mucin structure, aggregation, Physiological functions and biomedical applications', *Current Opinion in Colloidal and Interface Science* 11(2-3), 164-170.

17. Barnhart, K.T., Izquiedo, A., Pretorius, E.S., Shera, D.M., Shabbout, M. & Shannik, A., 2006, 'Baseline dimensions of the human vagina', *Human Reproduction* 21(6), 1618 -1622.

18. Bergmeier, L.A. & Lehner, T., 2006, 'Innate and adaptive mucosal immunity in protection against HIV infection', *Advances in Dental Research* 19(1), 21-28.

19. Blauvelt, A., Asada, H., Saville, M.N., Klaus-Kovtun, V., Altman, D.J. & Yarchoan, R., 1997, 'Productive infection of dentritic cells by HIV- and their ability to capture virus are mediated by separate pathways', *Journal of Clinical Investigation* 100(8), 2043-2053.

20. Bomsel, M., 1997, 'Transcytosis of infectious human immunodeficiency virus across a tight human epithelial cell line barrier', *Nature Medicine* 3(1), 42-47.

21. Box, G.E.P. & Behnken, D.W., 1960, 'Some new three level designs for the study of quantitative variables', *Technometrics* 2(4), 455-475.

22. Braccini, I. & Pérez, S., 2001, 'Molecular basis of Ca^{2+}-induced gelation of alginates and pectins: the egg-box model revisited', *Biomacromolecules* 2(4), 1089-1096.

23. Brannon-Peppas, L., 1992, 'Design and mathematical analysis of controlled release from microsphere-containing polymeric implants', *Journal of Controlled Release* 20(3), 201-208.

24. Broom, D.M., Mendl, M.T. & Zanella, A.J., 1995, 'A comparison of the welfare of sows in different housing conditions', *Animal Science* 61(20), 369-385.

25. Cai, R. & Arntfield, S.D., 1997, 'Thermal gelation in relation to binding of bovine serum albumin-polysaccharide systems', *Journal of Food Science* 62(6), 1129-1134.

26. Celia, C., Trapasso, E., Cosco D., Paolino D. & Fresta, M., 2009, 'Turbiscan Lab® Expert analysis of the stability of ethosomes® and ultradeformable liposomes containing a bilayer fluidizing agent', *Colloids and Surfaces B: Biointerfaces* 72(1), 155-160.

27. Celum, C., Wald, A., Hughes, J., Sanchez, J., Reid, S., Delany-Moretlwe, S., Cowan, F., Casapia, M., Ortiz, A., Fuchs, J., Buchbinder, S., Koblin, B., Zwerski, S., Rose, S., Wang, J., Corey, L. & HPTN 039 Protocol Team., 2008, 'Effect of acyclovir on HIV-1

acquisition in herpes simplex virus 2 seropositive women and men who have sex with men: a randomised, double-blind, placebo-controlled trial', *Lancet* 371(9630), 2109–2119.

28. Chan, D.C. & Kim, P.S., 1998, 'HIV entry and its inhibition', *Cell* 93(5), 681-684.

29. Chan, D.C., Fass, D., Berger, J.M. & Kim, P.S., 1997, 'Core structures of Gp41 from the HIV envelop glycoprotein, *Cell* 89(2), 263-273.

30. Clark, M.R., & Friend, D.R., 2012, 'Pharmacokinetics and topical vaginal effects of two tenofovir gels in rabbits', *AIDS Research and Human Retroviruses* 28(11), 1458-1466.

31. Cone, R.A., Hoen, T., Wong., X., Abusuwwa, R., Anderson, D.J. & Moench, T.R., 2006, 'Vaginal microbicides: detecting toxicities *in vivo* that paradoxically increase pathogen transmission', *BMC Infectious Diseases* 6, 1 June, 90.

32. CONRAD, *Cellulose sulphate gel*, viewed 14 February 2011, from http://www.conrad.org/f-3.html.

33. Coplan, P.M., Mitchnick, M. & Rosenberg, Z.F., 2004, 'Regulatory challenges in microbicide development', *Science* 25(5679), 1991-1952.

34. Costa, P., Lobo & J.M.S., 2001, 'Modeling and comparison of dissolution profiles', *European Journal of Pharmaceutical Sciences* 13(2), 123-133.

35. Crosby, R.A., DiClenente, R.J., Wingood, G.M., Salazar, F., Rose, E., Levine, D., Brown, L., Lescano, C., Pugatch, D., Flanigan, T., Fernandez, I., Schlenger, W. & Silver, B.J., 2005, 'Correlates of condom failure among adolescent males: an exploratory study' *Preventative Medicine* 41(5-6), 873-876.

36. Cunningham, A.L., Harman, A.N. & Donaghy, H., 2007, 'DC-SIGN 'AIDS' HIV immune evasion and infection', *Nature Immunology* 8(6), 556-558.

37. Cutler, B. & Justman, J., 2008, 'Vaginal microbicides and the prevention of HIV transmission, *Lancet Infectious Diseases* 8(11), 685-697.

38. D'cruz, O.J. & Uckun, F.M., 2007, 'Preclinical evaluation of a dual-acting microbicidal prodrug WHI-07 in combination with vanadocene dithiocarbomate in the female reproductive tract of rabbit, pig and cat', *Toxicologic Pathology* 35(7), 910-927.

39. D'cruz, O.J. & Uckun, F.M., 2008, 'Evaluation of local tolerance of the antiretroviral spermicide (WHI-07)-loaded gel-microemulsion in the porcine female reproductive tract', *Journal of Applied Toxicology* 28(3), 303-314.

40. D'cruz, O.J., Erbeck, D. & Uckun, F.M., 2005, 'A study of the pig as a model for the vaginal irritancy of benzakonium chloride in comparison to the non-irritant microbicide PHI-443 and the spemicide vanadocene dithiocarbamate', *Toxicologic Pathology* 33(4), 465-476.

41. D'Cruz, O.J., Samuel, P., Waurzyniak, B. & Uckun, F.M., 2003, '*In vivo* evaluation of a gel formulation of stampidine, a novel nonspermicidal broad-spectrum anti-HIV microbicide', *American Journal of Drug Delivery* 1(4), 275–285.

42. Das Neves, J. & Bahia, M.F., 2006, 'Gels as vaginal drug delivery systems', *International Journal of Pharmaceutics* 318(1-2), 1-14.

43. Dash, S., Murthy, P.N., Nath, L. & Chowdhury, P., 2010, 'Kinetic modeling on drug delivery systems', *Acta Poloniae Pharmaceutica - Drug Research* 67(3), 217-223.

44. De Witte, L., Nabatov, A. & Geijtenbeek, T.B.H., 2007, 'Distinct roles for DC-SIGN-dendritic cells and Langerhans cells in HIV-1 transmission', *Trends in Molecular Medicine* 14(1), 12-19.

45. Dekker, J., Rossen, J.W.A., Büller, H.A. & Einerhand, A.W.C., 2002, 'The MUC family: an obituary', *Trends in Biochemical Sciences* 27(3), 126-131.

46. Dell, R.B., Holleran, S. & Ramakrishnan, R., 2002, 'Sample size determination', *ILAR Journal* 43(4), 207-213.

47. Denniston, G.C. & Hill, G., 2007, 'Male circumcision in HIV prevention', *Lancet* 369(9573), 1598.

48. Donaghy, H., Wilkinson, J. & Cunningham, A.L., 2006, 'HIV infection with dendritic cells: has our focus been too narrow', *Journal of Leukocyte Biolology* 80(5), 1001-1012.

49. Du Toit, L.C., Pillay, V. & Choonara, Y.E., 2009, 'Nano-microbicides: challenges in drug delivery, patient ethics and intellectual property in the war against HIV/AIDS', *Advanced Drug Delivery Reviews* 62(4-5), 532-546.

50. Dumond, J.B., Patterson, K.B., Pecha, A.L., Werner, R.E., Andrews, E., Damle, B., Tressler, R., Worsley, J. & Kashuba, A.D., 2009, 'Maraviroc concentrates in cervicovaginal fluid and vaginal tissue of HIV-1 negative women', *Journal of Acquired Immune Deficiency Syndrome*, 51(5): 546-553.

51. Elechiguerra, J., Burt, J.L., Morones, J.R., Camacho-Bragado, A., Gao, X., Lara, H.H. & Yacaman, M.J., 2005, 'Interaction of silver nanoparticles with HIV-1', *Nanobiotechnology* 3, 29 June, 6.

52. Epple, H., Allers, K., Tröger, H., Kühl, A., Erben, U., Fromm, M., Zeitz, M., Loddenkemper, C., Schulzke, J.D. & Schneider, T., 2010, 'Acute HIV infection induces mucosal infiltration with $CD4^+$ and $CD8^+$ T cells, epithelial apoptosis and a mucosal barrier defect', *Gastroenterology* 139(4), 1289-13000.

53. Espinosa, M., Noé, G., Troucoso, C., Ho, S.B. & Villalón, M., 2002, 'Acidic pH and increasing [Ca^{2+}] reduce the swelling of mucin in primary cultures of human cervical cells', *Human Reproduction* 17(8), 1964-1972.

54. Feldblum, P.J., Adeiga, A., Bakare, R., Wevill, S., Lendvay, A., Obadaki, F., Olayemi, M.O., Wang, L., Nanda, K. & Rountree, W., 2008, 'SAVVY vaginal gel (C31G) for prevention of HIV infection: a randomized controlled trial in Nigeria', *PLoS One* 3(1), e1474.

55. Festing, M.F.W., 1994, 'Reduction of animal use: experimental design and quality of experiments', *Laboratory Animals* 28(3), 212-221.

56. FHI, *Cellulose sulphate ruled out as microbicide candidate*, viewed 14 February 2011,

from http://www.fhi.org/en/RH/Pubs/Briefs/HIVprevTrials/CS_microbide.htm.

57. Fox, J. & Fidler, S., 2010, 'Sexual transmission of HIV-1', *Antiviral Res* 85(1), 276-285.

58. Fukunag, T., Sasaki, M., Araki, K., Okamoto, T., Yasuoka, T., Tsujikawa, T., Fujiyama, Y. & Bamba, T., 2003, 'Effects of the soluble fibre pectin on intestinal cell proliferation, focal short chain fatty acid production and microbial population', *Digestion* 67(1-2), 42-49.

59. Gabby, M. & Gibbs, A., 1996, 'Does additional lubrication reduce condom failure', *Contraception* 53(3), 155-158.

60. Garcia, X., Scribing, E., Domenici, J., Quadrant, J. & Friezes, J., 2011, '*In vitro* characterization and *in vivo* analgesic and anti-alloying activity of PLGA-bupivacaine nanoparticles', *Journal of Nanoparticle Research* 13(5), 2213-2223.

61. Garg, S., Verman, K., Anderson, R.A. & Zaneveld, L.J., 2004, 'Rapidly disintegrating novel bioadhesive vaginal tablets of polystyrene sulfonate (PSS), a potential microbicide formulation', *15th International Conference of AIDS*, Bankok, Thailand, July 11-16, 2004 Abstract TuPeB4656.

62. Geijtenbeek, T.B., Know, D.S., Torensma, R., van Vliet, S.J., van Duijnhoven, G.C.F., Middel, J., Cornelissen, I.L.M.H.A., Nottet, H.S.L.M., KewalRamani, V.N., Littman, D.R., Figdor, C.G. & van Kooyk, Y., 2000, 'DC-SIGN, a dendritic cell-surface HIV-1-binding protein that enhances trans-infection of T cells', *Cell* 100(5), 587-597.

63. Geonnoti, A.R. & Katz, D.F., 2006, 'Dynamics of HIV neutralization by a microbicide formulation layer: biophysical fundamentals and transport theory', *Biophysical Journal* 91(6), 2121-2130.

64. Global Campaign for Microbicides, *Current trials*, viewed 14 February 2011, from http://www.global-campaign.org/microbicide-trials.htm.

65. Gonzalez, O., Gorka, I., Ferreirós, N., Maguregui, M.I., Alonso, R.M. & Jiménez, R.M., 2009, 'Optimization and validation of a SPE-HPLC-PDA-flourescence method for the simultaneous determination of drugs used in combined cardiovascular therapy in human plasma', *Journal of Pharmaceutical and Biomedical Analysis* 50(4), 63-639.

66. Grandin, T. (ed.), 2007, *Livestock handling and transport*, CABI Publishing, Oxford.

67. Grandin, T., 1997, 'Assessment of stress during handling and transport', *Journal of Animal Science* 75(1), 249-257.

68. Gray, R.H., 2008, 'Wawer MJ, 'Reassessing the hypothesis on STI control for HIV prevention', *Lancet* 371(9630), 2064–2065.

69. Gray, R.H., Kigozi, G., Serwadda, D., Makumbi, F., Watya, S., Nalugoda, F., Kiwanuka, N., Moulton, L.H., Chaudhary, M.A., Chen, M.Z., Sewankambo, N.K., Wabwire-Mangen, F., Bacon, M.C., Williams, C.F., Opendi, P., Reynolds, S.J., Laeyendecker, O., Quinn, T.C. & Wawer, M.J., 2007, 'Male circumcision for HIV prevention in men in Rakai, Uganda: a randomised trial', *Lancet* 369(9562), 657–66.

70. Gray, R.H., Wawer, M.J., Brookmeyer, R., Sewankambo, N.K., Serwadda, D., Wabwire-Mangen, F., Lutalo, T., Li, X., van Cott, T., Quinn, T.C. & Rakai Project Team., 2001, 'Probability of HIV-1 transmission per coital act in monogamous, heterosexual, HIV-1-discordant couples in Rakai, Uganda', *Lancet* 357(9263), 1149–53.

71. Gummuluru, S., Rogel, M., Stamatatos, L. & Emerman, M., 2003, 'Binding of human immunodeficiency virus type 1 to immature dendritic cells can occur independently of DC-SIGN and mannose binding C-type receptors via a cholesterol–dependent pathway', *Journal of Virology* 77(23), 12865-12874.

72. Gupta, J., Tao, J.Q., Garg, S. & Al-Kassas, R., 2011' 'Design and development of an in-vitro assay for evaluation of solid vaginal dosage forms', *Pharmacology & Pharmacy* 2, October, 289-298.

73. Gupta, K.M., 2008, 'Novel technologies for vaginal delivery of microbicides. PhD Thesis', Dept. Bioengineering, The University of Utah, US, pp.21.

74. Haase, A.T., 2005, 'Perils at mucosal front lines for HIV and SIV and their hosts', *Nature Reviews Immunology* 5(10), 783-792.

75. Haase, A.T., 2010, 'Targeting early infection to prevent HIV-1 mucosal transmission', *Nature* 464(7286), 217-223.

76. Harris, J.E., Paul, D.R. & Barlow, J.W., 1983, 'A comparison of miscible binary blend interaction parameters measured by different methods', *Polymer Engineering & Science* 23(12), 676-681.

77. Hassan, E.E. & Gallo, J.M., 1990, 'A simple rheological method for the in vitro assessment of mucin-polymer bioadhesive bond strength', *Pharmaceutical Research* 7(5), 491-495.

78. Hayes, R.J., Schulz, K.F. & Plummer, F.A., 1995, 'The cofactor effect of genital ulcers in the per-exposure risk of HIV-1 transmission in sub-Saharan Africa', *Journal of Tropical Medicine Hygiene* 98(1), 1-8.

79. Hemmerling, A., Harrison, W., Schroeder, A., Park, J., Korn, A., Shiboski, S. & Cohen, C.R., 2009, 'Phase I dose-ranging safety trial of lactobacillus cripatus CTV-05 (LACTIN-V) for the prevention of bacterial vaginosis', *Sexually Transmmited Diseases* 36(9), 564-569.

80. Hemmerling, A., Harrison, W., Schroeder, A., Park, J., Korn, A., Shiboski, S., Foster-Rosales, A. & Cohen, CR., 2010, 'Phase 2a study assessing colonization efficiency, safety, and acceptability of lactobacillus crispatus CTV-05 in women with bacterial vaginosis', *Sexually Transmitted Diseases* 37(12), 745-750.

81. Hemmerling, A., Potts, M., Walsh, J., Young-Holt, B. & Stefanski, D.A., 2007, 'Lime juice as a candidate microbicide? An open-label safety trial of 10% and 20% lime juice used vaginally', *Journal of Women's Health* 16(7), 1041-1051.

82. Hendrix, C.W., Cao, Y.J. & Fuchs, E.J., 2009, 'Topical microbicides to prevent HIV: clinical drug development challenges', *Annul Review of Pharmology and Toxicology* 49, February, 349-375.

83. Hester, R. & Kennedy, S., 2003, 'Candida infection as a risk factor for HIV-1 transmission', *Journal Women's Health (Larchmt)* 12(5), 487-494.

84. Hilber, A.M., Chersich, M.F., Van de Wijgert, J.H.H.M., Rees, H. & Temmerman, M., 2007, 'Vaginal practices, microbicides and HIV: what do we need to know?', *Sexually Transmitted Infections* 85, 505-508.

85. HIV Prevention Trials Network, *HPTN study status table*, viewed 14 February 2011, from http://www.hptn.org/research_studies/HPTNStudyStatusTable.asp.

86. Hladick, F. & Hope, T.J., 2009, 'HIV infection of the genital mucosa in women', *Current HIV/AIDS Reports* 6(1), 20-28.

87. Hladick, F. & McElrath, M.J., 2008, 'Setting the stage: host invasion by HIV', *Nature Reviews Immunology* 8(6), 447-457.

88. Hladik, F. & Doncel, G.F., 2010, 'Preventing mucosal HIV transmission with topical microbicides: challenges and opportunities', *Antiviral Research* 88(Suppl 1), S3-9.

89. Horwood, J., 2007, 'Cellulose sulphate trial halted', *Lancet Infectious Diseases* 7, 183.

90. Hosein, S.R. & Wilson, D.P., 2011, 'Incidence of HIV among men who have sex with men in France', *Lancet Infectious Diseases* 11(4), 262-263.

91. World Health Organisation, *HIV data*, viewed 24 July 2013, from http://www.who.int/hiv/data/en/.

92. Hu, Q., Frank, I., Williams, V., Santos, J.J., Watts, P., Griffin, G.E., Moore, J.P., Pope, M. & Shattock, R.J., 2004, 'Blockade of attachment and fusion receptors inhibits HIV-1 infection of human cervical tissue', *Journal of Experimental Medicine* 199(8), 1065-1075.

93. International Partnership for Microbicides, *IPM clinical trials table 2011*, viewed 25 July 2011, from http://www.ipmglobal.org/our-work/research/clinical-trial.

94. Iriarte, G., Gonzalez, O., Ferreirós, N., Maguregui, M.I., Alonso, R.M. & Jiménez, R.M., 2009, 'Validation of a fast liquid chromatography-UV method for the analysis of drugs used in combined cardiovascular therapy', *Journal of Chromatography* B 877(27), 3045-3053.

95. Jameson, B., Baribaud, F., Pohlmann, S., Ghavimi, D., Mortari, F., Doms, R.W. & Iwasaki, A., 2002, 'Expression of DC-SIGN by dendritic cells of intestinal and genital mucosae in human and rhesus macaques', *Journal of Virology* 76(4), 1866-1875.

96. Jiang, Y., Emau, P., Cairns, J.S., Flanary, L., Morton, W.R., McCarthy, T.D. & Tsai, C.C., 2005, 'SPL7013 gel as a topical microbicide for prevention of vaginal transmission of SHIV in macaques', *AIDS Research and Human Retroviruses* 21(3), 207–213.

97. Joshi, S.N., Katti, U., Godbole, S., Bharucha, K., B.K.K., Kulkarni, S., Risbud, A. & Mehendale, S., 2005, 'Phase I safety of praneem polyherbal vaginal tablet use among HIV-uninfected women in Pune, India', *Transactions of the Royal Society of Tropical Medicine and Hygiene* 99(10), 769-774.

98. Kaiser, G.M., Heuer, M.M., Frühauf, N.R., Kühne, C.A. & Broelsch, C.E., 2006, 'General handling and anaesthesia for experimental surgery in pigs, *Journal of Surgical Research* 130(1), 73-79.

99. Karnachi, A.A. & Khan, M.A., 1996, 'Box-Behnken design for the optimization of variables of indomentacin coprecipitates with polymer mixtures', *International Journal of Pharmaceutics* 131(1), 9-17.

100. Kawamura, T., Gulden, F.O., Sugaya, M., McNamara, D.T., Borris, D.L., Lederman, M.M., Orenstein, J.M., Zimmerman, P.A. & Blauvelt, A., 2003, 'R5 HIV productively infects Langerhans cells, and infection levels are regulated by compound CCR5 polymorphisms', *Proceedings of the National Academy of Sciences USA* 100(14), 8401-8406.

101. Kawamura, T., Kurtz, S.E., Blauvelt, A. & Shimada, S., 2005, 'The role of langerhans cells in the sexual transmition of HIV', *Journal of Dermatological Science* 40(3), 147-

155.

102. Kennedy, E.M., Gavegnano, C., Nguyeu, L., Slater, R., Lucas, A., Fromentin, E., Schinazi, R.F., & Kim, B., 2010, 'Ribonucleoside triphosphates as substrate of human immunodeficiency virus type 1 reverse transcriptase in human macrophages', *Journal of Biological Chemistry* 285(50), 39380-39391.

103. Khan, G.M. & Zhu, J. 1998, 'Formulation and *in vitro* evaluation of ibuprofen-carbopol® 974P-NF controlled release matrix tablets III: influence of co-excipients on release rate of the drug', *Journal of Controlled Release* 54(2), 185-190.

104. Khan, K.A. 1975, 'The concept of dissolution efficiency', *Journal of Pharmacy and Pharmacology* 27(1), 48-49.

105. Klaase, P.J., 2007, 'Modeling how many envelope glycoprotein trimers per viron particle in human immunodeficiency virus infectivity and its neutralization by antibody', *Virology* 369(2), 245-262.

106. Klaase, P.J., Shattock, R. & Moore, J.P. 2008, 'Antiretroviral drug-based microbicides to prevent HIV-1 sexual transmission', *Annual Review of Medicine* 59, February, 455-71.

107. Kozlowski, P.A. & Neutra, M.R., 2003, 'The role of mucosal immunity in prevention of HIV transmission', *Current Molecular Medicine* 3(3), 217-228.

108. Kumar, M., Mishra, R.K. & Banthia, A.K., 2010, 'Development of pectin based hydrogel membranes for biomedical applications', *International Journal of Plastics Technology* 14(2), 213-223.

109. Kumar, P., Pillay, V., Choonara, Y.E., Modi, G., Naidoo, D. & du Toit, L.C., 2011, 'In silico theoretical molecular modeling for Alzheimer's disease: the nicotine-curcumin paradigm in neuroprotection and neurotherapy', *International Journal of Molecular Sciences* 12(1), 694-724.

110. Kwon, D.S., Gregorio, G., Bittou, N., Hendrickson, W.A. & Littman, D.R., 2002, 'DC-SIGN-mediated internalization of HIV is required for trans-enhancement of T-cell

infections', *Immunity* 16(1), 135-144.

111. Lacey, C.J.N., Wright, A., Weber, J.N. & Profy, A.T., 2006, 'Direct measurement of in-vivo vaginal microbicide levels of Pro2000 achieved in a human safety study', *AIDS* 20(7), 1027-1039.

112. Lai, S.K., Hida, K., Shukair, S., Wang, Y.Y., Figueiredo, A., Cone, R., Hope, T.J. & Hanes, J., 2009, 'HIV is trapped by acidic but not by neutralized human cervicovaginal mucus', *Journal of Virology* 83(21), 11196 –11200.

113. Lai, S.K., Wang, Y. & Hanes, J., 2009, 'Mucus-penetrating nanoparticles for drug and gene delivery to mucosal tissues', *Advanced Drug Delivery Reviews* 61(2), 158-171.

114. Lamers, S.L., Salemi, M., McGrath, M.S. & Fogel, G.B., 2008, 'Prediction of R5, X4, and R5X4 HIV-1 coreceptor usage with evolved neural networks', *IEEE/ACM Transactions on Computational Biology and Bioinfomatics* 5(2), 291-300.

115. Lemarchand, C., Couvreur, P., Vauthier, C., Costantini, D. & Gref, R., 2003, 'Study of emulsion stabilization by graft copolymers using the optical analyzer Turbiscan', *International Journal of Pharmaceutics* 254(1), 77-82.

116. Li, S. & McCarthy, S., 1999, 'Further investigations on the hydrolytic degradation of poly(DL-lactide)', *Biomaterials* 20(1), 35-44.

117. Liu, L., Chen, G., Fishman, M.L. & Hicks, K.B., 2005, 'Pectin gel vehicles for controlled fragrance delivery', *Drug Delivery* 12(3), 149-157.

118. Liu, L., Fishman, M.L., Hicks, K.B. & Kende, M., 2005, 'Interactions of various pectin formulations with porcine colonic tissues', *Biomaterials* 26(29), 5907-5907.

119. Liu, S., Lu, H., Neurath, R. & Jiang, S., 2005, 'Combination microbicides cellulose acetate 1, 2 benzenedicarboxylate and UC781 has synergistic and complementary effects against human immunodeficiency virus type 1', *Antimicrobial Agents and Chemotherapy* 49(5), 1830-1836.

120. Lukashov, V.V. & Goudsmit, J., 1997, 'Founder virus population related to route of

virus transmission: a determination of intrahost human immunodeficiency virus type 1 evolution?', *Journal of Virology* 71(3), 2023-2030.

121. Magnus, C. & Regoes, R.R., 2010, 'Estimating the stoichiometry of HIV neutralization', *PLOS Computational Biology* 6(3), 1-11.

122. Magnus, C., Rusert, P., Bonhoeffer, S., Trkola, A. & Regoes, R.R., 2009, 'Estimating the stoichiometry of human immunodeficiency virus entry', *Journal of Virology* 83(3), 1523-1531.

123. Manson, K.H., Wyand, M.S., Miller, C. & Neurath, A.R., 2000, 'Effect of cellulose acetate phthalate topical cream on vaginal transmission of simian immunodeficiency virus in rhesus monkeys', *Antimicrobial Agents and Chemotherapy* 44(11), 3199–3302.

124. Marcorin, G.L., Da Ros, T. & Castellano, S., 2000, 'Design and synthesis of novel [60] fullerene derivatives as potential HIV aspartic protease inhibitors', *Organic Letters* 2(25), 3955-3958.

125. Matsuda, Y., Minamida, Y. & Hayashi, S-I, 1976, 'Comparative evaluation of tablet lubricants: effect of application method on tablet hardness and ejectability after compression', *Journal of Pharmaceutical Sciences* 65(8), 1155-1160.

126. Mayer, K.H. & Pizer, H.F., 2009, '*HIV prevention: a comprehensive approach*', Academic Press, London.

127. Mayer, K.H., Karim, S.A., Kelly, C., Maslankowski, L., Rees, H., Profy, A.T., Day, J., Welch, J. & Rosenberg, Z., HIV Prevention Trials Network (HPTN) 020 Protocol Team., 2003, 'The safety and tolerability of PRO 2000 Gel in sexually active HIV-uninfected and abstinent HIV-infected women', *AIDS* 17(3), 321-329.

128. McCarthy, T.D., Karellas, P., Henderson, S.A., Giannis, M., O'Keefe, D.F., Heery, G., Paull, J.R., Matthews, B.R. & Holan, G., 2005, 'Dentrimers as drugs, discovery and preclinical and clinical development of dentrimer-based microbicides for HIV and STI prevention', *Molecular Pharmacology* 2(4), 312-318.

129. McCormack, S., Ramjee, G., Kamal, A., Rees, H., Cook, A., Gafos, M., Jentsch, U., Pool, R., Chisembele, M., Kapiga, S., Mutemwa, R., Valley, A., Palanee, T., Profy, A., Nunn, A., Hayes, R. & Weber, J., 2010, 'Pro 2000 vaginal gel for prevention of HIV-1 infection (Microbicide Development Programme 301): a phase 3, randomized, double blind, parallel-group trial', *Lancet* 376(9749), 1329-1337.

130. McEwen, B., 2002, *The end of stress as we know it*, Joseph Henry Press, Washington DC

131. McGuckin, M.A., Lindén, S.L., Sutton, P. & Florin, T.H., 2001, 'Mucin dynamics and enteric pathogens', *Nature Reviews Microbiomolecules* 9(4), 265-278.

132. Mengual, O., Meunier, G., Cayre, I., Puech, K. & Snabre, P., 1999, 'Characterisation of instability of concentrated dispersions by a new optical analyser: the TURBISCAN MA 1000', *Colloids and Surfaces A: Physicochemical and Engineering* Aspects 152(1-2), 111-123.

133. Microbicide Trial Network, *Studies*, viewed 14 February 2011, from http://www.mtnstopshiv.org/node/studies.

134. Microbicide Trial Network, 2008, *Tenofovir gel provides high level of protection against HIV in rectal tissue*, viewed 25 July 2011, from http://www.mtnstopshiv.org/node/2931.

135. Miller, C.J. & Shattock, R.J., 2003, 'Target cells in vaginal HIV transmission', *Microbes and Infection* 5(1), 59-67.

136. Miller, C.J., Alexander, N.J., Sutjipo, S., Lackner, A.A., Gettie, A., Hendrickx, A.G., Lowenstine, L.J., Jennings, M. & Marx, P.A., 1989, 'Genital mucosal transmission of simian immunodeficiency virus: animal model for heterosexual transmission of human immunodeficiency virus', *Journal of Virology* 63(10), 4277-4284.

137. Miller, C.J., Li, Q., Abel, K., Kim, E.Y., Ma, Z.M., Wietgrefe, S., La Franco-Scheuch, L., Compton, L., Duan, L,. Shore, M.D., Zupancic, M., Busch, M., Carlis, J., Wolinsky, S. & Haase, A.T., 2005, 'Propagation and dissemination of infection after vaginal transmission of simian immunodeficiency virus', *Journal of Virology* 79(14), 9217-9227.

138. Mishra, R.K., Datt, M. & Banthia, A.K., 2008, 'Synthesis and characterization of pectin/PVP hydrogel membranes for drug delivery system', *AAPS PharmSciTech* 9(2), 395-403.

139. Mishra, R.K., Datt, M., Pal, K. & Banthia, A.K., 2008, 'Preparation and characterization of amidated pectin based hydrogels for drug delivery, *Journal of Material Science: Materials in Medicine* 19(6), 2275-2280.

140. Mohammadi, D., 2010, 'Trial results finally show potential for microbicidal HIV gel', *Lancet Infectious Diseases* 10(9), 587.

141. Moore, J.W. & Flanner, H.H., 1996, 'Mathematical comparison of dissolution profiles', *Pharmaceutical Technology* 1, 64-74.

142. Morrow, G., Vachot. L., Vagrnas, P. & Robbiani, M., 2007, 'Current concepts of HIV transmission', *Current HIV/AIDS Reports* 4(1), 29-35.

143. Mortazavi, S.A., 2003, 'Extended frequency sweep: a more realistic rheological approach to investigate the process of mucoadhesive polymer-mucus gel chain interpenetration', *Iran Polymer Journal* 12(5), 413-420.

144. Munarin, F., Guerriro, S.G., Grellier, M.A., Tanzi, M.C., Barbosa, M.A., Petrini, P. & Granja, P.L., 2011, 'Pectin-based injectable biomaterials for bone tissue engineering', *Biomacromolecules* 12(3), 568-577.

145. Munch, J., Standker, L., Adermann, K., Schulz, A., Schindler, M., Chinnadurai, R., Pöhlmann, S., Chaipan, C., Biet, T., Peters, T., Meyer, B., Wilhelm, D., Lu, H., Jing, W., Jiang, S., Forssmann, W.G. & Kirchhoff, F., 2007, 'Discovery and optimization of a natural HIV-1 entry inhibitor targeting the gp41 fusion peptide', *Cell* 129(2), 263-275.

146. Nanni Costa, L., 2009, 'Short-term stress: the case of transport and slaughter*', Italian Journal of Animal Science* 8, December, 241-252.

147. Nazli, A., Chan, O., Dobson-Belair, W.N., Ouellet, M., Tremblay, M.J., Gray-Owen, S.D., Arsenault, A.L. & Kaushic, C., 2010, 'Exposure to HIV-1 directly impairs mucosal epithelial barrier integrity allowing microbial translocation', *PLoS Pathogens* 6(4), e1000852.

148. Ndesendo, V.M.K., Pillay V., Choonara Y.E., Buchman E., Bayever D.N. & Meyer L.C.R., 2008, 'A review of current intravaginal drug delivery approaches employed for the prophylaxis of HIV/AIDS and prevention of sexually transmitted infections', *AAPS PharmSciTech* 9(2), 505-520.

149. Ndesendo, V.M.K., Pillay, V., Choonara, Y.E., du Toit, L.C., Buchman, E., Meyer, L.C.R., Khan, R.A. & Uwe, R., 2010, 'Investigation of the physicochemical and physicomechanical properties of a novel intravaginal bioadhesive polymeric device in the pig model*', AAPS PharmSciTech* 11(2), 793-808.

150. Ndesendo, V.M.K., Pillay, V., Choonara, Y.E., du Toit, L.C., Meyer, L.C.R., Buchman, E., Kumar, P. & Khan, R.A., 2011, 'In Vivo evaluation of the release of zidovudine and polystyrene sulfornate from a dual intravaginal bioadhesive polymeric device in the pig model', *Journal of Pharmaceutical Sciences* 100(4), 1416-1435.

151. Nordman, H., Davies, J.R., Herrmann, A., Karlsson, N.G., Hansson, G.C. & Carlstedt, I., 1997, 'Mucus glycoproteins from pig gastric mucosa: identification of different mucin populations from the surface epithelium', *Biochemical Journal* 326(Pt 3), 903-910.

152. Norvell, M.K., Berubi, G.I. & Thompson, R.J., 1984, 'Investigation of microtrauma after sexual intercourse', *Journal of Reproductive Medicine* 29(4), 269-271.

153. O'Hara, T., Dunne, A., Butler, J. & Devane, J., 1998, 'A review of methods used to compare dissolution profile data', *PSTT* 1(5), 214-223.

154. O'keefe, B.R., Shenoy, S.R., Xie, D., Zhang, W., Muschik, J.M., Currens, M.J.,

Chaiken, I. & Boyd, M.R., 2000, 'Analysis of the interaction between the HIV-inactivating protein cyanovirin-N and soluble forms of the envelope glycoprotein gp120 and gp41', *Molecular Pharmacology* 58(5),982-992.

155. Owen, D.H. & Katz, D.F., 1999, 'A vaginal fluid simulant', *Contraception* 59(2), 91-95.

156. Owen, D.H. & Katz, D.F., 2005, 'A review of the physical and chemical properties of human semen and the formulation of a semen simulant', *Journal of Andrology* 26(4), 459-469.

157. Patel, M.M., Smart, J.D., Nevell, T.G., Ewen, R.J., Eaton, P.J. & Tsibouklis, J., 2003, 'Mucin/poly(acrylic acid) interactions: a spectroscopic investigation of mucoadhesion', *Biomacromolecules* 4(5), 1184-1190.

158. Pearlman, D.A., Case, D.A., Caldwell, J.W., Ross, W.S., Cheatham, T.E., De-Bolt, S III, Ferguson, D., Seibel, G. & Kollman, P., 1995, 'AMBER, a package of computer programs for applying molecular mechanics, normal mode analysis, molecular dynamics and free energy calculations to simulate the structural and energetic properties of molecules', *Computer Physics Communications* 91(1-3), 1-41.

159. Perotti, M., Pirovano, A. & Phillips, D.M., 2003, 'Carageenan formulation prevents macrophage trafficking from vagina: implications for microbicide development', *Biology of Reproduction* 69(3), 933-939.

160. Pignet, V. & Blauvelt, A., 2002, 'Essential roles of dendritic cells in the pathogenesis and potential treatment of HIV disease', *Journal of Investigative Dermatology* 119(2), 365-369.

161. Pillay, V. & Danckwerts, M.P., 2002, 'Textural profiling and statistical optimization of crosslinked calcium-alginate-pectinate-cellulose acetophthalate gelisphere matrices', *Journal of Pharmaceutical Sciences* 91(12), 2559-2570.

162. Pillay, V., Mashingaidze, F., Choonara, Y.E., du Toit, L.C., Buchmann. E., Maharaj, V., Ndesendo & V.M.K., Kumar, P., 2012, 'Qualitative and quantitative intravaginal targeting: key to anti-HIV-1 microbicide delivery from test tube to *in vivo* success', *Journal of Pharmaceutical Sciences* 101(6), 1950-1968.

163. Pinkerton, S.D. & Abramson, P.R., 1997, 'Effectiveness of condoms in preventing HIV transmission' *Social Science & Medicine* 44(9), 1303-1312.

164. Piret, J., Lamontagne, J., Bestman-Smith, J., Roy, S., Gourde, P., Désormeaux, A., Omar, R.F., Juhász, J. & Bergeron, M.G., 2000, '*In vitro* and *in vivo* evaluations of sodium lauryl sulfate and dextran sulfate as microbicides against herpes simplex and human immunodeficiency viruses', *Journal of Clinical Microbiology* 38(1), 110–119.

165. Poignard, P., Saphire, E.O., Parren, P.W. & Burton, D.R., 2001, 'gp120: biologic aspects of structural features', *Annual Reviews Immunology* 19, April, 253-274.

166. Polson, C., Sarkar, P., Incledon, B., Raguvaran, V. & Grant, R., 2003, 'Optimization of protein precipitation based on effectiveness of protein removal and ionization effect in liquid chromatography-tandem mass spectrometry', *Journal of Chromatography B* 785(2), 263-275.

167. Pope, M. & Haase, A., 2003, 'Transmission, acute HIV-1 infection and the quest for strategies to prevent infection', *Nature Medicine* 9(7), 847-852.

168. Population Council, *Carraguard phase 3 clinical trial*, viewed 14 February 2011, from http://www.popcouncil.org/projects/90_ClinicalStudiesCarraguardPhaseIII.asp.

169. Ravi, P.R, Kotreka, U.K. & Saha, R.N., 2008, 'Controlled release matrix tablets of zidovudine: effect of formulation variables on the *in vitro* drug release kinetics', *AAPS PharmSciTech* 9(1), 302-313.

170. Raviolo, M.A. & Briñón, M., 2011, 'Preformulation studies of zidovudine derivatives: acid dissociation constants, differential scanning calorimetry, thermogravimetry, X-rays powder diffractometry and aqueous stability studies', Scientia *Pharmaceutica* 79(3), 479-491.

171. Richman, D.D., Wrin, T., Little, S.J. & Petropoulos, C.J., 2003, 'Rapid evolution of the neutralizing antibody response to HIV-1 type infection', *Proceedings of the National Academy of Sciences USA* 100(7), 4144 - 4149.

172. Rohan, L.C.C. & Sassil, A., 2009, 'Vaginal drug delivery system for hiv prevention' *AAPS Journal* 11(1), 78-87.

173. Rolin, C., 1993, *Industrial gums: polysaccharides and their derivatives*, Academic Press, New York.

174. Rossi, S., Bonferoni, M.C., Lippoli, G., Bertoni, M., Ferrari, G., Caramella, C. & Conte, U., 1995, 'Influence of mucin type on polymer-mucin rheological interactions', *Biomaterials* 16(14), 1073-1079.

175. Samanidou, V.F., Giannakis, D.E. & Papadaki, A., 2009, 'Development and validation of an HPLC method for the determination of seven penicillin antibiotics in veterinary drugs and bovine blood plasma', *Journal of Separation Science* 32(9), 1302-1311.

176. Santos, C.A., Freedman, B.D., Ghosan, S., Jacob, J.S., Scarpulla, M. & Mathiowitz, E., 2003, 'Evaluation of anhydride oligomer within polymer microsphere blends and their impact on bioadhesion and drug delivery *in vitro*', *Biomaterials* 24(20), 3571-3583.

177. Schuon, A., 2008, 'Positive initial results pave the way for definitive follow-up studies, Anti-HIV nanoviricide drug candidate demonstrate significant therapeutic efficacy in animal trails', in *Nanotechnology Now*, viewed 14 February 2011, from http://www.nanotech-now.com/news.cgi?story id=29215.

178. Sexton, A., Harman, S., Shattock, R.J. & Ma, K-C., 2009, 'Design, expression, and characterization of a multivalent, combination HIV microbicide', *FASEB Journal* 23(10), 3590-3600.

179. Shaikh, J., Ankola, D.D., Beniwal, V., Sing, D. & Ravi Kumar, M.N.V., 2009, 'Nanoparticle encapsulation improves oral bioavailability of curcumin by at least 9-fold when compared to curcumin administered with piperine as absorption enhancer', *European Journal of Pharmaceutical Sciences* 37(3-4), 223-230.

180. Sharma, R. & Ahuja, M., 2011, 'Thiolated pectin: Synthesis, characterization and evaluation as a mucoadhesive polymer', *Carbohydrate Polymers* 85(3), 658-663.

181. Shattock, R. & Solomon, S., 2004, 'Microbicides- aids to safer sex', *Lancet* 363(9414), 1002-1003.

182. Shen, R., Richter, H.E. & Smith, P.D. 2011, 'Early HIV-1 target cells in human vaginal and ectocervical mucosa', *American Journal of Reproductive Immunology* 65(3), 261-267.

183. Siegfried, N., Muller, M., Deeks, J., Volmink, J., Egger, M., Low, N., Walker, S. & Williamson, P., 2005, 'HIV and male circumcision- a systematic review with assessment of the quality of studies', *Lancet Infectious Diseases* 5(3), 165-173.

184. Siepmann, F., Eckart, K., Maschke, A., Kotler, K. & Siepmann, J., 2010, 'Modeling drug release from PVAc/PVP matrix tablets', *Journal of Controlled Release* 141(2), 216-222.

185. Smith, M., 2006, 'TMC 120 vaginal ring promising as microbicides carrier', *XVI International Conference*; Toronto, Canada. August 13-18, 2006.

186. Sriamornsak, P. & Wattanakorn, N., 2008, 'Rheological synergy in aqueous mixtures of pectin and mucin', *Carbohydrate Polymers* 74(3), 474-481.

187. Sriamornsak, P., Wattanakorn, N. & Takeuchi, H., 2010, 'Study on the mucoadhesion mechanism of pectin by atomic force microscopy and mucin-particle method', *Carbohydrate Polymers* 79(1), 54-59.

188. Sriamornsak, P., Wattanakorn, N., Nunthanid, J. & Puttipipatkhachorn, S., 2008, 'Mucoadhesion of pectin as evidence by wettability and chain interpenetration', *Carbohydrate Polymers* 74(3), 458-467.

189. Srivastava, P., Malviya, R. & Kulkarni, G.T., 2010, 'Formulation and evaluation of paracetamol tablets to assess binding property of orange peel pectin', International *Journal of Pharmaceutical Sciences Review and Research* 3(1), 31-34.

190. Stone, A., 2002, 'Microbicides: A new approach to preventing HIV and other sexually transmitted infections', *Nature Reviews Drug Discovery* 1(12), 977-985.

191. Tachet, A., Dulioust, E., Salmon, D., De Almeida, M., Rivalland, S., Finkielsztejn, L., Heard, I., Jouannet, P., Sicard, D. & Rouzioux, C., 1999 'Detection and quantification of HIV-1 in semen: identification of subpopulation of men at high potential risk of viral sexual transmission', *AIDS* 13(7), 823-831.

192. Tam, S.K., Dusseault, J., Polizu, S., Ménard, M., Hallé, J-P. & Yahia, L., 2005, 'Physicochemical model of alginate-poly-L-lysine microcapsules defined at the micrometric/nanometric scale using ATR-FTIR, XPS, and ToF-SIMS', *Biomaterials* 26(34), 6950-6961.

193. Templeton, D.J., 2010, 'Male circumcision to reduce transmission of HIV', *Current Opinion in HIV and AIDS* 5(4), 344-349.

194. Thakur, B.R., Singh, R.K. & Handa, A.K., 1997, 'Chemistry and uses of pectin-a review', *Critical Reviews in Food Science and Nutrition* 37(1), 47-73.

195. Thirawong, N., Kennedy, R.A. & Sriamornsak, P., 2008, 'Viscometric study of mucin-pectin interaction and its mucoadhesive bond strength', *Carbohydrate Polymers* 71(2), 170-179.

196. Thomas, J.A., Ott, D.E. & Gorelick, R.J., 2007, 'Efficiency of human immunodeficiency virus type 1 postentry infection process: evidence against disproportionate numbers of defective virions', *Journal of Virology* 81(8), 4367-4370.

197. Thormar, H., Bergsson, G., Gunnarsson, E., Georgsson, G., Witvrouw, M., Steingrímsson, O., De Clercq, E. & Kristmundsdóttir, T., 1999, 'Hydrogels containing monocaprin have potent microbicidal activities against sexually transmitted viruses and bacteria *in vitro*', *Sexually Transmmited Infections* 75(3), 181–185.

198. Tiller, A.R. & Gorella, B., 1994, 'Estimation of polymer compatibility from molecular mechanics calculations', *Polymer* 35(15), 3251-3259.

199. Tsai, C.C., Emau, P., Jiang, Y., Tian, B., Morton, W.R., Gustafson, K.R. & Boyd, M.R., 2003, 'Cyanovirin-N gel as a topical microbicide prevents rectal transmission of SHIV89.6P in macaques', *AIDS Research and Human Retroviruses* 19(7), 535–541.

200. Turvile, S.G., Santos, J.J., Frank, I., Cameron, P.U., Wilkinson, J., Miranda-Saksena, M., Dable, J., Stössel, H., Romani, N., Piatak, M. Jr., Lifson, J.D., Pope, M. & Cunningham, A.L., 2004, 'Immunodeficiency virus uptake, turnover, and 2-phase transfer in human dendritic cells', *Blood* 103(6), 2170-2179.

201. U.S. National Institutes of Health, *A study of the effects of Advantage 24 on the rectum*, viewed 25 July 2011, from http://clinicaltrials.gov/ct2/show/NCT00000929.

202. U.S. National Institutes of Health, *Safety, tolerance and acceptability trial of the Invisible Condom® in healthy women*, viewed 25 July 2011, from http://clinicaltrials.gov/ct2/show/NCT00136643.

203. Vaidya, A., Jain, A., Khare, P., Agrawal, R.K. & Jain, S.K., 2009, 'Metronizadole loaded pectin microspheres for colon targeting', *Journal of Pharmaceutical Sciences* 98(11), 4229-4236.

204. Valenta, C., 2005, The use of mucoadhesive polymers in vaginal delivery', *Advanced Drug Delivery Reviews* 57(11), 1692-1712.

205. Van Damme, L., Ranjee, G., Alary, M., Vuylsteke, B., Chandeying, V., Rees, H., Sirivongrangson, P., Mukenge-Tshibaka, L., Ettiègne-Traoré, V., Uaheowitchai, C., Karim, S.S., Mâsse, B., Perriëns, J., Laga, M. & COL-1492 study Group., 2002, 'Efficacy of COL- 1492, a nonoxynol-9 vaginal gel, on HIV transmission in female sex workers: a randomized trial', *Lancet* 360(9338), 971-977.

206. Van de Perre, P., Segondy, M., Foulongne, V., Ouedraogo, A., Konate, I., Huraux, J.M., Mayaud, P. & Nagot, N., 2008, 'Herpes simplex virus and HIV-1: deciphering viral synergy', *Lancet Infectious Diseases* 8(8), 490-497.

207. Van de Wijgert, J., Fullem, A., Kelly, G., Mehendale, S., Rugpao, S., Kumwenda, N., Chirenje, Z., Joshi, S., Taha, T., Padian, N., Bollinger. & R., Nelson, K., 2001, 'Phase I trial of the topical microbicide buffer gel: Safety results from four international sites', *Journal of Acquired Immune Deficiency Syndromes* 26(1), 21-27.

208. Van den Berg, N., Mayosi, B. & Khati, M., 2011, Efficacy and mode of action of a natural compound against HIV-1 subtype C', WITS Research update, University of

the Witwatersrand, 16 November.

209. Vernazza, P.L., Gillian, B.L., Dyer, S.A., Fiscus, S.A., Eron, J.J., Frank, A.C. & Cohen, M.S., 1997, 'Quantification of HIV in semen: correlation with antiviral treatment and immune status', *AIDS* 11(8), 987-993.

210. Von Mollendorf, C.E., Van Damme, L., Moyes, J.A., Rees, V.H., Callahan, M.M., Mauck, C.K., Puren, A.J., Tweedy, K. & Taylor, D., 2010, 'Results of a safety and feasibility study of the diaphragm used with ACIDFORM gel or KY jelly', *Contraception* 81(3), 232-239.

211. Walsh, T.L., Frezieres, R.G., Nelson, A.L, Wraxall, B.G.D. & Clark, V.A., 1999, 'Evaluation of prostate-specific antigen as a quantifiable indicator of condom failure in clinical Trials', *Contraception* 60(5), 289-298.

212. Wang, Y. & Annunziata, O., 2007, 'Comparison between Protein-Polyethylene Glycol (PEG) Interactions and the Effect of PEG on Protein-Protein Interactions Using the Liquid-Liquid Phase Transition', *Journal of Physical Chemistry B* 111(5), 1222-1230.

213. Warhurst, D.C., Craig, J.C., Adagu, I.S., Meyer, D.J. & Lee, S.Y., 2003, 'The relationship of physico-chemical properties and structure to the differential antiplasmodial activity of the cinchona alkaloids', *Malaria Journal* 2, 1 September, 26.

214. Wilkinson, E., 2007, 'Herpes treatment may limit HIV transmission and progression', *Lancet Infectious Diseases* 7(4), 249.

215. Witvrow, M., Fikkert, V., Pluymers, W., Matthews, B., Mardel, K., Schols, D., Raff, J., Debyser, Z., De Clercq, E. & Holan, G., Pannecouque, C., 2000, 'Polyanionic (i.e., polysulfonate) dendrimers can inhibit the replication of human immunodeficiency virus by interfering with both virus adsorption and later steps (reverse transcriptase/integrase) in the virus replicative cycle', *Molecular Pharmacology* 58(5), 1100-1108.

216. Wong, T.W., Chan, L.W., Lee, H.Y., Heng & P.W.S., 2002, 'Release characteristics of pectin microspheres prepared by an emulsion technique', *Journal of Microencapsulation* 19(4), 511-522.

217. Woolfson, A.D., Umrethia, M.L., Kett, V.L. & Malcolm, R.K., 2010, 'Freeze-dried, mucoadhesive system for vaginal delivery of the HIV microbicide dapivarine: optimization by an artificial neural network', *International Journal of Pharmaceutics* 388(1-2), 136-143.

218. UNAIDS, *World epidemic update 2009,* viewed 24 July 2012*, from* www.unaids.org.

219. World Health Organisation, *International HIV data 2009*, viewed 15 February 2011, from http://www.who.int/hiv/data/2009_global_summary.png.

220. World Health Organization, 2009, *Microbicides*, viewed 24 July 2012, from www.who.int/hiv/topic/microbicides/en/.

221. Wu, L. & KewalRamani, V.N., 2006, 'Dendritic–cell interactions with HIV: infection and viral dissemination', *Nature Reviews Immunology* 6(11), 859-868.

222. Wu, L., 2008, 'Biology of HIV mucosal transmission', *Current Opinion in HIV and AIDS* 3(5), 534-540.

223. Xie, X.L., Li, R.K.Y., Tjong, S.C. & Tang, C.Y., 2002, 'Flory-Huggins interaction parameters of LCP/thermoplastic blends measured by DSC analysis', *Journal of Thermal Analysis and Calorimetry* 70(2), 541-548.

224. Yacaman, M.J., Elechiquerra, J.L., Lara, H.H. & Burt, J.L., 2006, *Protein-Noble metal nano-particles*, World Intellectual Property Organization patent WO-06/053325.

225. Yang, X., Kurteva, S., Ren, X., Lee, S. & Sodroski, J., 2005, 'Stoichiometry of envelope glycoprotein trimers in the entry of human immunodeficiency virus type1', *Journal of Virology* 79(19), 12132-121147.

226. Yang, X., Kurteva, S., Ren, X., Lee, S. & Sodroski, J., 2006, 'Subunit stiochiometry of human immunodeficiency virus type 1 envelope glycoprotein trimers during virus entry into cells', *Journal of Virology* 80(9), 4388-4395.

227. Yu, B.Y., Chung, J.W. & Kwak, S-Y., 2008, 'Reduced Migration from Flexible

Poly(vinyl chloride) of a Plasticizer Containing β-Cyclodextrin Derivative', *Environmental Science & Technology* 42(19), 7522–7527.

228. Yu, C-Y., Cao, H., Zhang, X-C., Zhou, F-Z., Cheng S-X., Zhang X-Z. & Zhuo, R-X., 2009, 'Hybrid nanospheres and vesicles based on pectin as drug carriers', *Langmuir* 25(19), 11720-11726.

229. Zaitseva, M., Blauvelt, A., Lee, S., Lapham, C.K., Klaus-Kovtun, V., Mostowski, H., Manischewitz, J. & Golding, H., 1997, 'Expression and function of CCR5 and CXCR4 on human Langerhans cells and macrophages: implications for HIV primary infection', *Nature Medicine* 3(12), 1369-1375.

230. Zhang, L., He, T., Talal, A., Wang, G., Frankel, S.S. & Ho, D.D., 1998, 'Distribution of human immunodeficiency virus/simian immunodeficiency virus coreceptors: CXCR4, CCR3 and CCR5', *Journal of Virology* 72(6), 5035-5045.

231. Zhang, Y. & Moore, J.P., 1999, 'Will multiple coreceptors need to be targeted by inhibitors of human immunodeficiency virus type 1 entry', *Journal of Virology* 73(4), 3443-3448.

232. Zhang, Y., Huo, M., Zhou, J., Zou, A., Li, W., Yao, C. & Xie., S. 2010, 'DDSolver: An add-in program for modelling and comparison of drug dissolution profiles', *AAPS Journal* 12(3), 263-271.

233. Zhu, P, Chertova, BJr., Lifson, JD., Arthur, L.O., Liu, J., Taylor, K.A. & Roux, K.H., 2003, 'Electron tomography analysis of envelope glycoprotein trimers on HIV and simian immunodeficiency virons', *Proceedings of the National Academy of Sciences USA* 100(26), 15812-15817.

234. Zhu, P., Liu, J., Julian, BJr., Chertova, E., Lifson, J.D., Grisé, H., Ofek, G.A., Taylor, K.A. & Roux, K.H., 2006, 'Distribution and three-dimentional structure of HIV virus envelope spikes', *Nature* 441(7095), 847-852.

235. Zoeteweij, J.P. & Blauvelt, A., 1998, 'HIV-dendritic cell interactions promote efficient viral infection of T cells', *Journal of Biomedical Science* 5(4), 253-259.

APPENDICES

REVIEW

Qualitative and Quantitative Intravaginal Targeting: Key to Anti-HIV-1 Microbicide Delivery from Test Tube to *In Vivo* Success

VINESS PILLAY,[1] FELIX MASHINGAIDZE,[1] YAHYA E. CHOONARA,[1] LISA C. DU TOIT,[1] ECKHART BUCHMANN,[2] VINESH MAHARAJ,[3] VALENCE M. K. NDESENDO,[4] PRADEEP KUMAR[1]

[1]Department of Pharmacy and Pharmacology, Faculty of Health Sciences, University of the Witwatersrand, Parktown, 2193 Johannesburg, South Africa

[2]Department of Obstetrics and Gynecology, Faculty of Health Sciences, University of the Witwatersrand, Parktown, 2193 Johannesburg, South Africa

[3]Department of Biosciences, Council for Scientific and Industrial Research, Brummeria, Pretoria, South Africa

[4]School of Pharmacy and Pharmaceutical Sciences, St. John's University of Tanzania, Dodoma, Tanzania

Received 8 December 2011; revised 27 January 2011; accepted 9 February 2012

Published online in Wiley Online Library (wileyonlinelibrary.com). DOI 10.1002/jps.23098

ABSTRACT: The past decade has seen several effective anti-HIV-1 agent discoveries, yet microbicides continue to disappoint clinically. Our review expounds the view that unsatisfactory microbicide failures may be a result of inefficient delivery systems employed. We hereby propose a thorough scientific qualitative and quantitative investigation of important aspects involved in HIV-1 transmission as a prerequisite for microbicide delivery. Intravaginal targeting of HIV-1 increases the chances of microbicide success, wherein vaginal microenvironmental factors including pH should be maintained at HIV-1 prohibitive acidic levels simultaneously to ward off other sexually transmitted diseases, which compromise vaginal epithelial barrier properties. Furthermore, choice of receptors to target both on HIV-1 and on target cells is vital in deterring transmission. Appropriate modeling of virus–target cell interactions as well as targeting early stages of the HIV-1 infection accompanied by computation and delivery of appropriate microbicide quantities could revolutionize microbicide research, ultimately delivering a female-controlled HIV-1 prevention modality appropriately. © 2012 Wiley Periodicals, Inc. and the American Pharmacists Association J Pharm Sci

Keywords: targeted drug delivery; special populations; site-specific delivery; polymeric drug delivery systems; polymer–biopolymer interactions; physicochemical properties; pharmacokinetics/pharmacodynamics; permeability; mucosal delivery; macromolecular drug delivery

INTRODUCTION

Several novel anti-HIV-1 compounds are in the discovery pipeline and existing agents are being investigated for the treatment of the ever elusive HIV/AIDS, leading to a refocus toward prevention.[1,2] Contemporary strategies include microbicides, vaginally or rectally applied topical chemical agents, having the ability to block HIV-1 infection.[2] Nonoxynol-9 was the first chemical entity to be extensively tried as a preventative microbicide against HIV-1. It is quite effective as a viral membrane lysis agent; however, its efficacy *in vivo* as an HIV-1 preventative application was not demonstrated due to its detrimental and disruptive effects on the vaginal epithelia, which even led to an increase in HIV infection according to the COL-1492 study. Several microbicide trials have failed, restricting microbicide agents to test tube therapies.[3,4] They may be highly effective *in vitro* but not sufficiently effective *in vivo*.[5] Various reasons have been postulated to explain this failure of microbicides. This review focuses on microbicide formulation and delivery as the "Achilles heel" and as an aspect that can be manipulated to change microbicide fortunes if only appropriate scientific analysis, considerations, and designs are pursued.

Correspondence to: Viness Pillay (Telephone: +27-11-717-2274; Fax: +27-86-517-6890; E-mail: viness.pillay@wits.ac.za)

Journal of Pharmaceutical Sciences
© 2012 Wiley Periodicals, Inc. and the American Pharmacists Association

Society For Biomaterials

Exploration of the biomacromolecular interactions of an interpenetrating proteo-saccharide hydrogel network at the mucosal interface

Felix Mashingaidze,[1] Yahya E. Choonara,[1] Pradeep Kumar,[1] Lisa C. du Toit,[1] Vinesh Maharaj,[2] Eckhart Buchmann,[3] Valence M. K. Ndesendo,[4] Viness Pillay[1]

[1]University of the Witwatersrand, Faculty of Health Sciences, Department of Pharmacy and Pharmacology, 7 York Road, Parktown, 2193, Johannesburg, South Africa
[2]Council for Scientific and Industrial Research, Department of Biosciences, Meiring Naudé Road, Brummeria, Pretoria, South Africa
[3]University of the Witwatersrand, Faculty of Health Sciences, Department of Obstetrics and Gynecology, 7 York Road, Parktown, 2193, Johannesburg, South Africa
[4]St. John's University of Tanzania, School of Pharmacy and Pharmaceutical Sciences, Dodoma, Tanzania

Received 13 September 2012; revised 1 February 2013; accepted 5 February 2013
Published online 1 September 2013 in Wiley Online Library (wileyonlinelibrary.com). DOI: 10.1002/jbm.a.34664

Abstract: The relationship between mucin (MUC) and pectin (PEC) was explored in an attempt to understand the biomacromolecular interactions that occur at mucosal surfaces when mucus membranes are exposed to PEC-based materials. These interactions were explored through techniques, such as attenuated total reflection Fourier transform infrared (ATR-FTIR) spectroscopy, SEM imagery of lyophilized MUC–PEC blends, thermodynamic analysis, rheology investigations, and *in silico* static lattice atomistic simulations using a molecular mechanics energy relationships (MMER) approach. Three types of PEC that had different degrees of esterification and degrees of amidation were investigated at different MUC–PEC mass ratios (1:0, 1:1, 1:4, 1:9, and 0:1). The effect PEG 400 and Ca^{2+} in the MUC–PEC interactions were also studied. ATR-FTIR spectroscopy revealed broadening and strengthening of FTIR peaks at 3363 cm^{-1} and between 3000–3650 cm^{-1} due to stretching vibrations of the –OH, –COOH groups on MUC and PEC as well as the –N–H group on MUC. This suggested significant intra- and inter-molecular H-bonding. Morphologically, MUC-rich scaffolds were porous, thin, and multidirectional compared with the smooth, rigid, and unidirectional PEC-rich scaffolds. The Flory–Huggins interaction parameter (χ_{12}) for all MUC–PEC mass ratios was negative, thus confirming MUC–PEC miscibility and interactions. UV absorbance increased with increasing relative concentration of PEC in the aqueous MUC–PEC dispersions. Furthermore, rheology investigations demonstrated synergistic enhancement in viscosity (η) and dynamic moduli upon the addition of PEG 400 and Ca^{2+}. MMER analysis revealed several key MUC–PEC interactions that corroborated well with the experimental data. Notably, higher esterification and larger mass ratios of PEC yielded greater MUC–PEC interactions. © 2013 Wiley Periodicals, Inc. J Biomed Mater Res Part A: 101A: 3616–3629, 2013.

Key Words: pectin, Mucin, macromolecular interaction, synergistic enhancement in rheology, molecular mechanics energy relationships

How to cite this article: Mashingaidze F, Choonara YE, Kumar P, du Toit LC, Maharaj V, Buchmann E, Ndesendo VMK, Pillay V. 2013. Exploration of the biomacromolecular interactions of an interpenetrating proteo-saccharide hydrogel network at the mucosal interface. J Biomed Mater Res Part A 2013:101A:3616–3629.

INTRODUCTION

Mucin, a glycosylated protein and a major structural component of the mucus gel found lining human body cavities (such as the urogenital, gastrointestinal, eye, lungs, and other mucosal membranes) plays a major role in various frontline interactions with various materials from the external environment.[1,2] Mucus comprises approximately 95% water, 2% lipids (fatty acids, phospholipids, and cholesterol) and electrolytes, and the remaining 3% being mucin. Researchers have shown interest in mucin as the structural backbone of the gel-like layer that serves various functions such as lubrication of mucosal membranes to avoid abrasion, protection of mucosal lining from self-digestion as in the case of gastric mucus and it also acts as a gatekeeper, keeping at bay unwanted external materials and organisms such as bacteria and viruses.[3,4] The major functions of mucus are owed to the structural and molecular properties of mucin. Mucin is a large (0.5–20 MDa) glycoprotein consisting of a protein core composed of 4–5 amino acids (proline, serine, threonine, glycine, and glutamate) arranged in detached regions. One of

Correspondence to: V. Pillay; e-mail: viness.pillay@wits.ac.za
Contract grant sponsors: South African National Research Foundation (NRF); Council for Scientific and Industrial Research (CSIR) South Africa

© 2013 WILEY PERIODICALS, INC.

Formulation, optimization and characterization of mucin-pectin-polyethylene glycol microspheres for intravaginal anti-HIV-1 drug delivery

F. Mashingaidze[1], V. Pillay[1], Y. E. Choonara[1], L.C. du Toit[1], V. Maharaj[2], E. Buchmann[3], V.M.K.Ndesendo[4], P. Kumar[1]

[1]Department of Pharmacy and Pharmacology, University of the Witwatersrand, Johannesburg, South Africa
[2]Department of Biosciences, CSIR South Africa, Pretoria, South Africa
[3] Department of Obstetrics and Gynecology, University of the Witwatersrand, Johannesburg, South Africa
[4]School of Pharmacy & Pharmaceutical Sciences, St. John's University of Tanzania , Dodoma, Tanzania.

INTRODUCTION

The goal was to formulate, optimize and characterize mucin-pectin-polyethylene glycol microspheres for intravaginal anti-HIV-1 drug delivery.

MATERIALS AND METHODS

Porcine gastric mucin types III (MUC) and polyethylene glycol (PEG, Mw 400) were purchased from Sigma–Aldrich® Inc, St. Louis, USA. GENU® pectin type USP/100(PEC) was obtained from CP Kelco ApS, Lille Skensved, Denmark. The model anti-HIV-1 drug employed was zidovudine (AZT, Glaxo Smith Kline). Other materials employed included; calcium chloride, glucose and cyclohexane which were of analytical grade. Simulated vaginal fluid (SVF) was prepared from analytical grade chemicals [1].

1) *MUC-PEC-PEG microsphere formulation and characterization*: Microspheres where formulated using a crosslinking-emulsion technique. MUC, PEC, PEG and AZT were subsequently dispersed and dissolved in deionised water to form the aqueous phase whilst stirring for 15min and then crosslinked with calcium chloride [2].A water-in-oil (W/O) emulsion was prepared by ultrasonication with cyclohexane as the oil phase. The W:O ratio was 4:1 with span 85 added as the surfactant. The emulsion was centrifuged at 4000rpm for 1min and thereafter excess cyclohexane was decanted. The remaining concentrated microsphere emulsion was frozen at -80°C for 12hrs with glucose added as a lyoprotectant before lyophilization for 48hrs. Characterization of the microspheres involved; measurement of microsphere particle size, zeta potential (Zetasizer Nano ZS, Malvern Instruments Ltd, Worcestershire, United Kingdom) and observation of the shape, appearance and size under a (JEOL S100 Transmission Electron Microscope (Tokyo, Japan).

2) *Microsphere optimization and drug release studies*: For optimization, a Box-Behnken design of 15 experimental formulations was employed. AZT release from the microspheres was measured over 12hrs utilizing a dialysis method with SVF employed as the dissolution media [1]. The Mean Dissolution Time (MDT) and the dissolution profile were used to characterize AZT release from the MUC-PEC-PEG microspheres

RESULTS AND DISCUSSION

The optimized formulation had an average zeta potential of -35.0±0.940mV and released 99.783% of the encapsulated AZT in 9hrs with a MDT value of 3.209hrs as illustrated in Fig. 1a. Smooth-surfaced spherical microspheres with a particle size ranging from 0.2-0.5µm were formulated as depicted in Fig. 1b.

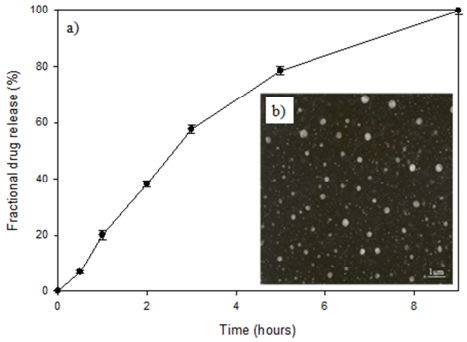


Fig. 1.a)Graphical illustration of the fractional AZT released from MUC-PEC-PEG microspheresb) transmission electron microscopy image of MUC-PEC-PEG microspheres (insert).

CONCLUSIONS

AZT-loaded MUC-PEC-PEG microsphereswere successfully formulated. These microspheres are intended for prolonged intravaginal delivery of anti-HIV-1 bioactives, microbicides and possibly antifungal drugs.

ACKNOWLEDGMENTS

We acknowledge the financial sponsorship we received from the South African National Research Foundation (NRF) and the Council of Scientific and Industrial Research (CSIR) South Africa.

REFERENCES

[1] D.H.Owen and D.F. Katz, "A vaginal fluid simulant" Contraception., 59 (1999) 91-95.
[2] P. Opanasopit, A. Apirakaramwong, T. Ngawhirunpat, T. Rojanarata andU. Ruktanonchai, "Development and Characterization of Pectinate Micro/Nanoparticles for Gene Delivery"AAPS. Pharm.Sci.Tech. 9 (2008) 67-74.

APPENDIX D

Pectin-mucin Interactions: Implication and Application in Microsphere Formulation for Drug Delivery

Felix Mashingaidze[1], Viness Pillay[1]*, Yahya E. Choonara[1], Vinesh Maharaj[2] and Lisa C. du Toit[1]

[1]University of the Witwatersrand, Department of Pharmacy and Pharmacology, 7 York Road, Parktown Johannesburg, 2193

[2]Department of Biosciences, CSIR South Africa, Meiring Naude Road, Brummeria, Pretoria, South Africa

*Correspondence: viness.pillay@wits.ac.za

Purpose:

All membranes covering human body cavities are lined by mucus. This is a viscoelastic gel-like secretion that has diverse properties and purposes which include; protecting the body against infection, lubricating the membranes they cover to prevent abrasion and preventing self digestion as in the case of gastric mucus. Equal to these benefits, mucus poses various challenges especially in pharmaceutical drug delivery. Our study is to determine the interactions of mucin, the major structural component of mucus, with a biodegradable and biocompatible polymer, pectin, commonly used in pharmaceutical formulations and to further harness this unique relationship to fabricate a unique drug delivery carrier in the form of pectin-mucin microspheres.

Methods:

Turbidity measurement by absorbance: Different ratios of aqueous pectin and mucin were examined for UV absorbance at 600nm using a nanophotometer. A comparison was done between the turbidity of aqueous solutions of pectin and mucin in combination and those of native pectin and mucin respectively. The difference in turbidity of the blended pectin-mucin solution and the sum of that of the individual native polymer solutions was regarded a measure of pectin-mucin interactions.

Rheological analysis: A modular advanced rheometer was used to determine the viscosity, loss and storage moduli of different aqueous ratios of pectin-mucin. Subsequent computation of the difference in the viscosity, loss and storage moduli of the pectin-mucin blend and the sum of the individual pectin and mucin was regarded a measure of the interactions of pectin and mucin.

Fourier transform infrared (FTIR) analysis of pectin-mucin: Dry lyophilized polymer blends of pectin and mucin were analyzed by FTIR to determine pectin-mucin interactions.

Fabrication and characterization of pectin-mucin microspheres: Pectin-mucin microspheres were fabricated using a crosslink-emulsion technique. 0.5g of a pectin-mucin blend with pectin: mucin ratio of 4:1 was solubilized in deionized water at 25°C by stirring for an hour then a crosslinking agent, calcium chloride ($CaCl_2$) and plasticizer, polyethylene glycol 400 (PEG 400) were added to further increase the pectin mucin interpenetration. This aqueous mixture was used as the aqueous phase, cyclohexane was used as the oil phase and span 85 was the surfactant in the sonication of pectin-mucin microspheres.

Results:

Results revealed turbidometric and rheological synergism between pectin and mucin and FTIR disclosed hydrogen bonding as a major contributor to the pectin-mucin interactions. The successful fabrication of microspheres of pectin and mucin with a size range of 0.2-0.5µm is also testimony of the intricate interpenetration of pectin and mucin to form one compatible polymer blend that can be utilized in pharmaceutical applications as a drug carrier.

PATENT JOURNAL

INCLUDING TRADE MARKS, DESIGNS AND COPYRIGHT IN CINEMATOGRAPH FILMS

SEPTEMBER 2011 VOL 44 • No.09

Companies and Intellectual Property Commission

a member of the dti group

Part II of II

ISSUED MONTHLY **DATE OF ISSUE: 28 SEPTEMBER 2011**

ISSN 2223-4837

PATENT JOURNAL

INCLUDING TRADE MARKS, DESIGNS AND COPYRIGHT IN CINEMATOGRAPH FILMS

VOL. 44 NO. 09 Date of Issue: 28 September 2011

PATENTS, TRADE MARKS, DESIGNS AND COPYRIGHT OFFICE

Official notices of proceedings under:

The Patents Act, 1978
The Designs Act, 1993
The Trade Marks Act, 1963
The Trade Marks Act, 1993
The Registration of Copyright in Cinematograph Films Act, 1977

Registrar of Patents, Trade Marks, Designs and Copyright

Note: CIPC acting on behalf of the Government of the Republic of South Africa, cannot guarantee the accuracy of its publications or undertake any responsibility for errors or omissions or their consequences.

2011/06565 ~ Provisional ~ 54: ROLING STOCK JACK ~ 71:JOHANNES STANDER 4 Burma Road Southport KZN 4230 ~ 72:JOHANNES STANDER
2011/06566 ~ Provisional ~ 54: DS-NET ~ 71:PETER MAXWELL 10 Dorothy Road Amalinda East London 5201 PETER LYUBA 16 Belgrave Road Southernwood East London 5201 ~ 72:PETER MAXWELL PETER LYUBA
2011/06567 ~ Provisional ~ 54: WATER AXEL ~ 71:WILLEM JACOBUS SWART 40 Alex Pienaar St Strand Western Cape 7140 ~ 72:Willem Jacobus SWART
2011/06568 ~ Provisional ~ 54: FLEXIBLE LIGHT WEIGHT EDGING CORNICE ~ 71:WILLEM JACOBUS SWART 40 Alex Pienaar St Strand Western Cape 7140 ~ 72:Willem Jacobus SWART
2011/06569 ~ Provisional ~ 54: POWER DRAIN PLUNGER ~ 71:WILLEM JACOBUS SWART 40 Alex Pienaar St Strand Western Cape 7140 ~ 72:Willem Jacobus SWART
2011/06570 ~ Complete ~ 54: SAFETY BARRIER REINFORCING ~ 71:STITCH WISE (PTY) LTD 1 Nursery Road Westerndeep Levels Carletonville ~ 72:KILLASSY NATALIE ~ 33: ZA ~ 31: 2010/06432 ~ 32: 08/09/2010
2011/06571 ~ Complete ~ 54: REINFORCING ELEMENT ~ 71:STITCH WISE (PTY) LTD 1 Nursery Road Westerndeep Levels Carletonville ~ 72:KILLASSY NATALIE ~ 33: ZA ~ 31: 2010/06433 ~ 32: 08/09/2010
2011/06572 ~ Provisional ~ 54: BARBECUE OR LIKE GRIDIRON ~ 71:VON SEIDEL MICHAEL 10 Leccino Terrace Helderberg Estate Somerset West 7130 CAPE PROVINCE ~ 72:VON SEIDEL MICHAEL
2011/06573 ~ Complete ~ 54: PROCESS FOR SEQUESTRATION OF FLUIDS IN GEOLOGICAL FORMATIONS ~ 71:DUSSEAULT MAURICE B 15532 Lorne Court White Rock British Columbia V4B 5J6 BILAK ROMAN 49 Macewan Park Close N W Calgary Alberta T3K3Z6 ~ 72:DUSSEAULT MAURICE B BILAK ROMAN ~ 33: US ~ 31: 61/173.301 ~ 32: 28/04/2009
2011/06574 ~ Complete ~ 54: BACK-UP FUEL CELL ELECTRIC GENERATOR COMPRISING A COMPACT MANIFOLD BODY,METHODS OF MANAGING THE OPERATION THEREOF ~ 71:ELECTRO POWER SYSTEMS S.P.A. Torino Via Livorno, 60 ~ 72:CHERCHI PIERPAOLO MERCANTE LUCA MUSSO ANDREA CEFFA DARIO BORELLO LUISA GIANOLIO GUISEPPE ~ 33: EP ~ 31: 09152671.5 ~ 32: 12/02/2009
2011/06575 ~ Complete ~ 54: THERMOSETTING COMPOSITIONS CONTAINING ISOCYANURATE RINGS ~ 71:COOK COMPOSITES AND POLYMERS COMPANY 820 East 14th Avenue North Kansas City MO 64114 ~ 72:ZHAO MING-YANG HSU CHIH-PIN ~ 33: US ~ 31: 61/166.281 ~ 32: 03/04/2009
2011/06576 ~ Complete ~ 54: METHOD FOR ALLOWING A SOLAR GENERATOR TO TRACK THE SUN,CONTROL FOR A SOLAR SYSTEM AND SOLAR SYSTEM ~ 71:FRAUNHOFER-GESELLSCHAFT ZUR FORDERUNG DER ANGERWANDTEN FORSCHUNG E.V Hansastrasse 27C 80686 Munchen ~ 72:BURGER BRUNO STALTER OLIVIER ~ 33: DE ~ 31: 10 2009 013 113.2 ~ 32: 13/03/2009
2011/06577 ~ Complete ~ 54: COMPOUNDS AND COMPOSITIONS FOR COGNITION-ENHANCEMENT,METHODS OF MAKING,AND METHODS OF TREATING ~ 71:MITHRIDION INC 505 Science Drive Suite C Madison WI 53711 ~ 72:TWOSE TREVOR M ABRAHAM BRENT D COPP RICHARD R FARNHAM JAMES G HANSON SETH A HENDRICKSON MICHAEL L OCKULY JEFFREY C VERDONE MELINDA L ~ 33: US ~ 31: 61/278.649 ~ 32: 09/10/2009
2011/06578 ~ Provisional ~ 54: PHARMACEUTICAL DOSAGE FORM ~ 71:UNIVERSITY OF THE WITWATERSRAND,JOHANNESBURG 1 JAN SMUTS AVENUE BRAAMFONTEIN JOHANNESBURG ~ 72:PILLAY VINESS CHOONARA YAHYA ESSOP MASHINGAIDZE FELIX KUMAR PRADEEP
2011/06579 ~ Complete ~ 54: ABDOMINAL EXERCISER WITH ROTATABLE SEAT AND TANDEM PULLEY FEATURES ~ 71:E. MISHAN & SONS, INC 230 Fifth Avenue Suite 800 New York NY 10001 ~ 72:MISHAN STEVEN MISHAN EDWARD I ~ 33: US ~ 31: 12/877.321 ~ 32: 08/09/2010
2011/06580 ~ Complete ~ 54: VESSEL CONTAINING FLUID DISTRIBUTION MEDIA ~ 71:SAINT-GOBAIN CERAMICS & PLASTICS, INC 1 New Bond Street Box Number 15138 Worcester Massachusetts 01615-0138 ~ 72:NIKNAFS HASSAN S SHERMAN DANIEL C ~ 33: US ~ 31: 61/152.912 ~ 32: 16/02/2009
2011/06581 ~ Complete ~ 54: SOLAR ENERGY COLLECTION APPARATUS ~ 71:VAN NIEKERK DANIEL GABRIEL 43 VIOOLTJIE STREET GROENEWEIDE BOKSBURG 1459 DAVIS BEVAN JOHN 141 Elsburg Road Delville Ext 1 Germiston 1401 Gauteng ~ 72:VAN NIEKERK DANIEL GABRIEL ~ 33: ZA ~ 31: 2009/01066 ~ 32: 16/02/2009
2011/06582 ~ Complete ~ 54: MULTI-DIMENSIONAL SIGNAL OF REDUCED PEAK-TO-RMS RATIO ~ 71:TELEFONAKTIEBOLAGET L M ERICSSON (PUBL) SE 164 83 Stockholm ~ 72:DENT PAUL W ~ 33: US ~ 31: 12/166.910 ~ 32: 02/07/2008
2011/06583 ~ Complete ~ 54: COM[POSITIONS AND METHODS FOR EXTENDED THERAPY WITH AMINOPYRIDINES ~ 71:ACORDA THERAPEUTICS INC 15 Skyline Drive Hawthorne New York 10532 ~ 72:BLIGHT ANDREW R COHEN RON ~ 33: US ~ 31: 61/299.259 ~ 32: 28/01/2010



First Time Inventor

Certificate awarded to

Felix Mashingaidze

for having disclosed their first Wits invention

Prof Helen Laburn, DVC Research, University of the Witwatersrand, Johannesburg

21 May 2013

This award is issued by the Technology Transfer Office of the University, located in Wits Enterprise. As a recipient of this award, the Technology Transfer Office welcomes you to the Wits Innovator's Forum, an elite group of Wits researchers who translate their research into innovations that have potential for use in society and industry for the benefit of South Africans.

Wits Enterprise
The Innovation Edge

UNIVERSITY OF THE WITWATERSRAND JOHANNESBURG

Wits Innovators Forum

APPENDIX G

AESC3

STRICTLY CONFIDENTIAL

ANIMAL ETHICS SCREENING COMMITTEE (AESC)

CLEARANCE CERTIFICATE NO. 2011/44/05

APPLICANT: **Mr F Mashingaidze**

DEPARTMENT: **Pharmacy and Pharmachology**

PROJECT TITLE: ***In Vivo intravaginal delivery of a drug combination (zidovudine and BP36) in the pig model employing a composite polymeric delivery system***

Number and Species

20 Large White Pigs

Approval was given for to the use of animals for the project described above at an AESC meeting held on **27 September 2011**. This approval remains valid until **30 September 2013**.

The use of these animals is subject to AESC guidelines for the use and care of animals, is limited to the procedures described in the application form and to the following additional conditions:

Approved with the following conditions and recommendations:

Conditions that must be met

1. Possible side-effects should be specified and discussed with Dr Leith Meyer.

Recommendations for consideration

1. The experimental design should be randomized.

Signed: _____ (Chairperson, AESC) Date: 10/10/2011

I am satisfied that the persons listed in this application are competent to perform the procedures therein, in terms of Section 23 (1) (c) of the Veterinary and Para-Veterinary Professions Act (19 of 1982)

Signed: _____ (Registered Veterinarian) Date: 25/10/2011

cc: Supervisor:
Director: CAS

APPENDIX H

Which AESC 2009

Please note that only typewritten applications will be accepted. Should additional space be required for section "I" and/or "j", please use the back of this form.

ANIMAL ETHICS SCREENING COMMITTEE

MODIFICATIONS AND EXTENSIONS TO EXPERIMENTS

a. Name: Felix Mashingaidze

b. Department: Pharmacy and Pharmacology

c. Experiment to be modified / extended **AESC NO:**

Original AESC number	2011	44	05
Other M&E's :			

d. Project Title: *In vivo* intravaginal delivery of a drug combination (zidovudine and BP36) in the pig model employing a composite polymeric delivery system.

e.	Number and species of animals **originally approved**:	20	
f.	Number of additional animals **previously allocated on M&Es**:	0	
g.	Total number of animals **allocated** to the experiment to date:	0	
h.	Number of animals **used** to date:	0	

i. Specific modification / extension requested:
- Reduction in zidovudine dosage from 300mg to150mg whilst increasing the dosage of BP36 from 60mg to 600mg (only in group C pigs) to enable better detection and quantification of the bioactive.
- Vaginal mucosa biopsies to be obtained from group C pigs only at time intervals 3, 7, 14, 21, 28 days.
- Permission to commence with the main study after 5 days of closely observing the pilot study.
- Permission to include vaginal swabbing just behind the urethral junction using absorbent cotton material at time points 3, 7, 14, 21, 28 days as an additional technique to enable vaginal mucosal surface drug detection and quantification

j. Motivation for modification / extension:
- *Ex vivo* permeability studies we performed using excised pig vaginal mucosa showed that AZT is easily detectable and quantifiable in plasma yet BP36 is not so detectable and it is difficult to quantify hence the need to increase the dosage.
- Due to the low detectability of BP36 an additional technique of obtaining vaginal biopsies which will then be processed to detect BP36 is essential.
- To reduce the amount of time spent for the whole study and to avoid overgrowth of Large White pigs whilst in housing before experimentation. This also reduces total cost of study as a result of less feeds necessary to sustain the pigs.
- Vaginal swabs will aid in the detecting the vaginal mucosal surface drug.

Date: 10/12/2012 Signature:

RECOMMENDATIONS:
Approved.

Date: 13 December 2012 Signature: .
Chairman, AESC

AESC 2013

Please note that only typewritten applications will be accepted. Should additional space be required for section "I" and/or "j", please use the back of this form.

ANIMAL ETHICS SCREENING COMMITTEE

MODIFICATIONS AND EXTENSIONS TO EXPERIMENTS

a. Name: Felix Mashingaidze

b. Department: Pharmacy and Pharmacology

c. Experiment to be modified / extended **AESC NO:**

Original AESC number	2011	44	05
Other M&E's : 3			

d. Project Title: *In vivo* intravaginal delivery of a drug combination (zidovudine and BP36) in the pig model employing a composite polymeric delivery system.

e.	Number and species of animals **originally approved**:	20	
f.	Number of additional animals **previously allocated on M&Es**:	0	
g.	Total number of animals **allocated** to the experiment to date:	12	
h.	Number of animals **used** to date:	12	
i.	Specific modification / extension requested: -Collection of small intestinal tissue for ex vivo studies for Mr. Angus Hibbins **-Mr. Angus Hibbins: AESC No. 2011/33/04** Excision of small intestinal tissue from one euthanized pig for the purposes of ex vivo drug permeability studies		
j.	Motivation for modification / extension: - Ex vivo studies necessary to augment main in vivo studies. - No pain or suffering will be experienced by the euthanized pigs.		

Date: 07/05/2013 Signature:

RECOMMENDATIONS:
Approved: collection of small intestinal tissue

Date: 8 May 2013 Signature:

Chairman, AESC